Supramolecular Studies with Functionalised Group 15 Ligands

By

Noelia M. Sánchez Ballester

Supervisors: Dr. Mark R. J. Elsegood and Martin B. Smith

A Doctoral Thesis submitted in partial fulfilment of the requirements for the award of Doctor of Philosophy

At Loughborough University
Chemistry Department

November 2009

ACKNOWLEDGMENTS

I would like to thank every person who has helped me achieve my PhD in Loughborough University:

I would like to thank my supervisors: Dr. Mark R.J. Elsegood and Dr. Martin B. Smith for allowing me to join this research group and giving me the opportunity to start a PhD in Loughborough and for giving me support and enthusiasm during these three years. I would like to thank Loughborough University for funding this research. I would like to thank Dr. Caroline A. Kirk for the powder XRD analysis and the technical service in the department, especially Dr. Mark Edgar, Pauline King, John Kershaw, Alistair Daley and Andy Kowalski. I would like to thank the EPSRC National Crystallography Service at the University of Southampton for the data collection of **2.21**, **3.2**, **4.58** and **5.25**.

I would like to thank my family for the constant support during the course of my studies and in my personal life.

I wish to thank all the members of the inorganic chemistry section past and present: Julia Barreira, Joanne Smith, Chris Kirk, Gavin Brown, Allen Ekubo, Andrew Lake, Chris Raw, Benoit Genevier, Paul Staniland, Sandie Dann, Paul Kelly, Vickie McKee, Leanne James, Rob King, Jenna Crisp, Lee Fan, Ralf Kulmaczewski, Anna Ma, Soraya Sanchez, Voro, David, Carlos and many other people that I met here.

I would like to thank Silvia, Jesus, Jasón, Cristina, Hayley, Adela, Aranxa, Ed, Sylvain, Eric, Abdul, Claire, Noemi, Suzy (I hope I have not forgotten anyone!) for all our EHB lunches, parties, chats, support and very good moments together!

I would like to thank Yohan Chan for the patience, support and comprehension he has given me during all this time.

GENERAL ABBREVIATIONS

Ad	Adamantane
bpy	4,4'-bipyridine
$B(OH)_3$	Boric acid
BNCT	Boron neutron capture therapy
CSD	Cambridge Structural Database
cod	1,5-cyclooctadiene
DMF	Dimethylformamide
DMSO	Dimethylsulfoxide
dpp	1,3-bis(diphenylphosphino)propane
d	Doublet
dd	Doublet of doublets
eq	Equivalents
EtOH	Ethanol
glygly	glycylglycine
Hz	Hertz
IR	Infrared
MHz	Megahertz
Me	Methyl
MOF	Metal-organic framework
$[2,n\text{-Hpzdca}]^-$	*n*-carboxy-pyrazine-2-carboxylate
nbd	η^2-norbornadiene
NMR	Nuclear Magnetic Resonance
ppm	Parts per million
phen	phenanthroline
Ph	Phenyl
x-Hpyca	Pyridine-*x*-carboxylic acid
$[x\text{-pyca}]^-$	Pyridine-*x*-carboxylate
x,y-H_2pydca	Pyridine-*x*,*y*-dicarboxylic acid
$[x,y\text{-Hpydca}]^-$	*y*-carboxy-pyridine-*x*-carboxylate
$[x,y\text{-pydca}]^{-2}$	Pyridine-*x*,*y*-dicarboxylate
2-Hpzca	Pyrazine-2-carboxylic acid

$[2\text{-pzca}]^-$	Pyrazine-2-carboxylate
2,*n*-H_2pzdca	Pyrazine-2,*n*-dicarboxylic acid
$[2,n\text{-pzdca}]^{-2}$	Pyrazine-2,*n*-dicarboxylate
s	Singlet
THF	Tetrahydrofuran
tht	Tetrahydrothiophene
tpy	2,2':6',2''-terpyridine
trygly	triglycine
t	Triplet
XRD	Powder X-ray Diffraction
δ	Chemical shift

ABSTRACT

This thesis has been divided into five sections. The first chapter introduces the main themes of this thesis, including the description of the concepts of supramolecular chemistry, crystal engineering, hydrogen bonding and graph set analysis. The final section of chapter one describes a typical X-ray experiment used to determine the structures of the compounds presented in this thesis.

Chapter two describes the synthesis and single crystal structures of copper(I) complexes with pyridine- and pyrazine-carboxylic acids. A series of novel solvent inclusion compounds of copper(I) complexes with pyridine- and pyrazine-carboxylic acids and the hydrogen bonding patterns adopted are also discussed.

Chapter three reports the potential uses of boronic acids as building blocks for the design of novel solid-state architectures utilising hydrogen bonds. Novel copper(I) pyridine-/pyrazine-carboxylate complexes with boronic acid co-crystals are presented in which the heterodimeric boronic···carboxylate $R^2_2(8)$ ring motif is present in all cases.

Chapter four discusses the synthesis of novel ditertiary phosphines bearing functional groups with hydrogen bonding potential either *via* a three-step or single step synthetic route which involves a well known method of reductive amination followed by an efficient Mannich-based condensation. Complexation studies of these *P*,*P*-bidentate ligands with various transition metal centres such as Pt(II), Mo(0), Ru(II) and Au(I) are also presented. The effect on the structural motifs observed in these series of compounds by the regioselective incorporation of functional groups with potential hydrogen bonding capability such as hydroxyl and amide is also given.

Finally, chapter five contains the synthesis and coordination studies of new phosphorus donor ligands leading to ideas for further work.

CONTENTS

Chapter 1

Introduction

1.1 Introduction

This chapter will introduce the main themes of this thesis – the concepts of supramolecular chemistry, crystal engineering, hydrogen bonding and graph set analysis. The final section describes a typical X-ray experiment used to determine the structures of the compounds presented in this thesis. Specific introductions regarding the chemistry reported are included at the start of each experimental chapter.

1.2 Supramolecular Chemistry

The term "supramolecular chemistry" has been defined by Nobel Prize winner Jean-Marie Lehn, as "*chemistry beyond the molecule*",[1,2] the association of molecular or ionic entities held together reversibly by intermolecular forces to yield organised arrays of higher complexity.

Supramolecular chemistry is a multidisciplinary field, encircling the traditionally distinct disciplines of organic, inorganic and physical chemistry. Supramolecular self-assembly of components causes the reversible, spontaneous formation of organised structures driven by molecular recognition between two or more units under the intermolecular control of relatively labile non-covalent interactions.[2,3] The reversibility of supramolecular self-assembly is key to form the thermodynamically most favourable structure. Biological examples of self-assembly include the DNA double helix in which two strands are linked together by hydrogen bonds and π-π stacking interactions and, the formation of the quaternary structures of proteins, *e.g.* in the synthesis of viral components.[4] Molecular recognition is made possible by the complementarity of the subunits, often through the utilisation of the geometric and chemical features of the molecular fragments.[5]

Supramolecular, non-covalent bonding interactions include:

- Ion-ion interactions (100-350 $kJmol^{-1}$)
- Ion-dipole interactions (50-200 $kJmol^{-1}$)
- Dipole-dipole interactions (5-50 $kJmol^{-1}$)
- Hydrogen bonding (4-120 $kJmol^{-1}$)
- π-π stacking (0-50 $kJmol^{-1}$)
- Van der Waals forces (<5 $kJmol^{-1}$)

As a result of its relative strength and directionality,[6] and its importance in biological examples of self-assembly, hydrogen bonding has been described as the "*masterkey interaction in supramolecular chemistry*".[5]

1.3 Hydrogen Bonding

Hydrogen bonding is a donor-acceptor interaction involving hydrogen atoms.[7] The necessary criteria for a hydrogen bond are:[7-9]

- The hydrogen bond donor (*D*–H), relatively polarised bonds, where *D* includes O, N, F or C, and
- The hydrogen bond acceptor (*A*), normally having a basic lone pair or having polarisable π electrons; negatively charged acceptors are also common.

The hydrogen bond is symbolised in the rest of this work as D–H···A, where the distance D–H is smaller than the distance H···A. The net effect in the D–H···A system is a weakening and lengthening in the D–H bond. The strength of hydrogen bonding interactions is greater than the van der Waals interactions, but considerably weaker than covalent bonding and dependent on its environment.[9] Categorisation of the strength of hydrogen bonding is itself ambiguous, with many sources having overlapping and contradictory categories.[5,7] The categories adopted by Desiraju, Steed and Atwood, shown in Table 1.1, will be used for the remainder of this work.[4,10]

Table 1.1 Classification of the strength of hydrogen bonding.

	Very strong	Strong	Weak
D···A / Å	2.2-2.5	2.5-3.2	3.2-4.0
Bond Angles / °	175-180	130-180	90-180
Bond energy / kJ mol^{-1}	60-120	16-60	< 12

The weakest of the interactions commonly thought of as hydrogen bonds involve π-acceptors. For example, D–H donor groups can form hydrogen bond with the π-system of a phenyl ring. D–H···π interactions follow a similar pattern in strength to their stronger relatives, with the hydrogen bond being weaker when D = N compared to D = O, and considerably weaker still when D = C.

Gilli and Gilli have presented the *Electrostatic-Covalent H-Bond Model* (*ECHBM*) which derives from the systematic analysis of structural and spectroscopic data of a large number of homonuclear O–H···O and heteronuclear N–H···O/O–H···N hydrogen bonds.[11] This model leads to a thorough classification of hydrogen bonds in chemical classes which can be used to predict the hydrogen bond strength from the simple knowledge of the chemical formula.

1.3.1 The Study of Hydrogen Bonding

Spectroscopic methods, such as NMR spectroscopy, have become standard methods to investigate hydrogen bonds in the solid state. However, the effects of weaker hydrogen bonds are not generally detected as easily.[10] The effect of weak hydrogen bonding can be detected by single crystal X-ray diffraction and neutron diffraction. As X-rays interact with the electrons in a structure, the placing of electron-poor hydrogen atoms within structures containing heavy, electron-rich atoms can be more of a challenge, yet the donor atom-acceptor atom distance D···A is still accurately found. Where the accurate positioning of hydrogen atoms is needed, neutron diffraction can be used. Here the neutrons interact with the nuclei of the system, allowing the hydrogen atoms to be accurately located.

1.4 Supramolecular Synthons and Crystal Engineering

The combination of hydrogen bonds and/or intermolecular interactions using a "designed placement of functional groups" generates supramolecular synthons, some of the many examples are shown in Figure 1.1.[5,12] Supramolecular synthons allow molecular recognition to occur: the chemical nature and geometrical placement of the functional groups in the two or more molecular fragments producing intermolecular interactions which result in the assembly (self-assembly) of supramolecular arrays.[5,6]

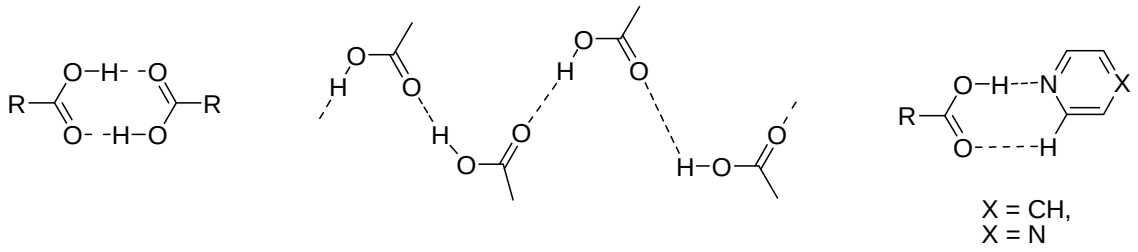

Figure 1.1 Examples of supramolecular synthons: carboxylic acid head-to-tail; carboxylic acid chain and carboxylic acid-pyridine.

Crystal engineering has been defined as the understanding of intermolecular interactions in the context of crystal packing and the utilisation of such understanding in the design of new solids with desired physical and chemical properties.[13] It is a multidisciplinary area involving, for example, materials chemistry, supramolecular chemistry, molecular recognition and biology.

Crystal engineering concentrates on the use of molecules or ions with exofunctionality that are capable of forming one-dimensional, two-dimensional or three-dimensional networks; the goal of crystal engineering is to recognise and design synthons that are robust enough to be exchanged from one network structure to another, which ensures generality and predictability.[5] Some authors consider that crystal engineering is not yet at the stage where crystal structures are entirely predictable,[13-15] with progress needed in the areas of target identification, synthetic methodology and synthetic strategy. Recently, various computational methods have been developed in order to predict the thermodynamically feasible crystal structures of organic molecules.[16,17]

1.5 Graph Set Analysis

Etter *et al*. have constructed a set of rules for the assignment of nomenclature to hydrogen bond patterns displayed in the solid state.[18-20] Without these rules, much confusion can result, with authors utilising their own nomenclature. The rules, an application of graph theory, are termed "graph set analysis" and the graph sets assigned to the hydrogen bond patterns take the form:

$$G^{a}_{d}(r)$$

Where

G = pattern designator
r = degree of the pattern
a = number of acceptors
d = number of donors

The pattern designator, G, can take the assignments S, C, R and D:

- S denotes an intramolecular bond
- C denotes an infinite chain
- R denotes rings
- D denotes non-cyclic dimers and other finite hydrogen-bonded sets.

The degree of the pattern, r, is either the number of atoms in the ring or the repeat length of the chain, traversing the shortest pathway from the hydrogen atom of the hydrogen bond to the acceptor atom of the next.

Etter concluded that all good donor and acceptor groups tend to be used in hydrogen bonding, and that the strongest donors tend to hydrogen bond with the strongest acceptors.[18-20]

In this work, graph set analysis will be used to describe the hydrogen bonding patterns significant to the structures, particularly in comparing motifs between structures. Two examples of packing modes of carboxylic acids are termed $\mathbf{R^2_2(8)}$ and **C(4)** (Figure 1.2).

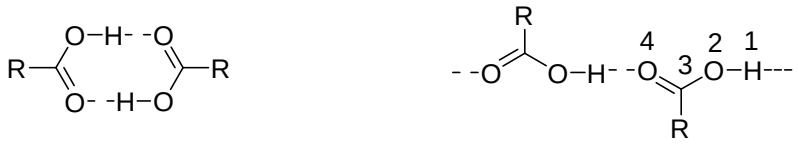

$\mathbf{R^2_2(8)}$ **C(4)**

(a) (b)

Figure 1.2 Examples of graph set analysis, applied to the packing modes of carboxylic acids. (a) $R^2_2(8)$ ring motif, an eight-membered ring with two donors and two acceptors; (b) C(4) chain motif with four atoms in the repeat length.

1.6 The Cambridge Structural Database (CSD)

The Cambridge Structural Database (hereafter "the CSD") is a crystallographic database containing data for approximately 450,000 structures.[21,22] While not being a store of information on all structurally determined compounds due to the quantity of unpublished structures and the ongoing imbalance in journal publication times compared to structural data collection times, the CSD is, however, a source of information useful in the rationalisation of crystal structures, particularly the geometry of molecules and of hydrogen bonding motifs.

1.7 Solvates and Co-crystals

The term co-crystal has not been well-defined and a number of possible definitions such as molecular complexes, molecular adducts, clathrates and inclusion compounds have been utilised. Often these terms describe the same family of chemical compounds.[23]

The work presented below will adhere to the following definitions/rules:[23,24]

- The term co-crystal is used to denote togetherness of two or more molecular components that must themselves be solids under ambient conditions, but without the implication that either component should retain any degree of its individual crystalline identity within the co-crystal.

- The term solvate is used to describe the corresponding solid/liquid combination. This in itself is a departure from the accepted understanding of a solvate, which is a multi-component molecular crystal that has been obtained from solution, where molecules of the crystallisation solvent have become incorporated into the crystal (the accompanying special case hydrate applies specifically when the solvent is water).

1.8 General X-ray Experimental

The experimental which follows is a generalised description of the single crystal X-ray diffraction technique used at Loughborough University to determine the structures within this thesis. Where applicable, exceptions to this general X-ray experimental are noted in the experimental sections of each chapter, for example where data have been collected using X-ray sources other than the laboratory X-ray source. Structural studies on small and weakly diffracting materials have been performed at the SRS Daresbury Laboratory, on stations 9.8 and 16.2SMX, using synchrotron radiation.

A suitable crystal (typically with dimensions in the range 0.1 to 0.8), which extinguished polarised light, was mounted onto a glass fibre on the goniometer head using a drop of inert oil. The goniometer head was transferred to the Bruker SMART 1000 CCD or Bruker APEX 2 CCD diffractometer, and placed in a pre-cooled N_2 gas stream (typically 150 K). The crystal was centred in the X-ray beam and a set of 3 runs of 50 frames each (typically 5 seconds per frame) was collected using graphite-monochromated Mo-K_α (λ = 0.71073 Å) radiation. The reflections from these frames were then indexed automatically using the Bruker SMART or Apex II program to give a unit cell and an orientation matrix.[25,26] The unit cell was checked against the data stored

in the CSD using CrystalWeb and against unit cells determined in the home laboratory to prevent replication.[27]

A full sphere of data was collected using narrow frames (0.3° steps in ω), with the exposure time dependent on the intensity of the reflections observed in the initial frames collected for indexing, typically ranging from 5 seconds per frame to 40 seconds per frame. The data were integrated using the Bruker SAINT program.[28] A semi-empirical absorption correction was applied using the SADABS program based on equivalent and repeated reflections and the data reduction carried out.[29] The program XPREP within the SHELXTL suite of programs was used to detect any higher, missed symmetry and the space group was determined.[30] The structure was solved using the program XS using either direct methods or Patterson synthesis as appropriate.[30] The structure was refined using the program SHELXL-97 by full-matrix least-squares methods on F^2.[30] Non-hydrogen atoms were initially refined isotropically, then later anisotropically. Hydrogen atoms, except hydrogen atoms noted in the further discussion in each chapter, were placed in geometrically calculated positions. $U_{iso}(H)$ values were set to be 1.2 times U_{eq} of the carrier atom for aryl C*H*, methylene CH_2 and methine C*H*, and 1.5 times U_{eq} of the carrier atom for O*H*, N*H* and CH_3.

The program XP was used to produce graphics.[31] Hydrogen bonds are shown as thin dashed lines in the diagrams within this thesis. Thick dashed lines are used to signify the η^6-bonding of the arene to the ruthenium(II) metal centre in Chapter IV.

Chapter 2

Coordination Chemistry Involving Pyridine and Pyrazine Carboxylic Acids and Bis(triphenylphosphine)copper(I) Borohydride

2. Coordination Chemistry Involving Pyridine and Pyrazine Carboxylic Acids and Bis(triphenylphosphine)copper(I) Borohydride

2.1. Introduction

The reasons for incorporating metal ions into supramolecular networks are numerous, for example, they give access to physical properties that are less common in organic compounds, such as magnetic properties, conductivity and catalytic activity.[32-36] Metal ions also display a range of coordination geometries allowing greater flexibility in constructing materials with specific dimensions and topologies.[37]

Crystal engineering using coordination complexes in general can be broadly categorised into three areas:

- Coordination polymers based on covalent-coordinate bonds.
- Hydrogen-bonded networks of coordination complexes.
- Hybrid networks based on both coordination and hydrogen bonds.

The first category is self-explanatory, but the latter two are often confused.[38] Hydrogen bonded networks of coordination complexes contain coordination bonds only within the coordination complexes, with no peripheral coordination, so the dimensionality of the array is determined by the hydrogen bonding. Hybrid networks based on both coordination and hydrogen bonds use a combination of the two types of bond to form the array.

2.2 The use of Pyridine- and Pyrazine- Carboxylic Acids in Supramolecular Chemistry

Organic compounds displaying exodentate functionality are often utilised as the nodes within metal-free networks.[39] The nine pyridine- (Figure 2.1) and three pyrazine-carboxylic acids (Figure 2.2) display such functionality in the form of their carboxylic acids groups, and the variety of angles between these groups have been used in the

production of networks. These ligands also possess a nitrogen atom for metal-coordination which can combine with an acid group at the *ortho* position to give metal-chelation.

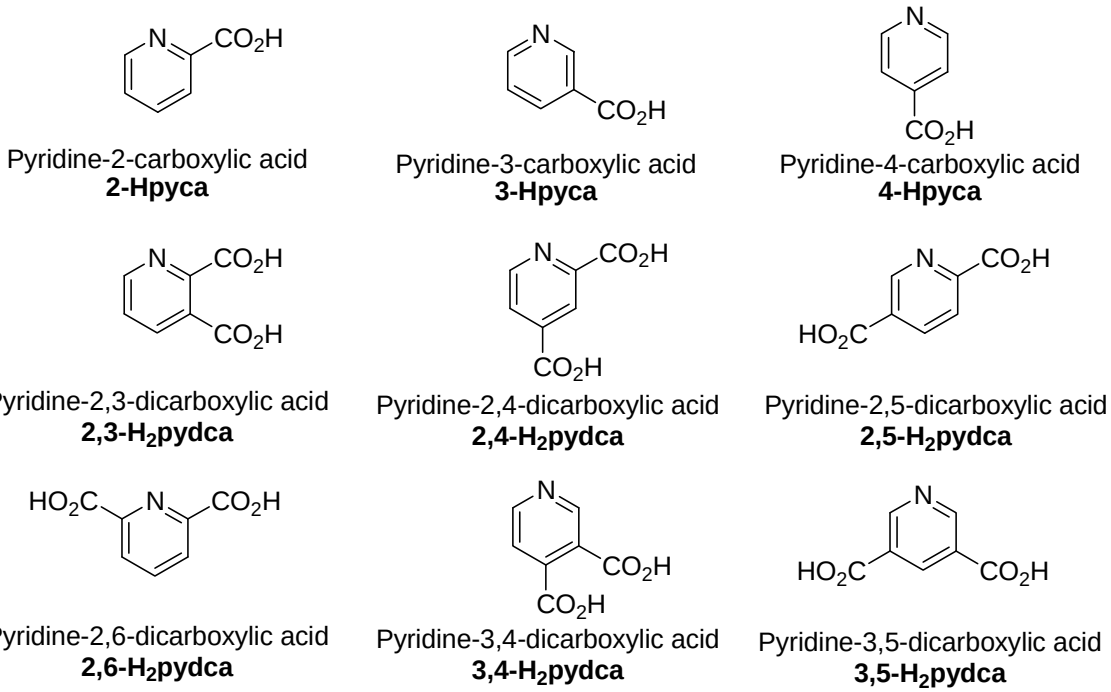

Figure 2.1 The range of pyridine-carboxylic acids and the abbreviations used in this thesis.

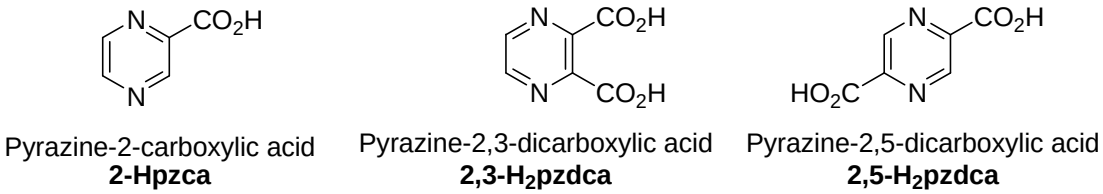

Figure 2.2 The range of pyrazine-carboxylic acids and abbreviations used in this thesis.

In recent years, pyridine- and pyrazine-carboxylic acids have been extensively studied because they can act as excellent building blocks with versatile coordination behaviour and their ability to form hydrogen-bonds in the construction of metal-organic coordination frameworks (MOF) with porosity, photoluminescent or magnetic properties.[40-45]

A search of the Cambridge Structural Database (hereafter "the CSD", version 5.30, November 2008 plus 4 updates) highlights numerous literature examples of single crystal structures containing pyridine- and pyrazine-carboxylic acids groups attached to transition metals.[46-49] In contrast, there is very little documented with regards to complexes of Cu(I) with these organic ligands.[50-52] A brief survey of copper chemistry with pyridine- and pyrazine-carboxylic acids is discussed below.

2.2.1 Copper Complexes with Pyridine Carboxylic Acids

Pyridine-2-carboxylic acid is known to chelate to metal centres including alkali metal cations and transition metals through the nitrogen atom as well as through one oxygen of the carboxylate group.[53-55] This is also seen in pyridine-2,*n*-dicarboxylic acid, where the carboxylic group at the *n* position may remain protonated (Figure 2.3) or be deprotonated and coordinate to a further metal site (Figure 2.4).[32,56]

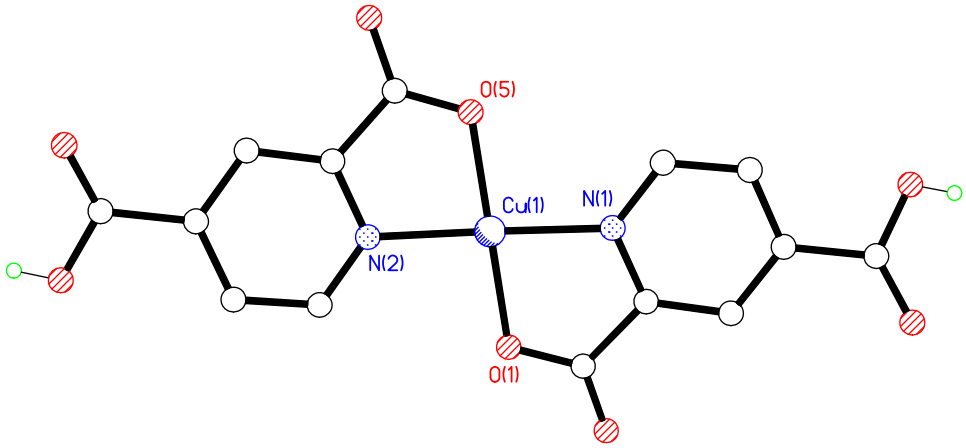

Figure 2.3 View of Cu(2,4-Hpydca)$_2$ in which the CO_2H group at the 4-position remains protonated.

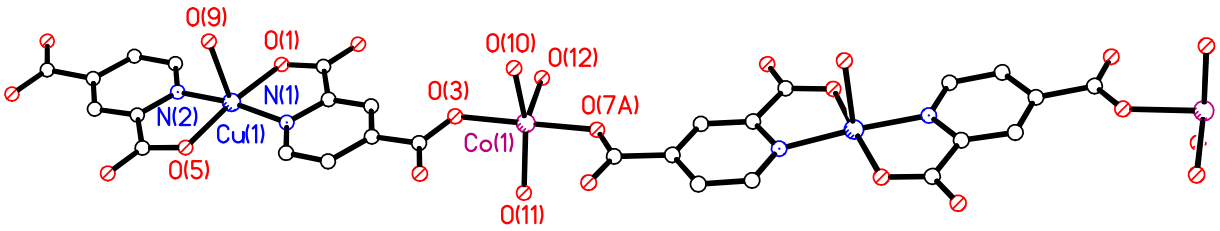

Figure 2.4 View of $[Co(2,4pydca)Cu(H_2O)_4]_n$ in which the CO_2H group at the 4-position is deprotonated and coordinated to Co^{2+}.

The exodentate nature of the 3-pyridine and 4-pyridine carboxylate ions makes them a valuable tecton for designing high-dimensional structures. These compounds combine the coordination ability of the pyridyl moiety with the various modes of the carboxylato group to act as a chelate [Figure 2.5 (a)] and bridging ligand.[57-65] Furthermore, 3-pyridine and 4-pyridine carboxylic acids, nicotinic acid and isonicotinic acid respectively, provide potential extension of the dimensionality *via* the classical cyclic hydrogen bonded carboxylic acid ring motif $R^2_2(8)$ [Figure 2.5 (b)].[52,66,67]

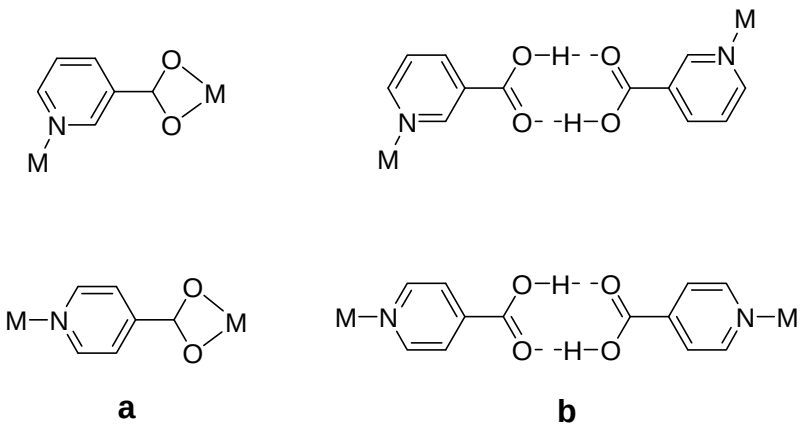

Figure 2.5 (a) Chelating mode of nicotinic and isonicotinic acids; **(b)** The $R^2_2(8)$ cyclic hydrogen bonded carboxylic acid ring motif.

Goher has studied copper(I) halide adducts with nicotinic and isonicotinic acids, but only two crystal structures have been reported, $Cu(3\text{-}Hpyca)_2Cl$ and Cu(4-Hpyca)Cl.[51,52,66] Pyridine-3-carboxylic acid crystallises as a polymeric 2:1 complex with copper(I) chloride, $Cu(3\text{-}Hpyca)_2Cl$, (Figure 2.6). The coordination geometry

about the metal centre is approximately tetrahedral with Cu(I) and Cl ligands arranged alternately forming a zigzag chain extending along the *a* axis.

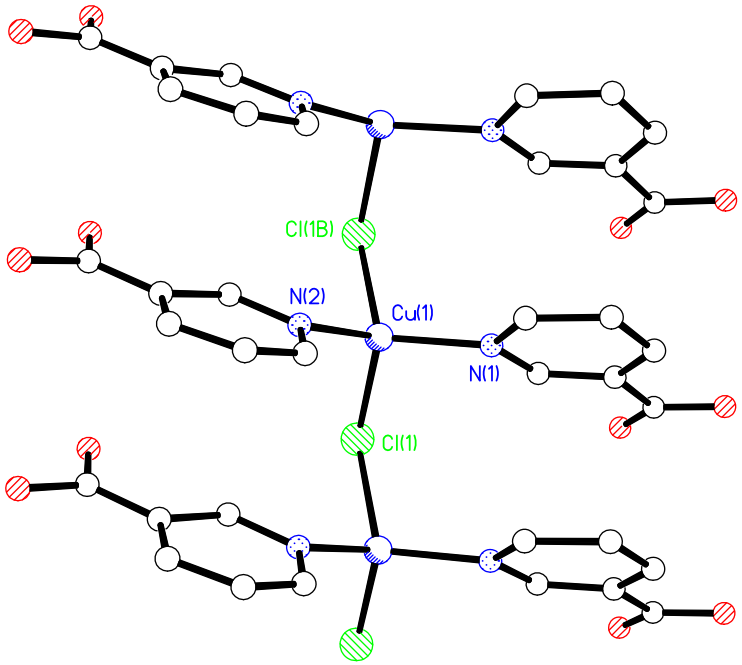

Figure 2.6 Zigzag chain of $Cu(3\text{-}Hpyca)_2Cl$. Hydrogen atoms have been omitted for clarity.

Pyridine-4-carboxylic acid crystallises as a polymeric 1:1 adduct with copper(I) chloride, Cu(4-Hpyca)Cl, (Figure 2.7) with the 4-Hpyca ligand bridging two symmetry-related metal centres forming a ribbon of edge-sharing Cu_2Cl_2 parallelograms propagating along the *b* axis.

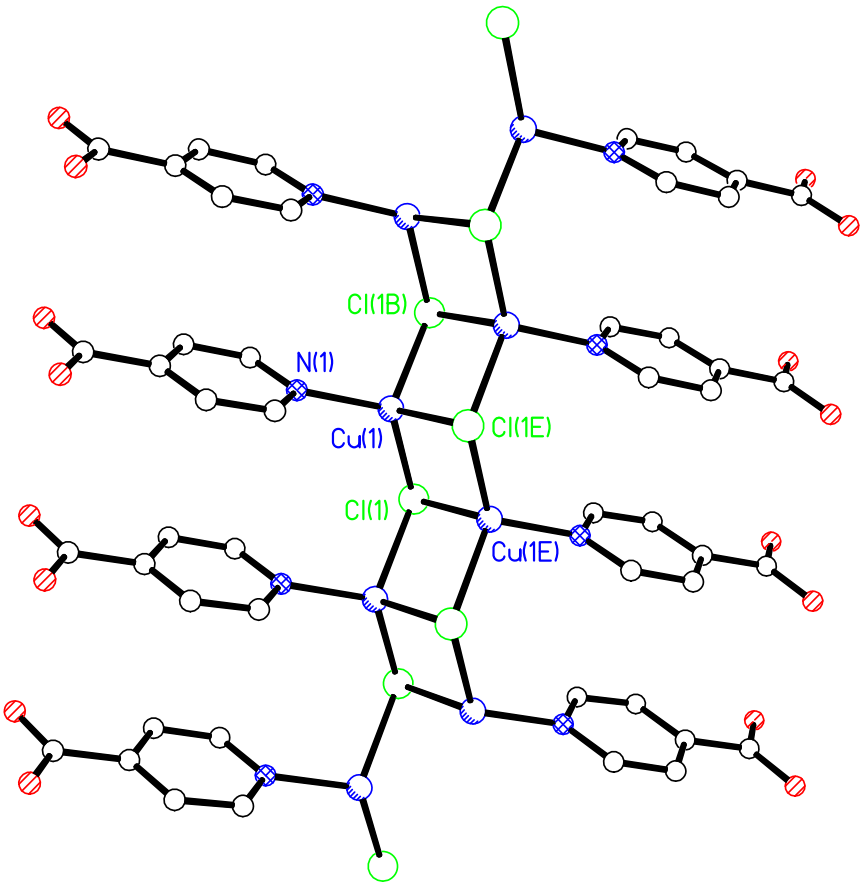

Figure 2.7 View of Cu(4-Hpyca)Cl. Hydrogen atoms have been removed for clarity.

Yu has reported another interesting example of copper(I) halides coordinated to isonicotinic acid forming also a one-dimensional ribbon-like structure.[68] Yu and Goher have used a copper(II) halide as a starting material, but only copper(I) is present at the end of the reaction as Cu(II) halides are reduced to the corresponding Cu(I) derivative in the presence of organic species, particularly compounds containing a pyridine ring.[69-71]

In contrast to the high occurrence of copper complexes with pyridine-3-carboxylic acid in the single crystal X-ray structures contained in the CSD (version 5.30, November 2008), there is very little reported about pyridine-3,*n*-dicarboxylic acids. These ligands possess two potential carboxylic acid coordinating sites, which can each be deprotonated, resulting in a divalent anion, and a third, neutral aromatic nitrogen coordinating site. An example showing this three-connected mode of the $[3,4\text{-pydca}]^{2-}$ has been described by Tong with the synthesis of a three-dimensional coordination polymer $(NMe_4)_{2n}[Cu_3(3,4\text{-pydca})_4(H_2O)_4]_n \cdot 4nH_2O$.[72] The X-ray structure contains two

unique doubly deprotonated [3,4-pydca]$^{2-}$ ligands and two crystallographically independent Cu(II) atoms, one with five-coordinate square bipyramidal geometry and one with six-coordinate octahedral geometry. The five-coordinated Cu(II) centre coordinates to two *trans* carboxylate oxygen atoms and two *trans* pyridyl nitrogen atoms of four [3,4-pydca]$^{2-}$ ligands with a water molecule filling the remaining coordination site. The octahedral Cu(II) ion is coordinated to four carboxylate oxygen atoms and two *trans* water ligands (Figure 2.8). There is extensive hydrogen bonding between the coordinated water ligands and the carboxylate oxygen atoms of the [3,4-pydca]$^{2-}$ ligands which may play a templating role.

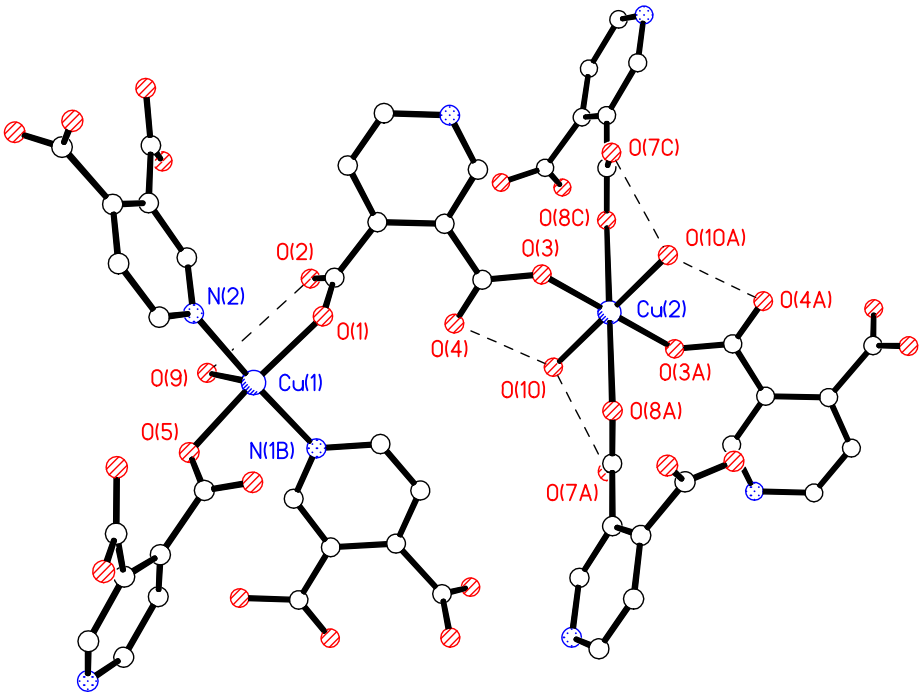

Figure 2.8 View of the coordination geometries around the metal centres in $(NMe_4)_{2n}[Cu_3(3,4\text{-pydca})_4(H_2O)_4]_n{\cdot}4nH_2O$. Hydrogen atoms, NMe_4^+ ions and non coordinated water molecules have been removed for clarity.

One interesting example of the pyridine-3,5-carboxylic acid ligand exhibiting different coordination modes and forming different crystal architectures, under similar conditions, except for pH has been reported by Wang.[73,74] Upon heating a mixture of 3,5-H_2pydca and the Cu(2,2':6',2''-terpyridine) adduct under neutral conditions a one-dimensional framework, **A**, with the Cu(tpy) moieties bridging the [3,5-pydca]$^{2-}$ was

obtained (Figure 2.9). Interestingly, the nitrogen atom in $[3,5\text{-pydca}]^{2-}$ remains uncomplexed affording an additional potential complexation site.

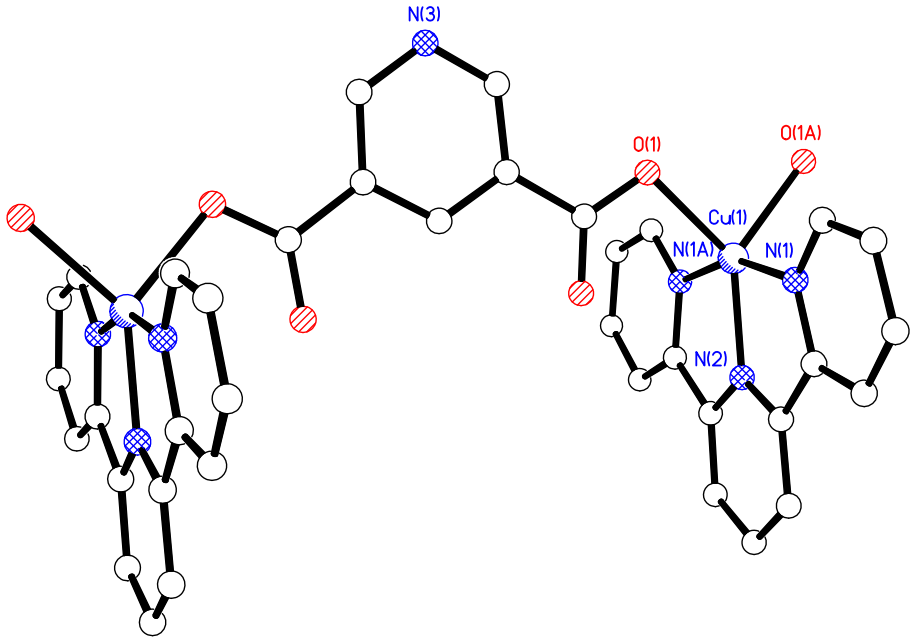

Figure 2.9 View of copper(II) complex **A** obtained under neutral conditions. Hydrogen atoms have been removed for clarity.

In contrast, the treatment of complex **A** with a monovalent metal, $[Cu(MeCN)_4](PF_6)$, in the presence of base afforded a rearranged one-dimensional structure, **B**, where one of the carboxylate moieties is no longer coordinated to a [Cu(tpy)] adduct. The cleaved Cu–O covalent bond was replaced by a new Cu–N bond resulting from the coordination of the [Cu(tpy)] to the pyridine nitrogen (Figure 2.10). Notably, the crystal structure of **B** shows two crystallographically independent [Cu(tpy)] moieties, one coordinated to a carboxylate oxygen atom and a nitrogen atom of two different $[3,5\text{-pydca}]^{2-}$ ligands and one coordinated to a carboxylic oxygen of a $[3,5\text{-pydca}]^{2-}$ ligand and one water molecule.

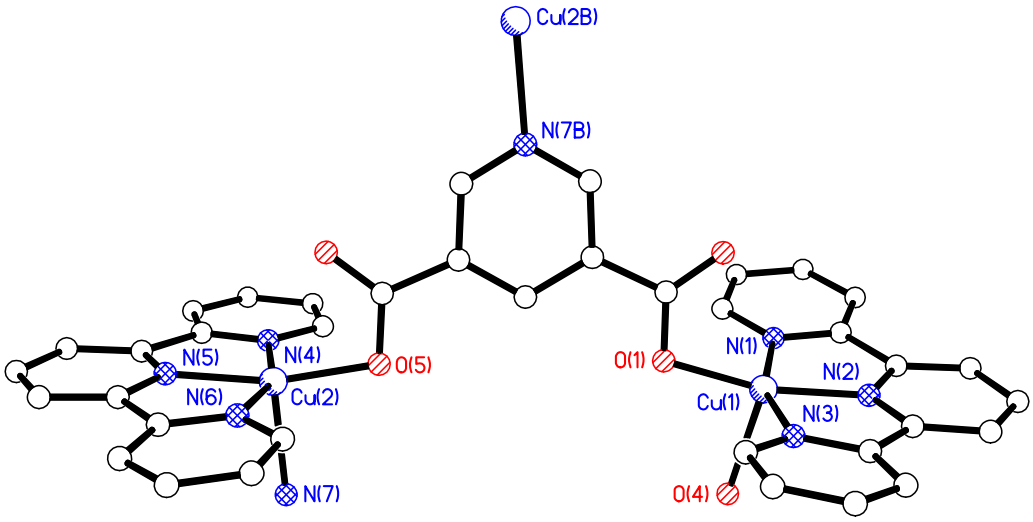

Figure 2.10 View of complex **B** obtained under basic conditions. $[PF_6]^-$ anions and hydrogen atoms have been removed for clarity.

2.2.2 Copper Chemistry of Pyrazine Carboxylic Acids

Pyrazine-2-carboxylic acid is a multidentate ligand which combines the coordination properties of the pyridine-2-carboxylic acid acting as a chelating ligand through the nitrogen atom and the carboxylate group (Figure 2.11).[75] The pyrazine moiety has also an additional nitrogen donor site which can further participate in the assembly of a polymeric structure by an exo-binding mode to another metal centre or by supramolecular interactions with nearby hydrogen-bonding donors (Figure 2.12).[6,76]

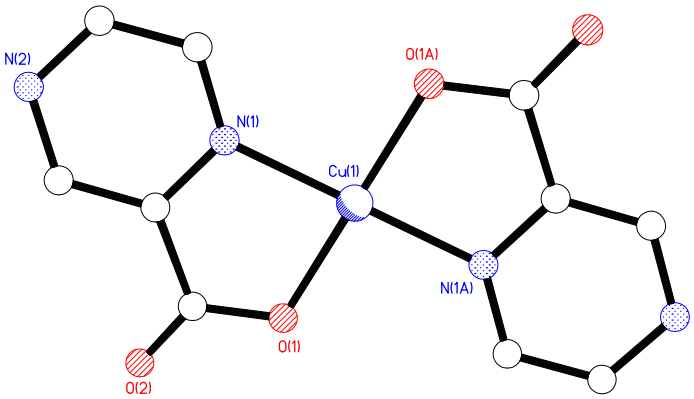

Figure 2.11 An example of the pyrazine-2-carboxylate acting as a chelating ligand - $Cu(2\text{-pzca})_2$.

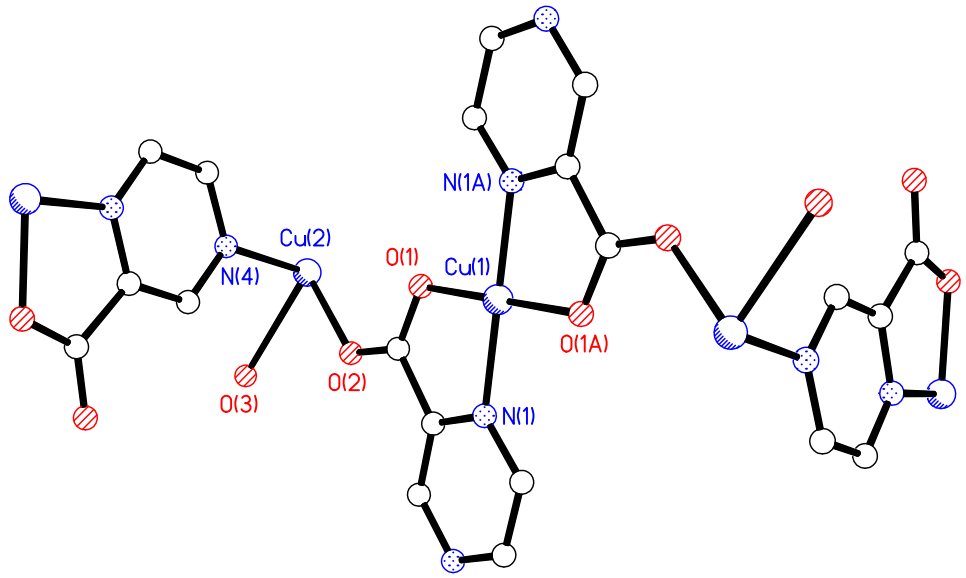

Figure 2.12 Fragment of a copper(II) coordination polymer containing pyrazine-2-carboxylate ligand – $\{Cu_3(2\text{-pzca})_4(H_2O)_2\}$.

Pyrazine-2-carboxylate complexes of copper(II) have been used to construct several novel mixed-metal and mixed-valent coordination polymers.[42,49,77-79] The attractiveness of these complexes as a metal-containing building block for the construction of novel framework materials of varying dimensionality lies in their donor-acceptor versatility. Chelation of the Cu(II) centre by the pyrazine-2-carboxylate ligand leaves a *para*-N-donor and one free carboxylate oxygen available for intermolecular bonding and supramolecular interactions.

Recently, Liu reported a three dimensional Cu(I)/Cu(II) coordination polymer, $\{[Cu^{I}Cu^{II}(2\text{-pzca})_2(N_3)]\}_n$, which was isolated under hydrothermal conditions.[80] The coordination sphere of the copper ions (Figure 2.13) shows each Cu(I) atom situated in a tetrahedral environment coordinated to two azide ligands and two nitrogen atoms from two pyrazine-2-carboxylate ligands. The Cu(II) ion presents an octahedral geometry coordinating to two oxygen atoms and two nitrogen atoms from two chelating pyrazine-2-carboxylate ligands, an azide ligand and a water molecule.

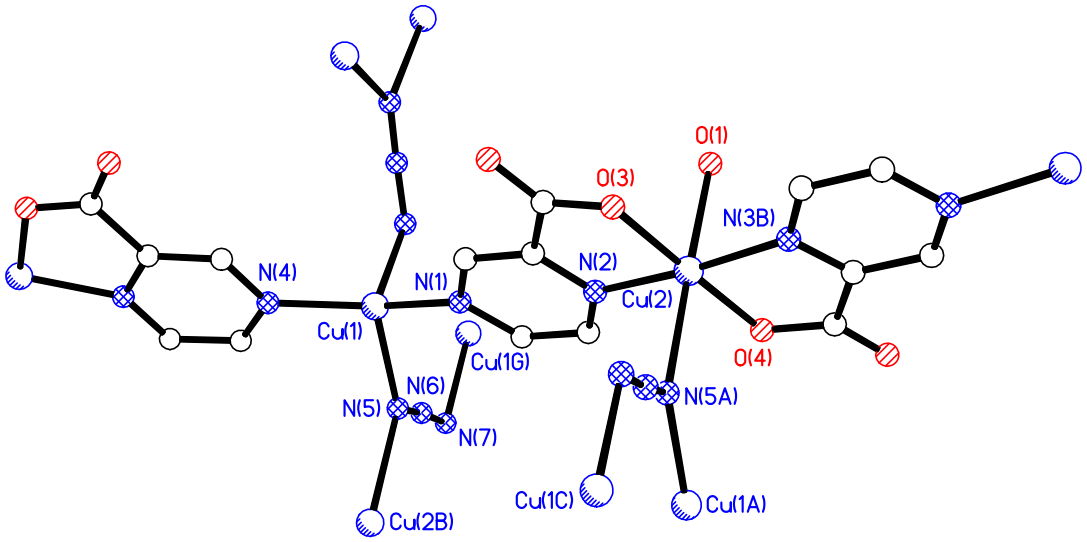

Figure 2.13 View of $\{[Cu^{I}Cu^{II}(2\text{-pzca})_2(N_3)]\}_n$. Hydrogen atoms have been removed for clarity.

In recent years, the synthesis and characterisation of metal coordination polymers based on the pyrazine-2,3-dicarboxylate ligand has evolved rapidly mostly because of two reasons. Firstly, the presence of two carboxylate groups as substituents in the *N*-heterocyclic pyrazine ring allows multiple coordination modes. Secondly, the steric hindrance between these groups (donor O atoms) and the pyrazine ring (donor N atoms), which helps to increase the dimensionality of the assembled covalent networks. Due to these interesting features, a number of coordination modes of the six donor atoms of the 2,3-H_2pzdca ligand have been reported (Figure 2.14).[43,81-92] A brief description of literature examples of copper(II) complexes with pyrazine-2,3-dicarboxylic acid and their different coordination modes are described.

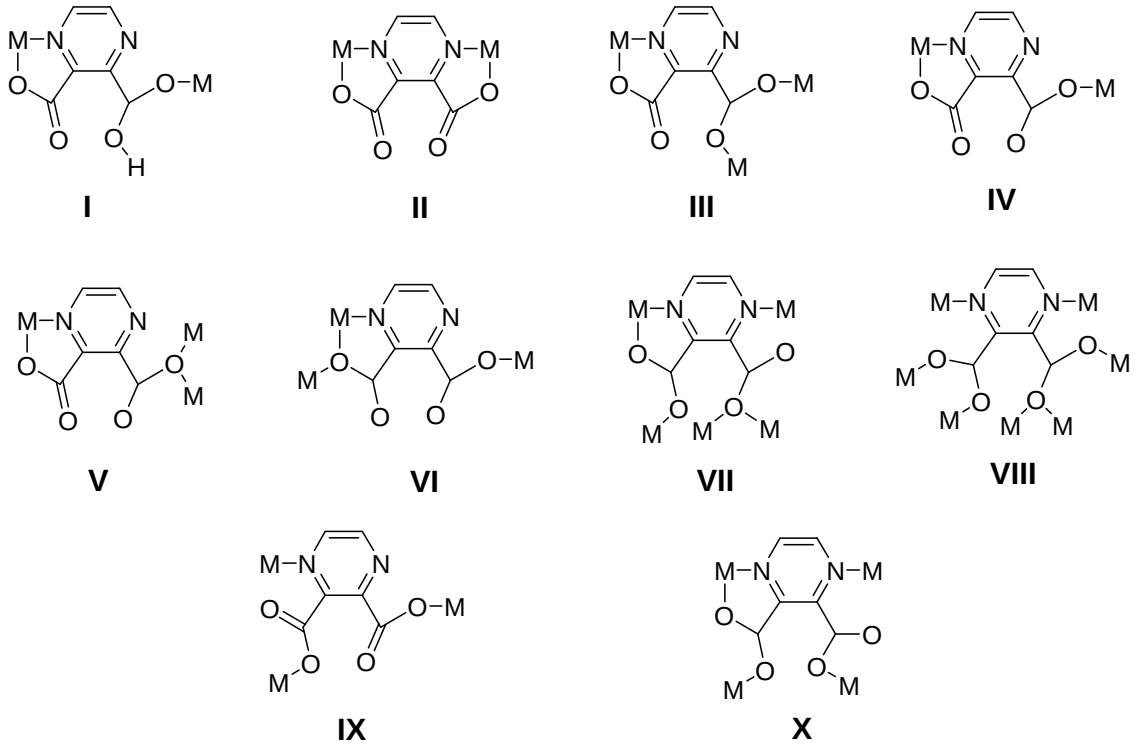

Figure 2.14 Coordination modes of 2,3-H_2pzdca.

Xiang has reported the crystal structure of a copper(II) compound, {[Cu(2,3-Hpzdca)$_2$]·2C_3H_7NO}$_n$, which is a good example of 2,3-H_2pzdca coordination mode type **I**.[92]

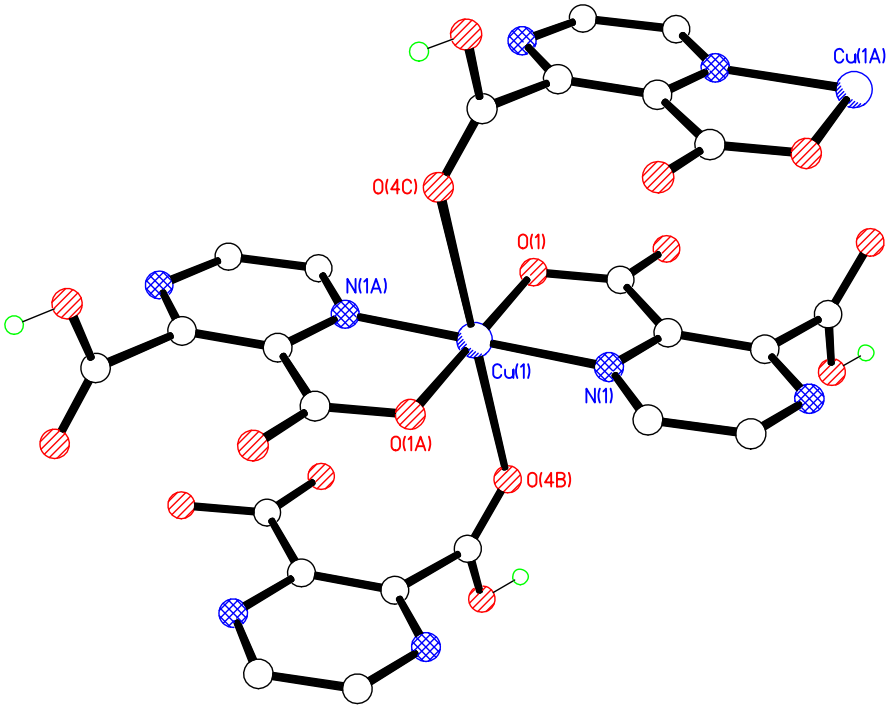

Figure 2.15 View of $\{[Cu(2,3\text{-}Hpzdca)_2]\cdot 2C_3H_7NO\}_n$ showing the type **I** coordination environment of the Cu(II) metal centre. Molecules of DMF and hydrogen atoms on aromatic rings have been removed for clarity.

Konar has described the crystal structure of compound $[Cu(2,3\text{-}Hpzdca)(H_2O)_2]\cdot H_2O$ which shows ligand coordination type **IV**. The copper(II) compound is five-coordinate having two $[2,3\text{-}pzdca]^{2-}$ ligands coordinated to the metal centre through one pyrazinic nitrogen atom and one carboxylate oxygen atom from each ligand. The remaining two coordination sites are occupied by water molecules (Figure 2.16).[93]

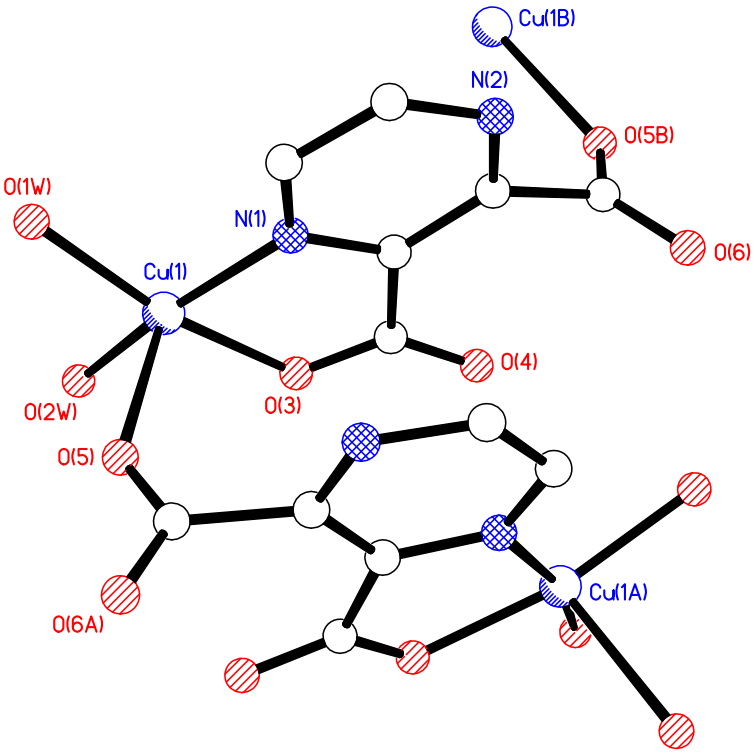

Figure 2.16 View of $[Cu(2,3\text{-}Hpzdca)(H_2O)_2]\cdot H_2O$ showing the type **IV** coordination environment of the Cu(II) metal centre. Hydrogen atoms have been removed for clarity.

The copper(II) complexes with 2,5-H_2pzdca are the least studied of the pyrazine carboxylic acids ligands described in this chapter. In contrast with the 2,3-H_2pzdca, the pyrazine-2,5-dicarboxylate anion does not present steric hindrance, and as a consequence, both carboxylate groups are nearly coplanar with the pyrazine ring.[94,95]

The work of Boabide aimed at investigating the magnetic properties of transition metal complexes based on the 2,5-H_2pzdca ligand, has led to the crystallisation of only three examples of copper(II) complexes with pyrazine-2,5-dicarboxylic acid reported in the CSD (version 5.30, November 2008).[40,41] The two first examples, $\{[Cu(2,5\text{-}pzdca)(NH_3)(H_2O)]\cdot H_2O\}_n$ and $\{[Cu(2,5\text{-}pzdca)(NH_3)_2]\cdot 2H_2O\}_n$, consist of one-dimensional polymeric chains in which metal centres are linked by bidentate [2,5-Hpzdca]$^{2-}$ ligands (Figure 2.17).

The typical Cu(II) octahedral coordination environments in both complexes exhibit some differences. Compound $\{[Cu(2,5\text{-}pzdca)(NH_3)(H_2O)]\cdot H_2O\}_n$ has one [2,5-

Hpzdca]$^{2-}$ ligand and two crystallographically independent copper atoms with centres of symmetry sited on the metals. The apical positions along the chain are occupied by alternate ammonia and water molecules. In contrast, in compound {[Cu(2,5-pzdca)$(NH_3)_2$]·$2H_2O$}$_n$ there is only one [2,5-Hpzdca]$^{2-}$ ligand and one copper(II) ion crystallographically distinguishable and the centres of symmetry are placed on the metal ions and in the centre of the aromatic ring; the ammonia molecule is the unique terminal ligand coordinated to the metal ion.

(a)

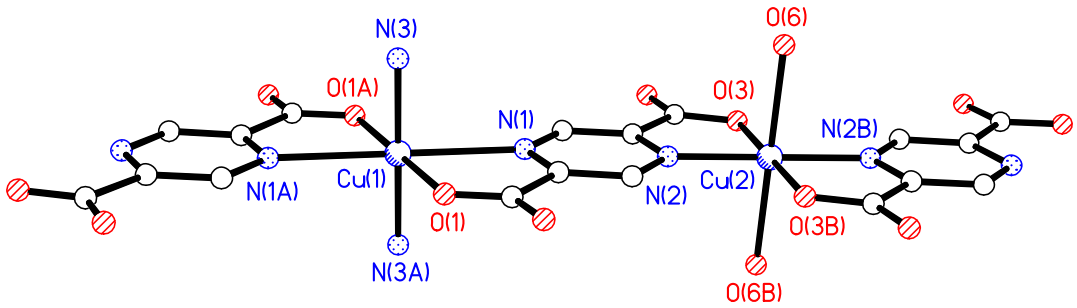

(b)

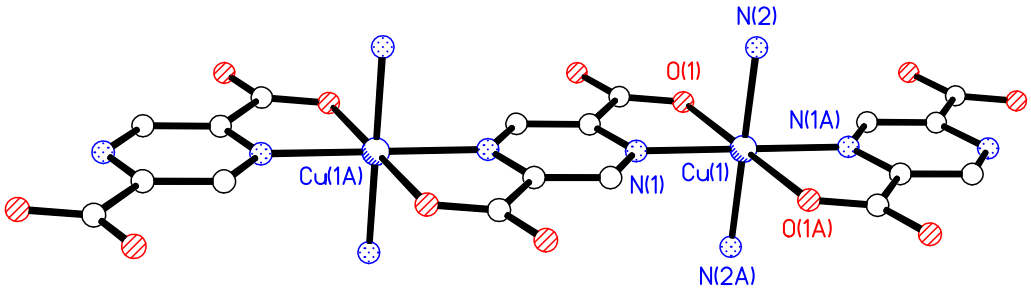

Figure 2.17 View of a fragment of the one-dimensional chain for compounds {[Cu(2,5-pzdca)$(NH_3)(H_2O)$]·H_2O}$_n$ **(a)** and {[Cu(2,5-pzdca)$(NH_3)_2$]·$2H_2O$}$_n$ **(b)**. Hydrogen atoms and water molecules not involved in coordination have been removed for clarity.

The last example of a copper(II) complex with pyrazine-2,5-dicarboxylic acid was synthesised by Boabide, $[Cu_2$(2,5-pzdca)$(phen)_4](NO_3)_2$·$10H_2O$,[40] from a mixture of 2,5-H_2pzdca·$2H_2O$, $Cu(NO_3)_2$·$3H_2O$ and phenanthroline. This complex crystallises as a dimeric structure in which a bidentate [2,5-Hpzdca]$^{2-}$ ligand bridges two copper atoms with a Cu···Cu distance of 7.112 Å. The distorted octahedral environment around each

copper ion is completed by four nitrogen atoms of two phenanthroline ligands (Figure 2.18).

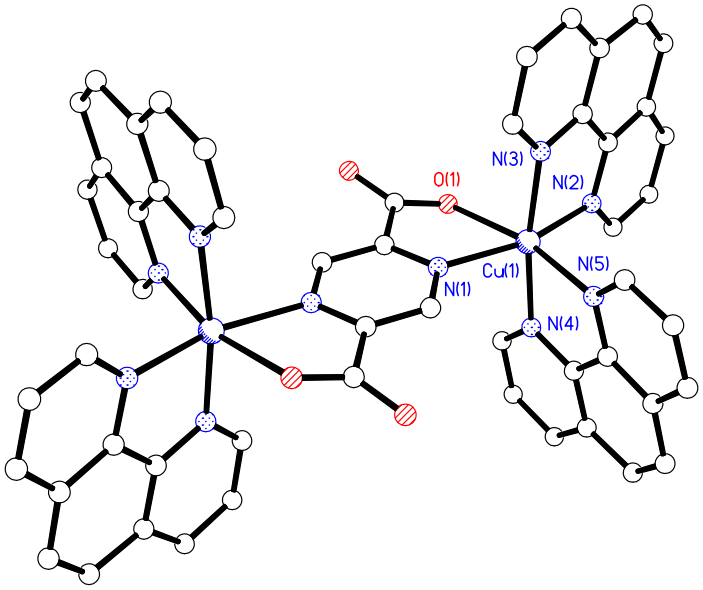

Figure 2.18 View of the dimeric compound $[Cu_2(2,5\text{-pzdca})(phen)_4](NO_3)_2 \cdot 10H_2O$. Hydrogen atoms, nitrate anions and water molecules have been removed for clarity.

The limited examples of single crystal structures of copper(I) complexes with pyridine- and pyrazine-carboxylic acids highlights this area as a suitable target for research. Analysis of the different solvates obtained in this study may allow us to get a better comprehension of the varied hydrogen bonding patterns they can adopt. It is in this area and with these aims that the research in this chapter is presented.

2.3 Results and Discussion

2.3.1 The Complexation of Pyridine Carboxylic Acids to the $[Cu(PPh_3)_2]^+$ Fragment

In preliminary work carried out by Cariati,[50] copper(I) complexes with pyridine- and pyrazine- carboxylic acids were synthesised. This study also reported the two first crystal structure examples of $[Cu(PPh_3)_2]^+$ metal salts of 3-Hpyca and 2,3-H_2pydca collected at room temperature. In Cu(3-pyca)$(PPh_3)_2$, each copper(I) metal centre is coordinated to two molecules of triphenylphosphine and two nicotinate anions, one *via* the pyridinic nitrogen atom and the other through one carboxylate oxygen forming a polymeric zigzag chain (Figure 2.19).

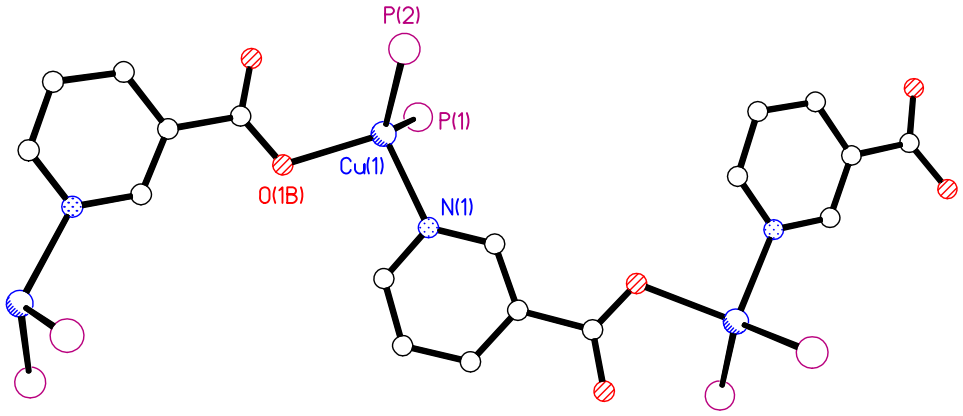

Figure 2.19 Zigzag chain of Cu(3-pyca)$(PPh_3)_2$. Hydrogen atoms and phenyl rings have been removed for clarity.

Compound Cu(2,3-Hpydca)$(PPh_3)_2$, crystallises as a discrete unit in which the copper(I) atom is in a tetrahedral coordination, being bonded to two molecules of triphenylphosphine, chelated to one 2,3-Hpydca anion through the pyridine nitrogen atom and to the carboxylate oxygen atom in the *ortho* position (Figure 2.20).

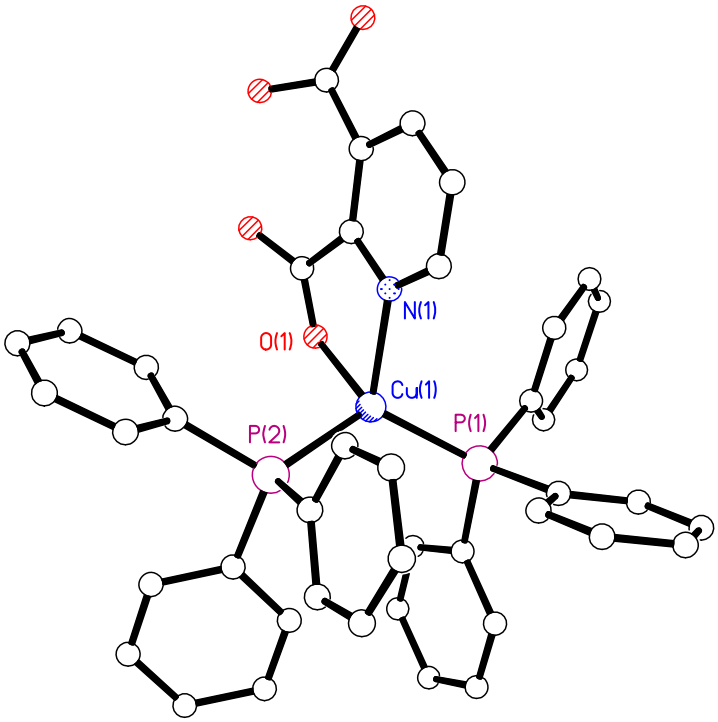

Figure 2.20 Asymmetric unit of Cu(2,3-Hpydca)(PPh_3)$_2$. Hydrogen atoms have been removed for clarity.

Cariati also predicted the crystal structures of the copper(I) complexes with pyridine- and pyrazine-carboxylic acids under study in this chapter, based on infrared spectroscopic evidence:[50] i) From the values of the ν_{as}(COO) and ν_s(COO) stretching vibrations Cariati concluded that compounds shown in Table 2.1 present the same type of coordination, the metal atom is being bonded through the nitrogen atom and one of the oxygen atoms of the carboxylate group. ii) Compounds Cu(2-pyca)(PPh_3)$_2$ and Cu(2-pzca)(PPh_3)$_2$ form monomeric complexes with five-membered chelate rings. iii) Compounds Cu(2,*n*-pydca)(PPh_3)$_2$ (n = 3–6) and Cu(2,3-Hpzdca)(PPh_3)$_2$, show similar values for ν_{as}(COOH) and ν_{as}(COO) as compound Cu(2,3-Hpydca)(PPh_3)$_2$, therefore they probably present the same discrete structure as Cu(2,3-Hpydca)(PPh_3)$_2$ described above. iv) Pyridine carboxylic acids without carboxylic groups in *ortho* position with respect to the nitrogen atom form polymeric molecular structures like compound Cu(3-pyca)(PPh_3)$_2$ also described above. v) Because compounds Cu(2,3-pzdca)(PPh_3)$_2$ and Cu(2,5-pzdca)(PPh_3)$_2$ do not exhibit the ν(COOH) stretching vibrations, the formation of dimeric complexes is expected.

Table 2.1 IR spectral data (cm^{-1}) for Cu(I) complexes synthesised by Cariati.[50]

	ν_{as}(COOH)	ν_{s}(COOH)	ν_{as}(COO)	ν_{s}(COO)	$\Delta\nu$[a]
Cu(2-pyca)$(PPh_3)_2$	-	-	1635	1352	283
Cu(3-pyca)$(PPh_3)_2$	-	-	1605	1392	213
Cu(4-pyca)$(PPh_3)_2$	-	-	1615	1360	255
Cu(2,3-Hpyca)$(PPh_3)_2$	1700	-	1625	1362	263
Cu(2,4-Hpyca)$(PPh_3)_2$	1705	1340	1610	1385	225
Cu(2,5-Hpyca)$(PPh_3)_2$	1705	-	1620	-	-
Cu(2,6-Hpyca)$(PPh_3)_2$	1700	-	1602	1360	242
Cu(3,4-Hpyca)$(PPh_3)_2$	1705	-	1600	1355	245
Cu(3,5-Hpyca)$(PPh_3)_2$	1715	-	1650	1375	275
Cu(2-pzca)$(PPh_3)_2$	-	-	1640	1350	290
Cu(2,3-Hpzca)$(PPh_3)_2$	1735	1350	1625	1375	250
Cu(2,3-pzca)$(PPh_3)_2$	-	-	1625	1350	275
Cu(2,5-pzca)$(PPh_3)_2$	-	-	1640	1355	285

[a] $\Delta\nu = \nu_{as}(COO) - \nu_{s}(COO)$

The work presented below will show the inaccuracy of some of these reported statements, support some of the conclusions and also present interesting versatile behaviour of these complexes depending on the crystallisation solvent.

2.3.2 Synthesis of $(PPh_3)_2Cu(BH_4)$

Using a synthetic method first introduced by Cariati and Naldini,[96] and later adapted by Lippard and Ucko,[97] the reduction of copper(II) sulfate hexahydrate with sodium borohydride in the presence of triphenylphosphine in warm ethanol affords the copper(I) compound, $(PPh_3)_2Cu(BH_4)$, in 82% yield (Equation 2.1).

$$CuSO_4 \cdot 6H_2O \xrightarrow[\text{ii) } NaBH_4]{\text{i) } PPh_3,\ EtOH} Cu(PPh_3)_2(BH_4)$$

Equation 2.1

The solid-state structure of $(PPh_3)_2Cu(BH_4)$ has been previously determined by X-ray diffraction showing how the borohydride group is bonded to the copper(I) ion through two hydrogen atoms giving a distorted tetrahedral geometry at Cu(I) with two triphenylphosphine phosphorus atoms occupying the remaining two sites (Figure 2.21).[98,99]

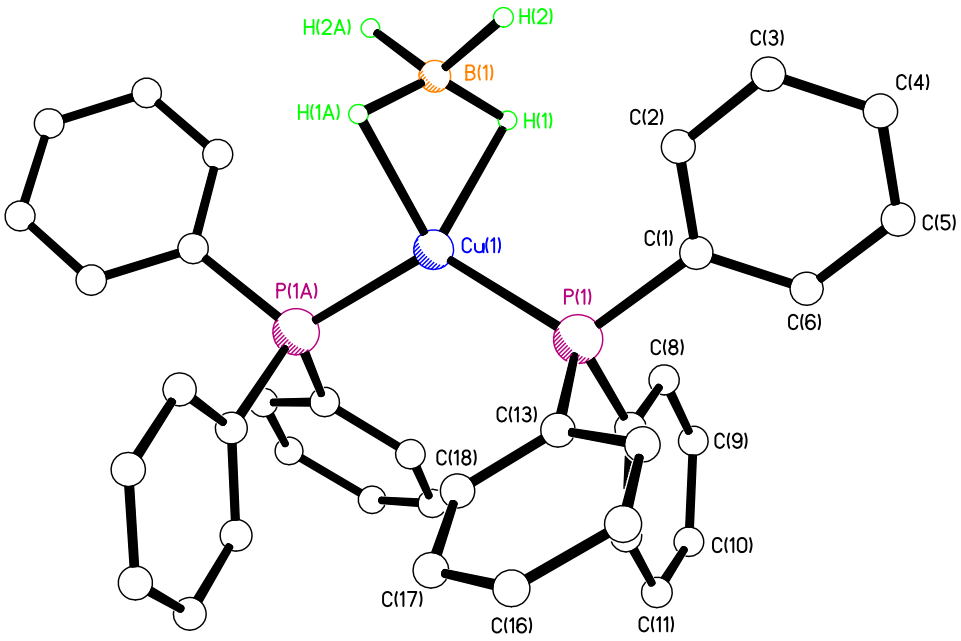

Figure 2.21 View of the asymmetric unit of $(PPh_3)_2Cu(BH_4)$.

The copper(I) complex, $(PPh_3)_2Cu(BH_4)$, is easy to synthesise cleanly in high yield and is soluble in many organic solvents. The evolution of its coordination reactions with suitable organic ligands can be easily followed using ^{31}P NMR. Therefore, $(PPh_3)_2Cu(BH_4)$ is a good choice as starting material for the further complexation studies with pyridine- and pyrazine-carboxylic acids as a potential building blocks to make polymeric species or units able to link *via* hydrogen bonds or other weak interactions.

2.3.3 Crystallisation of Cu(*n*-pyca)$(PPh_3)_2$ Complexes (*n* = 2–4)

Initially, the complexation of the pyridine- monocarboxylic acids *n*-Hpyca (*n* = 2–4) to the $[Cu(PPh_3)_2]^+$ fragment was attempted stirring the mixture in dichloromethane at

room temperature over 12 h (Equation 2.2).[50] The products, Cu(2-pyca)$(PPh_3)_2$, Cu(3-pyca)$(PPh_3)_2$ and Cu(4-pyca)$(PPh_3)_2$, were easy to isolate as yellow precipitates in excellent yield, 83-89%, by adding diethyl ether. Later, the same reactions were carried out under reflux (assumed to ensure the complete displacement of the $[BH_4]^-$ unit by the pyridine-*n*-carboxylic acid), resulting in the same high yield of precipitate, but with considerably shorter reaction times (within 3 h).

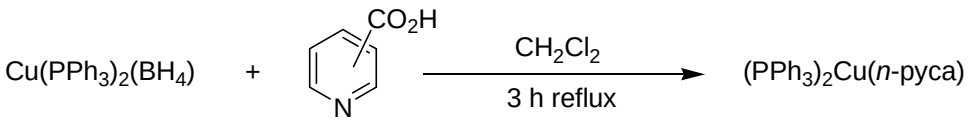

Equation 2.2

Most relevant infrared spectroscopic data for compounds Cu(2-pyca)$(PPh_3)_2$, Cu(3-pyca)$(PPh_3)_2$ and Cu(4-pyca)$(PPh_3)_2$, are presented in Table 2.2. The difference between the asymmetric and symmetric stretch, $\Delta\nu$, gives information on the carboxylate bonding mode in the complexes obtained. All the compounds show the strong carboxylate stretching frequencies $\nu_{as}(COO)$ and $\nu_s(COO)$ in the characteristic range of copper carboxylate compounds in agreement with the data reported by Cariati.[50,100,101] The $\Delta\nu$ separation values of $\nu(COO^-)$ bands indicates that the coordination of the carboxylate group is monodentate.[102]

Table 2.2 IR spectral data (cm^{-1}) for $(PPh_3)_2Cu(I)$ complexes of 2-Hpyca, 3-Hpyca and 4-Hpyca ligands

	$\nu(COO)_{as}$	**$\nu(COO)_s$**	**$\Delta\nu$**
Cu(2-pyca)$(PPh_3)_2$	1635	1352	283
Cu(3-pyca)$(PPh_3)_2$	1606	1383	223
Cu(4-pyca)$(PPh_3)_2$	1612	1368	244

2.3.3.1 Solvates of Cu(2-pyca)$(PPh_3)_2$

The first aim of this research was to obtain the crystal structures of these copper(I) pyridine monocarboxylic acids predicted by Cariati.[50] Interestingly, in preliminary work carried out by Helena Ascroft and Agnese Cecchin, the structures of Cu(2-

pyca)(PPh_3)$_2$·2MeOH **2.1**, Cu(2-pyca)(PPh_3)$_2$·EtOH **2.2** and Cu(2-pyca)(PPh_3)$_2$·*i*-PrOH **2.3** were determined. These studies revealed a solvent dependency with regards to the crystallisation conditions.

Compound Cu(2-pyca)(PPh_3)$_2$·2MeOH **2.1** was crystallised from a solution containing MeOH, including two solvent molecules per complex in the structure (Figure 2.22). The carboxylate oxygen is hydrogen bonded to two molecules of MeOH through two strong (solvent)O–H···O(carboxylate) hydrogen bonds (Table 2.3).

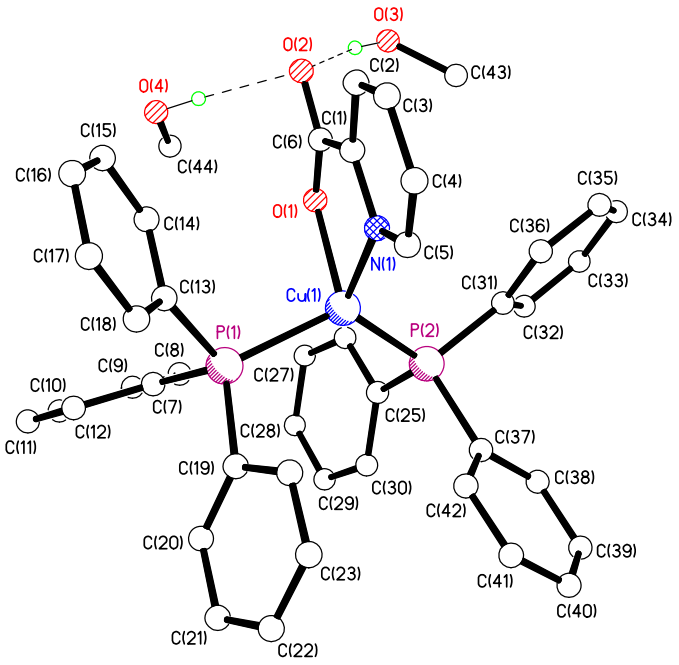

Figure 2.22 Asymmetric unit of Cu(2-pyca)(PPh_3)$_2$·2MeOH **2.1**. Hydrogen atoms not involved in hydrogen bonding have been omitted for clarity.

Table 2.3 Selected hydrogen bonding parameters for **2.1**.

D–H···A	D···A/Å	D–H/Å	H···A/Å	D–H···A/°
O(4)–H(4)···O(2)	2.875(3)	0.84	2.04	174
O(3)–H(3)···O(2)	2.748(2)	0.84	1.93	163

While the crystallisation of Cu(2-pyca)(PPh_3)$_2$ in the presence of MeOH occurs in a 1:2 stoichiometry, the inclusion of the next homologues in the alcohols series, EtOH, *n*-PrOH and *i*-PrOH, into the crystal structure of Cu(2-pyca)(PPh_3)$_2$ occurs in a 1:1

stoichiometry. The solvates Cu(2-pyca)(PPh_3)$_2$·X, where X = EtOH (**2.2**), *n*-PrOH (**2.3**) or *i*-PrOH (**2.4**) present two independent molecules of Cu(2-pyca)(PPh_3)$_2$·X in the asymmetric unit, which differ in the disposition of the phenyl rings. Interestingly, while the solvent molecules in compounds **2.2** and **2.4** present a similar relative position with respect to the Cu(2-pyca)(PPh_3)$_2$ complex [Figure 2.23 (**a**)], in **2.3** the two independent molecules also differ in the position of the solvent molecule with respect to the copper(I) complex [Figure 2.23 (**b**)].

(a)

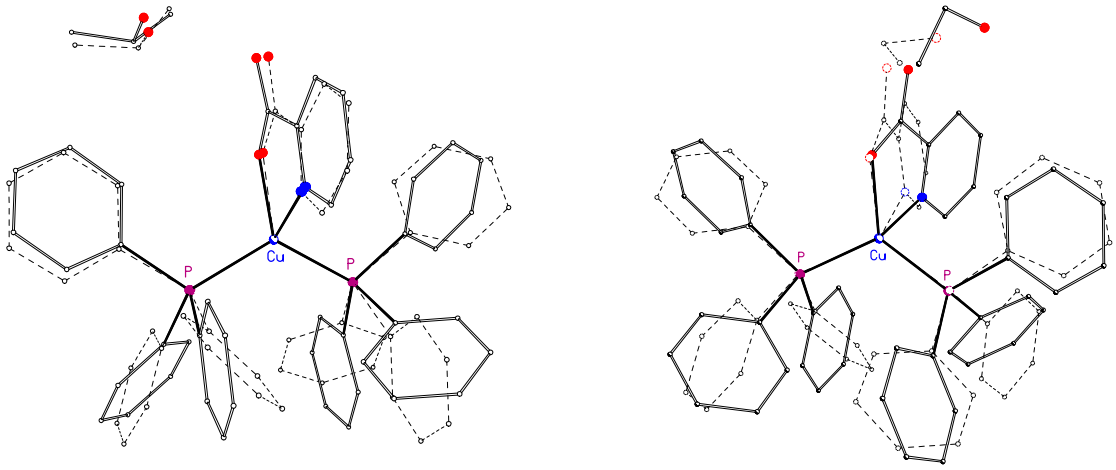

(b)

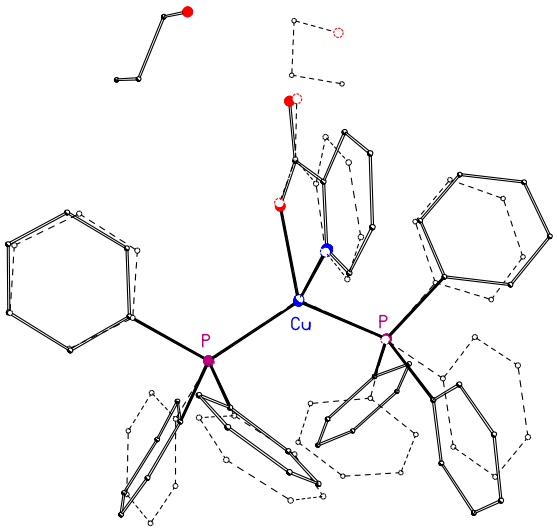

Figure 2.23 Overlay view of the two independent solvate pairs in **(a)** Cu(2-pyca)(PPh_3)$_2$·EtOH **2.2** (left) and Cu(2-pyca)(PPh_3)$_2$·*i*-PrOH **2.4** (right). **(b)** Cu(2-pyca)(PPh_3)$_2$·*n*-PrOH **2.3**, solvent disorder components have been omitted for clarity. Hydrogen atoms have been omitted for clarity.

Compounds **2.2**-**2.4** crystallise showing a similar (solvent)O–H···O(carboxylate) interaction as seen for compound **2.1** (Table 2.4). Solvate Cu(2-pyca)(PPh_3)$_2$·*i*-PrOH **2.4** contains an almost identical hydrogen bonding pattern to that seen in compounds **2.2** and **2.3**, except that the hydrogen bond (solvent)O–H···O(carboxylate)is slightly longer than those observed in **2.2** and **2.3**, presumably due to the inclusion of the bulkier, branched alcohol, *i*-PrOH.

Table 2.4 Selected hydrogen bonding parameters for **2.2**-**24**.

	D–H···A	**D···A/Å**	**D–H/Å**	**H···A/Å**	**D–H···A/º**
2.2	**O(5)–H(5)···O(2)**	2.704(3)	0.884(19)	1.83(2)	172(5)
	O(6)–H(6)···O(4)	2.706(3)	0.816(19)	1.891(19)	176(4)
2.3	**O(5)–H(5)···O(2)**	2.734(4)	0.84	1.93	159.3
	O(6)–H(6)···O(4)	2.689(4)	0.90(7)	1.80(7)	169(7)
2.4	**O(5)–H(5)···O(2)**	2.759(2)	0.79(3)	1.98(3)	171(3)
	O(6)–H(6)···O(4)	2.7694(19)	0.79(3)	1.99(3)	169(3)

The use of Platon to analyse the solvent accessible voids within the "solvent-free" structures of **2.2**-**2.4** allows the calculation of the percentage volume of each structure accessible to the relevant solvents (Table 2.5).[103] Compounds **2.1**-**2.4** have a clear correlation in their solvent accessible volume showing an increment with the increasing alcohol size. Interestingly, the effect is more pronounced in **2.2** (EtOH) and **2.3** (*n*-PrOH) than the one observed in **2.4** (*i*-PrOH) for a more bulky alcohol. The 1:1 alcohol solvate **2.3** (*n*-PrOH) shows a 2.3% expansion of the unit cell volume with respect to solvate **2.2** (EtOH) in order to accommodate a larger solvent. Although *i*-PrOH is a more sterically demanding branched alcohol this effect is less pronounced in **2.4** (*i*-PrOH).

Table 2.5 Comparison of unit cell dimensions of **2.1**-**2.4** Cu(2-pyca)(PPh_3)$_2$·*n*Solvent.

	2.1	**2.2**	**2.3**	**2.4**
n Solvent	2MeOH	EtOH	*n*-PrOH	*i*-PrOH
a/Å	12.8237(5)	13.9684(7)	14.5287(15)	11.1667(7)
b/Å	15.7911(6)	15.2341(7)	15.3652(16)	17.5876(11)
c/Å	19.2068(7)	18.4128(9)	18.4940(19)	20.1282(12)
α/°	90	74.777(2)	78.366(2)	82.333(2)
β/°	97.398(2)	82.880(2)	70.820(2)	86.315(2)
γ/°	90	82.744(2)	87.215(2)	77.497(2)
Space Group	$P2_1/c$	$P\bar{1}$	$P\bar{1}$	$P\bar{1}$
Solvent accessible volume[a]/Å^3	238.5	398.4	477.6	481.3
Cell volume/Å^3	3857.0(3)	3733.5(3)	3818.6(7)	3822.3(4)
Cell volume increase %[b]	-	-	2.3	2.4

[a]For each molecule of solvent.

[b]Volume increase as a percentage compared to **2.2**.

Attempts to include the larger alcohols *tert*-butanol or *n*-butanol into the structure of Cu(2-pyca)(PPh_3)$_2$, using similar crystallisation conditions to those used in the formation of **2.1**-**2.4**, failed to produce a solvate, instead crystallising the monomeric solvent-free structure, Cu(2-pyca)(PPh_3)$_2$ **2.5** (Figure 2.24). Compound **2.5** lies on a mirror plane, resulting in the asymmetric unit comprising half of a molecule.

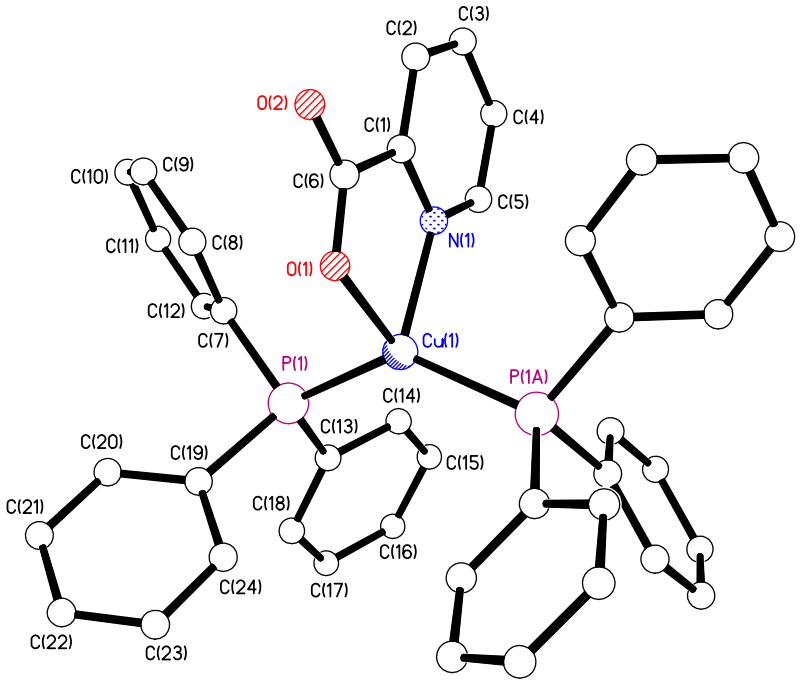

Figure 2.24 View of Cu(2-pyca)$(PPh_3)_2$ **2.5**. Hydrogen atoms have been omitted for clarity.

Weak C–H···O hydrogen bonds, [where H···O distances are 2.58 Å], maintain the packing of **2.5** forming one-dimensional chains by $R^1_2(12)$ motifs along the crystallographic *b* axis (Figure 2.25).

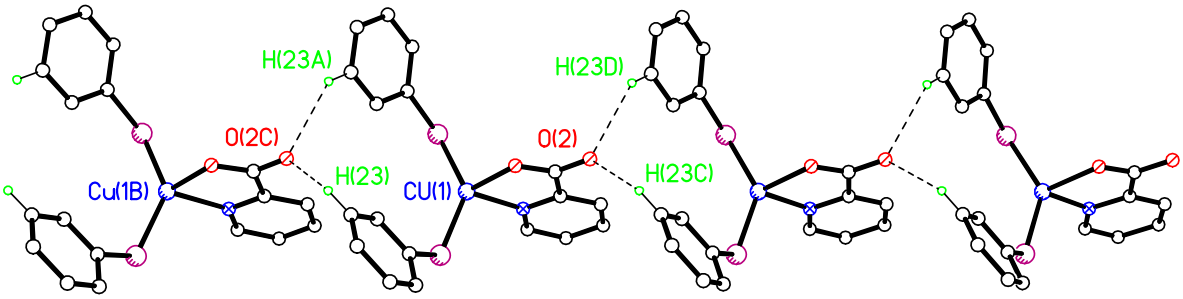

Figure 2.25 View of the hydrogen bonded chain formed by **2.5**. Most phenyl groups and hydrogen atoms not involved in hydrogen bonding have been removed for clarity.

2.3.3.2 Solvates of Cu(3-pyca)$(PPh_3)_2$

Cariati has reported the solvent-free crystal structure of Cu(3-pyca)$(PPh_3)_2$ **2.6**,[50] but there is no previous literature evidence of this compound forming solvates. Because compound Cu(3-pyca)$(PPh_3)_2$ shows excellent solubility in the same range of alcohols previously used with the Cu(2-pyca)$(PPh_3)_2$ system, the potential formation of solvates Cu(3-pyca)$(PPh_3)_2$·X, where X = MeOH, EtOH, *n*-PrOH, *i*-PrOH, *n*-BuOH and *tert*-BuOH has also been investigated.

The slow evaporation of a solution of Cu(3-pyca)$(PPh_3)_2$ in methanol leads to the formation of colourless plates Cu(3-pyca)$(PPh_3)_2$·MeOH **2.7**. The copper(I) centre is coordinated to two symmetry related [3-pyca]$^-$ ligands through one pyridinic nitrogen atom and one carboxylate oxygen atom from each ligand forming one-dimensional zigzag chains which propagate in the [1 1 0] direction (Figure 2.26). The MeOH molecule is hydrogen bonded alternately on either side of the chain to the second caboxylate oxygen forming a similar (solvent)O–H···O(carboxylate) interaction as seen previously for compounds **2.1**-**2.4** (Table 2.6).

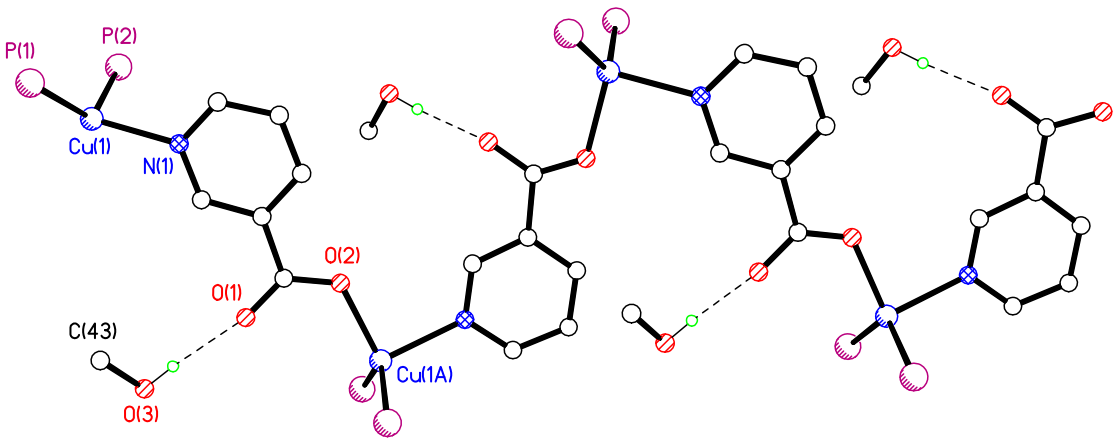

Figure 2.26 Zigzag chains of Cu(3-pyca)$(PPh_3)_2$·MeOH **2.7** propagating in the [110] direction. Phenyl rings and hydrogen atoms not involved in hydrogen bonding have been omitted for clarity.

Table 2.6 Selected hydrogen bonding parameters for **2.7**.

D–H···A	D···A/Å	D–H/Å	H···A/Å	D–H···A/°
O(3)–H(3)···O(1)	2.720(3)	0.78(4)	1.94(4)	173(4)

The crystallisation of Cu(3-pyca)$(PPh_3)_2$ from an ethanolic solution by Agnese Cecchin resulted in the solvate, Cu_2(3-pyca)$_2(PPh_3)_4$·2EtOH **2.8**, which is dimeric (Figure 2.27). The two symmetry-related copper ions are linked by two bridging [3-pyca]$^-$ ligands through the pyridinic nitrogen atom and one carboxylate oxygen atom on each ligand, forming a twelve-membered ring with a distance of 6.909 Å between symmetry-related metal centres. The unique ethanol molecule is hydrogen bonded to the carboxylate oxygen, O(2), *via* one strong (solvent)O–H···O(carboxylate) hydrogen bond (Table 2.7).

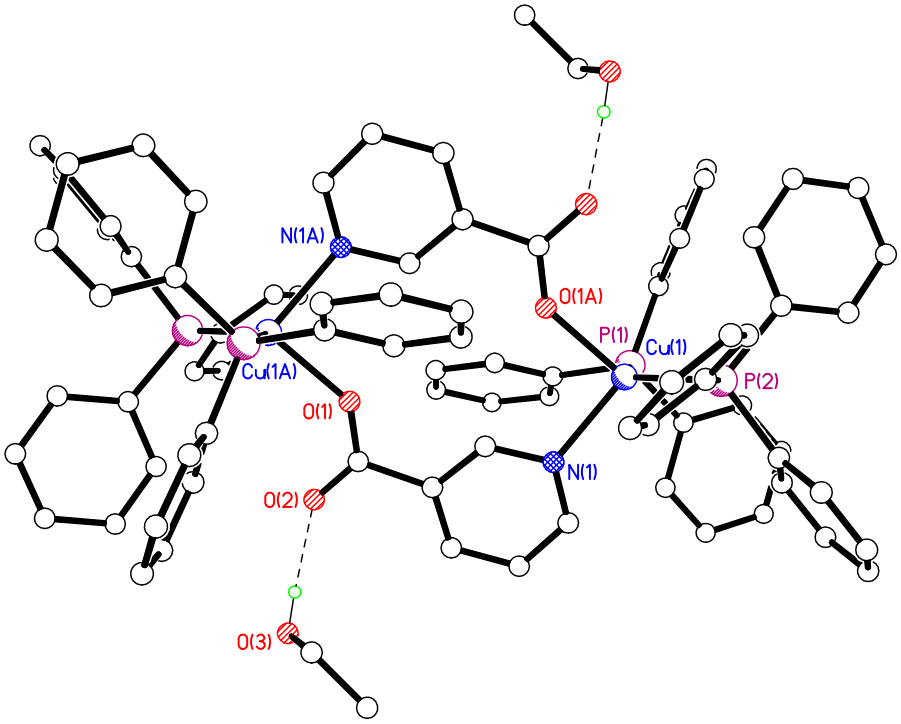

Figure 2.27 The dimeric structure of Cu_2(3-pyca)$_2(PPh_3)_4$·2EtOH **2.8**. Hydrogen atoms not involved in hydrogen bonding have been removed for clarity.

Table 2.7 Selected hydrogen bonding parameters for **2.8**.

D–H···A	D···A/Å	D–H/Å	H···A/Å	D–H···A/°
O(3)–H(3)···O(2)	2.674(3)	0.81(4)	1.86(4)	177(4)

The coordination geometry at the nitrogen atom is highly strained, the angle at nitrogen between the ring centroid of the pyridinic ring and the copper atom is 24.7° away from the expected linear geometry (Figure 2.28). The distortion is required to prevent unfavourable steric interactions between H(1) and H(1A), which are left on different planes. Analysis of the Cu–N bond lengths in compounds **2.7** and **2.8** shows similar values, 2.1261(19) Å and 2.154(2) Å respectively.

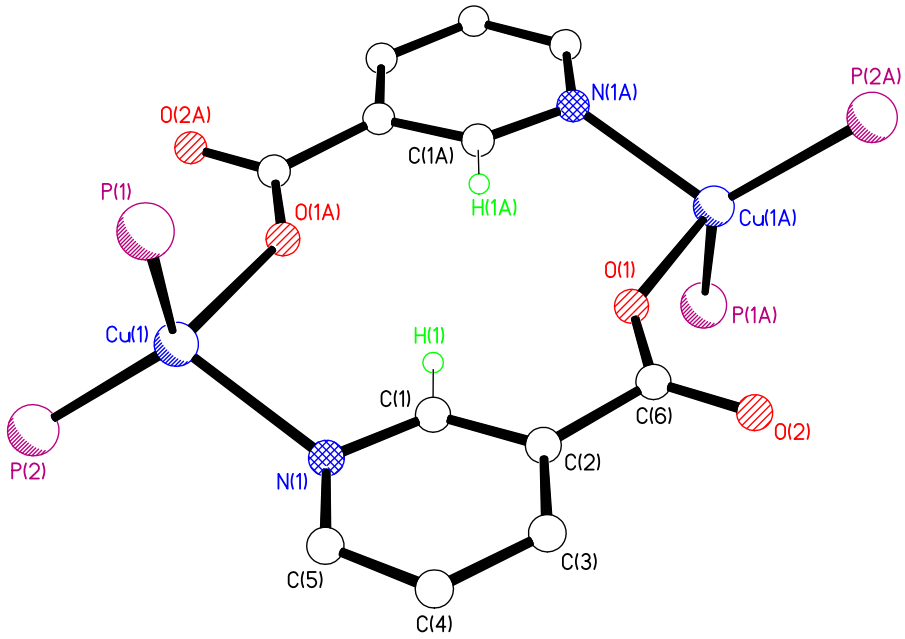

Figure 2.28 View of **2.8** showing the strained angles in the coordination geometry at the nitrogen atoms. Phenyl groups and hydrogen atoms apart from H(1) and H(1A) have been omitted for clarity.

Although the solvent-free Cu(3-pyca)(PPh_3)$_2$ is known to pack in the crystalline state in one-dimensional chains,[50] in the presence of EtOH, the formation of the chains is prevented and **2.8** packs as a zero-dimensional dimer; behaviour that was not predicted by Cariati.

$Cu(3\text{-pyca})_2(PPh_3)_2$ was originally crystallised by Cariati and co-workers from dichloromethane, and the structure determined at room temperature.[50] In this study complex $Cu(3\text{-pyca})_2(PPh_3)_2$ **2.6**, has been isolated from a range of different alcohols such as, *n*-PrOH, *i*-PrOH, *n*-BuOH and *tert*-BuOH and the structure re-determined using low-temperature single crystal X-ray diffraction (Figure 2.29). The same structure is found in each case, ruling out larger solvents being incorporated in this system. The re-determination at low temperature (150 K) gives a big improvement in the final *R* value (2.3% compared to 4.1%), with reductions of 0.6, 0.6 and 0.4% in the *a*, *b* and *c* unit cell dimensions, resulting in an overall 1.6% contraction in the unit cell volume compared to that determined at room temperature.

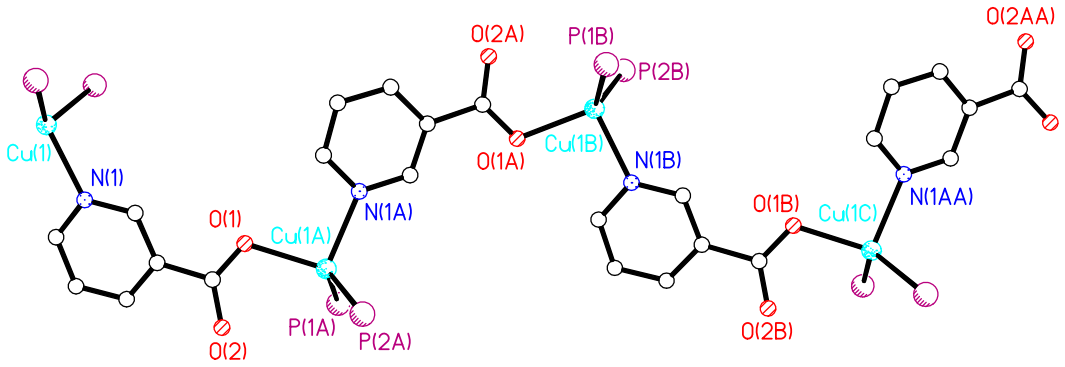

Figure 2.29 $Cu(3\text{-pyca})(PPh_3)_2$ **2.6**. Phenyl groups and hydrogen atoms have been omitted for clarity.

Attempts to include larger alcohols such as, *n*-PrOH, *i*-PrOH into the structure of $Cu(3\text{-pyca})(PPh_3)_2$ as seen previously for structures **2.3** and **2.4** failed to yield solvates, instead crystallising as the solvent-free structure **2.6**.

2.3.3.3 Solvates of $Cu(4\text{-pyca})(PPh_3)_2$

Inspired by the success of the $Cu(2\text{-pyca})(PPh_3)_2$ and $Cu(3\text{-pyca})(PPh_3)_2$ analogues, crystallisation of $Cu(4\text{-pyca})(PPh_3)_2$ was attempted using the same alcohols as above. Due to the low solubility of $Cu(4\text{-pyca})(PPh_3)_2$ **2.9** in almost all alcohols, the crystallisation of **2.9** was only possible from methanol.

The Cu(4-pyca)$(PPh_3)_2$ complex was crystallised by Agnese Cecchin, and structurally characterised by the author of this thesis, from a solution of methanol, including three molecules of solvent (methanol and water) per complex in the structure. The asymmetric unit comprises $[Cu(PPh_3)_2$4-py(COO)$]_2 \cdot 2MeOH \cdot 0.765(4)MeOH \cdot 0.235(4)H_2O$ **2.9** (Figure 2.30). In Figure 2.30, only the version of the structure with three molecules of methanol is shown. The disorder in methanol and water solvent molecules involved only one of the possible three molecules present in the structure, actually molecules C(87)–O(7)–H(7A) and C(85)–O(5)–H(5) are not disordered. Molecule C(86)–O(6)–H(6) was modelled over two sets of positions [part MeOH/part water] in the ratio 76.5(4):23.5(4)%. Selected hydrogen bonding parameters for **2.9** are shown in Table 2.8.

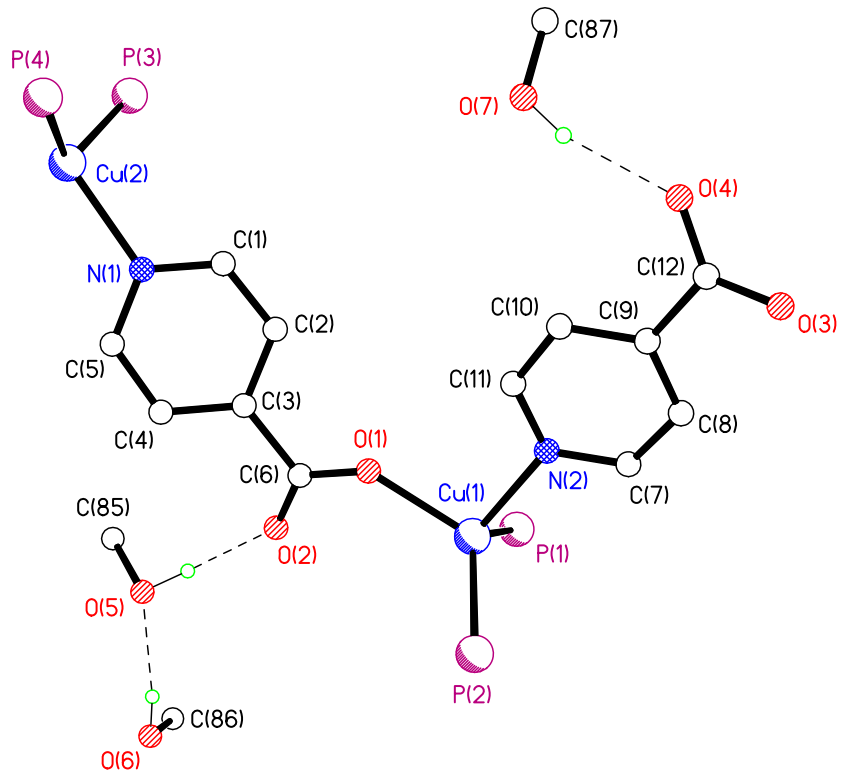

Figure 2.30 View of the asymmetric unit of solvate **2.9**. Water molecule, phenyl groups and hydrogen atoms not involved in hydrogen bonding have been removed for clarity.

Table 2.8 Selected hydrogen bonding parameters for **2.9**.

D–H···A	D···A/Å	D–H/Å	H···A/Å	D–H···A/º
O(5)–H(5)···O(2)	2.725(3)	0.92(5)	1.80(5)	178(5)
O(6)–H(6)···O(5)	2.827(5)	0.84	2.00	168
O(7)–H(7A)···O(4)	2.810(3)	0.84	1.99	164

The structure of **2.9** is polymeric, as Cariati predicted, with one-dimensional zigzag chains running parallel to the *a* direction. Neighbouring chains interlock *via* their phenyl groups to form pseudo-sheets in the *ac* plane through weak C–H···O hydrogen bonds [2.53 Å]. These sheets form layers stacked on top of each other in the *b* orientation (Figure 2.31).

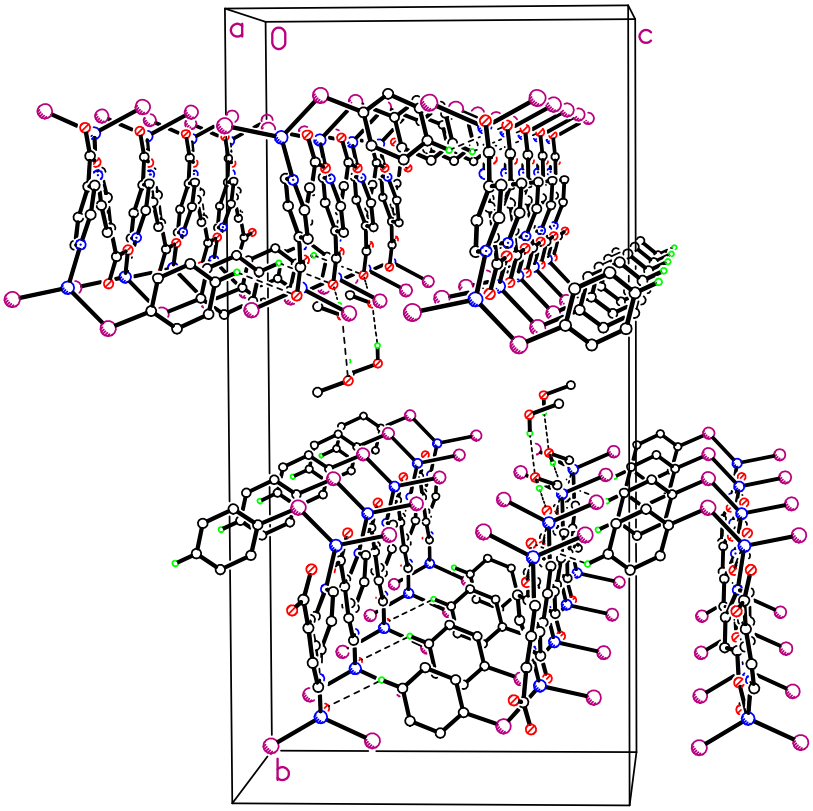

Figure 2.31 Packing plot of compound **2.9**, viewed along the crystallographic *c* axis. Water molecules, phenyl groups and hydrogen atoms not involved in hydrogen bonding have been omitted for clarity.

2.3.3.4 Discussion of the General Structural Features of Complexes 2.1-2.9

There is little variation in the P–Cu, O–Cu and N–Cu bond lengths in complexes **2.2-2.9** (Table 2.9) and they are consistent with the values reported for other copper(I) complexes.[104,105] The P–Cu–P bond angles are similar to reported values for other *bis*(triphenylphosphine)copper(I) compounds.[106-109] In all complexes obtained, the copper(I) ion is in a distorted tetrahedral environment. The chelated O–Cu–N bite angle (79.77-80.16°) is the origin of this distortion. The geometry of complexes **2.2-2.5** are in general agreement with the mean values collected from the CSD survey, (Version 5.30, November 2008 plus 4 updates), the O–Cu–N bond angle values are similar to those reported for other examples of five-membered chelate C–O–Cu–N–C systems (83.50-76.23º).[110-113]

Complexes **2.2-2.5** and **2.6** show a large difference between the P–Cu–P bond angles, (9.9-13.7º), (Table 2.9). A possible reason for this difference could be: in complex **2.6**, there are two sets of possible H···H repulsive interactions on the phenyl rings from the triphenylphosphine molecules, causing additional opening of the P–Cu–P, while in complexes **2.2-2.5** there are two sets of weak edge to face C–H···π attractive phenyl-phenyl interactions (Table 2.10) contracting the angle to a smaller value (Figure 2.32).

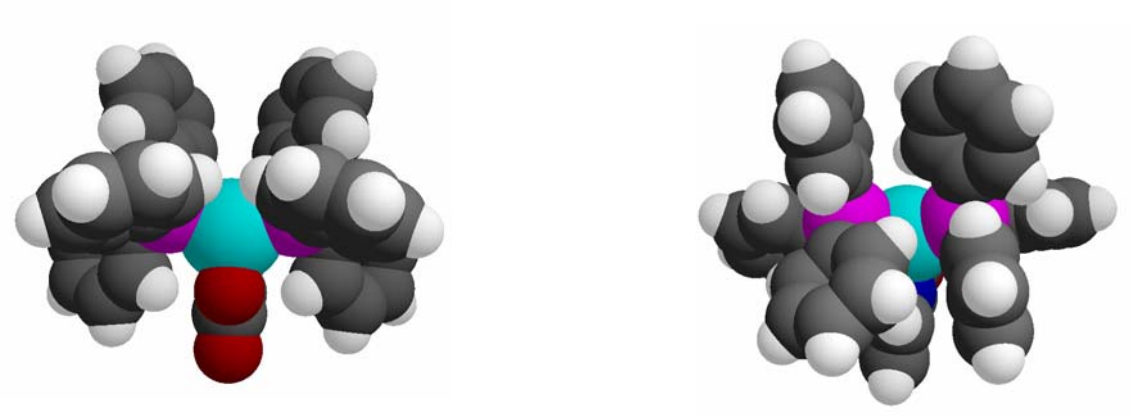

a **b**

Figure 2.32 Space filling plots. **a.** Complex **2.6**, **b.** Complex **2.4**.

There is a large difference, (6.9-8.8º), between the P–Cu–P bond angles for the complexes **2.6**-**2.8** (Table 2.9). A possible explanation for this difference in the P–Cu–P bond angles between these solvates could be: the structures **2.6** and **2.7** both crystallise including molecules of solvent which can be accommodated in the void between the phenyl groups at the expense of some angular distortions at the copper(I) tetrahedral environment. However, **2.8** crystallises as a solvent-free structure, hence **2.8** does not accommodate solvent molecules in the structure giving smaller values for the P–Cu–P bond angle.

The values for the α and β parameters [α= angle defined between planes P(1)-Cu(1)-P(2) or P(1)-Cu(1)-P(1A) and O(1)-Cu(1)-N(1) and β= angle defined between planes P(3)-Cu(2)-P(4) and N(2)-Cu(2)-O(3)] (Table 2.9) in **2.2**-**2.6** show the deviations of angles N–Cu–O and P–Cu–P from the tetrahedral environment presented by the copper(I) centre in all these structures. As expected, the formation of the strong O–H···O hydrogen bond interactions with the solvent molecules may be the reason of the slight deviation of these values from 90°.

Table 2.9 Selected bond lengths (Å) and bond angles (°) for **2.1-2.9**.

	2.1	**2.2**	**2.3**	**2.4**	**2.5**	**2.6**	**2.7**	**2.8**	**2.9**
P–Cu	2.2465(5)	2.254	2.2512(8)	2.2610(5)	2.2608(7)	2.2512(7)	2.2720(8)	2.2589(4)	2.258(7)
O–Cu	2.1091(13)	2.0792(16)	2.092(2)	2.0908(12)	2.084(2)	2.0497(16)	2.0700(19)	2.1238(11)	2.069(17)
N–Cu	2.0651(15)	2.102	2.101(2)	2.1055(14)	2.090(3)	2.1261(19)	2.154(2)	2.1299(13)	2.134(2)
O(1)–Cu(1)–N(1)	79.92(6)	80.13(7)	80.01(8)	79.77(5)	80.16(10)	92.01(7)	90.45(8)	95.10(5)	92.00(7)
O(3)–Cu(2)–N(2)	-	79.73(8)	79.71(9)	79.79(5)	-	-	-	-	90.76(7)
P–Cu(1)–P	124.853(18)	122.33(2)	126.14(3)	124.024(18)	136.05(4)	125.47(3)	123.55(3)	116.656(16)	123.94(3)
α	97.9	96.6	94.3	90.9	90.0	-	-	-	-
P(3)–Cu(2)–P(4)	-	124.66(2)	123.28(3)	124.014(18)	-	-	-	-	118.98(3)
β	-	93.9	94.8	93.1	-	-	-	-	-

α= angle defined between planes P(1)-Cu(1)-P(2) or P(1)-Cu(1)-P(1A) and O(1)-Cu(1)-N(1).

β= angle defined as described for α but applied to the second molecule of complex in the asymmetric unit. P(3)-Cu(2)-P(4) and N(2)-Cu(2)-O(3).

Table 2.10 Edge to face C–H···π attractive phenyl-phenyl interactions (Å) for **2.2**-**2.5**.

	2.2	**2.3**	**2.4**	**2.5**
C–H···π	2.847/3.228	3.091/3.274	2.913/3.184	3.115/3.340

2.3.4 Synthesis and Crystallisation of Cu(2,*n*-Hpyca)$(PPh_3)_2$ (*n* = 3-6) Complexes

The reactions of $Cu(PPh_3)_2(BH_4)$ with pyridine-2,*n*-dicarboxylic acid (*n* = 3-6) were carried out under reflux in dichloromethane yielding compounds **2.10**-**2.14**. The reactions took up to 3 h to complete and the products were easily isolated in excellent yield as yellow-orange precipitates by addition of light petroleum ether to the concentrated reaction mixture (Equation 2.3).

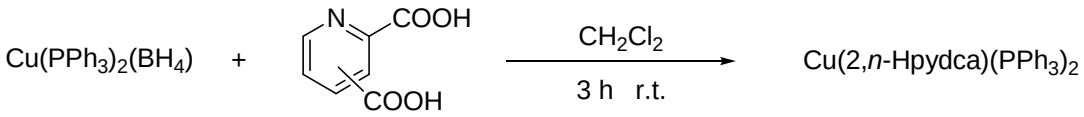

Equation 2.3

Cu(2,3-Hpydca)$(PPh_3)_2$ **2.10** crystallises with an intramolecular *S*(7) graph set hydrogen bond (Figure 2.33), a common motif for adjacent carboxylic acid groups.[114,115] The same motif is seen in the zwitterionic form of 2,3-H_2pydca,[116,117] with very similar O···O distances for both of them, 2.408(2) Å in compound **2.10** and 2.400(2) Å in 2,3-H_2pydca, the *N*,*O* metal coordination does not create any distortions in the ligand. As seen previously in compound **2.7**, the re-determination at low temperature (150 K) gives a slight improvement in the final R value (4.93% compared to 5.30%).

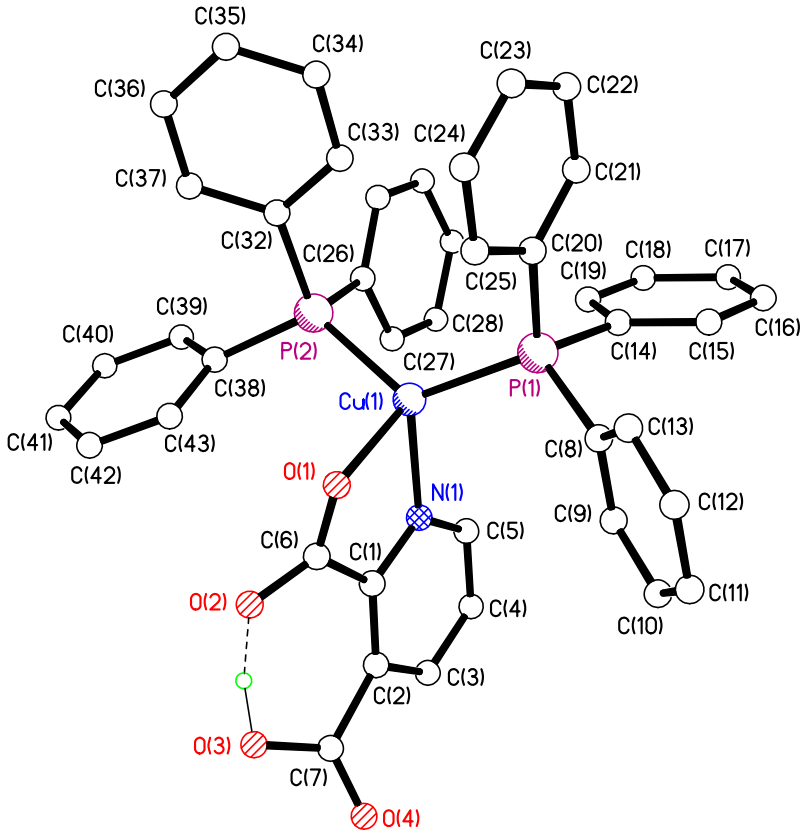

Figure 2.33 View of the asymmetric unit of Cu(2,3-Hpydca)(PPh_3)$_2$ **2.10**. Hydrogen atoms except O*H* have been removed for clarity.

The intramolecular hydrogen bonding of the protonated carboxylic acid group in **2.10** limits the dimensionality of the packing of the complex, with molecules of **2.10** forming centrosymmetric dimers *via* weak C–H···O hydrogen bonding interactions [where C···O distance is 3.50 Å], producing an $R^2_2(26)$ graph set motif with a distance of 9.248 Å between symmetry-related metal centres. The dimers are also stabilised by the presence of an edge-to-face C–H···π(centroid) interaction (2.490 Å) between the aromatic rings of the two symmetry related molecules (Figure 2.34). Selected hydrogen bonding parameters for **2.10** are shown in Table 2.11.

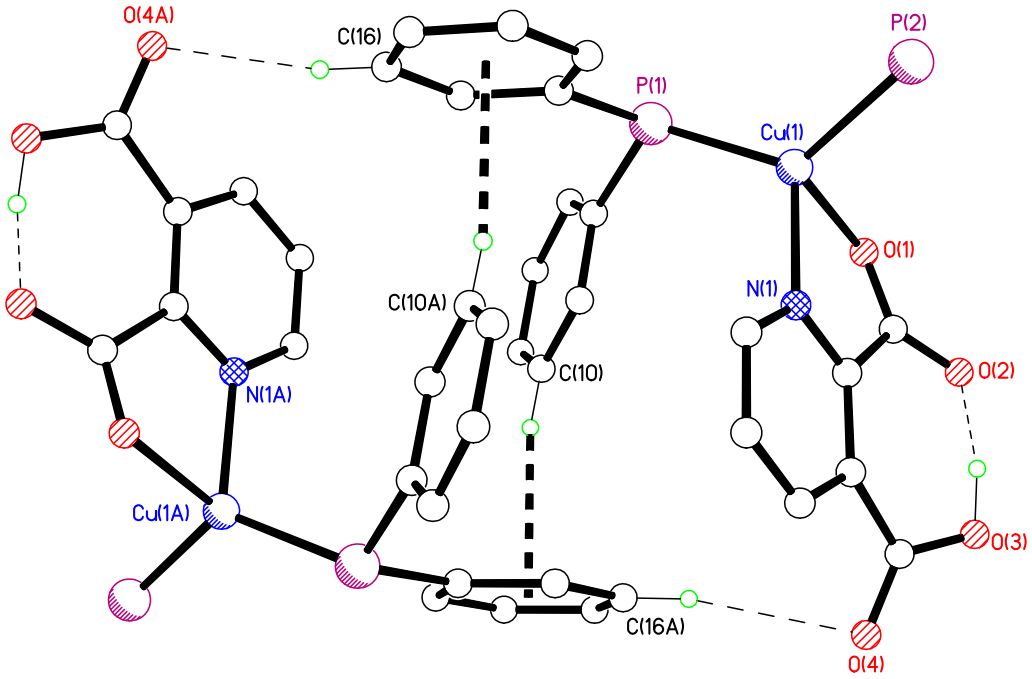

Figure 2.34 View of the hydrogen bonded dimers of Cu(2,3-Hpydca)(PPh_3)$_2$ **2.10**. Phenyl groups and hydrogen atoms not involved in hydrogen bonding have been omitted for clarity.

Table 2.11 Selected hydrogen bonding parameters for **2.10**.

D–H···A	D···A/Å	D–H/Å	H···A/Å	D–H···A/°
O(3)–H(3)···O(2)	2.408(2)	0.95(3)	1.47(3)	167(3)

It is interesting to note that the re-determination of the full structure of compound **2.10** at low temperature allows a better location of the hydrogen atoms in the structure, showing the formation of dimers and the presence of the intramolecular hydrogen bond which were not discussed by Cariati. Crystallisation of Cu(2,3-Hpydca)(PPh_3)$_2$ **2.10** was also performed from MeOH, EtOH, *n*-PrOH and *i*-PrOH with no solvates formed and only the solvent-free structure was observed.

Cu(2,4-Hpydca)(PPh_3)$_2$·$CHCl_3$ **2.11** was crystallised from a chloroform solution (Figure 2.35). The asymmetric unit of **2.11** contains two molecules of the complex and two molecules of chloroform. Careful inspection of the disposition of the two unique molecules shows that the compound has crystallised with two similar conformations of

the complex molecules and they only differ significantly in the disorder present in one of the solvent molecules.

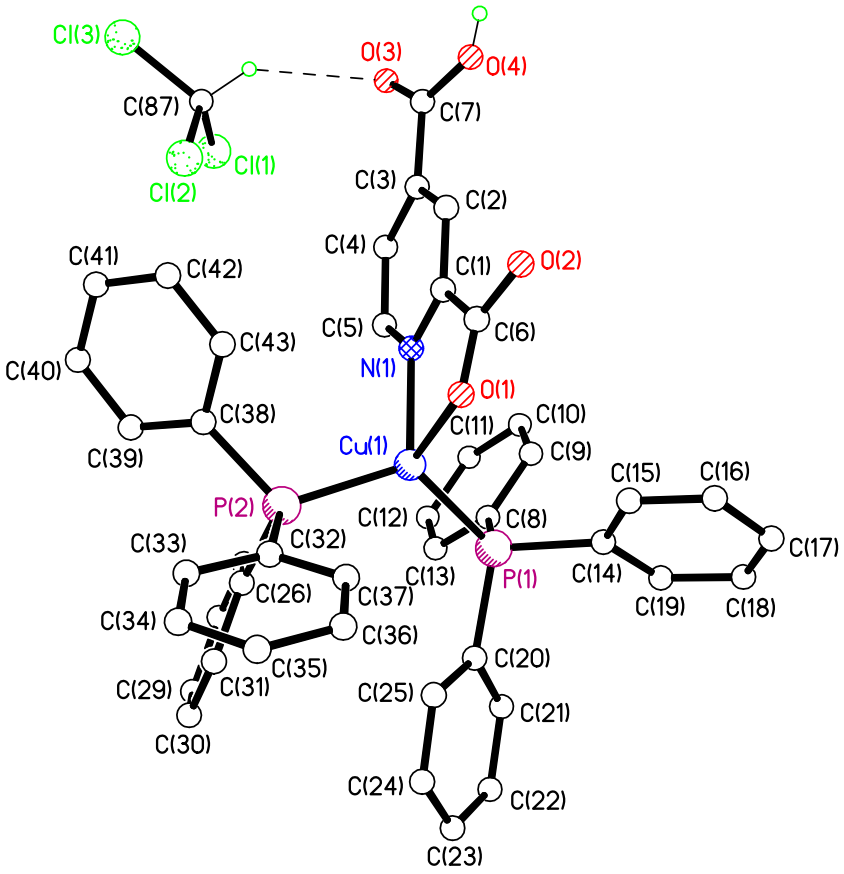

Figure 2.35 View of one of the two independent Cu(2,4-Hpydca)$(PPh_3)_2$·$CHCl_3$ units in **2.11**. Hydrogen atoms not involved in hydrogen bonding and the disordered solvent molecule have been omitted for clarity.

The $R^2_2(8)$ head-to-tail carboxylic acid dimer is not found in **2.11** (Figure 2.36); instead are series of ring motifs are formed using a combination of strong (acid)O–H···O(carboxylate) and weak (aromatic)C–H···O(carboxylate) hydrogen bonds (Table 2.12). The combination of these interactions with a symmetry related molecule results in an $R^2_2(14)$ ring motif. The outer carboxyl groups of each molecule also interact with a phenyl group producing an $R^3_3(11)$ graph set motif. This creates chains running parallel to the *b* direction and stacking on top of each other in the *a* orientation. The chloroform molecules are located between the chains and hydrogen bond to the carboxylic acid group through (solvent)C–H···O(acid) hydrogen bond.

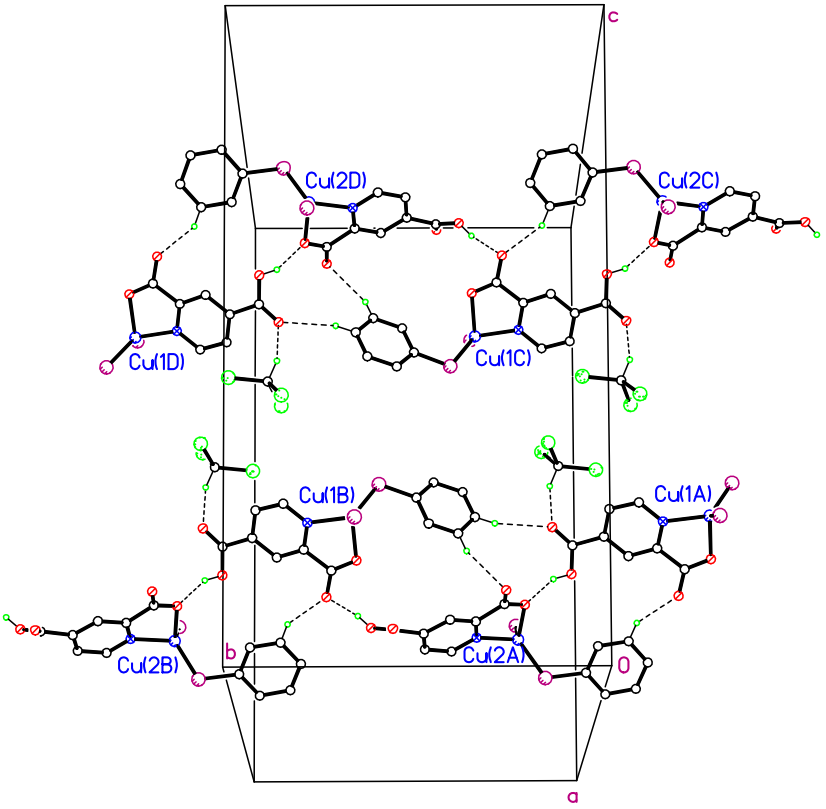

Figure 2.36 View of the packing plot of compound **2.11**, viewed down the crystallographic *a* axis. Most phenyl groups and hydrogen atoms not involved in hydrogen bonding have been removed for clarity.

Table 2.12 Selected hydrogen bonding parameters for **2.11**.

D–H···A	D···A/Å	D–H/Å	H···A/Å	D–H···A/º
O(4)–H(4)···O(5A)^{i}	2.511(4)	0.84	1.73	154
O(8)–H(8)···O(2A)^{i}	2.468(4)	0.84	1.64	166

Symmetry operation: ^{i}-x+1/2, y+1/2, -z+1/2.

The addition of an extra carboxylic acid group compared to **2.1**-**2.5** provided an additional hydrogen bonding group which resulted in the extension of the zero-dimensional molecular structures into a one-dimensional network through hydrogen bonds in **2.11**.

The Cu(2,5-Hpydca)$(PPh_3)_2$ was crystallised by Agnese Cecchin, and structurally characterised by the author of this thesis, from a methanolic solution. It was observed to include one molecule of water per molecule of complex, yielding Cu(2,5-

Hpydca)$(PPh_3)_2 \cdot H_2O$ **2.12** (Figure 2.37). The inclusion of water molecules into the structure provides suitable O*H* donors to the system. The H_2O molecule hydrogen bonds to the two carboxylate oxygen atoms through a bifurcated (solvent)O–H···O(acid) hydrogen bond, with the formation of an $R^2_1(4)$ ring motif. Selected hydrogen bonding parameters for **2.12** are shown in Table 2.13.

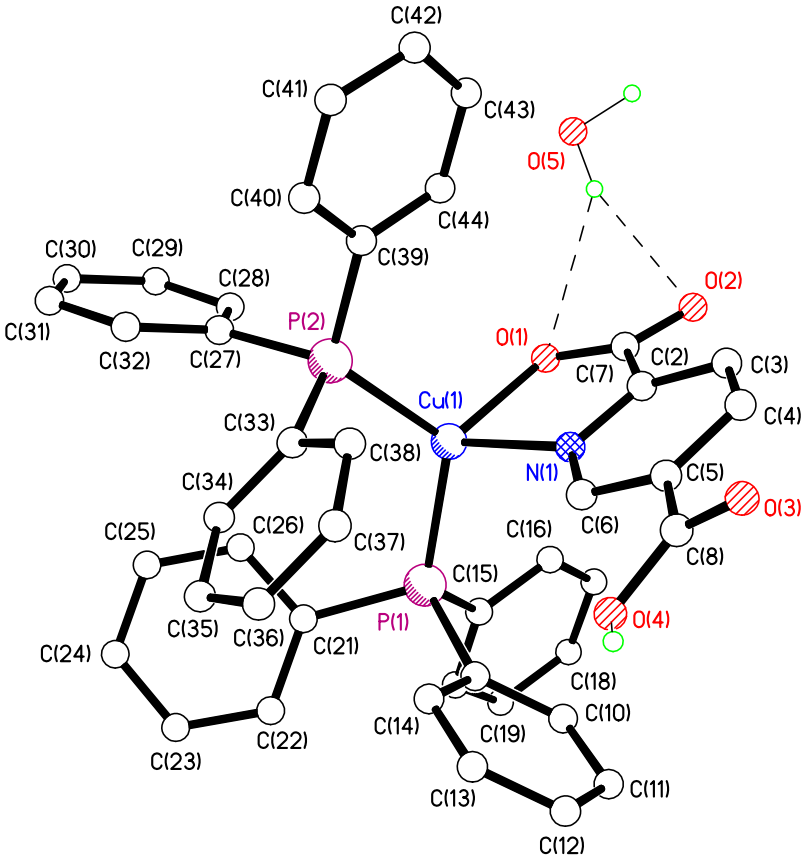

Figure 2.37 View of the asymmetric unit of Cu(2,5-Hpydca)$(PPh_3)_2 \cdot H_2O$ **2.12**. Hydrogen atoms from the phenyl groups have been removed for clarity.

Table 2.13 Selected hydrogen bonding parameters for Cu(2,5-Hpydca)$(PPh_3)_2 \cdot H_2O$ **2.12**.

D–H···A	D···A/Å	D–H/Å	H···A/Å	D–H···A/°
O(4)–H(4)···O(2A)^{i}	2.6009(17)	0.84	1.77	170
O(5)–H(5B)···O(2)	3.091(2)	0.89(3)	2.27(3)	152(3)
O(5)–H(5B)···O(1)	3.320(2)	0.89(3)	2.60(3)	139(2)
O(5)–H(5A)···O(3B)^{ii}	2.864(2)	1.02(3)	1.85(3)	171(3)

Symmetry operations: ^{i}x, -y+1/2, z-1/2 and ^{ii}-x+2, -y, -z+1.

The molecules of **2.12** form chains *via* a single, strong (carboxylic acid)O–H···O(carboxylate) hydrogen bond propagating parallel to the *c* axis (Figure 2.38). The water molecules of crystallisation then aid the formation of an extended two-dimensional hydrogen bonding array by donating each of its O*H* groups to two symmetry related molecules of complex *via* two strong O–H···O hydrogen bonds, with the uncoordinated carboxylate *O* atom from one and one the carboxylic acid *O* atom from the other allowing the formation of $R^4_4(22)$ and $R^8_8(36)$ ring motifs.

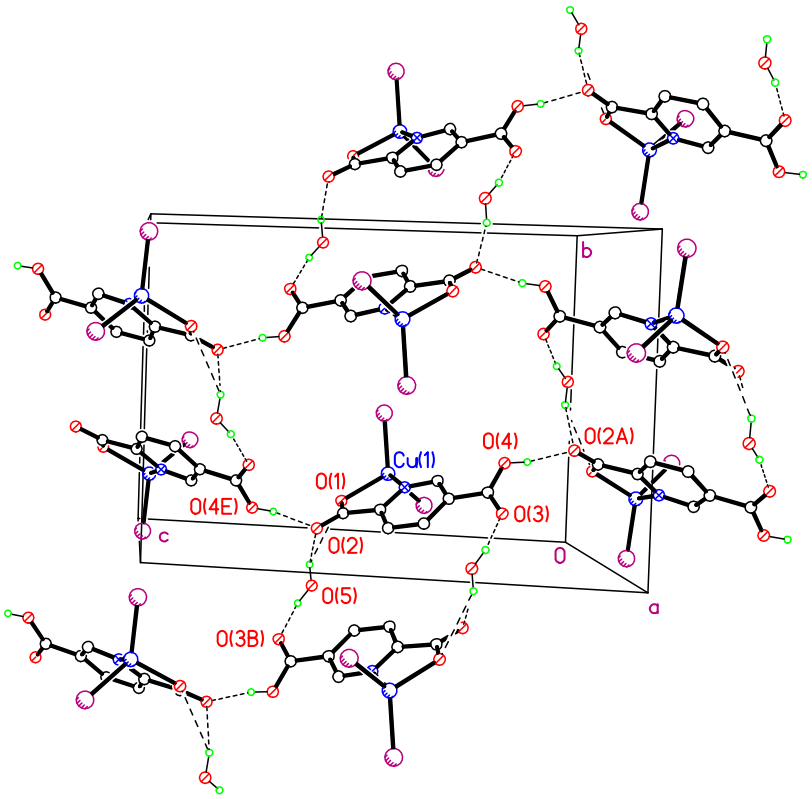

Figure 2.38 Packing plot of compound Cu(2,5-Hpydca)$(PPh_3)_2 \cdot H_2O$ **2.12**. Hydrogen not involved in hydrogen bonding and phenyl groups have been removed for clarity.

When Cu(2,5-Hpydca)$(PPh_3)_2$ was crystallised *via* the vapour diffusion of hexane into a chloroform/methanol solution; a chloroform solvate, Cu(2,5-Hpydca)$(PPh_3)_2 \cdot 2CHCl_3$ **2.13**, was isolated (Figure 2.39).

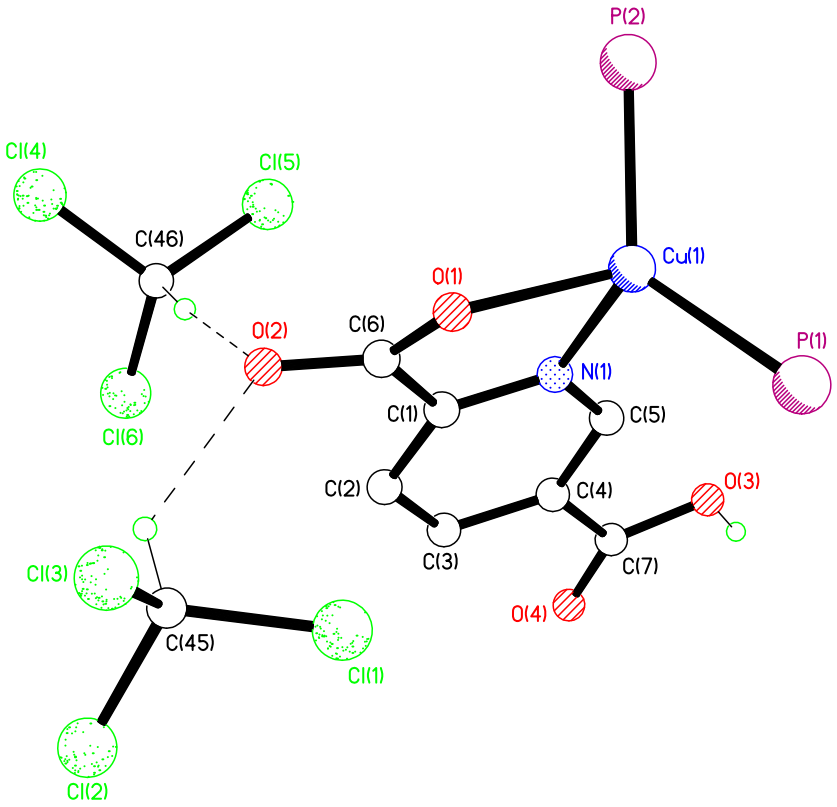

Figure 2.39 View of the asymmetric unit of compound Cu(2,5-Hpydca)$(PPh_3)_2 \cdot 2CHCl_3$ **2.13**. Phenyl groups and hydrogen atoms except O*H* have been omitted for clarity.

As seen above for **2.12**, a single strong (carboxylic)O–H···O(carboxylate) hydrogen bond holds the molecules of **2.13** into chains (Table 2.14) and complementary interactions with the solvent molecules, (phenyl)C–H···Cl(solvate) and (solvate)C–H···O(carboxylic/carboxylate) [2.90 Å, 2.87 Å, 2.46 Å, 2.41 Å], extend the dimensionality of the structure into sheets, this disposition is unsurprising considering the positioning of the carboxylic group in the molecule (Figure 2.40). The chloroform molecules bridge adjacent different chains. Here, chloroform facilitates the formation of a supramolecular array, rather than limiting the dimensionality as seen in compound **2.10**.

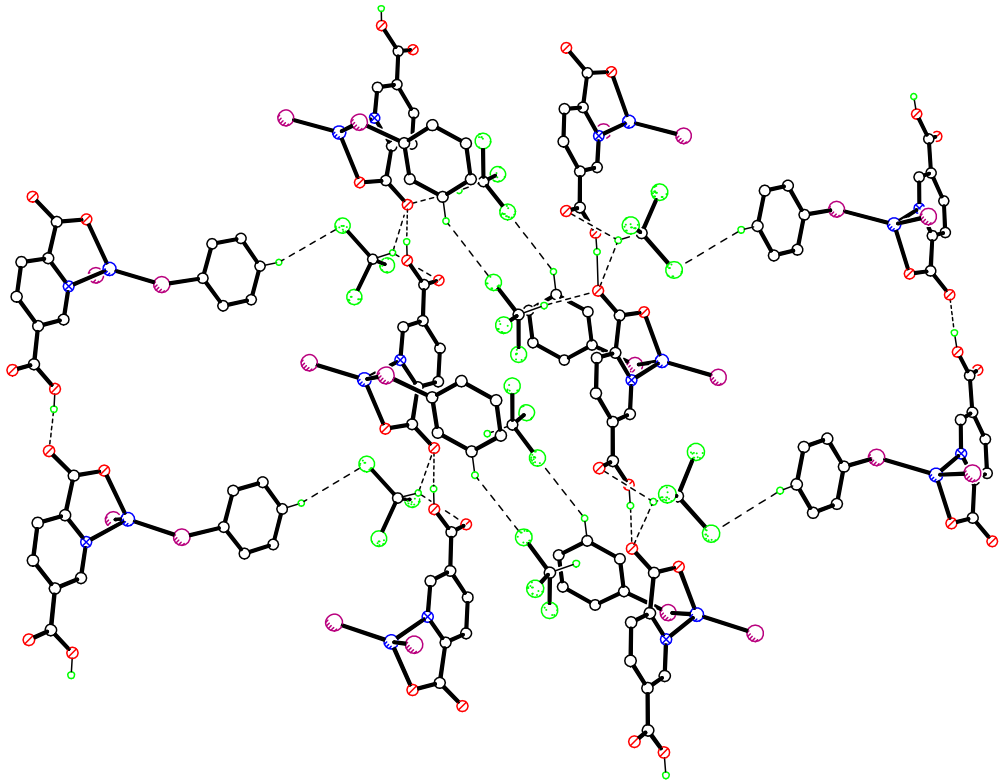

Figure 2.40 Packing of Cu(2,5-Hpydca)$(PPh_3)_2 \cdot 2CHCl_3$ **2.13**. Hydrogen not involved in hydrogen bonding and most phenyl groups have been removed for clarity.

Table 2.14 Selected hydrogen bonding parameters for **2.13**

D–H···A	D···A/Å	D–H/Å	H···A/Å	D–H···A/º
O(3)–H(3A)···O(2)	2.553(3)	0.84	1.71	177

Symmetry operations: [1]x+1, y, z.

The X-ray diffraction data for compound Cu(2,6-Hpydca)$(PPh_3)_2 \cdot H_2O$ **2.14** was collected at the EPSRC National X-ray Service at Daresbury Laboratory due to the weak intensity of the reflections. The hydrogen atoms of one of the water molecules, O(11), could not be located in the Fourier difference map. Compound **2.14** crystallises with two formula units in the asymmetric unit and three water molecules of crystallisation. The two unique molecules crystallise in two different conformations and they also differ in the number of water molecules hydrogen bonded to the complex (Figure 2.41).

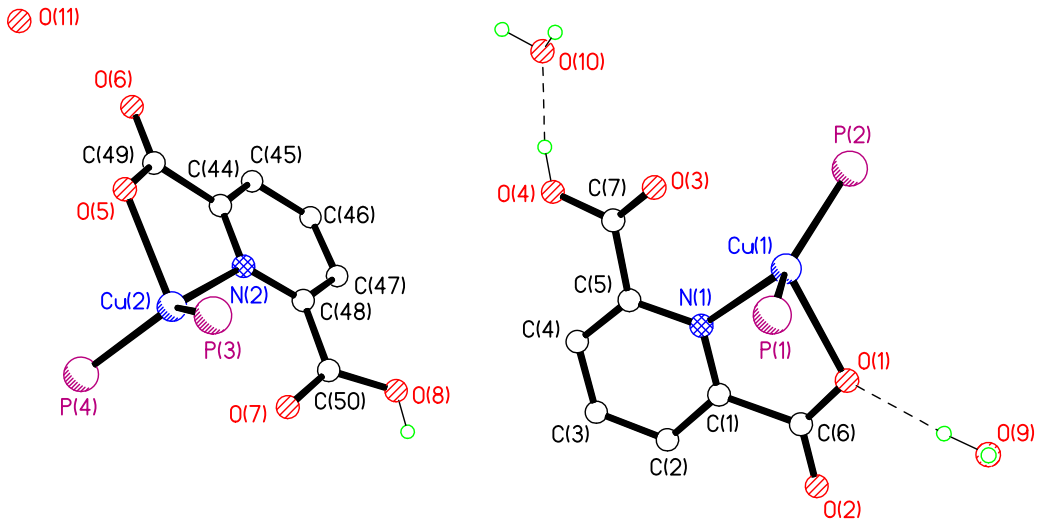

Figure 2.41 View of the asymmetric unit of **2.14**. Phenyl groups and hydrogen atoms not involved in hydrogen bonding have been removed for clarity.

In the case of compound **2.14**, two of the water molecules hydrogen bond to a symmetry related molecule and to the carboxylate *O* of one copper(I) complex molecule, forming an $R^3_3(8)$ motif. The network of strong hydrogen bonds creates a stepped-chain structure which extends in the [1 0 1] direction (Figure 2.42). The pyridyl rings of neighbouring complex molecules interlock allowing (pyridyl)C–H···O(carboxylate) hydrogen bonding interactions (2.563 Å). Selected hydrogen bonding parameters for **2.14** are shown in Table 2.15.

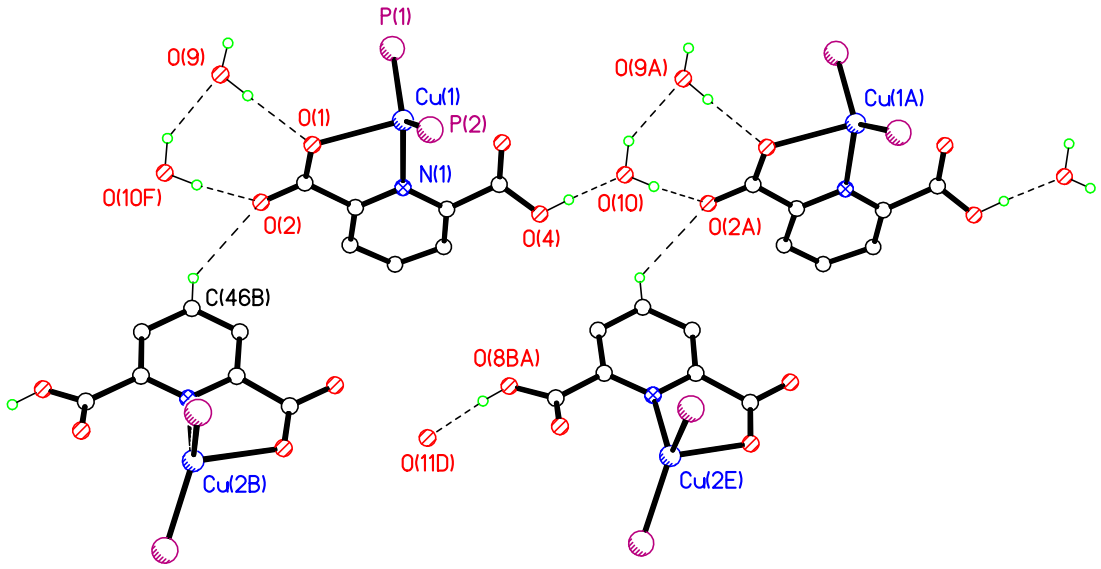

Figure 2.42 View of the hydrogen bonded chain formed by compound **2.14**. Phenyl groups and hydrogen atoms not involved in hydrogen bonding have been removed for clarity.

Table 2.15 Selected hydrogen bonding parameters for **2.14**.

D–H···A	D···A/Å	D–H/Å	H···A/Å	D–H···A/°
O(4)–H(4)···O(10)	2.516(8)	0.84	1.69	169
O(10)–H(10B)···O(9)^{i}	2.767(9)	0.84(2)	2.03(5)	145(7)
O(9)–H(9B)···O(1)	2.777(8)	0.83(2)	1.95(2)	177(11)
O(10)–H(10A)···O(2)^{i}	2.635(8)	0.83(2)	1.83(3)	164(10)
O(8)–H(8)···O(11)^{ii}	2.558(8)	0.84	1.72	173

Symmetry operations: ^{i}x, y+1, z; ^{ii}x, y-1, z.

Cariati failed to predict the structures of **2.10**-**2.14**, because the reported analysis was based on the comparison of the infrared spectra of these compounds: all complexes presented very similar υ_{as}(COOH) and υ_{as}(COO) and Cariati supposed that their structures were identical. However, the work has shown that **2.10** crystallises as discrete dimers, whereas complexes **2.11**-**2.14** crystallise as polymeric structures where different types of hydrogen bonding patterns, such as single, strong (carboxylic)O–H···O(carboxylate) or secondary interactions with solvent molecules, hold the molecules together yielding higher dimensionality networks.

The coordinated carboxylate group only deviates slightly from co-planarity with the pyridine ring of the bidentate ligand in **2.14** bearing [2,6-Hpydca]$^-$ (the maximum twist angle is 3.1°). However, when the bidentate ligands are [2,3-Hpydca]$^-$, [2,4-Hpydca]$^-$ and [2,5-Hpydca]$^-$, this deviation is greater, with the greatest twist angle being 18.8°, observed in **2.13**. With the exception of complex **2.13**, the carboxylic acid groups of the [2,*n*-Hpydca]$^-$ ligands (*n* = 3-6) show greater deviations from co-planarity with the pyridine ring of the bidentate ligand than do the carboxylate group. The most notable example is complex **2.11**, where the carboxylic acid group lies at an angle of 36.2° to the pyridine ring of the bidentate ligand.

2.3.5 Synthesis and Crystallisation of Cu(3,*n*-pyca)$(PPh_3)_2$ (*n* = 4, 5) Complexes

The next step was to study the hydrogen bonding capability of copper(I) complexes containing 3,*n*-H_2pydca (*n* = 4, 5) ligands. The method used to synthesise them is described above for complexes **2.1**-**2.14** giving good to high yields (Equation 2.4). Crystallisation was attempted for both compounds using a wide range of solvent systems, however both compounds only crystallised as solvent-free structures. Experimental data such as, microanalysis, ^{1}H and ^{31}P NMR spectral data, clearly show the presence of the expected compounds in both cases.

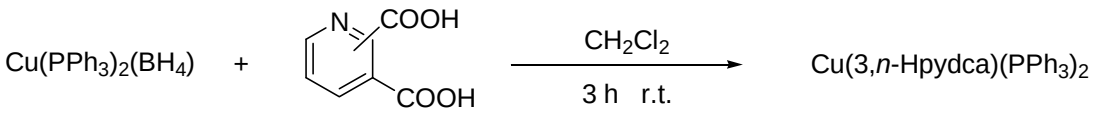

Equation 2.4

The crystal structure of compound Cu(3,4-Hpydca)$(PPh_3)_2$ **2.15** shows that the 3,4-pyridine ligand bridges covalently two copper(I) centres through the pyridine nitrogen atom and an oxygen from the carboxylate group *para* to the nitrogen atom forming covalently bonded chains. The second carboxylate oxygen is hydrogen bonded to the carboxylic acid *OH* group *meta* to the nitrogen atom forming a intramolecular *S*(7) graph set strong O–H···O motif (Table 2.16), a common occurrence in 1,2-disubstituted dicarboxylic acids in their neutral form and when deprotonated (Figure 2.43).[116,118] The

coordinated carboxylate and carboxylic acid groups deviate slightly from co-planarity with the pyridine ring of the bidentate ligand with the greatest twist angle being 18.1°.

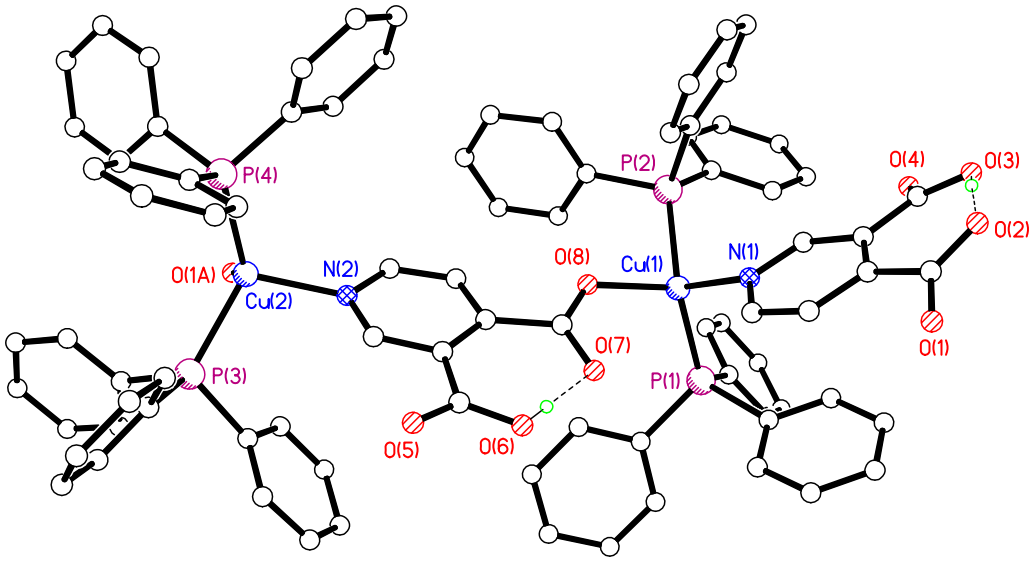

Figure 2.43 View of the asymmetric unit of compound $[Cu(3,4\text{-}Hpydca)(PPh_3)_2]_n$ **2.15**. Hydrogen atoms not involved in hydrogen bonding have been removed for clarity.

Table 2.16 Selected hydrogen bonding parameters for **2.15**.

D–H···A	D···A/Å	D–H/Å	H···A/Å	D–H···A/º
O(3)–H(3)···O(2)	2.432(3)	0.84	1.60	170
O(6)–H(6)···O(7)	2.416(4)	0.84	1.58	176

The intramolecular hydrogen bonding of the protonated carboxylic acid group in **2.15** limits the dimensionality of the packing of the complex. The one-dimensional polymeric zigzag chains propagate parallel to the *a* axis (Figure 2.44).

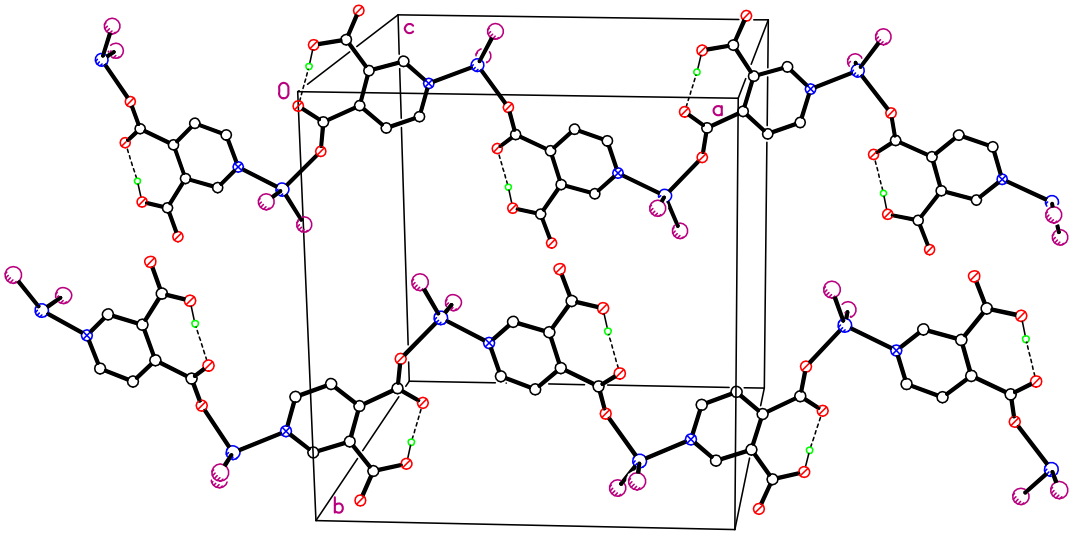

Figure 2.44 Packing plot of **2.15**, viewed along the crystallographic *b* axis. Phenyl groups and hydrogen atoms except O*H* have been removed for clarity.

Crystals of compound Cu(3,5-Hpydca)(PPh_3)$_2$ **2.16** were obtained by Helena Ascroft and represent the first example of copper(I) coordinated to the 3,5-H_2pydca ligand. Wang and co-workers have described an example of a copper(II) complex with 3,5-H_2pydca ligand presenting a similar hydrogen bonding pattern to the one observed in **2.16** where the metal centers are coordinated to the *O* atoms from the carboxylic/carboxylate functionalities instead of involving also the pyridyl *N* which is more common.[73,119] Compound **2.16** crystallises forming zigzag chains where each copper(I) atom is tetrahedrally coordinated by two molecules of triphenylphosphine, one carboxylate oxygen from one [3,5-Hpydca]$^-$ ligand and by one carboxylic oxygen from a symmetry related [3,5-Hpydca]$^-$ ligand (Figure 2.45). Complex **2.16** shows smaller deviations from co-planarity of the pyridine ring with the carboxylate and carboxylic acid groups than the ones observed in **2.15** (the maximum twist angle in **2.16** is 9.8°).

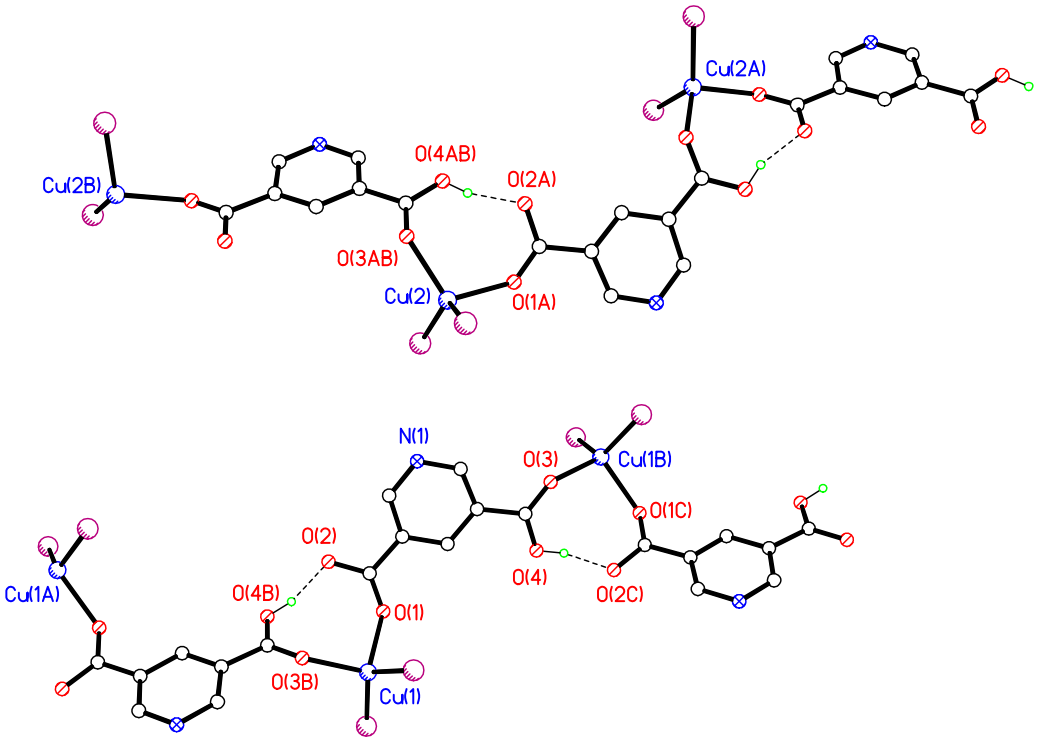

Figure 2.45 View of the zigzag chains of Cu(3,5-Hpydca)$(PPh_3)_2$ **2.16**. Phenyl groups and hydrogen atoms not involved in hydrogen bonding have been removed for clarity.

The carboxylic acid and the carboxylate oxygen of the $[3,5\text{-Hpydca}]^-$ do indeed participate in hydrogen bonding, forming the $R^1{}_1(8)$ carboxylic acid-carboxylate graph set motif through one strong O–H···O hydrogen bond (Table 2.17).

Table 2.17 Selected hydrogen bonding parameters for **2.16**.

D–H···A	D···A/Å	D–H/Å	H···A/Å	D–H···A/°
O(4)–H(4)···O(2C)^{i}	2.442(4)	0.84	1.62	164
O(4B)–H(4B)···O(2)^{ii}	2.452(4)	0.84	1.65	160

Symmetry operations: ^{i}x+1/2, -y+1, z; ^{ii}x+1/2, -y+2, z.

Cariati predictions for compounds without groups in the *ortho* position with respect to the pyridinic nitrogen such as, **2.15** and **2.16** were proved correct as they do crystallise forming polymeric structures.

2.3.5 Synthesis and Crystallisation of Copper(I)-Pyrazinecarboxylic Acid Complexes

As seen previously, pyridine carboxylate ligands bind well to metal centres and, therefore, have been extensively used in the construction of metal/organic networks. The functionalised homologues, the pyrazine carboxylates, although less used,[93,120] are another class of very good ligands for the construction of new framework materials because of their extensive bonding versatility. In pyrazine carboxylate ligands, two coordination sites, neutral and/or charged, chelate to the metal centre while the remaining donor sites can further participate in the assembly of a polymeric structure by an exo-binding mode to other metal centres or by supramolecular interactions to nearby H-bonding donors.

All compounds described below, Cu(2-pzca)$(PPh_3)_2$ **2.17**, Cu(2,3-Hpzdca)$(PPh_3)_2$ **2.18**, Cu(2,3-pzdca)$(PPh_3)_4$ **2.19** and Cu(2,5-pzdca)$(PPh_3)_2$ **2.20**, have been synthesised following the same reaction conditions described previously in this chapter. The crystallisation of pyrazine copper(I) complexes **2.17-2.20** all proceeded smoothly, through slow vapour diffusion into a saturated complex solution or by simple evaporation. Interestingly, in the case of compound Cu(2-pzca)$(PPh_3)_2$ **2.17**, the crystallisation of two different polymorphic forms was observed depending on the solvent system. The first polymorph of **2.17** which was obtained by slow vapour diffusion of hexane into a chloroform solution of Cu(2-pzca)$(PPh_3)_2$, crystallises in the triclinic crystal system while the second polymorph, which was obtained using diethyl ether instead of hexane, crystallises as monoclinic. Both forms crystallise as solvent-free structures with one molecule of **2.17** in the asymmetric unit (Figure 2.46).

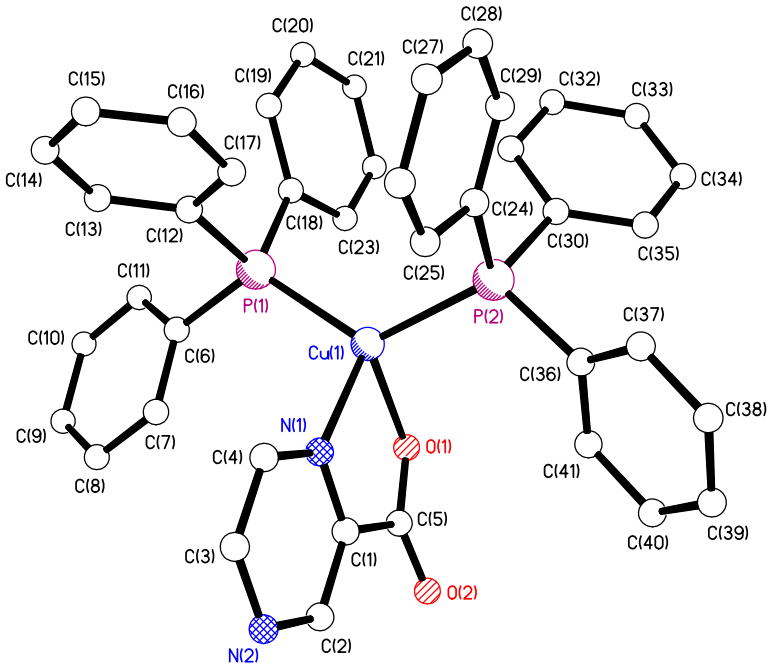

Figure 2.46 View of the asymmetric unit of the triclinic polymorph of Cu(2-pzca)(PPh_3)$_2$ **2.17**. Hydrogen atoms have been omitted for clarity.

Carboxylate oxygen atoms are involved in weak secondary hydrogen bond (phenyl)C–H···O(carboxylate) interactions, H···O = 2.52 Å and 2.44 Å, producing alternate $R^4_4(30)$ and $R^2_2(20)$ motifs, which creates a one dimensional stepped structure extending parallel to the *b* direction (Figure 2.47).

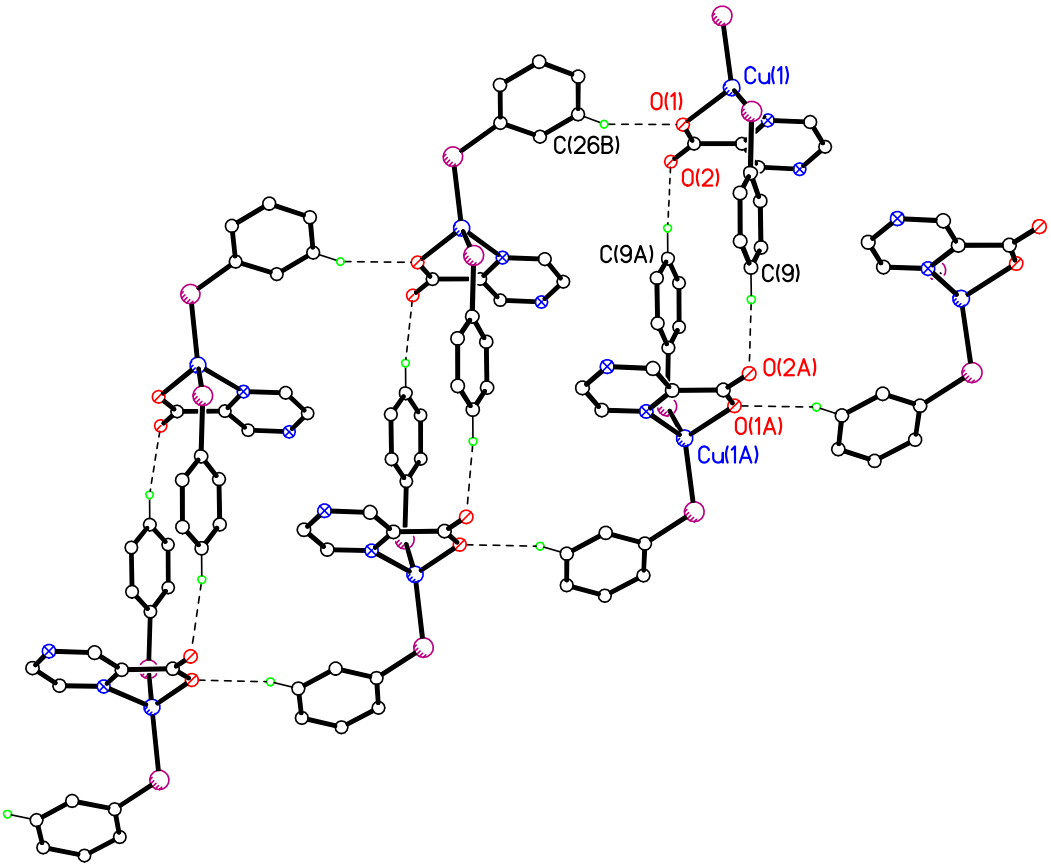

Figure 2.47 View of the stepped chain motif in **2.17**. Most phenyl groups and hydrogen atoms not involved in hydrogen bonding have been omitted for clarity.

In contrast to the solvent dependency trend observed in **2.1**-**2.5**, attempts to include the same alcohols, MeOH, EtOH, *n*-PrOH and *i*-PrOH, into the structure of Cu(2-pzca)$(PPh_3)_2$ **2.17** failed to produce solvates, crystallising instead as the solvent-free triclinic polymorph **2.17A**.

The reaction of one equivalent of $(PPh_3)_2Cu(BH_4)$ with one equivalent of 2,3-H_2pzdca yields compound Cu(2,3-Hpzdca)$(PPh_3)_2$ **2.18**. Complex **2.18** crystallises with the carboxylate group involved in chelation almost coplanar with the pyrazine ring [dihedral angle of 3.3°] and the carboxylic acid group almost perpendicular to the pyrazine ring [dihedral angle of 95.1°] preventing the formation of the intramolecular O–H···O hydrogen bond observed in Cu(2,3-Hpydca)$(PPh_3)_2$ **2.9** (Figure 2.48).

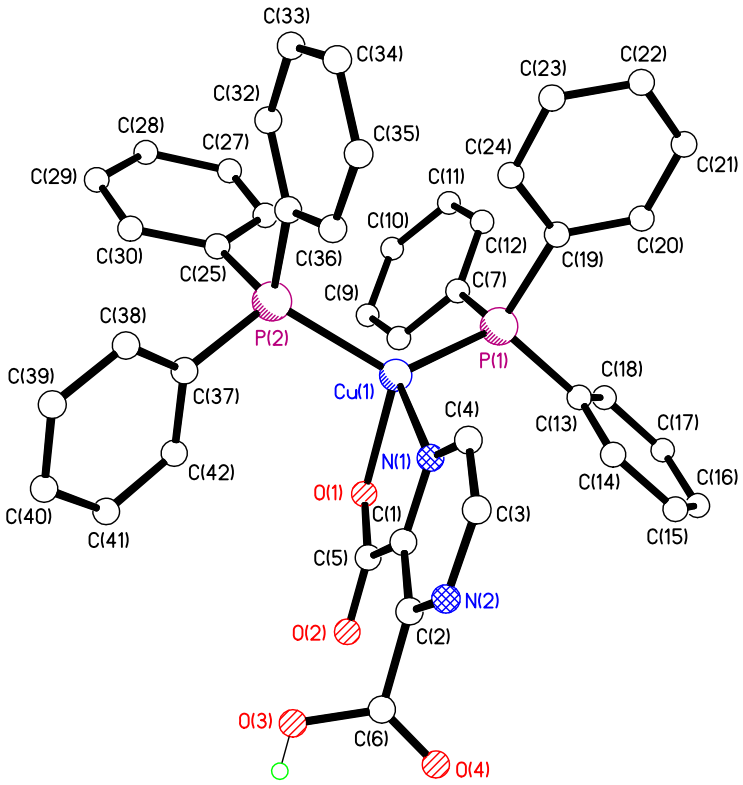

Figure 2.48 View of the asymmetric unit of **2.18**. Hydrogen atoms except O*H* have been omitted for clarity.

Instead, O–H···O hydrogen bonds generate dimers in which two monomers of complex **2.18** are held in an $R_2^2(14)$ motif, with a distance of 11.920 Å between symmetry-related copper atoms (Figure 2.49). Cariati predictions of compound **2.18** crystallising as discrete units also failed as seen previously for Cu(2,3-Hpydca)$(PPh_3)_2$ **2.10**. Selected hydrogen bonding parameters for **2.18** are shown in Table 2.18.

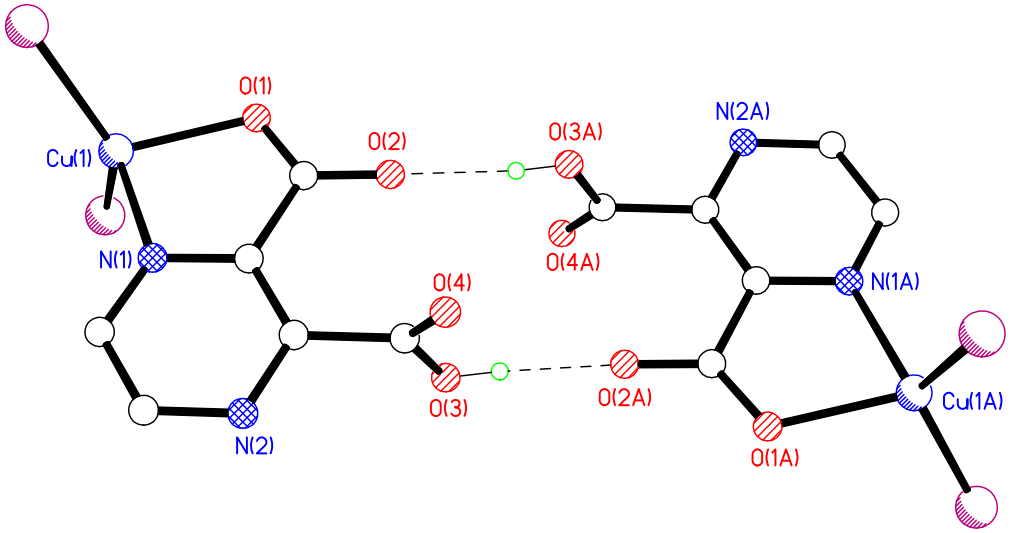

Figure 2.49 View of the $R_2^2(14)$ graph set motif between monomers of **2.18**, producing dimers. Phenyl groups and hydrogen atoms except those involved in hydrogen bonding have been omitted for clarity.

Table 2.18 Hydrogen bonding parameters for **2.18**.

D–H···A	D···A/Å	D–H/Å	H···A/Å	D–H···A/º
O(3)–H(3A)···O(2)^{i}	2.600(3)	0.77(4)	1.87(5)	159(5)

Symmetry operation: ^{i}-x+1, -y+1, -z.

When one equivalent of 2,3-H_2pzdca was reacted with two equivalents of $(PPh_3)_2Cu(BH_4)$, the pyrazine ligand bridges two metal centres yielding Cu_2(2,3-pzdca)$(PPh_3)_4$ **2.19**. The same compound, **2.19**, was also obtained by adding one equivalent of $(PPh_3)_2Cu(BH_4)$ to **2.18**. Compound **2.19** presents a two-fold axis, resulting in the asymmetric unit comprising half of a molecule (Figure 2.50). The asymmetric unit also contains two methanol molecules of crystallisation, one of them disordered across a two-fold axis. The hydrogen atoms of the disordered methanol molecule could not be located in the Fourier difference map. As expected, electronic repulsions force the adjacent carboxylate groups away from the plane of the pyrazine ring, with a dihedral angle of 31.2°. Selected hydrogen bonding parameters for **2.19** are shown in Table 2.19.

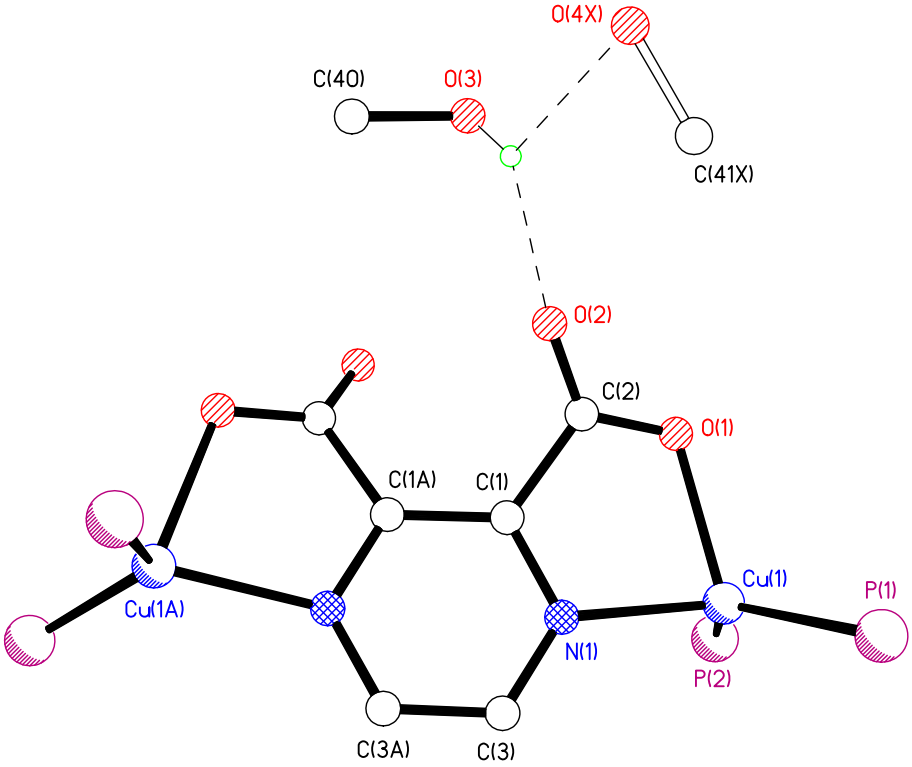

Figure 2.50 View of Cu_2(2,3-pzdca)$(PPh_3)_4$ **2.19**. Phenyl groups and hydrogen not involved in hydrogen bonding have been removed for clarity. Only one of the components of the disordered methanol C41–O4 is shown for clarity.

Table 2.19 Selected hydrogen bonding parameters for **2.19**.

D–H···A	D···A/Å	D–H/Å	H···A/Å	D–H···A/º
O(3)–H(3)···O(2)	2.609(10)	0.84	2.06	123
O(3)–H(3)···O(4X)	2.93(2)	0.84	2.51	112

Complex Cu_2(2,5-pzdca)$(PPh_3)_4$ **2.20** shows similarities with the reported compound $Cu_2[(2,5\text{-pzdca})(phen)_4](NO_3)_2 \cdot 10H_2O$ reported by Beobide and co-workers, but without any included solvent in this case.[40] Both compounds crystallise on a crystallographic centre of symmetry where the bidentate $[2,5\text{-pzdca}]^{2-}$ ligand bridges two copper atoms with a Cu···Cu distance slightly smaller for **2.20**, 6.852 Å, than the one reported for $Cu_2[(2,5\text{-pzdca})(phen)_4](NO_3)_2 \cdot 10H_2O$, 7.112 Å (Figure 2.51).

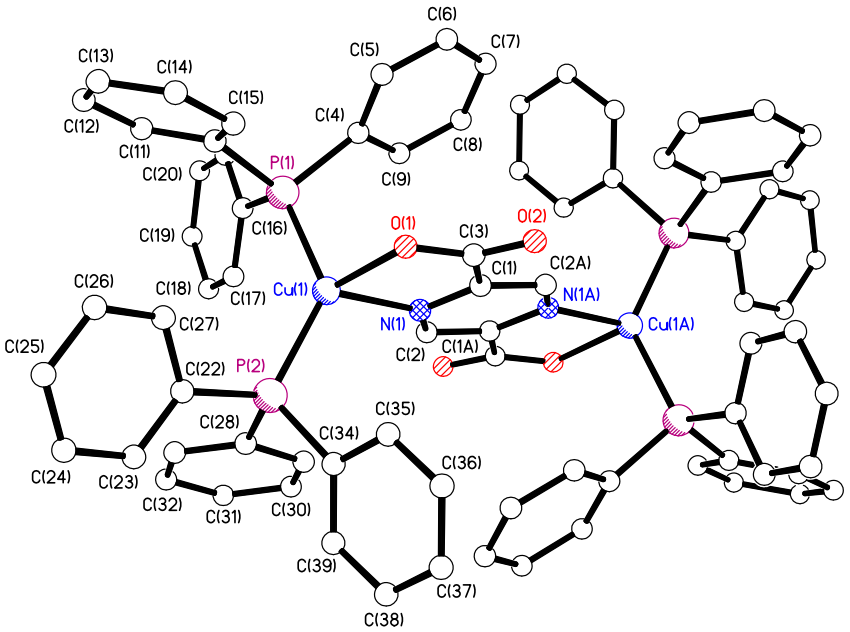

Figure 2.51 View of centro-symmetric compound **2.20**. Hydrogen atoms have been omitted for clarity.

The hydrogen bonded undulating chains, produced as a result of the 2,5-substitution of **2.20**, extend in the *ab* plane through weak C–H···O hydrogen bonds [where C···O distances are 3.09 Å, 3.12 Å and 3.19 Å] forming $R^2_2(14)$ and $R^2_2(22)$ graph set motifs (Figure 2.52).

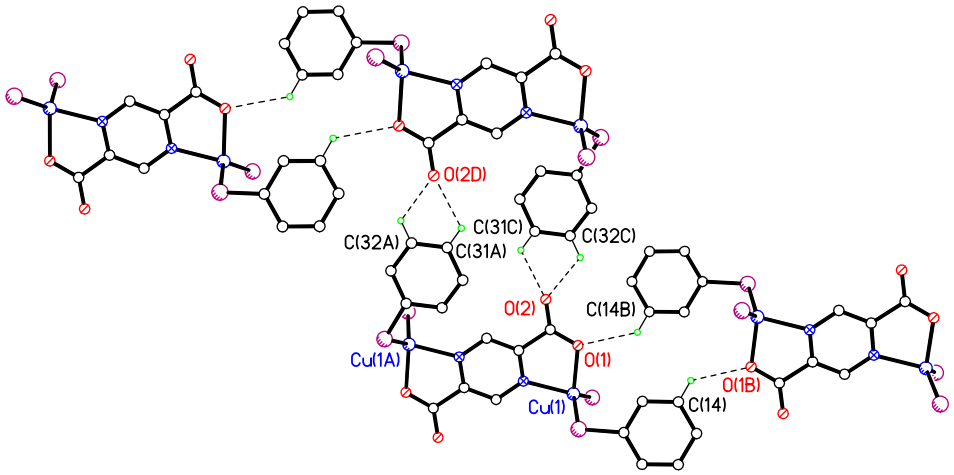

Figure 2.52 View of Cu_2(2,5-pzdca)$(PPh_3)_4$ **2.20**. Most phenyl groups and hydrogen atoms not involved in hydrogen bonding have been removed for clarity.

The copper(I) complexes with 2,3-H_2pzdca and 2,5-H_2pzdca described in this chapter have similar pK_1 and pK_2 values.[50] However, while the crystallisation of the 1:1 and 1:2 adducts, ligand:$[Cu(PPh_3)_2]^+$, was possible using 2,3-H_2pzdca as a ligand, only the 1:2 adduct was crystallised from the reaction with 2,5-H_2pzdca. An explanation for this behaviour may be that the Cu(2,3-Hpzdca)$(PPh_3)_2$ **2.18** complex in solution, like other 1,2-disubstituted acids, adopts the favourable cyclic arrangement *via* intramolecular hydrogen bonding, and this slows the process of losing the second proton making possible the isolation of the 1:1 adduct. In contrast, the structure of pyrazine-2,5-dicarboxylic acid prevents the formation of intramolecular hydrogen bonds, therefore both protons are equivalent and the isolation of 1:1 adduct was not possible.

The infrared spectrum of **2.18** confirms the formation of the 1:1 adduct, with strong asymmetric and symmetric carboxylate absorptions at 1626 and 1353 cm^{-1} respectively, in addition to an absorption at 1737 cm^{-1} corresponding to the carbonyl double bond of the protonated carboxylic acid group.

2.4 Conclusions

The crystal structures of eighteen novel copper(I) complexes with pyridine and pyrazine carboxylic acids and the re-determination at low temperature for compounds, Cu(3-pyca)(PPh_3)$_2$ and Cu(2,3-Hpydca)(PPh_3)$_2$, have been presented in this chapter.

Compounds Cu(2-pyca)(PPh_3)$_2$ and Cu(2-pzca)(PPh_3)$_2$ crystallise as the molecular structures Cariati predicted, forming monomeric complexes with five-membered chelate rings being coordinated to the metal ion through the nitrogen atom and the unidentate carboxylic group. Interestingly, the use of a varied range of solvent systems has allowed the crystallisation of Cu(2-pyca)(PPh_3)$_2$ solvates, **2.1**-**2.5**, displaying a solvent dependency not seen in compound Cu(2-pzca)(PPh_3)$_2$ **2.17**, where the change of solvent system only led to the isolation of two different, triclinic and monoclinic, polymorphic forms. Solvents such as, *n*-BuOH and *tert*-BuOH failed to produce Cu(2-pyca)(PPh_3)$_2$ solvate structures suggesting that these molecules are too large to comfortably fill the voids in the crystal lattice used by the smaller homologues. Therefore, the adjustability of the void size is probably a limiting factor determining which solvents can be accommodated.

Structural analysis of **2.1**-**2.5** shows that these structures are very flexible in order to accommodate the solvent molecules, the bond angles at the copper ion can take quite a range of values; *e.g.* P–Cu–P 116.66-136.05º. Solvates structures **2.1**-**2.5** exhibit similar (solvate)O–H···O(carboxylate) hydrogen-bonding motifs with comparable distances and angles.

Although compounds Cu(3-pyca)(PPh_3)$_2$ **2.6** and Cu(3-pyca)(PPh_3)$_2$·MeOH **2.7** pack in the crystalline state in one-dimensional chains as Cariati predicted, in the presence of EtOH, the formation of the chains is prevented and Cu(3-pyca)(PPh_3)$_2$·EtOH **2.8** packs as a zero-dimensional dimer; behaviour that was not predicted by Cariati. The modification of the solvent causes a variation in the hydrogen bonding array of the Cu(3-pyca)(PPh_3)$_2$ molecules, with the resulting solvates having zero-dimensional or one-dimensional architectures. Following on from the inclusion of solvent molecules into the lattices of Cu(2-pyca)(PPh_3)$_2$ and Cu(3-pyca)(PPh_3)$_2$, the incorporation of solvents such as, EtOH, *n*-PrOH, *i*-PrOH failed for Cu(4-pyca)(PPh_3)$_2$, only being

possible the isolation of $[Cu(PPh_3)_2$4-py(COO)$]_2$·2MeOH·0.765(4)MeOH·0.235(4)H_2O **2.9**. The poor solubility of Cu(4-pyca)$(PPh_3)_2$ in these solvents may be the reason for this failure.

The structures of compounds **2.10**-**2.14** could not be predicted from infrared spectroscopic evidence and from the trend seen in Cu(2,3-Hpyca)$(PPh_3)_2$ previously reported by Cariati.[50] These structures provide an insight into the structural diversity that these copper(I) complexes can exhibit.

Extensive hydrogen bonding exists in **2.10**-**2.14**, with the strong (carboxylic acid)O–H···O(carboxylate) hydrogen bond interaction present in all cases forming intramolecular *S*(7) graph set or one-dimensional zig-zag chains depending on the disposition of the carboxylic groups in the pyridine ring. The combination of this O–H···O interaction with weaker interactions involving molecules of solvent, varying geometries and substitution pattern of carboxylic acid of the pyridine carboxylic acids employed, has led to the creation of a range of supramolecular arrays, from zero-dimensional to two-dimensional supramolecular structures.

Cariati predictions also failed for compound Cu(2,3-Hpzdca)$(PPh_3)_2$ **2.18** which crystallises as a dimer through O–H···O hydrogen bonds instead of discrete units. Once more, the structure of compound **2.18** could not be predicted from infrared spectroscopic evidence.

The analysis of the compounds presented here provides information on the varied hydrogen bonding patterns they can adopt, which can only contribute to the current level of understanding in solid state structure prediction.

2.5 EXPERIMENTAL

Starting Materials

The starting materials (2-Hpyca, 3-Hpyca, 4-Hpyca, 2,3-H_2pydca, 2,4-H_2pydca, 2,5-H_2pydca, 2,6-H_2pydca, 3,4-H_2pydca, 2,5-H_2pydca, 2-Hpzca, 2,3-H_2pzdca, 2,5-H_2pzdca $Cu(SO_4)\cdot 6H_2O$, were purchased from commercial sources Aldrich, Lancaster, Avocado and Acros. All solvents were purchased from Aldrich, Fisher or Lancaster. CH_2Cl_2 was distilled from CaH_2 under nitrogen, and diethyl ether distilled from Na under nitrogen.

Physical Measurements

All NMR spectra were recorded in $CDCl_3$ unless otherwise stated. NMR spectra (^1H and ^{31}P) were obtained on a Bruker DPX-400 MHz operating at 400.13 MHz for ^1H with chemical shifts (δ) in ppm relative to $SiMe_4$ and operating at 161.98 MHz for ^{31}P with chemical shifts (δ) in ppm relative to 85% H_3PO_4. Infrared spectra were recorded as KBr disks in the range 4000 – 200 cm^{-1} on a Perkin-Elmer System 2000 Fourier transform spectrometer. Elemental analyses (Perkin-Elmer 2400 CHN elemental analyser) were carried out by the Loughborough University Analytical Service within the Department of Chemistry.

Syntheses

$Cu(PPh_3)_2(BH_4)$ 2.1 Hydrated copper(II) sulfate (1.500 g, 5.607 mmol; previously ground to a fine powder using a pestle and mortar) was added to a solution of triphenylphosphine (7.567 g, 28.84 mmol) in absolute ethanol (100 ml). The mixture was stirred and warmed on a hotplate for 15 min until all the copper(II) sulfate dissolved. Powdered sodium borohydride (1.498 g, 39.63 mmol) was added whilst carefully stirring for 1 h, until the effervescence stopped and precipitation was complete. The crude white solid product was filtered off and stirred with chloroform (75 ml). The mixture was filtered and the filtrate warmed to 50 ºC on a hot plate at which point absolute ethanol (75 ml) was added dropwise until the initial faint cloudiness became fine white crystals. The mixture was cooled and the product isolated. The white

crystals were washed with a small amount of diethylether and dried in air. Yield 2.741 g, 82%, mp 164-165 ºC (lit. 165-166 ºC).[97]

^{1}H NMR (400 MHz, $CDCl_3$) δ 7.70-7.23 (30*H*, m, ArH).
^{31}P NMR: δ -1.20 ppm.
Analysis calculated for $C_{36}H_{34}CuP_2B$: C, 71.71; H, 5.68. Found: C, 71.63; H, 5.54%.

Unless stated otherwise, the following method was used for the synthesis of all compounds presented in this chapter. To a stirring solution of $Cu(PPh_3)_2(BH_4)$ **2.1** in DCM was added either pyridine-*n*-carboxylic acid (*n* = 2, 3, 4), pyrazine-2-carboxylic acid, pyridine-2,*n*-dicarboxylic acid (*n* = 3–6) (0.5 eq.), pyridine-3,*n*-dicarboxylic acid (*n* = 4, 5) (0.5 eq.) or pyrazine-2,*n*-dicarboxylic acid (*n* = 3, 5) (0.5 eq.) respectively. The resulting mixtures were then refluxed for 3 h. The products were isolated by concentration of the reaction solution to ≈ 5 ml and precipitation of the solids through the addition of Et_2O (≈ 15 ml). The precipitates were washed with Et_2O and dried in air before storage in a desiccator containing silica gel.[50]

Compound Cu(2-pyca)$(PPh_3)_2$
Yield 0.4811 g, 89%.
IR υ_{max} (KBr)/cm^{-1} 3049 (Ar C-H), 1610 (asymm. CO_2^-), 1435 (C-O), 1382 (symm. CO_2^-), 841, 757 and 739 (Ar C-H).
^{1}H NMR (400 MHz, $CDCl_3$) δ 8.28 (1*H*, d, *J* 4 Hz), 7.91 (1*H*, d, *J* 2.4 Hz), 8.25 (1*H*, d, *J* 7.6 Hz) 7.09-7.63 (31*H*, m).
^{31}P NMR data: δ -2.08 ppm.
Analysis calculated for $C_{42}H_{34}NCuO_2P_2 \cdot H_2O$: C, 69.27; H, 4.98; N, 1.92. Found: C, 69.36; H, 4.93; N, 2.06%.

Compound Cu(2-pyca)$(PPh_3)_2$ was crystallised from different solvents, methanol, ethanol, *i*-propanol, *n*-propanol to yield the solvates **2.1**, **2.2**, **2.3** and **2.4** respectively, when *t*-butanol and *n*-butanol were used as crystallisation solvents, the same compound **2.5** was obtained.

Compound Cu(3-pyca)(PPh_3)$_2$

Yield 0.515 g, 88%.

IR υ_{max} (KBr)/cm^{-1} 3050 (Ar C-H), 1615 (asymm. CO_2^-), 1436 (C-O), 1383 (symm. CO_2^-), 843, 834, 757 and 739 (Ar C-H).

^{1}H NMR (400 MHz, $CDCl_3$) δ 9.22 (1*H*, bs), 8.60 (1*H,* bs), 8.25 (1*H*, d, *J* 7.6 Hz) 7.00-7.62 (31*H*, m).

^{31}P NMR data: δ -1.95 ppm.

Analysis calculated for $C_{42}H_{34}NCuO_2P_2 \cdot 0.5H_2O$: C, 70.15; H, 4.90; N, 1.95. Found: C, 70.17; H, 4.84; N, 1.88%.

Compound Cu(3-pyca)(PPh_3)$_2$ was crystallised from different solvents, such as methanol, ethanol to yield the solvates **2.6** and **2.7** respectively. When *i*-propanol, *n*-propanol, *t*-butanol and *n*-butanol were used as crystallisation solvents, the same compound **2.8** was obtained.

Compound Cu(4-pyca)(PPh_3)$_2$

Yield 0.497 g, 83%.

IR υ_{max} (KBr)/cm^{-1} 3050 (Ar C-H), 1609 (asymm. CO_2^-), 1435 (C-O), 1368 (symm. CO_2^-), 863, 838, 774 and 741 (Ar C-H).

^{1}H NMR (400 MHz, $CDCl_3$) δ 8.60 (2*H*, bs), 7.80 (2*H,* bs), 7.00-7.65 (30*H*, m).

^{31}P NMR data: δ -1.80 ppm.

Analysis calculated for $C_{42}H_{34}NCuO_2P_2 \cdot 0.5H_2O$: C, 70.15; H, 4.56; N, 1.95. Found: C, 70.46; H, 4.56; N, 1.74%.

X-ray quality crystals for compound **2.9** were grown by the slow evaporation of a solution of Cu(4-pyca)(PPh_3)$_2$ in methanol.

Compound Cu(2,3-Hpydca)(PPh_3)$_2$

Yield 0.494 g, 73%.

IR υ_{max} (KBr)/cm^{-1} 3051 (Ar C-H), 1697 (asymm. CO_2^-), 1432 (C-O), 1363 (symm. CO_2^-), 854, 838, 812 and 744 (Ar C-H).

^{1}H NMR (400 MHz, $CDCl_3$) δ 8.90 (1*H*, dd, *J* 1.6, 8.0 Hz), 8.14 (1*H,* dd*, J* 1.6, 5.2 Hz), 7.00-7.65 (31*H*, m).

^{31}P NMR data: δ 0.34 ppm.

Analysis calculated for $C_{43}H_{34}NCuO_4P_2$: C, 68.48; H, 4.54; N, 1.86. Found: C, 68.51; H, 4.76; N, 1.95%.

X-ray quality crystals for compound **2.10** were grown by the slow evaporation of a solution of Cu(2,3-Hpydca)$(PPh_3)_2$ in chloroform.

Compound Cu(2,4-Hpydca)$(PPh_3)_2$

Yield 0.542 g, 80%.

IR υ_{max} (KBr)/cm^{-1} 3050 (Ar C-H), 1716 (C=O, acid), 1621 (broad, asymm. CO_2^-), 1360 (symm. CO_2^-), 883, 813, 793 and 742 (Ar C-H).

^{1}H NMR (400 MHz, $CDCl_3$) δ 9.03 (1*H*, s), 8.05 (1*H,* d*, J* 4.0 Hz), 7.83 (1*H*, d, *J* 4.8 Hz) 7.60-7.07 (30*H*, m).

^{31}P NMR data: δ -0.34 ppm.

Analysis calculated for $C_{43}H_{34}NCuO_4P_2$: C, 68.48; H, 4.54; N, 1.86. Found: C, 68.36; H, 4.61; N, 2.04%.

X-ray quality crystals for compound **2.11** were grown by vapour diffusion of hexane into a chloroform solution of Cu(2,4-Hpydca)$(PPh_3)_2$.

Compound Cu(2,5-Hpydca)$(PPh_3)_2$

Yield 0.291 g, 52%.

IR υ_{max} (KBr)/cm^{-1} 3052 (Ar C-H), 1706 (C=O, acid), 1597 (asymm. CO_2^-), 1434 (C-O), 1365 (symm. CO_2^-), 884, 818, 781 and 744 (Ar C-H).

^{1}H NMR (400 MHz, $CDCl_3$) δ 7.00-7.68 (33*H*, m).

^{31}P NMR data: δ 3.25 ppm.

Analysis calculated for $C_{43}H_{34}NCuO_4P_2$: C, 68.48; H, 4.54; N, 1.86. Found: C, 68.52; H, 4.99; N, 1.80%.

X-ray quality crystals of solvate **2.12** were grown from slow evaporation of a methanol solution of Cu(2,5-Hpydca)$(PPh_3)_2$. X-ray quality crystals for compound **2.13** were grown by vapour diffusion of hexane into a chloroform/methanol solution of Cu(2,5-Hpydca)$(PPh_3)_2$.

Compound Cu(2,6-Hpydca)(PPh_3)$_2$

Yield 0.238 g, 94%.

IR υ_{max} (KBr)/cm^{-1} 3052 (Ar C-H), 1696 (broad, asymm. CO_2^-), 1432 (C-O), 1373 (symm. CO_2^-), 896, 880, 849, 797 and 742 (Ar C-H).

^{1}H NMR (400 MHz, $CDCl_3$) δ 8.17 (2*H*, bs), 6.70-7.61 (31*H*, m).

^{31}P NMR data: δ -1.27 ppm.

Analysis calculated for $C_{43}H_{34}NCuO_4P_2$: C, 68.48; H, 4.54; N, 1.86. Found: C, 68.16; H, 4.95; N, 1.80%.

X-ray quality crystals for compound **2.14** were grown from recrystallisation of Cu(2,6-Hpydca)(PPh_3)$_2$ in the minimum amount of methanol.

Compound Cu(3,4-Hpydca)(PPh_3)$_2$

Yield 0.257 g, 71%.

IR υ_{max} (KBr)/cm^{-1} 3051 (Ar C-H), 1650 (broad, asymm. CO_2^-), 1434 (C-O), 1361 (symm. CO_2^-), 849, 809 and 742 (Ar C-H).

^{1}H NMR (400 MHz, $CDCl_3$) δ 8.33 (1*H*, d, *J* 5.2 Hz), 8.07 (1*H,* d*, J* 5.2 Hz), 7.54-7.07 (31*H*, m).

^{31}P NMR data: δ -0.54 ppm.

Analysis calculated for $C_{43}H_{34}NCuO_4P_2$: C, 68.48; H, 4.54; N, 1.86. Found: C, 68.37; H, 4.13; N, 1.84%.

X-ray quality crystals for compound **2.15** were grown by vapour diffusion of diethyl ether into a dichloromethane solution of Cu(3,4-Hpydca)(PPh_3)$_2$.

Compound Cu(3,5-Hpydca)(PPh_3)$_2$

Yield 0.514 g, 85%.

IR υ_{max} (KBr)/cm^{-1} 3048 (Ar C-H), 1650 (broad, asymm. CO_2^-), 1434 (C-O), 1372 (symm. CO_2^-), 878, 820, 794 and 743 (Ar C-H).

^{1}H NMR (400 MHz, $CDCl_3$) δ 9.20 (2*H*, bs), 8.82 (1*H,* t*, J* 1.8 Hz), 7.62-7.23 (30*H*, m).

^{31}P NMR data: δ -1.95 ppm.

Analysis calculated for $C_{43}H_{34}NCuO_4P_2$: C, 68.48; H, 4.54; N, 1.86. Found: C, 68.46; H, 4.49; N, 1.89%.

X-ray quality crystals for compound **2.16** were grown from recrystallisation of Cu(3,5-Hpydca)(PPh_3)$_2$ in the minimum amount of methanol.

Compound Cu(2-pzca)(PPh_3)$_2$

Yield 0.435 g, 74%.

IR υ_{max} (KBr)/cm^{-1} 3050 (Ar C-H), 1645 (asymm. CO_2^-), 1433 (C-O), 1343 (symm. CO_2^-), 865, 839, 792 and 748 (Ar C-H).

^{1}H NMR (400 MHz, $CDCl_3$) δ 9.47 (1*H*, d, *J* 1.6 Hz), 8.43 (1*H*, d, *J* 2.8 Hz), 7.77 (1*H*, dd, *J* 2.8, 1.6 Hz), 7.62-7.11 (30*H*, m).

^{31}P NMR data: -0.23 ppm.

Analysis calculated for $C_{41}H_{33}N_2O_2P_2Cu$: C, 69.24; H, 4.68; N, 3.94. Found: C, 68.98; H, 4.63; N, 3.72%.

X-ray quality crystals for compound **2.17** were grown by vapour diffusion of hexane into a chloroform solution of Cu(2-pzca)(PPh_3)$_2$.

Compound Cu(2,3-Hpzdca)(PPh_3)$_2$

Yield 0.226 g, 64%.

IR υ_{max} (KBr)/cm^{-1} 3053 (Ar C-H), 1737 (C=O, acid), 1626 (asymm. CO_2^-), 1434 (C-O), 1353 (symm. CO_2^-), 871, 844, 794 and 748 (Ar C-H).

^{1}H NMR (400 MHz, $CDCl_3$) δ 8.78 (1*H*, bs), 8.27 (1*H*, bs), 7.70-7.01 (30*H*, m).

^{31}P NMR data: 1.31 ppm.

Analysis calculated for $C_{41}H_{33}N_2O_2P_2Cu$: C, 66.80; H, 4.40; N, 3.71. Found: C, 66.48; H, 4.06; N, 3.67%.

X-ray quality crystals for compound **2.18** were grown by vapour diffusion of hexane into a chloroform solution of Cu(2,3-Hpzdca)(PPh_3)$_2$.

Compound Cu_2(2,3-pzdca)(PPh_3)$_4$

Yield 0.448 g, 73%.

IR υ_{max} (KBr)/cm^{-1} 1715 (broad, asymm. CO_2^-), 1445 (C-O), 1356 (symm. CO_2^-), 869, 835, 792 and 746 (Ar C-H).

^{1}H NMR (400 MHz, $CDCl_3$) δ 7.00-7.60 (62*H*, m).

^{31}P NMR data: 1.44 ppm.

Analysis calculated for $C_{42}H_{33}N_2O_4P_2Cu$: C, 66.80; H, 4.40; N, 3.71. Found: C, 66.21; H, 4.44; N, 3.80%.

X-ray quality crystals for compound **2.19** were grown by slow evaporation of a solution of Cu_2(2,3-pzdca)$(PPh_3)_4$ in chloroform.

Compound Cu_2(2,5-pzdca)$(PPh_3)_4$

Yield 0.124 g, 73%.

IR υ_{max} (KBr)/cm^{-1} 3050 (Ar C-H), 1641 (asymm. CO_2^-), 1434 (C-O), 814 and 742 (Ar C-H).

^{1}H NMR (400 MHz, $CDCl_3$) δ 8.78 (2*H*, s), 7.00-7.63 (60*H*, m).

^{31}P NMR data: 0.34 ppm.

Analysis calculated for $C_{78}H_{62}N_2O_4P_4Cu_2 \cdot 2MeOH \cdot CH_2Cl_2$: C, 65.23; H, 4.87; N, 1.88. Found: C, 65.62; H, 4.95; N, 2.17%.

X-ray quality crystals for compound **2.20** were grown by vapour diffusion of diethyl ether into a dichloromethane solution of Cu_2(2,5-pzdca)$(PPh_3)_4$.

2.6 Crystallographic Experimental

Data for compounds **2.1-2.13**, **2.16**, **2.17**, **2.19** and **2.20** were collected using a Bruker SMART 1000 CCD diffractometer using graphite-monochromated Mo-K_α radiation (λ = 0.71073 Å). Data for compounds **2.14** and **2.15** was collected using a Bruker APEX 2 CCD diffractometer using synchrotron radiation (λ = 0.8457 Å) at Daresbury SRS Station 16.2SMX. Data for compound **2.18** was collected using a Bruker APEX 2 CCD diffractometer using synchrotron radiation (λ = 0.6910 Å) at Daresbury SRS Station 9.8. Data for compound **2.21** was collected using a Bruker-Nonius 95 mm CCD camera on κ-goniostat diffractometer using graphite-monochromated Mo-K_α radiation (λ = 0.71073 Å).

All structures were solved by direct methods (except structures **2.3**, **2.4**, **2.10**, **2.11**, **2.14** and **2.20** which were solved using Patterson synthesis) and refined by full-matrix least-squares methods on F^2, producing CIF files which have been checked using the IUCr CheckCif routines. All *H* atoms, except water *H* atoms, were initially placed in geometrically calculated positions and were refined using a riding model (aryl C–H 0.95 Å, methyl C–H 0.98 Å, methylene C–H 0.99 Å, methine C–H 1.00 Å and hydroxyl O–H 0.84 Å). $U_{iso}(H)$ values were set to be 1.2 times U_{eq} of the carrier atom for aryl C*H*, methylene and methine C*H*, and 1.5 times U_{eq} of the carrier atom for O*H* and CH_3. Water *H* atoms in **2.12** were located in the difference Fourier map and the coordinates allowed to freely refine, however water *H* atoms could not be located in **2.9**. The coordinates of O*H* hydrogen atoms in compounds **2.4**, **2.6**, **2.7**, **2.10** and **2.19** were then allowed to refine freely.

Unless stated, all structural determinations proceeded without the need for further restraints or disorder modelling.

Compound **2.1** was found to contain a disordered methanol molecule with the C–O fragment modelled over two sets of positions, with refined occupancies major:minor = 74.7(5):25.3(5)%. The solvent *H* atom for the minor component was not located in the difference Fourier map.

Disorder in one of the two ethanol molecules in the asymmetric unit was modelled in compound **2.2**. The C_2H_5 fragment was modelled over two sets of positions, with refined occupancies 56.8(9):43.2(9)% with O(6) common to the two fragments. Compound **2.3** was found to contain a disordered phenyl ring, which was modelled over two sets of positions 59.7(9):40.3(9)%. It also contains a highly disordered ethanol molecule which was modelled over three sets of positions 55.7(6):28.9(6):15.4(6)% with O*H* group coincident. The ethanolic H(6) atom was located in the difference Fourier map and coordinates allowed to freely refine. The remaining O*H* hydrogen atom was placed in a geometrical position.

Compound **2.9** was found to contain disorder in methanol and water molecules involving only two of the possible three molecules in the structure. While methanol molecule C(87)–O(7)–H(7A) is not disordered, it was found to have either C(85)–O(5)–H(5) and C(86)–O(6)–H(6) for 76.5% of the time or C(85X)–O(5)–H(5) and O(7) for 23.5% of the time. The methanolic H(5) atom was located in the difference Fourier map and the coordinates allowed to freely refine. The remaining O*H* hydrogen atoms were placed in geometric positions.

Compound **2.11** was found to contain a disordered chloroform molecule with the Cl and H atoms modelled over two sets of positions, with refined occupancies 62.1(6):37.9(6)% with C(88) common to the two fragments. The disordered chloroform molecule in compound **2.13** was modelled over two sets of positions 69.2(3):30.8(3)%.

Water *H* atoms in compound **2.14** were located in the difference Fourier map and the coordinates allowed to freely refine, however hydrogen atoms were not located on the water molecule containing O(11) which also presents disorder but no satisfactory model could be found. Compound **2.14** showed a disordered phenyl ring, which was modelled over two sets of positions 50.1(11):49.9(11)%. *H* atoms were not found on the disordered MeOH molecule in **2.20** which was modelled over two sets of positions 54.0(19):46(19)%.

Programs used during data collection, data reduction, refinement and production of graphics were Bruker SMART, Bruker APEX 2, SAINT, SHELXTL and local programs.[25,26,28,121-123]

Chapter 3

Novel Crystal Engineering Studies Using Boronic Acids

3. Novel Crystal Engineering Studies Using Boronic Acids

3.1 Introduction

Boronic acids continue to receive widespread attention for their versatile behaviour in diverse areas such as organic synthesis, catalytic transformations, as fire retardants, as chemosensors for the recognition of carbohydrates and as therapeutic agents for Boron Neutron Capture Therapy.[124-133] An area of particular current interest is the use of boronic acids as building blocks for the design of novel solid-state architectures utilising hydrogen bonds or *via* covalent interactions when used directly as a ligands.[134-136]

The most common hydrogen bond motif formed by boronic acids [Figure 3.1 (**I**)] is very similar to the cyclic head-to-tail carboxylic acid ring motif $R^2_2(8)$ [Figure 3.1 (**II**)]. The energies of the carboxylic and boronic acid dimers are also comparable (-19.3 kcal/mol and -53.9 kJ/mol respectively).[137]

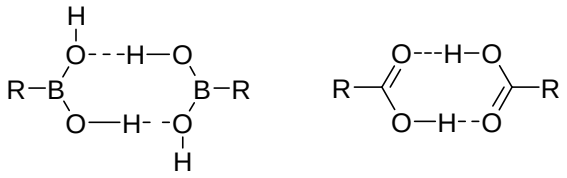

I **II**

Figure 3.1 (I) Dimers of boronic acids. **(II)** The $R^2_2(8)$ cyclic hydrogen bonded carboxylic acid ring motif.

The two additional hydrogen atoms in boronic acid dimers allow the interaction of homodimeric units in the solid state through hydrogen bonding, which is not available to carboxylic acid dimers. An example of this type of connectivity is shown by 2-bromophenylboronic acid where each dimer is interacting with other dimers by hydrogen bonds forming ribbons generating the hydrogen bonding motif **III** (Figure 3.2).[138]

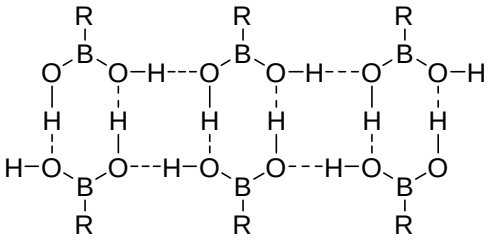

III

Figure 3.2 Schematic representation of the homodimeric 2-bromophenylboronic acid dimers in the solid state [R = 2-BrPh–].

The R–$B(OH)_2$ moiety adopts mainly three different conformations, as shown in Figure 3.3, which yield different hydrogen-bonding networks. Among these arrangements, while the syn-anti conformation is observed in a majority of structures, the syn-syn and anti-anti conformations are relatively uncommon.[139]

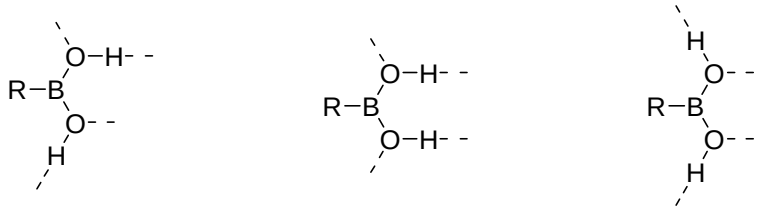

syn, anti syn, syn anti, anti

Figure 3.3 Conformations of the –$B(OH)_2$ moiety.

Due to the close similarity between the –$B(OH)_2$ and –COOH groups, efforts have been made to synthesise the hetero-dimeric hydrogen-bonded motifs (Figure 3.4).

IV **V**

Figure 3.4 Schematics of the hetero-dimeric boronic acid-carboxylate **IV** and boronic acid-carboxylic acid **V** motifs.

Rodríguez-Cuamatzi and co-workers studied the hydrogen bonding interaction energies for the homo- and hetero-dimers **I**, **II**, **IV** and **V**.[137] The results show that the stability of these systems decrease in the following order: $RB(OH)_2\cdots^{-}OOCR$ (**IV**) > $RCOOH\cdots HOOCR$ (**II**) > $RB(OH)_2\cdots HOOCR$ (**V**) > $RB(OH)_2\cdots(OH)_2BR$ (**I**), where R = Me, Ph. The robust boronic acid-carboxylate synthon **IV** is also capable of competing successfully with strong interactions such as the charge assisted $N–H^{+}\cdots O^{-}$ hydrogen bond.[140] Although the hetero-dimeric $RB(OH)_2\cdots^{-}OOCR$ system presents an interesting alternative to the use of carboxylic acid dimers in supramolecular synthesis and crystal engineering, only a few literature examples have been described making it an interesting target for study.[141]

The $RB(OH)_2\cdots^{-}OOCR$ (**IV**) interaction has also been reported as a highly efficient carrier system for the transport of amino acids from neutral aqueous solutions across organic media.[142] It is based on the synergistic action of arylboronic acids/crown ethers, which bind the carboxylate and ammonium moieties, respectively, the zwitterionic form of amino acids being lipophilised by formation of a three-component supramolecular species (Figure 3.5).

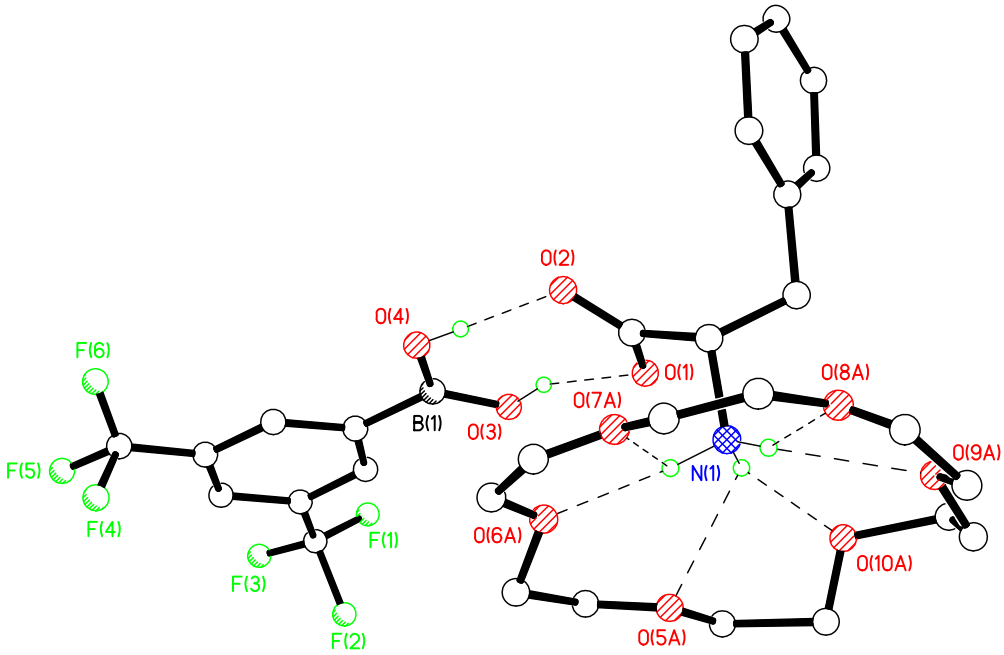

Figure 3.5 Molecular structure of the three-component system.

A search of the CSD (version 5.30, plus 4 updates, November 2008) shows a recent increase of attention toward the use of boronic acids in supramolecular chemistry. Interestingly, many of these supramolecular systems containing boronic acids do not contain any transition metal complexes.[137,143] This is rather surprising given the unique ability to tune various properties of transition metal complexes by ligand manipulation thereby influencing factors such as metal oxidation state, coordination numbers, solubility and charge. Literature examples of supramolecular work utilising boronic acids in the design of organometallic assemblies are presented below.

3.1.1 Boronic Acids in the Design of Metal Containing Supramolecular Assemblies

A recent approach whereby transition metals have been investigated, includes the organometallic studies with ferrocene-derived boronic acids, $[Fe\{\eta^5\text{-}C_5H_4(B(OH)_2\}_2]$ and $[Fe(\eta^5\text{-}C_5H_4\text{-}4\text{-}C_5H_4N)\{\eta^5\text{-}C_5H_4\text{-}(B(OH)_2\}_2]$, reported by Braga and co-workers.[144] Ferrocene-1,1'-diboronic acid, $[Fe\{\eta^5\text{-}C_5H_4(B(OH)_2\}_2]$, was prepared following a reported procedure from 1,1'-dilithioferrocene and tri-*n*-butyl borate, followed by hydrolysis of the resulting dibutylboronate.[145] In the X-ray structure of $[Fe\{\eta^5\text{-}C_5H_4(B(OH)_2\}_2]$ the two boronic acid groups bridge adjacent ferrocenyl moieties into chains through the boronic acid $R^2_2(8)$ dimer. These chains criss-cross in the crystal structure creating a two-dimensional corrugated sheet arrangement *via* lateral hydrogen bonding with $-B(OH)_2$ moieties adopting *anti* conformation producing $R^6_6(16)$ ring motifs (Figure 3.6).

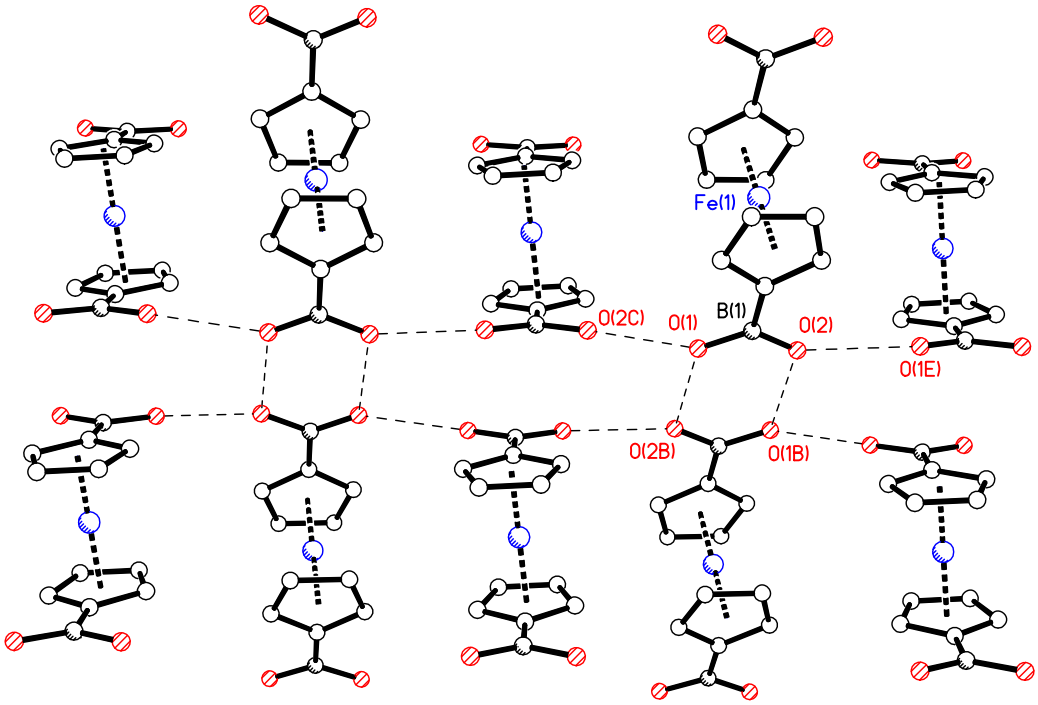

Figure 3.6 View of the sheet structure of [Fe{η^5-C_5H_4($B(OH)_2$}$_2$].

The simultaneous presence of one boronic acid group and one pyridyl group in the compound [Fe(η^5-C_5H_4-4-C_5H_4N){η^5-C_5H_4-($B(OH)_2$}$_2$] generates several supramolecular bonding options for this molecule. The –$B(OH)_2$ unit is capable of multiple hydrogen bonding donations as seen above with [Fe{η^5-C_5H_4($B(OH)_2$}$_2$], and the pyridyl ligand can donate an electron pair to a suitable Lewis acid or act as a hydrogen bond acceptor from a suitable proton donor. Compound [Fe(η^5-C_5H_4-4-C_5H_4N){η^5-C_5H_4-($B(OH)_2$}$_2$] has been shown, by single X-ray analysis, to form three different forms depending on the crystallisation conditions. Single crystals of the anhydrous form **A** were obtained by slow evaporation of a dichloromethane-methanol solution of 1'-(4-pyridyl)ferrocene-1-boronic acid at low temperature. Interestingly, the $R^2_2(8)$ head-to-tail boronic acid dimer is not found in **A** (Figure 3.7); in its place the ferrocenyl moieties form dimers *via* strong O–H···N interactions. The dimers are linked in a secondary pattern by single lateral O–H···N hydrogen bonds.

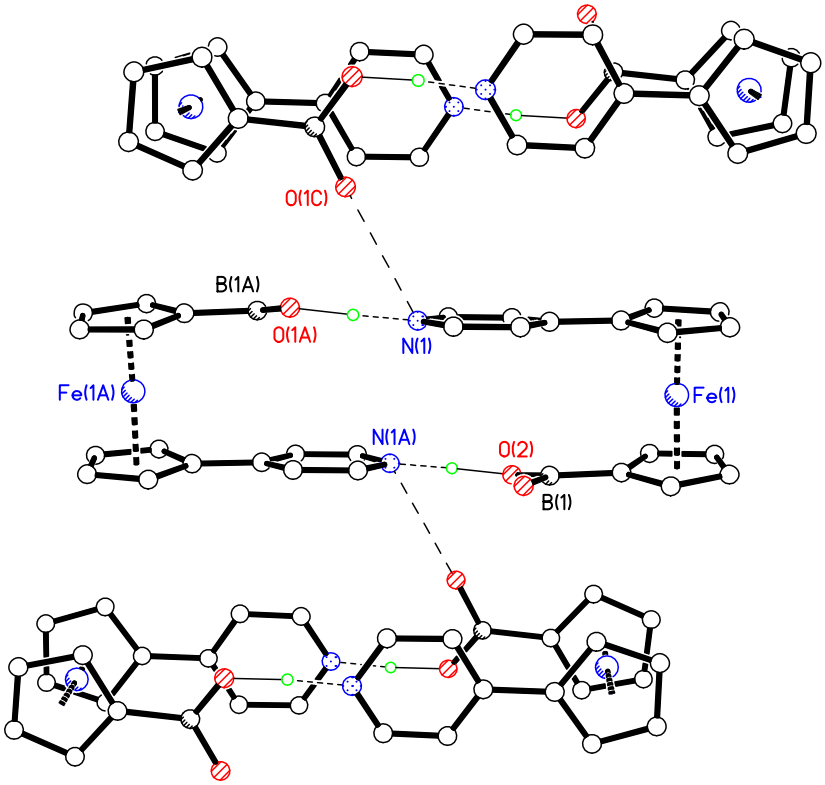

Figure 3.7 View of [Fe(η^5-C_5H_4-4-C_5H_4N){η^5-C_5H_4-$(B(OH)_2\}_2$] as the anhydrous form **A**.

Monohydrated form **B** was obtained by slow evaporation at room temperature from a solution of [Fe(η^5-C_5H_4-4-C_5H_4N){η^5-C_5H_4-$(B(OH)_2\}_2$] in acetone-water. In form **B**, the primary motif is the $R^2_2(8)$ boronic acid dimer based on O–H···O intermolecular bonds, while dimers are formed through O–H···N interactions between the lateral O–H groups and the pyridyl acceptors (Figure 3.8). Although compound **B** is a hydrated form, the water molecules do not seem to play any particular role in the packing.

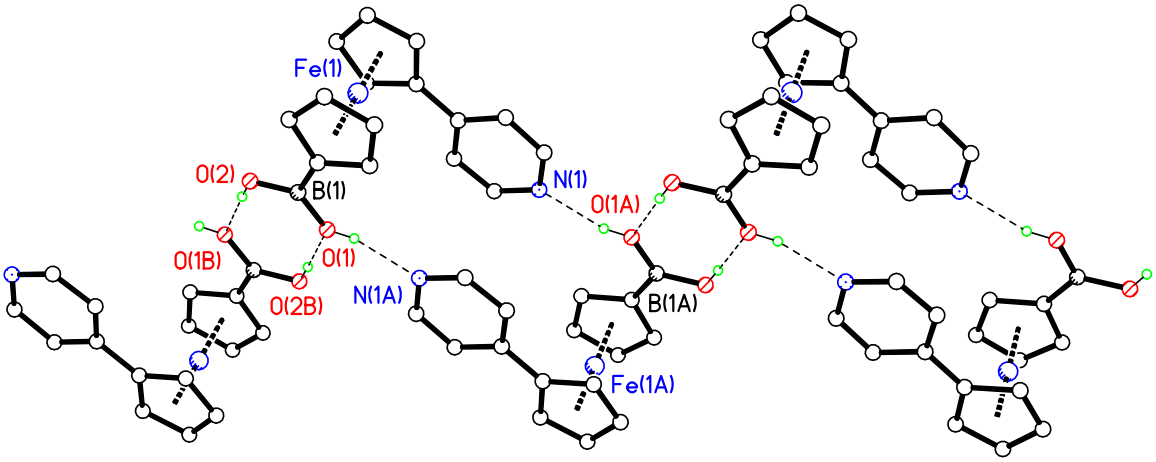

Figure 3.8 View of the zigzag chain structure of form **B**. Water molecules have been omitted for clarity.

Finally, form **C**, which is obtained from the slow evaporation of a solution of [Fe(η^5-C_5H_4-4-C_5H_4N){η^5-C_5H_4-$(B(OH)_2\}_2$] in acetone-$NH_{3(aq)}$ at low temperature, has an almost intermediate topology between the two forms described above. Although the molecules adopt the conformation seen in **B**, based on O–H···O interactions forming $R^2_2(8)$ boronic acid rings, there are also lateral O–H···O bonds, previously seen in **A** leading to a complex two-dimensional pattern (Figure 3.9).

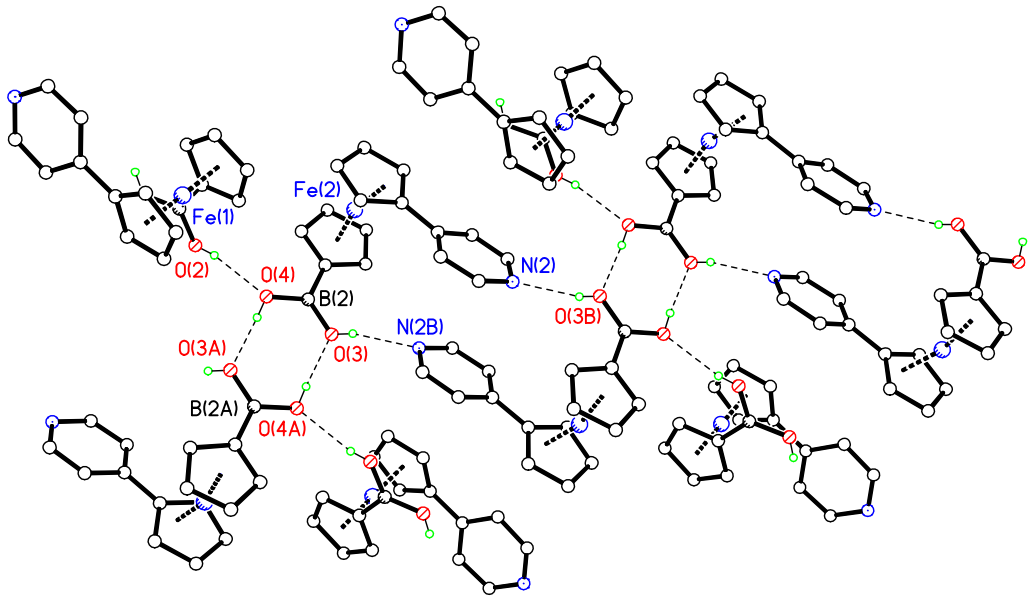

Figure 3.9 View of [Fe(η^5-C_5H_4-4-C_5H_4N){η^5-C_5H_4-$(B(OH)_2\}_2$] as form **C**.

Batsanov and Norrild have independently investigated two other interesting examples of ferrocene derived boronic acids.[146,147] Both authors synthesised aminoarylboronic acid systems based on a ferrocene framework in which the formation of an intramolecular hydrogen bond, which determines the orientation of the ferrocene substituents, seems to prevail over a conceivable B–N bond. This observed behaviour may allow these two functional groups to act cooperatively in potential catalytic processes, including the important area of *in situ* direct amide formation from amines and carboxylic acids.[148]

Recently, SeethaLekshmi and Pedireddi crystallised the first examples of metal hybrids of (4-carboxyphenyl)boronic acid with Mn(II), Co(II) and Ni(II).[149] The failure to form complexes between phenylboronic acid and transition metals ions was also highlighted. Using a substituted phenylboronic acid containing a carboxylate functional group, the desired complexes were obtained: compounds $[Co(H_2O)_6]^{2+}\cdot 4H_2O\cdot 2\{C_6H_4[B(OH)_2]4\text{-}CO_2^-\}$, $[Mn(H_2O)_6]^{2+}\cdot 4H_2O\cdot 2\{C_6H_4[B(OH)_2]4\text{-}CO_2^-\}$ and $[Ni(H_2O)_6]^{2+}\cdot 4H_2O\cdot 2\{C_6H_4[B(OH)_2]4\text{-}CO_2^-\}$ are isomorphic and isostructural. Analysis of the molecular arrangement of these compounds reveals that the (4-carboxyphenyl)boronic acid is not covalently coordinated to the metal ions. Instead, the metal centres are coordinated to six water molecules. The water molecules of crystallisation maintain an extensive hydrogen array through hydrogen bond interactions with the (4-carboxyphenyl)boronic acid (Figure 3.10).

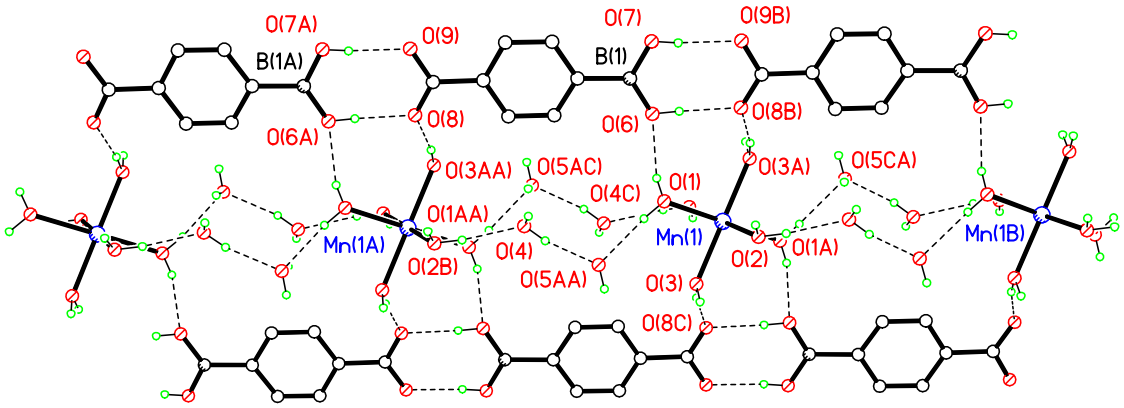

Figure 3.10 View of $[Mn(H_2O)_6]^{2+}\cdot 4H_2O\cdot 2\{C_6H_4[B(OH)_2]4\text{-}CO_2^-\}$.

Kara and co-workers utilised isomeric pyridinium boronic acid cations, (Figure 3.11), in the crystallisation of a series of salts with the square-planar metal bis-dithiooxalate

dianions $[M(S_2C_2O_2)_2]^{2-}$ (where M = Cu, Ni, Pd and Pt).[150] The use of **VI** and **VII** allowed for the importance of the geometry of the hydrogen bond donor groups in the design of different supramolecular architectures to be probed.

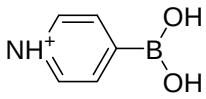

VI

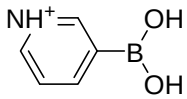

VII

Figure 3.11 4-pyridinium boronic acid cation, $[C_5H_4B(OH)_24\text{-}NH]^+$ **(VI)** and 3-pyridinium boronic acid cation, $[C_5H_4B(OH)_23\text{-}NH]^+$ **(VII)**.

Crystals of $[C_5H_4B(OH)_24\text{-}NH]_2[M(S_2C_2O_2)_2]\cdot 2H_2O$ (where M = Cu, Ni, Pd and Pt) are isostructural and isomorphous. The cations $[C_5H_4B(OH)_24\text{-}NH]^+$ **VI** are linked in pairs through strong hydrogen bonds between their boronic acid moiety and two water molecules forming $R^3_3(8)$ motifs. The planar dianions $[M(S_2C_2O_2)_2]^{2-}$ are hydrogen bonded by a N^+–H···O interaction at both ends creating two $R^2_1(5)$ synthons. As a result, a neutral hydrogen bonded ribbon is formed (Figure 3.12).

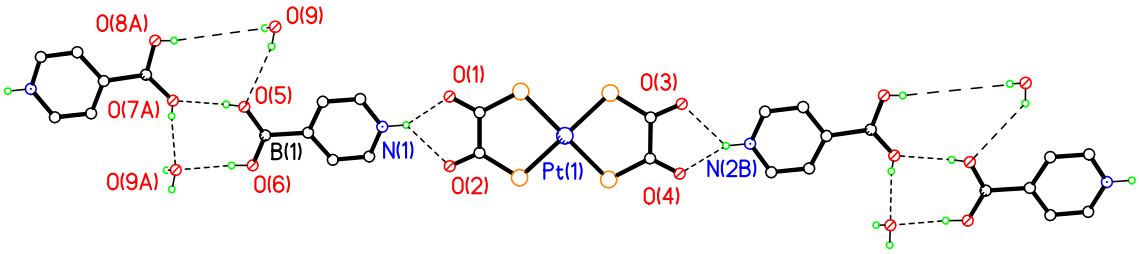

Figure 3.12 View of $[C_5H_4B(OH)_24\text{-}NH]_2[Pt(S_2C_2O_2)_2]\cdot 2H_2O$.

In contrast, isostructural salts of the isomeric cation **VII**, $[C_5H_4B(OH)_23\text{-}NH]_2[M(S_2C_2O_2)_2]$ (where M = Cu, Ni, Pd and Pt), crystallise as solvent-free structures. The boronic acid groups are involved in O–H···O hydrogen bonding with the thiocarboxylate moieties (through the carboxylate oxygen atoms) of neighbouring molecules, generating the expected head-to-tail $R^2_2(8)$ dimer for boronic acids in the *syn* conformation.[137,139,140] The pyridinium ion forms the N^+–H···O interaction with the

carboxylate oxygen atoms as seen previously. The resulting one-dimensional structure has large $R^8_6(18)$ ring motifs and a stepped chain appearance (Figure 3.13).

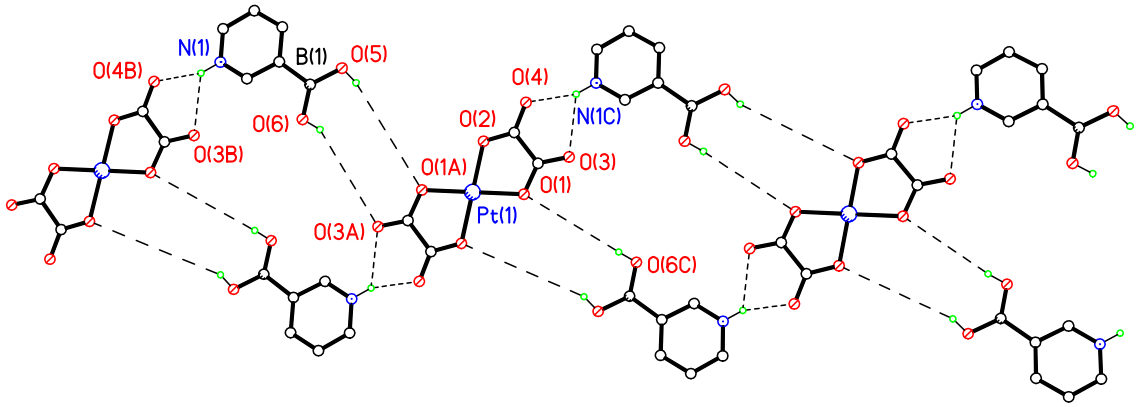

Figure 3.13 View of $[C_5H_4B(OH)_23\text{-}NH]_2[Pt(S_2C_2O_2)_2]$.

Other notable examples where the boric acid is used as a template to synthesise zincophosphates under hydrothermal conditions have been independently described by Zhong and Wiebcke.[151,152] In both examples, the trigonal planar boric acid molecules form centrosymmetric dimers by strong hydrogen bonding interactions linking two adjacent zincophosphate layers into a two-dimensional network. It is important to note the critical role of boric acid in the growth and stabilisation of these compounds as no crystals were obtained of the reaction product in the absence of $B(OH)_3$.

3.1.2 Uses of Boronic Acids

Boronic acids have been used in the field of medicinal chemistry as boron neutron capture (BNCT) therapy agents,[153] for the development of enzyme inhibitors like protease inhibitors,[154] antibody mimics for polysaccharides,[155] and as antibacterial agents.[156] Boron neutron capture therapy is a binary methodology for treating tumours in which a chemical agent containing at least one ^{10}B atom and thermal or isothermal neutrons are directed to a tumour where they combine to release a lethal dose of radiation to the cell. The development of ^{10}B-containing compounds for the treatment of tumours by BNCT requires the synthesis and evaluation of non-toxic agents that selectively target malignant cells rather than adjacent normal tissue and are retained intracellulary. Hatanaka and Mishima independently reported the first clinical results

demonstrating the effectiveness of this binary system, for the treatment of malignant gliomas and melanoma, respectively, using sodium mercaptoundecahydrododecaboronate ($Na_2B_{12}H_{11}SH$) and L-*p*-boronophenylalanine (L-*p*-BPA). More recently, *second generation* boron compounds, initially provided by DuPont Co., have been shown to cure a particular type of gliomas, and further research is ongoing in this field.[128,157]

Boronic acid-containing molecules have been utilised as chemosensors for the recognition of carbohydrates as they are known to reversibly bind diols with high affinity to form cyclic esters.[158]. There has been much interest focused on the design of boronic acid-containing fluorescent glucose sensors that operate under physiological conditions.[159-161] Gamsey and Cordes have highlighted the use of bidentate binding with diboronic acids to increase the selectivity toward glucose over other physiologically significant monosaccharides, such as fructose, and develop a successful *in vivo* boronic acid-based glucose sensor.[162,163] The spacing between the boronic acids could be adjusted through synthetic modifications in order to create a glucose-specific binding pocket.[131]

The uses of boronic acids are renowned in organic synthesis,[164,165] especially covering a number of cross-coupling reactions.[166,167] Parry and co-workers have described the syntheses of heteroaryl-substituted pyridines through the derivation of air-stable pyridylboronic acids under Suzuki cross-coupling conditions.[168] Recently, Liebeskind and Srogl developed a novel carbon–carbon cross-coupling protocol, involving the Pd(0)-catalysed, Cu(I)-mediated coupling of a variety of different thio-compounds with boronic acids under neutral conditions.[169-171] The Liebeskind-Srogl cross-coupling protocol can also be applied to cyclic thioureas and thioamides.[172] Recently, Billingsley and Buchwald have successfully developed a highly active catalyst system for the Suzuki-Miyaura cross-coupling of heteroaryl boronic acids and esters using dialkyl phosphine ligands.[173]

In recent years, boronic acids have also been used as building blocks in crystal engineering.[140,141] Following these studies, the main scope of the present chapter concentrates on obtaining and characterising new co-crystal systems including a range of boronic acids, $–R(OH)_2$, aiming to contribute to the understanding of less common

hydrogen bonding functionalities such as $RB(OH)_2\cdots^{-}OOCR$ (**IV**). This could provide alternatives, in terms of robustness and transferability, to the strong hydrogen bonding groups usually employed to link organometallic building blocks in molecular crystals.

3.2 Results and Discussion

3.2.1 Co-crystallisation of $Cu(2\text{-pyca})(PPh_3)_2$, $Cu(2\text{-pzca})(PPh_3)_2$ and $Cu_2(2,5\text{-pzdca})(PPh_3)_4$ with Boric Acid

The range of copper(I) complexes discussed in Chapter II shows interesting supramolecular behaviour linking complexes together either *via* hydrogen bonds using the non-coordinated carboxylic acid groups in pyridine and pyrazine carboxylates or through hydrogen bonding interactions with suitable solvent molecules of crystallisation. In one occurrence during the previous studies, compound $Cu(2\text{-pyca})(PPh_3)_2{\cdot}B(OH)_3$ **3.1** was isolated as X-ray quality single crystals from the reaction of 2-Hpyca with $(PPh_3)_2Cu(BH_4)$ in a mixture of dichloromethane and *tert*-BuOH (Figure 3.14). Boric acid may have been derived from the hydrolysis of borane BH_3, a by-product of the reaction, or borohydride in the presence of trace amounts of water.

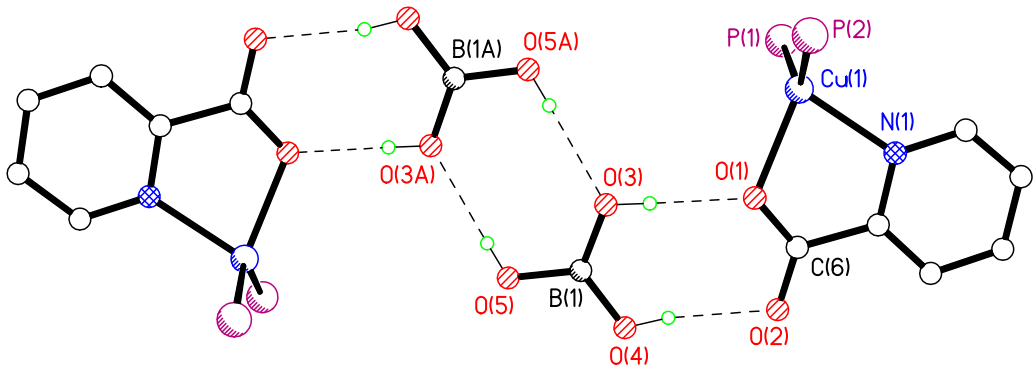

Figure 3.14 Dimers of $Cu(2\text{-pyca})(PPh_3)_2{\cdot}B(OH)_3$ **3.1**. Phenyl groups and hydrogen atoms not involved in hydrogen bonding have been removed for clarity.

In the crystal structure of $Cu(2\text{-pyca})(PPh_3)_2{\cdot}B(OH)_3$ **3.1**, two symmetry related boric acids in the *syn* conformation bridge adjacent $Cu(2\text{-pyca})(PPh_3)_2$ moieties into dimers through two different centrosymmetric head-to-tail $R^2_2(8)$ hydrogen bond motifs (Table 3.1). It is notable that the Etter system does not differentiate between them.[18,19] Although boric acid is capable of multiple hydrogen bonding donations,[174] in compound **3.1** the threefold symmetry of the $B(OH)_3$ molecule is destroyed by the strong O–H···O hydrogen bonding with the carboxylate oxygen atoms which limits the dimensionality

of the packing of the complex. Therefore, **3.1** is essentially zero-dimensional as no further propagation of hydrogen bonds is possible here.

Table 3.1 Selected hydrogen bonding parameters for **3.1**.

D–H···A	D···A/Å	D–H/Å	H···A/Å	D–H···A/º
O(3)–H(3)···O(1)	2.6701(15)	0.80(2)	1.88(2)	174(2)
O(4)–H(4)···O(2)	2.8120(18)	0.82(3)	2.00(3)	171(3)
O(5)–H(5)···O(3A)^{i}	2.818(2)	0.76(3)	2.06(3)	175(3)

Symmetry operation: ^{i}-x+1, -y+2, -z+1.

The intentional synthesis of the 1:1 Cu(2-pyca)$(PPh_3)_2 \cdot B(OH)_3$ adduct, **3.1**, was achieved upon adding a stoichiometric amount of boric acid to the reaction mixture (Equation 3.1). Due to the poor solubility of boric acid in CH_2Cl_2, the reaction was carried out in a mixture of dichloromethane and *tert*-BuOH. While at room temperature the reaction was complete after 48 h (analysis of the bulk material, by IR spectroscopy, obtained after 4, 12 and 24 h showed the presence of starting material), heating the mixture under reflux considerably shortened the reaction time (about 4 h). Crystals of compound **3.1** were isolated after slow evaporation of the saturated solution. The alcohol was also carefully chosen as competition could occur between small alcohols: MeOH, EtOH, *i*-PrOH and *n*-PrOH, and boric acid in the co-crystallisation with the copper(I) complex Cu(2-pyca)$(PPh_3)_2$ as seen previously in Chapter II.

$$\text{Cu(2-pyca)(PPh}_3)_2 + \text{B(OH)}_3 \xrightarrow[\text{CH}_2\text{Cl}_2/^t\text{BuOH}]{\text{Reflux}} \text{Cu(2-pyca)(PPh}_3)_2 \cdot \text{B(OH)}_3$$

Equation 3.1

Microanalyses and IR spectroscopy all indicate that the boric acid was present in the bulk samples.

In order to evaluate whether boric acid could be co-crystallised with similar metal complexes, Cu(2-pzca)$(PPh_3)_2$ **2.17** and Cu_2(2,5-pzdca)$(PPh_3)_4$ **2.20** were selected. These complexes are attractive for a number of reasons: (i) they contain two or four carboxylate oxygen atom sites, that can be used in hydrogen bonding, as seen previously in **3.1**, (ii) these copper(I) compounds are easily synthesised following the

synthetic procedure described in Chapter II and III with the $Cu(2\text{-pyca})(PPh_3)_2$ successfully co-crystallised with boric acid, it was clear that co-crystallisation of the boric acid with $Cu(2\text{-pzca})(PPh_3)_2$ and $Cu_2(2,5\text{-pzdca})(PPh_3)_4$ could be possible.

Compounds $Cu_2(2,5\text{-pzdca})(PPh_3)_4{\cdot}2B(OH)_3$ **3.2** and $Cu(2\text{-pzca})(PPh_3)_2Cl{\cdot}B(OH)_3$ **3.3** were obtained in the same manner as **3.1**. One or two equivalents of boric acid were used, depending on the pyrazine copper(I) complex under study, using reflux to fully dissolve the mixture as described above for compound **3.1**.

The co-crystallisation of $Cu_2(2,5\text{-pzdca})(PPh_3)_4$ **2.20** with boric acid yields yellow crystals of $Cu_2(2,5\text{-pzdca})(PPh_3)_4{\cdot}2B(OH)_3$ **3.2** (Figure 3.15). The symmetrical nature of the $Cu_2(2,5\text{-pzdca})(PPh_3)_4$ lends itself to its position on a centre of inversion, with the unique molecule of boric acid in the asymmetric unit hydrogen-bonded to the coordinated carboxylate group *via* the hetero-dimeric boric acid-carboxylate $R^2_2(8)$ dimer.

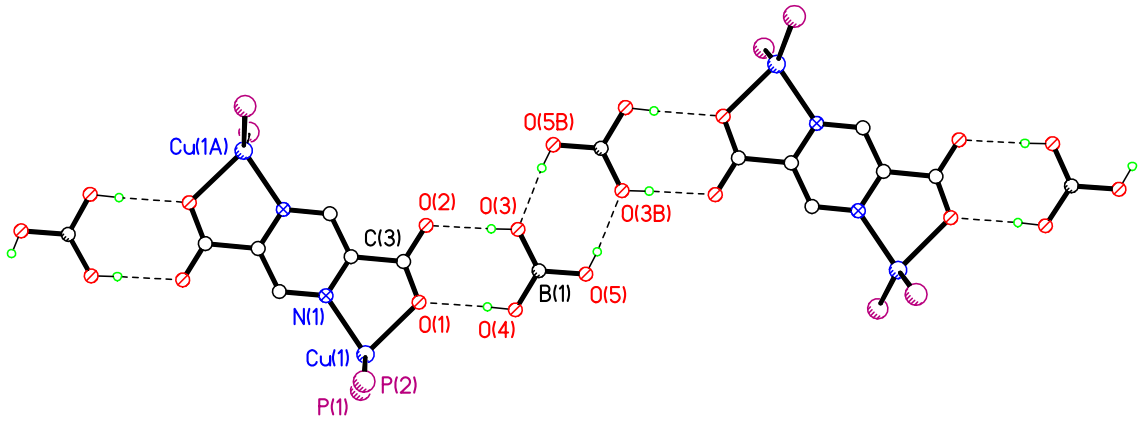

Figure 3.15 Chains of $Cu_2(2,5\text{-pzdca})(PPh_3)_4{\cdot}2B(OH)_3$ **3.2**. Phenyl rings and hydrogen atoms except O*H* have been omitted for clarity.

Complex **3.2** exhibits a similar trend to that observed in **3.1** but by virtue of the second carboxylate group further H-bonding can be observed leading to the formation of a 1-D structure propagating along the [1 1 0] direction. Selected hydrogen bonding parameters for **3.2** are shown in Table 3.2.

Table 3.2 Selected hydrogen bonding parameters for **3.2**.

D–H···A	D···A/Å	D–H/Å	H···A/Å	D–H···A/º
O(3)–H(3)···O(2)	2.6528(19)	0.77(3)	1.88(3)	175(3)
O(4)–H(4)···O(1)	2.8002(19)	0.82(3)	1.98(3)	178(3)
O(5)–H(5)···O(3B)^{i}	2.781(2)	0.76(3)	2.02(3)	173(3)

Symmetry operations: ^{i}-x+1, -y+1, -z+1.

The infrared spectrum of compound **3.2** shows the vibration modes of $B(OH)_3$ at ν = 1366 and 1432 cm^{-1} which belong to the vibrations of B–O bonds in triangular coordination mode.[151] The ν = 1432 cm^{-1} vibration should have contributions from the stretching vibration ν(C–O) of the carboxylate group.

Compound $Cu(2\text{-pzca})(PPh_3)_2$ **2.17** crystallises incorporating one molecule of dichloromethane in the crystal structure yielding $Cu_2(2\text{-pzca})(PPh_3)_4Cl{\cdot}B(OH)_3{\cdot}CH_2Cl_2$ **3.3**. The 2-pyrazine carboxylate acts as a bridging ligand between Cu(I) centres and leaves a potentially reactive chloride metal-coordinated maintaining charge neutrality (Figure 3.16). The solvent molecule did not change the packing of **3.3** which exhibits equivalent $R^2_2(8)$ motifs to those observed previously for compounds **3.1** and **3.2** (Table 3.3). There are two crystallographically independent Cu(I) centres which have different coordination environments. At Cu(2) the $[2\text{-pzca}]^-$ ligand coordinates through the *N* atom with two molecules of PPh_3 and a chloride completing the pseudo-tetrahedral geometry. The same $[2\text{-pzca}]^-$ ligand coordinates to Cu(1) in a bidentate fashion *via* the other N atom and a carboxylate O atom, the remaining coordination sites are occupied by two triphenylphosphine ligands.

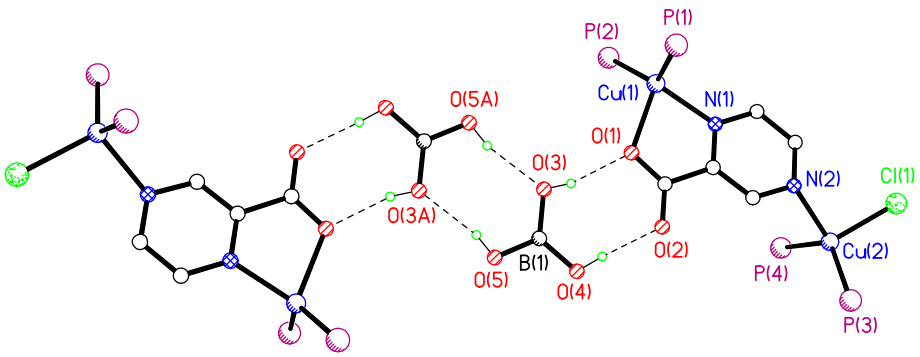

Figure 3.16 $Cu_2(2\text{-pzca})(PPh_3)_4Cl{\cdot}B(OH)_3{\cdot}CH_2Cl_2$ **3.3**. Phenyl groups, dichloromethane and hydrogen atoms not involved in hydrogen bonding have been omitted for clarity.

Table 3.3 Selected hydrogen bonding parameters for **3.3**.

D–H···A	D···A/Å	D–H/Å	H···A/Å	D–H···A/º
O(3)–H(H3A)···O(1)	2.742(3)	0.84	1.93	163
O(4)–H(4)···O(2)	2.684(3)	0.84	1.85	170
O(5)–H(5)···O(3A)^{i}	2.740(3)	0.84	1.96	154

Symmetry operations: ^{i}-x+1, -y, -z+1.

The chloride ligand forms a bifurcated (aromatic)C–H···Cl weak hydrogen bond, H···Cl 2.58 Å and 2.90 Å, with a symmetry generated molecule and *vice versa*, producing $R^1_2(10)$ and $R^2_2(12)$ ring motifs (Figure 3.17).

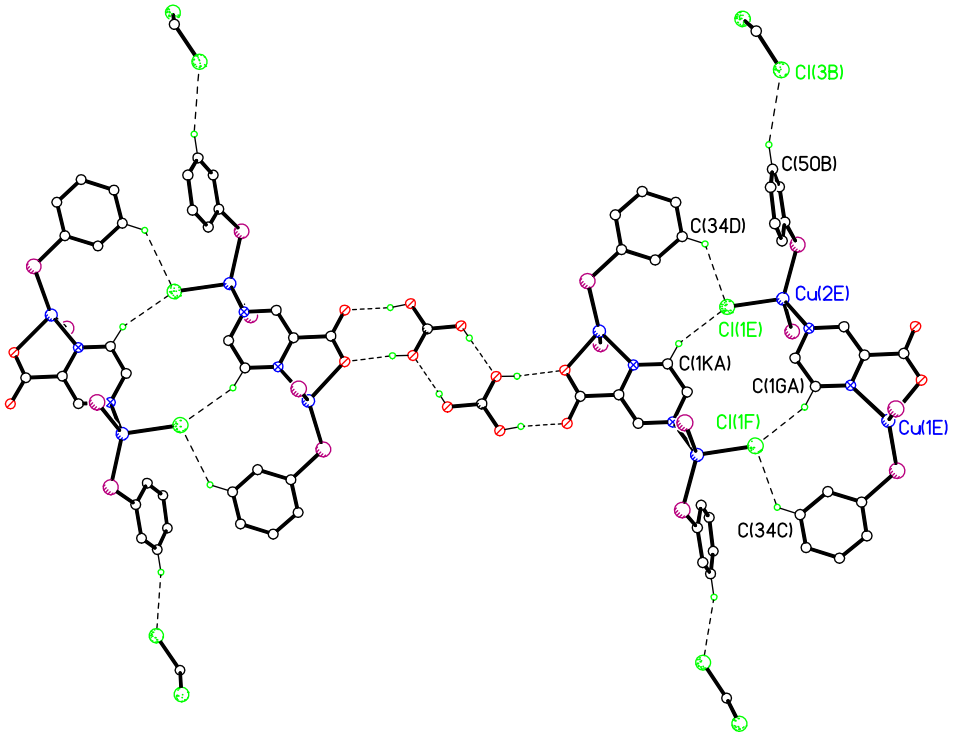

Figure 3.17 View of the hydrogen bonding motifs in **3.3**. Phenyl groups and hydrogen atoms not involved in hydrogen bonding have been removed for clarity.

The CH_2Cl_2 molecules are found on alternate sides of the one-dimensional structure and are also involved in weak (aromatic)C–H···Cl hydrogen bonds, 2.89 Å. The weak hydrogen bonding combined with the $R^2_2(8)$ motifs yields a pseudo-layer parallel to [0 1 1]. Further chemistry can be explored in order to extend the dimensionality of compound Cu_2(2-pzca)$(PPh_3)_4Cl{\cdot}B(OH)_3{\cdot}CH_2Cl_2$ **3.3** involving the chloride as a potential acceptor.[175-177]

3.2.2 Co-crystallisation of $Cu_2(2,5\text{-pzdca})(PPh_3)_4$ with Organoboronic Acids

Having successfully reproduced the co-crystallisation of $Cu_2(2,5\text{-pzdca})(PPh_3)_4$ with boric acid yielding compound **3.2**, which exhibits an extended one-dimensional hydrogen bonding network, further investigations were made in order to extend the dimensionality of this system. For this purpose, the co-crystallisation of $Cu_2(2,5\text{-pzdca})(PPh_3)_4$ was attempted with a variety of commercially available boronic acids which bear functional moieties such as, –COOH, $–NH_2$, −Br or an extra $-B(OH)_2$ (Figure 3.18).

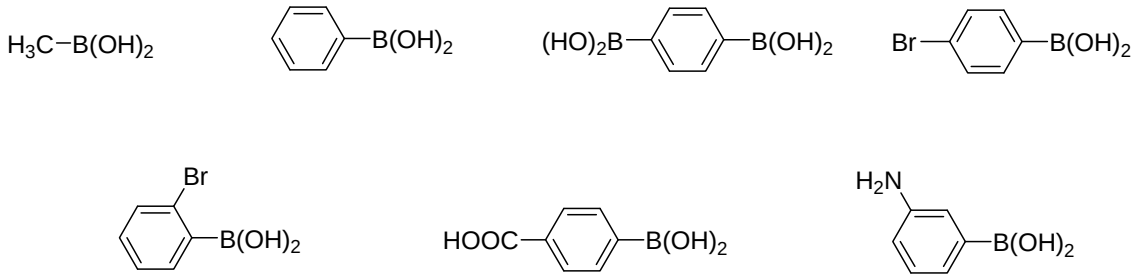

Figure 3.18 Boronic acids used in this study.

The synthesis of compounds **3.4**–**3.11** followed the same experimental conditions described above for compounds **3.1–3.3** with X-ray quality crystals obtained by slow evaporation of the saturated solutions.

Initially, the study was focused on the comparison between two similar boronic acid systems: (i) aliphatic methylboronic acid, $CH_3B(OH)_2$ and (ii) aromatic phenylboronic acid, $C_6H_5B(OH)_2$. Although both molecules lack other hydrogen bond acceptors/donors other than the $-B(OH)_2$ group, phenyl boronic acid could potentially be involved in weaker supramolecular interactions such as π-π interactions with phenyl rings of neighbouring molecules.[178,179]

3.2.2.1 Co-crystallisation of $Cu_2(2,5\text{-pzdca})(PPh_3)_4$ with Methylboronic Acid

Attempts to co-crystallise methylboronic acid with $Cu_2(2,5\text{-pzdca})(PPh_3)_4$ using similar synthetic procedures to those used in the formation of **3.1**–**3.3**, failed to produce the

desired co-crystal, instead crystallising a polymorphic form of **3.2**, Cu_2(2,5-pzdca)$(PPh_3)_4$·2B$(OH)_3$ **3.4**. The boric acid may have been present as a by-product in the original synthesis of Cu_2(2,5-pzdca)$(PPh_3)_4$ from the hydrolysis of borane BH_3 or $[BH_4]^-$ in the presence of trace amounts of water. In the presence of both boronic acids, $CH_3B(OH)_2$ and $B(OH)_3$, the co-crystallisation with the latter appears more favourable under the crystallisation conditions used. Both polymorphic forms, **3.2** and **3.4**, crystallise in the triclinic crystal system. They differ in the number of molecules of Cu_2(2,5-pzdca)$(PPh_3)_4$ and boric acid present in the asymmetric unit. While **3.2** crystallises with one half-molecule of Cu_2(2,5-pzdca)$(PPh_3)_4$ and one molecule of boric acid in the asymmetric unit. Compound **3.4** presents two molecules of Cu_2(2,5-pzdca)$(PPh_3)_4$ in the asymmetric unit lying on centres of inversion, with two unique boric acid molecules hydrogen bonded to the carboxylate group *via* the (boric acid)O−H···O(carboxylate) $R^2_2(8)$ graph set motif (Figure 3.19).

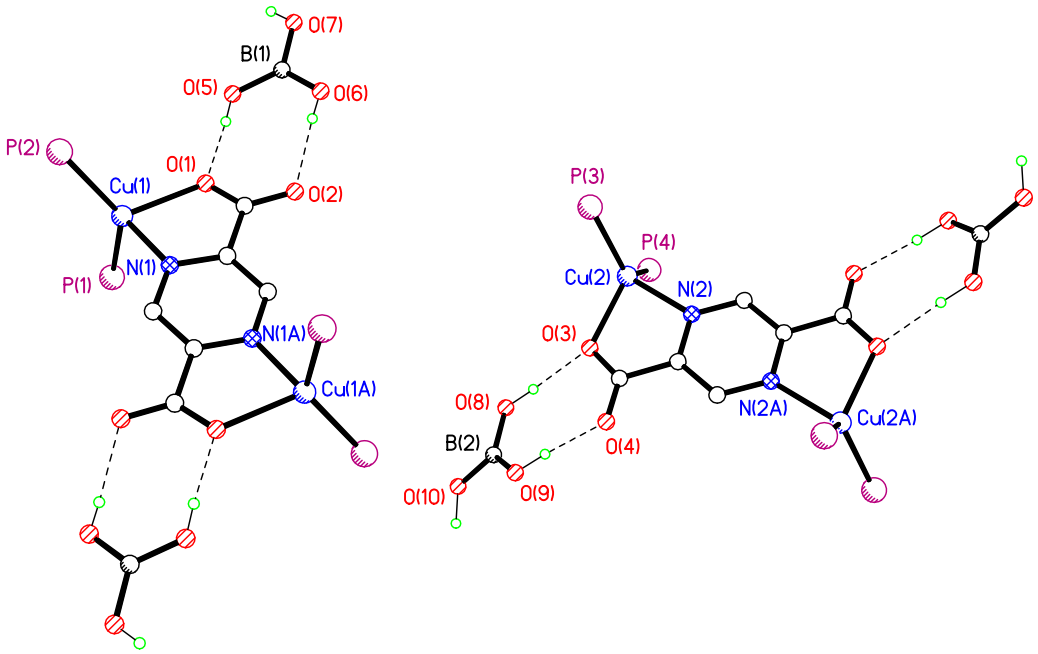

Figure 3.19 View of co-crystal Cu_2(2,5-pzdca)$(PPh_3)_4$·2B$(OH)_3$ **3.4**. Phenyl groups and hydrogen atoms not involved in hydrogen bonding have been omitted for clarity.

The two unique molecules exhibit identical hydrogen bonding patterns but differ geometrically making the one-dimensional polymeric zigzag chains obtained propagate in approximately perpendicular directions (Figure 2.44). Selected hydrogen bonding parameters for **3.4** are shown in Table 3.4.

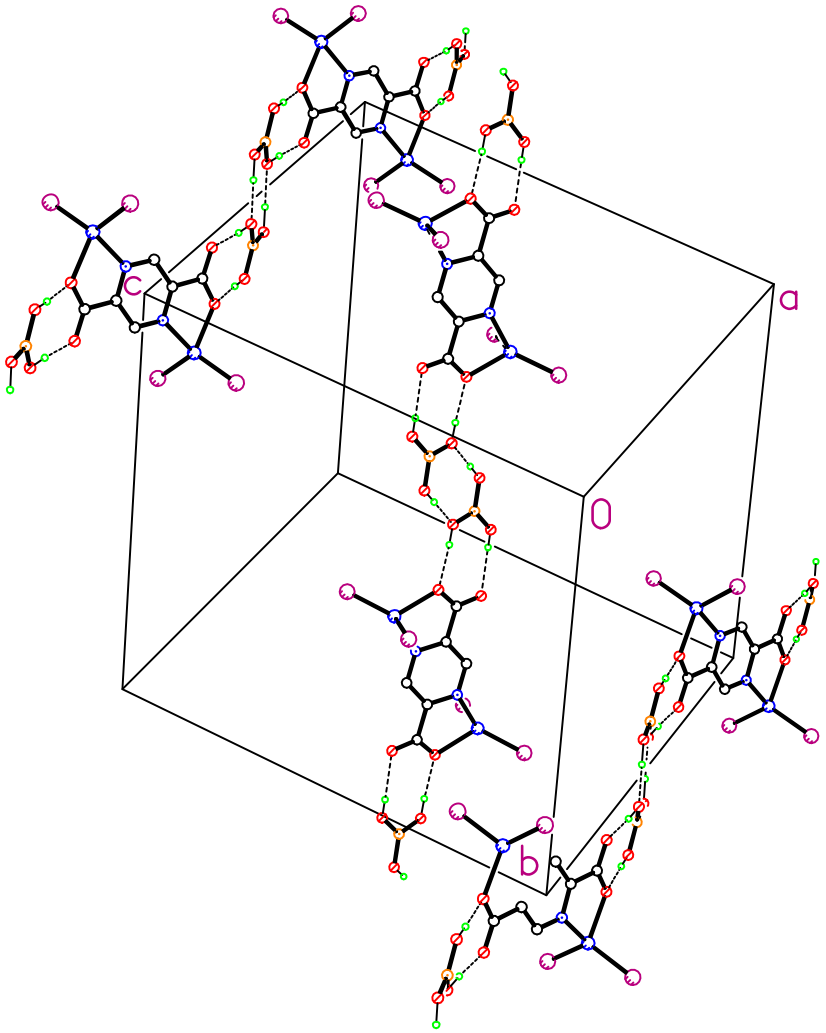

Figure 3.20 View of the hydrogen bonding motifs in co-crystal **3.4**. Phenyl groups and hydrogen atoms not involved in hydrogen bonding have been omitted for clarity.

Table 3.4 Selected hydrogen bonding parameters for **3.4**.

D–H···A	D···A/Å	D–H/Å	H···A/Å	D–H···A/º
O(5)–H(5)···O(1)	2.687(2)	0.83(3)	1.86(3)	176(3)
O(6)–H(6)···O(2)	2.707(3)	0.74(3)	1.97(3)	173(4)
O(7)–H(7)···O(5)^{i}	2.733(3)	0.84(4)	1.90(4)	173(4)
O(8)–H(8)···O(3)	2.826(3)	0.93(4)	1.90(4)	177(4)
O(9)–H(9)···O(4)	2.631(3)	0.89(3)	1.75(3)	176(3)
O(10)–H(10)···O(9)^{ii}	2.715(3)	1.00(4)	1.72(4)	175(3)

Symmetry operations: ^{i}-x+1, -y+1, -z+1, ^{ii}-x+1, -y, -z+2.

Although microanalyses of bulk powdered samples indicate the presence of $CH_3B(OH)_2$, numerous attempts to obtain crystals of compound Cu_2(2,5-pzdca)$(PPh_3)_4 \cdot 2CH_3B(OH)_2$ failed.

3.2.2.2 Co-crystallisation of Cu_2(2,5-pzdca)$(PPh_3)_4$ with Phenylboronic Acid

Phenylboronic acid has been co-crystallised with various aza-donor molecules such as, 4,4'-bipyridine (bpy) and *trans*-1,2-bis(4-pyridyl)ethane, by Pedireddi and SeethaLekshmi, producing a variety of networks in the form of sandwich, ladder and molecular blocks.[135] Interestingly, previous attempts to co-crystallise metal complexes with phenylboronic acid have failed.[149]

[Cu_2(2,5-pzdca)$(PPh_3)_4 \cdot 2C_6H_5(B(OH)_2)$][$Cu_2$(2,5-pzdca)$(PPh_3)_4$] **3.5** represents the first example of a metal complex co-crystallised with phenylboronic acid (CSD, version 5.30, plus 4 updates, November 2008). In contrast to the 1:2 copper(I) complex:boric acid stoichiometry observed in **3.4**, compound **3.5** crystallises in a 1:1 stoichiometry where only one of the two independent molecules of Cu_2(2,5-pzdca)$(PPh_3)_4$ present in the asymmetric co-crystallises with two phenylboronic acid molecules (Figure 3.21). Attempts to include two more molecules of phenylboronic acid in the asymmetric unit using an excess of the boronic acid during the synthesis were not successful yielding crystals of **3.5**. Compound **3.5** exhibits the expected hydrogen bonding $R^2_2(8)$ graph set motif seen previously for compounds **3.1**-**3.4** (Table 3.5). The $-B(OH)_2$ group only deviates slightly from planarity with respect to the aromatic ring (5.2°).

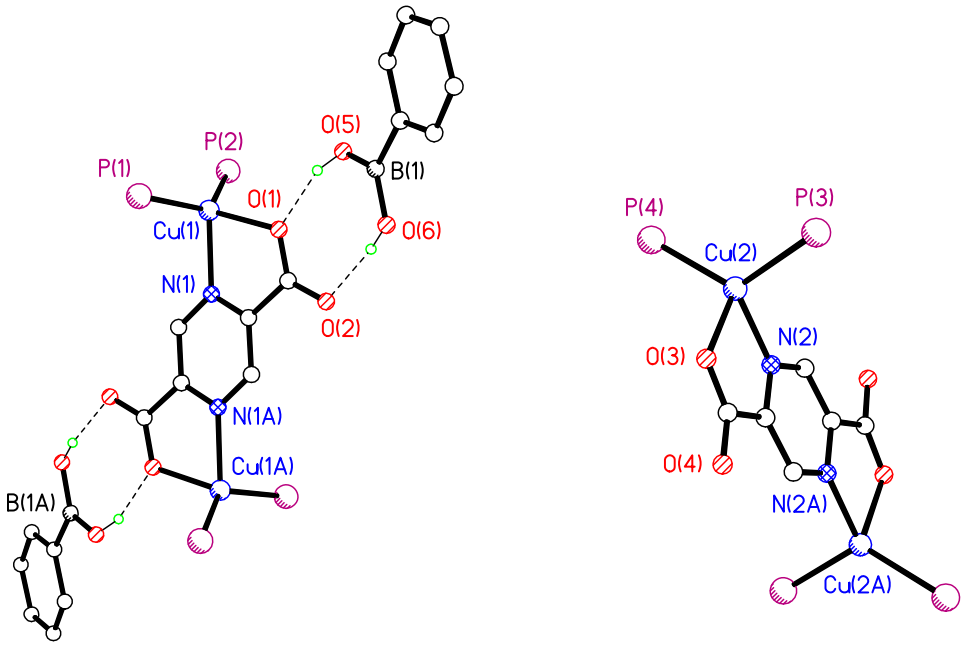

Figure 3.21 View of compound $[Cu_2(2,5\text{-pzdca})(PPh_3)_4{\cdot}2C_6H_5(B(OH)_2)][Cu_2(2,5\text{-pzdca})(PPh_3)_4]$ **3.5**. Phenyl groups and hydrogen atoms not involved in hydrogen bonding have been omitted for clarity.

Table 3.5 Selected hydrogen bonding parameters for **3.5**.

D–H···A	D···A/Å	D–H/Å	H···A/Å	D–H···A/º
O(6)–H(6)···O(2)	2.856(7)	0.93(3)	1.94(3)	166(7)
O(5)–H(5)···O(1)	2.729(6)	0.85(3)	1.90(4)	162(8)

Although aromatic rings are present in compound **3.5**, no face-to-face or edge-to-face stacking interactions are observed. However, packing of molecules in the crystal lattice of **3.5** is stabilised by weak (aromatic)C–H···O(carboxylate) interactions, H···O 2.45 Å and 2.50 Å, creating cavities where the phenylboronic acid molecules reside (Figure 3.22).

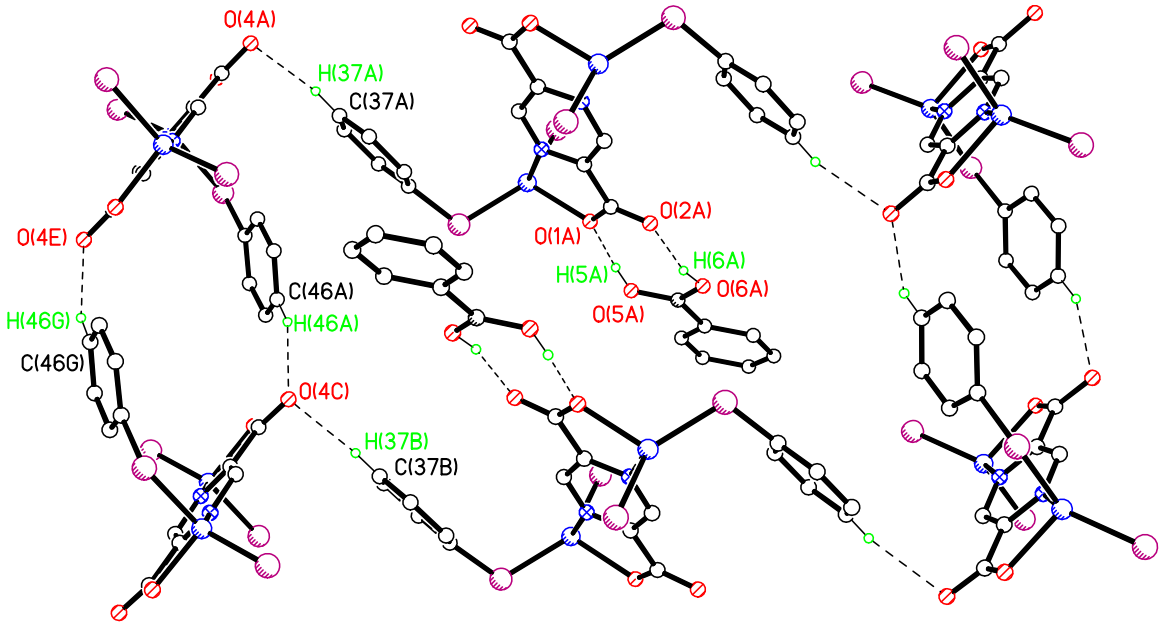

Figure 3.22 View of co-crystal **3.5** showing the hydrogen bonding motifs. Phenyl groups and hydrogen atoms not involved in hydrogen bonding have been omitted for clarity.

The infrared spectrum of pure phenylboronic acid contains a broad O–H stretching band at ν = 3279 cm^{-1} which appears as one broad band at ν = 3421 cm^{-1} on formation of $RB(OH)_2\cdots{}^{-}OOCR$ in compound **3.5**. The band characteristic for the asymmetric stretching vibration of the carboxylate group appears at ν = 1647 cm^{-1}. The broad band at ν = 1368 cm^{-1} should have contributions of the symmetric stretching vibration $\nu(COO^{-})$ and ν(B–O) stretching vibration, which for the pure phenylboronic acid is located at ν = 1348 cm^{-1}.

3.2.2.3 Co-crystallisation of Cu_2(2,5-pzdca)$(PPh_3)_4$ with 1,4-Phenyldiboronic Acid

The successful co-crystallisation of phenylboronic acid with Cu_2(2,5-pzdca)$(PPh_3)_4$ **2.20** led to the consideration of 1,4-phenyldiboronic acid as the addition of an extra $-B(OH)_2$ group compared to **3.5** could provide an additional hydrogen bonding group.

The structure of Cu_2(2,5-pzdca)$(PPh_3)_4\cdot C_6H_4${1,4-$B(OH)_2$} **3.6** was determined using synchrotron radiation on station 9.8 at the SRS, Daresbury Laboratory, due to the small crystal dimensions. In contrast with the phenylboronic acid, the inclusion of 1,4-

phenyldiboronic acid into the crystal structure of the Cu_2(2,5-pzdca)$(PPh_3)_4$ occurs in a 1:1 ratio. As observed previously in **3.1-3.5**, Cu_2(2,5-pzdca)$(PPh_3)_4 \cdot C_6H_4${1,4-$B(OH)_2$} **3.6** exhibits the typical (boronic acid)O−H···O(carboxylate) hydrogen bonds, producing an $R^2_2(8)$ graph set motif. The symmetrical nature of both 1,4-phenyldiboronic acid and [Cu_2(2,5-pzdca)$(PPh_3)_4$] lend themselves to their positions on inversion centres. Although the weak (aromatic)C–H···O(carboxylate) interactions observed in the solid state structure of **3.5** are not seen in **3.6**, the addition of an extra $-B(OH)_2$ provides an additional hydrogen bonding group resulting in the formation of one-dimensional chains propagating in the [1 0 1] direction (Figure 3.23). Selected hydrogen bonding parameters for **3.6** are shown in Table 3.6.

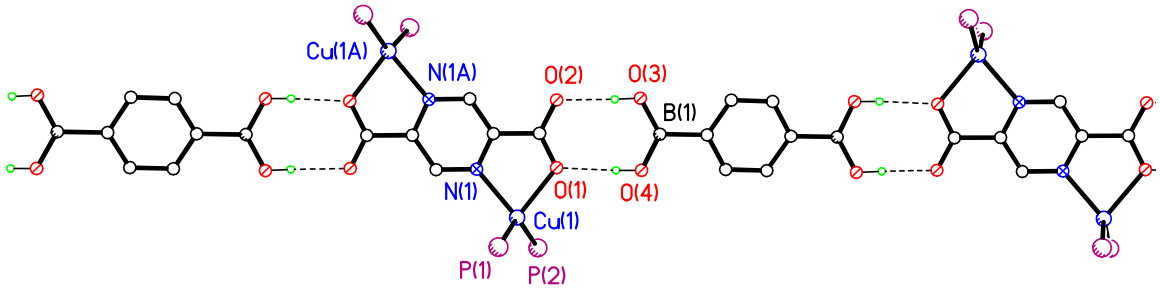

Figure 3.23 Chains of co-crystal **3.6**. Phenyl groups and hydrogen atoms not involved in hydrogen bonding have been omitted for clarity.

Table 3.6 Selected hydrogen bonding parameters for **3.6**.

D-H···A	D···A/Å	D–H/Å	H···A/Å	D–H···A/º
O(3)–H(3)···O(2)	2.748(3)	0.838(10)	1.94(2)	163(7)
O(4)–H(4)···O(1)	2.763(3)	0.833(10)	1.931(11)	176(5)

While the twists of the $-B(OH)_2$ groups out of the mean plane of the phenyl group in 1,4-phenylenediboronic acid and its tetrahydrate are 35° and 7° respectively,[180] the twist for compound **3.6** has an intermediate value of 19.4°, apparently as a result of the hydrogen bonding requirements.

Comparing the infrared spectra of the starting materials and **3.6**, similar changes to the cases discussed above were observed. Also, in this case the band at ν = 1366 cm^{-1} is broad and should have the contributions from the symmetric stretching vibration $\nu(COO^-)$ and ν(B–O).

3.2.2.4 Co-crystallisation of Cu_2(2,5-pzdca)$(PPh_3)_4$ with 2-Bromophenylboronic Acid

Cu_2(2,5-pzdca)$(PPh_3)_4$ co-crystallises with 2-bromophenylboronic acid in a 1:1 ratio yielding Cu_2(2,5-pzdca)$(PPh_3)_4 \cdot C_6H_4${$B(OH)_2$}2-Br **3.7**, which was obtained by slow diffusion of diethyl ether into a dichloromethane solution containing **3.7** (Figure 3.24). The Cu_2(2,5-pzdca)$(PPh_3)_4$ molecule lies on a crystallographic centre of symmetry. The crystal structure of **3.7** shows, as seen previously, that the $-B(OH)_2$ group is strongly hydrogen bonded as a double donor to the two carboxylate oxygen atoms in the Cu(I) complex (Table 3.7). Although the 2-bromophenylboronic acid possesses a halogen atom in the *ortho* position which can act as a good hydrogen-bonding acceptor,[181,182] due to the lack of strong hydrogen bond donors, extending the dimensionality of the system was unsuccessful, the structure of **3.7** is essentially zero-dimensional.

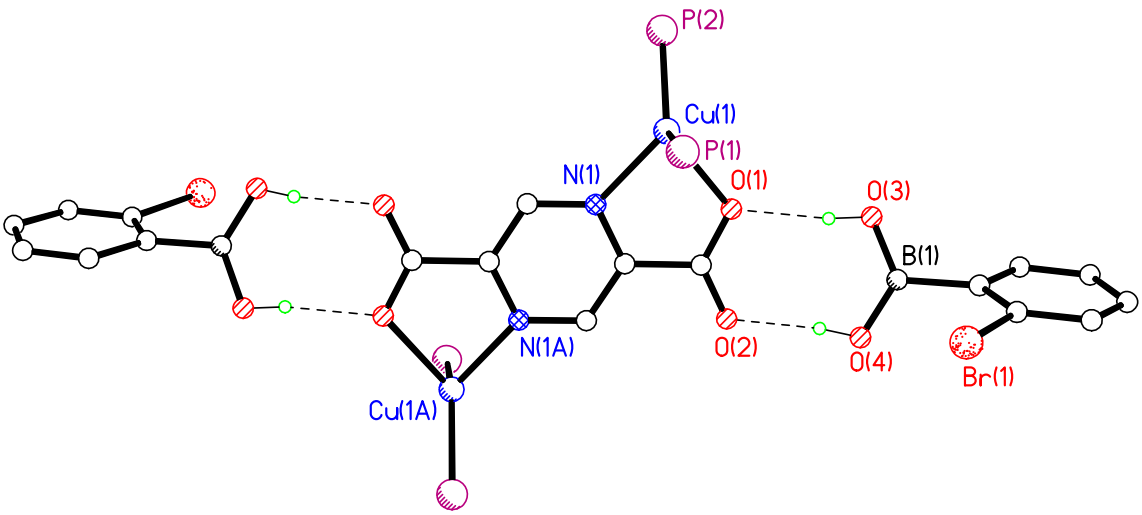

Figure 3.24 View of **3.7**. Phenyl groups and hydrogen atoms not involved in hydrogen bonding have been omitted for clarity.

While the –Br group is essentially coplanar with the C_6H_4 ring, the plane formed by O(3)/B(1)/O(4) is twisted out of the C_6H_4 plane by 64.1°, this distortion is more severe than that observed in the solid state structure of 2-bromophenylboronic acid, 34.0°.[138] It appears reasonable to ascribe this distortion to the sterically more demanding *ortho*-Br group in **3.7**.

Table 3.7 Selected hydrogen bonding parameters for **3.7**.

D–H···A	D···A/Å	D–H/Å	H···A/Å	D–H···A/º
O(3)–H(3)···O(1)	2.763(2)	0.84	1.94	168
O(4)–H(4)···O(2)	2.694(2)	0.84	1.86	170

While 4-bromophenylboronic acid is known to form an extended intermolecular hydrogen bonding network through (boronic acid)O–H···O(boronic acid) and Br···Br interactions,[183,184] numerous attempts to co-crystallise it with the copper(I) complex to yield Cu_2(2,5-pzdca)$(PPh_3)_4$·C_6H_4{$B(OH)_2$}4-Br **3.8** failed.

3.2.2.5 Co-crystallisation of Cu_2(2,5-pzdca)$(PPh_3)_4$ with 3-Aminophenylboronic Acid

The simultaneous presence of one –$B(OH)_2$ and one –NH_2 group in 3-aminophenylboronic acid generates several supramolecular bonding options for this molecule. From the failure to extend the dimensionality of our systems with **3.7**, a boronic acid containing an –NH_2 group in the *meta* position as a hydrogen bonding donor was studied. The co-crystal of Cu_2(2,5-pzdca)$(PPh_3)_4$ with 3-aminophenylboronic acid also includes additional molecules of water and dichloromethane in the lattice, giving the asymmetric unit [Cu_2(2,5-pzdca)$(PPh_3)_4$·C_6H_4{$B(OH)_2$}3-NH_2][Cu_2(2,5-pzdca)$(PPh_3)_4$]·H_2O·CH_2Cl_2 **3.9** (Figure 3.25). The hydrogen atoms of the water molecule O(7) could not be located in the Fourier difference map.

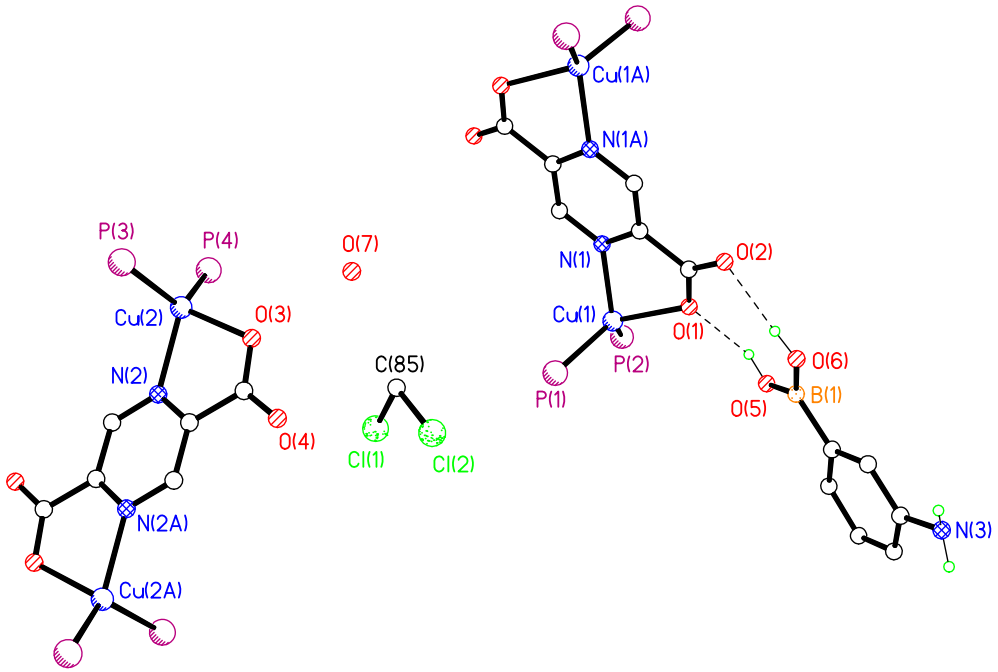

Figure 3.25 View of compound **3.9**. Phenyl groups and hydrogen atoms not involved in hydrogen bonding have been omitted for clarity.

The $-NH_2$ group of the 3-aminophenylboronic acid interacts with a carboxylate *O* atom through an intermolecular N−H···O hydrogen bond. This cooperates with the common boronic···carboxylate $R^2_2(8)$ ring motif formed in all the co-crystals described above, producing one-dimensional polymeric chains (Figure 3.26). As seen with **3.5**, the $-B(OH)_2$ group is almost co-planar (4.6°) with the aromatic ring. Selected hydrogen bonding parameters for **3.9** are shown in Table 3.8.

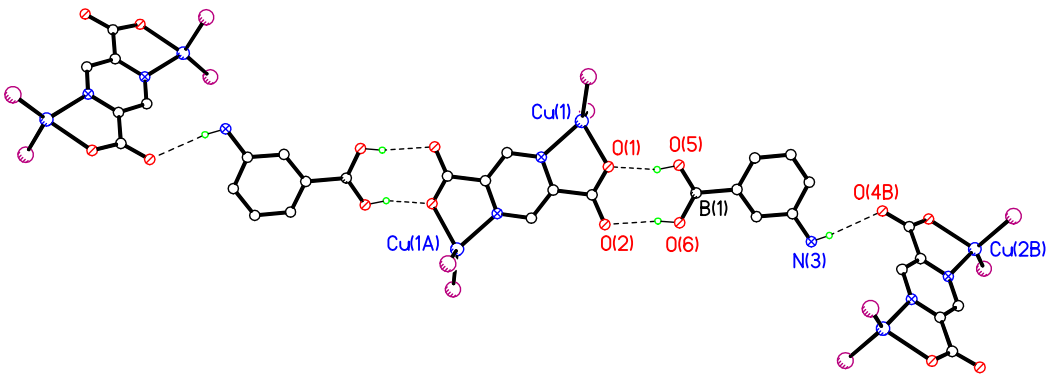

Figure 3.26 View of co-crystal **3.9**, showing a hydrogen bonded chain. Phenyl groups and hydrogen atoms not involved in hydrogen bonding have been removed for clarity.

Table 3.8 Selected hydrogen bonding parameters for **3.9**.

D–H···A	D···A/Å	D–H/Å	H···A/Å	D–H···A/°
O(5)–H(5A)···O(1)	2.686(2)	0.84	1.88	160
O(6)–H(6A)···O(2)	2.859(2)	0.84	2.03	171
N(3)–H(3B)···O(4B)^{i}	3.093(3)	0.84(3)	2.29(3)	160(3)

Symmetry operations: ^{i}-x+3, -y+1, -z+1.

While the dichloromethane molecule in **3.3** does not participate in the extension of the dimensionality of the supramolecular array formed, in compound **3.9** the solvent molecules interact with the Cu_2(2,5-pzdca)$(PPh_3)_4$ molecules using a combination of (phenyl)C–H···Cl(solvent), (solvent)C–H···O(carboxylate), (solvent)C–H···O(solvent) and (phenyl)C–H···O(solvent) hydrogen bonds, [2.87 Å, 2.38 Å, 2.20 Å and 2.56 Å], in order to form a two-dimensional architecture (Figure 3.27).

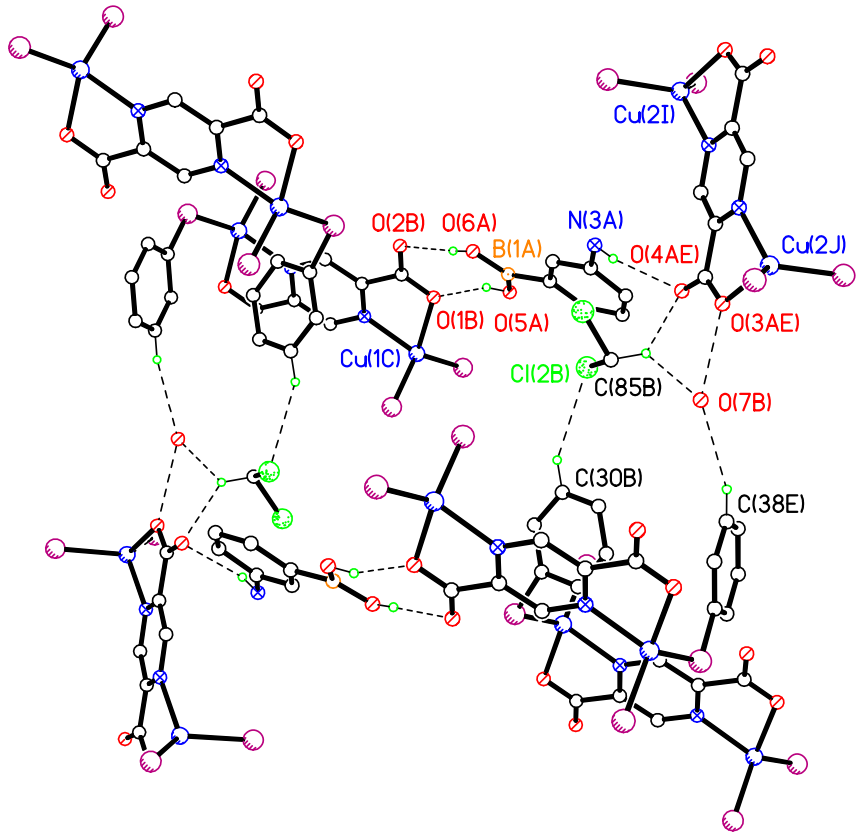

Figure 3.27 View of the hydrogen bonding motifs in co-crystal **3.9**. Phenyl groups and hydrogen atoms not involved in hydrogen bonding have been omitted for clarity. Close O···O [2.73 Å] contacts involving O(7B) are shown with dashed lines.

The infrared spectrum of **3.9** contains a broad band at ν = 3373 cm^{-1} assigned to contributions of the O–H and N–H vibrations. The strong bands at ν = 1631 and 1368 cm^{-1} should also have contributions from ν(asymm. CO_2^-)/ν(N-H) vibrations, and the ν(symm. COO^-)/ν(B–O) stretching vibration respectively.

Attempts to obtain suitable crystals for X-ray crystallography for Cu_2(2,5-pzdca)$(PPh_3)_4 \cdot C_6H_4$(1-COOH){4-$B(OH)_2$} **3.10** from organic solvents by different crystallisation methods such as (i) slow evaporation of dichloromethane/^{t}BuOH solution of **3.10** (ii) slow vapour diffusion of hexane into a dichloromethane solution of **3.10** (iii) slow vapour diffusion of diethyl ether into a dichloromethane solution of **3.10** were not successful.

Numerous attempts to co-crystallise the boronic acids described above with Cu(2-pyca)$(PPh_3)_2$ and Cu(2-pzca)$(PPh_3)_2$ complexes, such as Cu(2-pzca)$(PPh_3)_2 \cdot C_6H_4(B(OH)_2)$ **3.11**, using the same crystallisation conditions described for **3.9** failed. Crystallisation of the reaction mixtures gave crystals of the starting materials only. Elemental analysis data and IR spectroscopy indicate the presence of **3.10** and **3.11** (Experimental section). Further work could be done on the optimisation of the crystallisation method for these compounds.

While the $CO_2^-/B(OH)_2$ $R^2_2(8)$ synthon has relatively few examples reported in the CSD compared with the analogous, well studied, carboxylic acid-carboxylate $R^2_2(8)$ synthon, the majority of the CSD structures containing the carboxylate-boronic acid group synthon do involve boric acid or phenylboronic acid, indicating the more general carboxylate-boronic acid group as a supramolecular synthon worthy of study. Possible future work could include the co-crystallisation of pyrazine- and pyridine-carboxylic acids with other poly(boronic) acid analogues (Figure 3.28).[134,136,185]

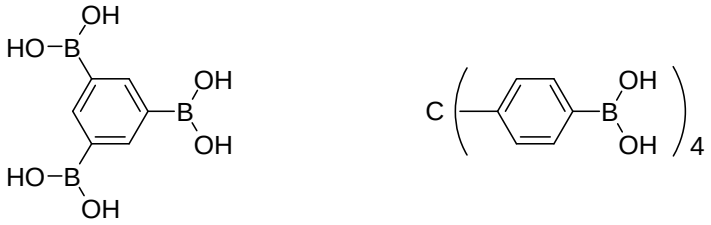

Figure 3.28 Examples of poly(boronic) acids that could be used in future studies.

The controlled and efficient synthesis of molecules of this type would provide synthetic underpinning for the molecular-engineering approach to design and construction of complex two and three-dimensional architectures.

3.2.3 Discussion of the General Structural Features of Compounds 3.1-3.7, 3.9 and 3.10

In the solid state, compounds **3.1-3.7**, **3.9** and **3.10** aggregate and present the common boronic···carboxylate $R^2_2(8)$ centrosymmetric dimer (Figure 3.29), formed by a pair of complementary O–H···O hydrogen bonding interactions characterised by O···O distances of 2.65-2.86 Å and O–H···O angles of 154-178° which are comparable to existing examples.[137,140,149,174,180] Deprotonation of the carboxylic acids, through metal chelation, converted them into perfect ditopic hydrogen bond acceptors for boronic acids in a *syn* conformation.

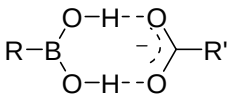

Figure 3.29 Common synthon in compounds **3.1-3.7**, **3.9** and **3.10**.

In all cases except compounds **3.6** and **3.7** the $–B(OH)_2$ groups are approximately co-planar with the C_6 ring (dihedral angles are all less than 6°). The heterodimeric unit $RB(OH)_2···^-OOCR$ (Figure 3.29) is non planar as shown by the α and β, (boronic acid)B–O···O–C(carboxylate), torsion angles shown in Table 3.9. These values are in good agreement with those observed in the literature.[137]

Table 3.9 Torsion angles (°) of compounds **3.1-3.7** and **3.9**.[i]

	3.1	**3.2**	**3.3**	**3.4**	**3.5**	**3.6**	**3.7**	**3.9**
α	9.0	12.4	8.9	9.5	16.5	15.1	23.7	21.1
β	0.5	12.7	14.0	15.6	12.0	11.8	29.1	19.8

[1] Where α and β = torsion angles (boronic acid)B–O···O–C(carboxylate).

Selected bond lengths and angles for the structurally characterised co-crystals **3.1**-**3.7**, **3.9** and **3.10** are shown in Table 3.10. There is little difference between these parameters for this series of complexes, and these bond lengths compare well with those in Cu_2(2-pyca)$(PPh_3)_2$·*X*, (*X* = MeOH, EtOH, *n*-PrOH or *i*-PrOH) **2.1**-**2.4**, (Table 2.10), Cu(2-pzca)$(PPh_3)_2$ **2.17** and Cu_2(2,5-pzdca)$(PPh_3)_4$ **2.20**. The B–O and O–B–O values are also in good agreement with those observed in the literature.[140,142,186] The small differences may be caused by the dissimilarity of the hydrogen bonding shell around the carboxylate group and the different steric environments.

Table 3.10 Selected bond lengths (Å) and angles (°) for compounds **3.1**-**3.7**, **3.9** and comparison with those of **2.1**-**2.4**, **2.17** and **2.20**.

	B−O[a]	**O−B−O**[i]	**C−O**	**Cu−O**	**O−Cu−N**
3.1	1.365	117.27(18) 118.82(18) 123.89(16)	1.2751(18) 1.2380(18)	2.0961(10)	78.92(4)
3.2	1.363	116.29(18) 119.92(18) 123.77(18)	1.265(2) 1.238(2)	2.1517(12)	79.44(5)
3.3	1.362	115.8(3) 119.6(3) 124.5(3)	1.242(3) 1.263(3)	2.175(2)	79.66(8)
3.4	1.35(4) [1.362(4)]	117.3(3)/[118.2(3)] 119.2(3)/[124.3(3)] 123.5(3)/[117.4(3)]	1.268(3)/[1.267(3)] 1.236(3)/[1.245(3)]	2.1395(17) [2.1252(18)]	78.88(7) [79.39(8)]
3.5	1.360	123.6(8)	1.280(8) 1.248(8)	2.142(5)	78.3(2)
3.6	1.351	124.3(3)	1.264(3) 1.238(3)	2.126(2)	78.74(8)
3.7	1.344	125.6(2)	1.270(3) 1.235(3)	2.1622(15)	78.61(6)
3.9	1.363(3)	123.8(2)	1.273(3) 1.236(3)	2.1183(17)	78.25(7)
2.1	-	-	1.259(2) 1.254(2)	2.1091(13)	79.92(6)
2.2	-	-	1.264(3) 1.249(3)	2.0792(16)	79.73(8)
2.3	-	-	1.266(3) 1.243(3)	2.092(2)	79.71(9)
2.4	-	-	1.264(2) 1.245(2)	2.0908(12)	79.77(5)
2.17	-	-	1.262(3) 1.239(3)	2.0698(17)	80.14(7)
2.20	-	-	1.2652(17) 1.2327(17)	2.0802(9)	81.32(4)

[a]O−H average distances; [i] Values in square brackets are for the second molecule in the asymmetric unit.

3.2.4 Discussion of Powder Diffraction Studies of Compound 3.2

Unfortunately, accurate characterisation of the bulk material for compounds **3.1**-**3.12** proved challenging to obtain. Powder X-ray diffraction (XRD) data were collected on compound **3.2** in order to determine the phases present in this sample. The powder XRD pattern collected from the bulk sample of **3.2,** shows a complicated mixture of phases to be present. Only two phases could be identified (Figure 3.30) through searching the International Centre for Diffraction Data (ICDD) Powder Diffraction File (PDF); the starting material $Cu(PPh_3)_2(BH_4)$, represented as purple lines in Figure 3.30 and boric acid, shown as green lines.

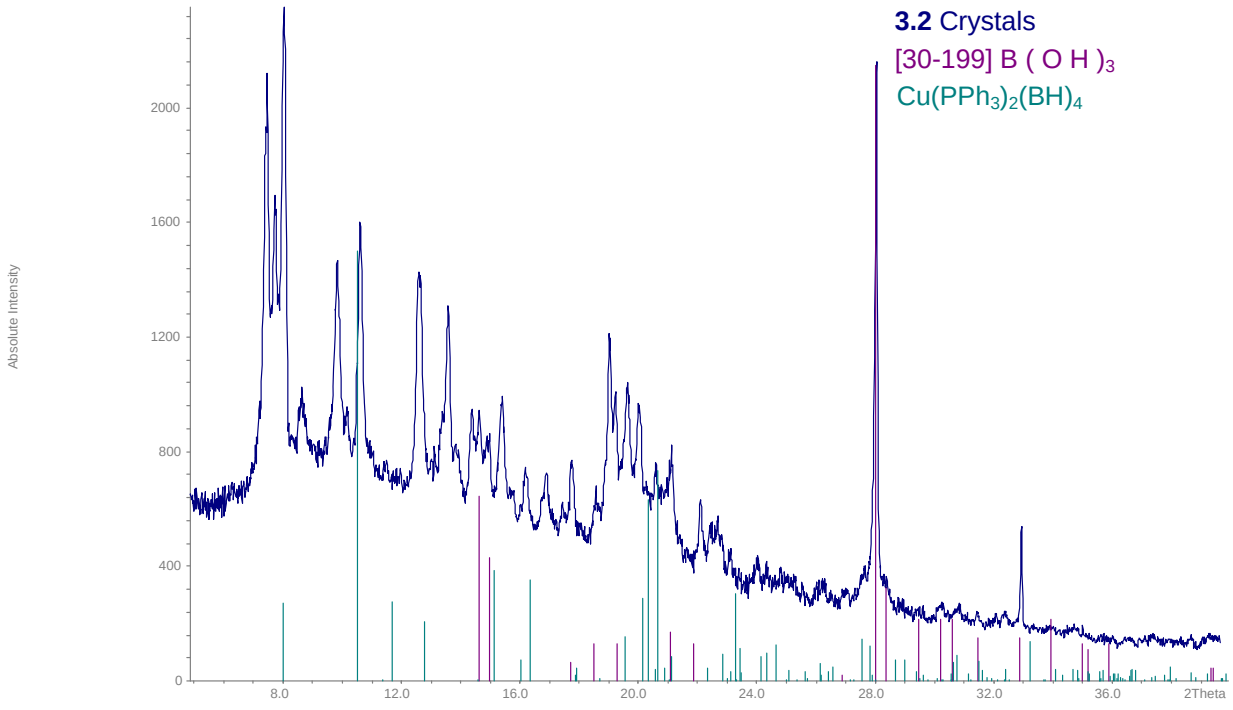

Figure 3.30 Powder diffraction patterns of **3.2**, $Cu(PPh_3)_2(BH_4)$ and $B(OH)_3$.

Using the structural model determined through single crystal analysis of compound **3.2**, a theoretical powder XRD pattern was calculated. Comparison of this with the observed data is shown in Figure 3.31 and it is clear that either this phase is not present in the bulk sample, only present in very small quantities too small to be detected by powder

XRD experiments or is very poorly crystalline and does not exhibit sharp diffraction peaks.

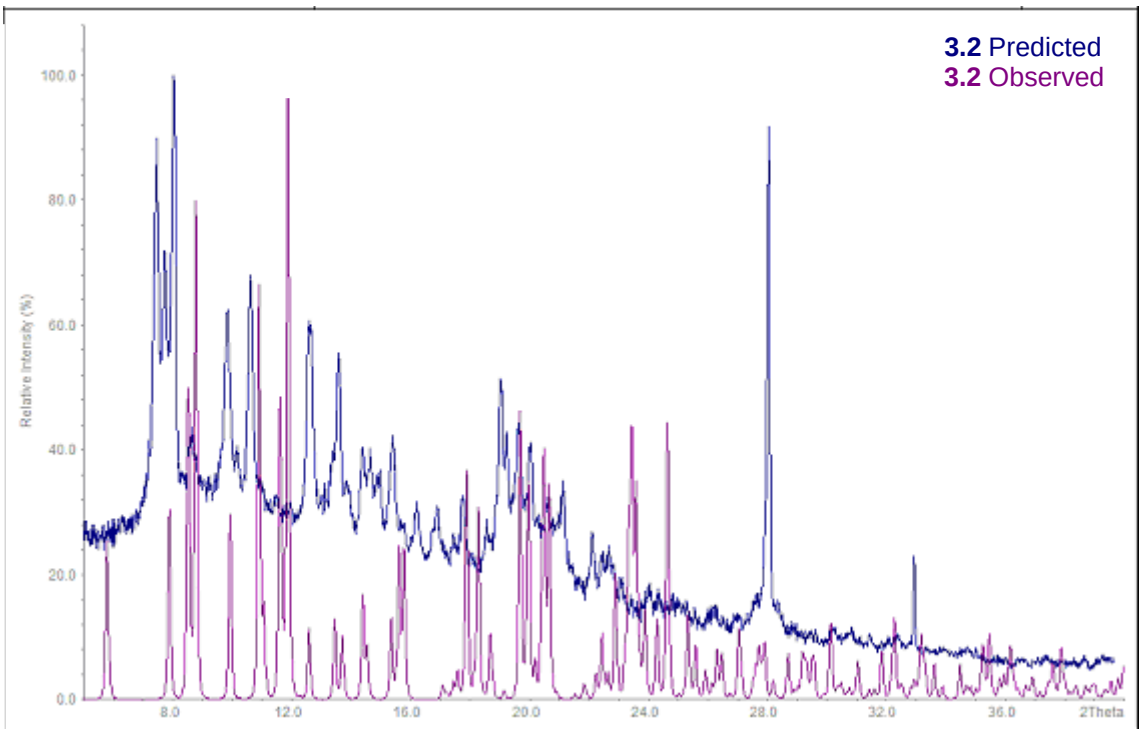

Figure 3.31 Powder diffraction patterns of **3.2** theoretical pattern and **3.2**.

The presence of $Cu(PPh_3)_2(BH_4)$ may come from the synthesis of Cu_2(2,5-pzdca)$(PPh_3)_4$ **2.20**. In order to obtain a sample without starting materials, compound **2.20** was re-crystallised from dichloromethane. Comparison of compound **2.20** before and after the re-crystallisation shows that the intense diffraction peaks in the 2θ region 4-8°, which belong to an unidentified phase, reduce in intensity. The powder diffraction pattern also shows that the amount of $Cu(PPh_3)_2(BH_4)$ present is slightly reduced (Figure 3.32).

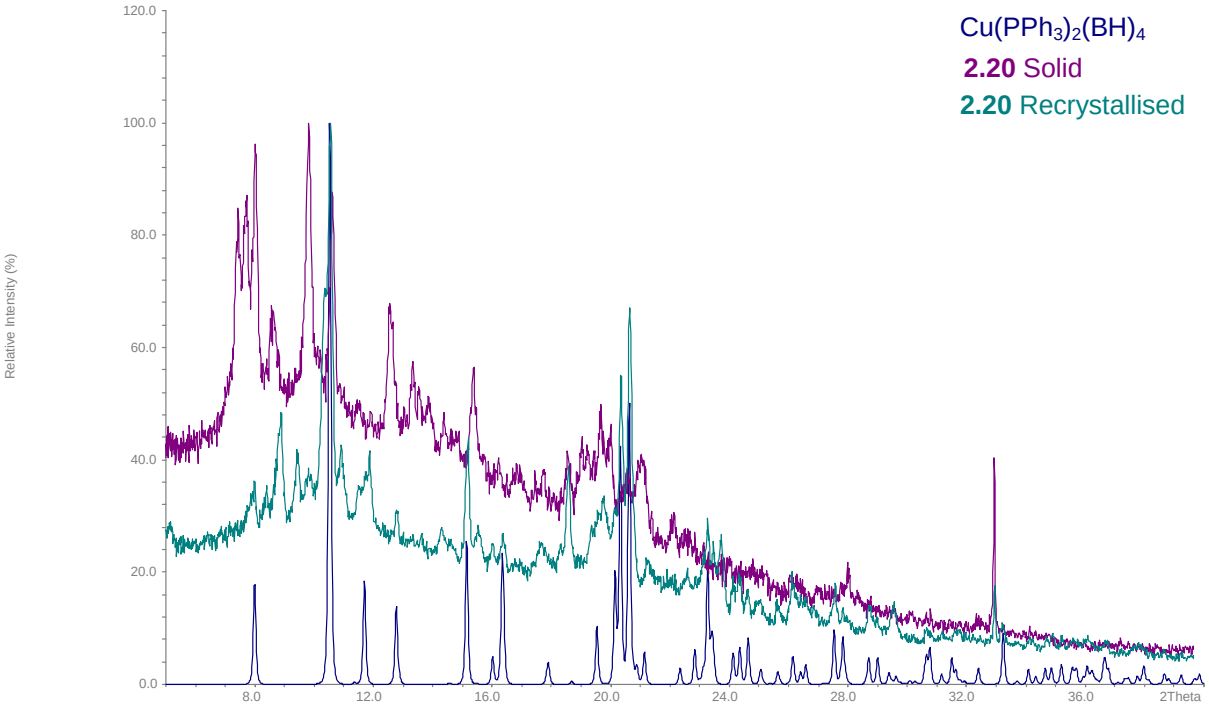

Figure 3.32 Powder diffraction patterns of **2.20**, **2.20** re-crystallised and $Cu(PPh_3)_2(BH_4)$.

As found previously for **3.2**, comparison between the theoretical and observed XRD patterns of **2.20** shows that some reflections can be identified as known phases, but there are still many unidentified peaks relating to the presence of, perhaps, several unknown phases (Figure 3.33).

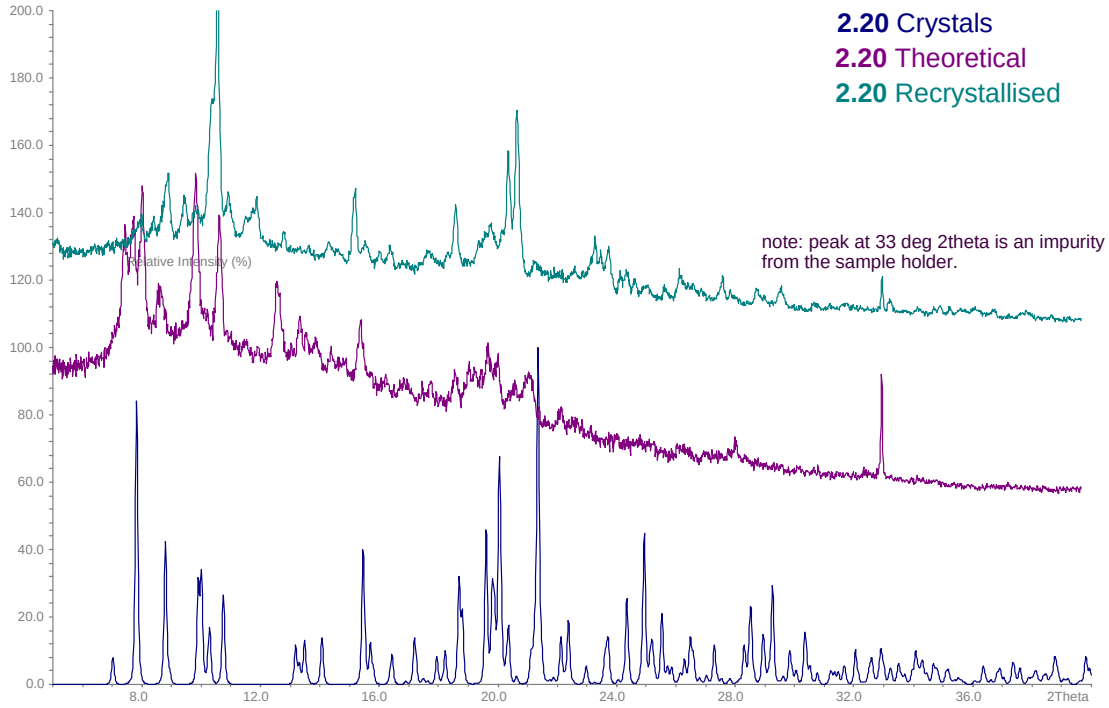

Figure 3.33 Powder diffraction patterns of **2.20** theoretical pattern, **2.20** and **2.20** re-crystallised.

Compound **3.2** was synthesised using the Cu_2(2,5-pzdca)$(PPh_3)_4$ **2.20** obtained from the re-crystallisation and the powder X-ray diffraction data collected is shown in Figure 3.34.

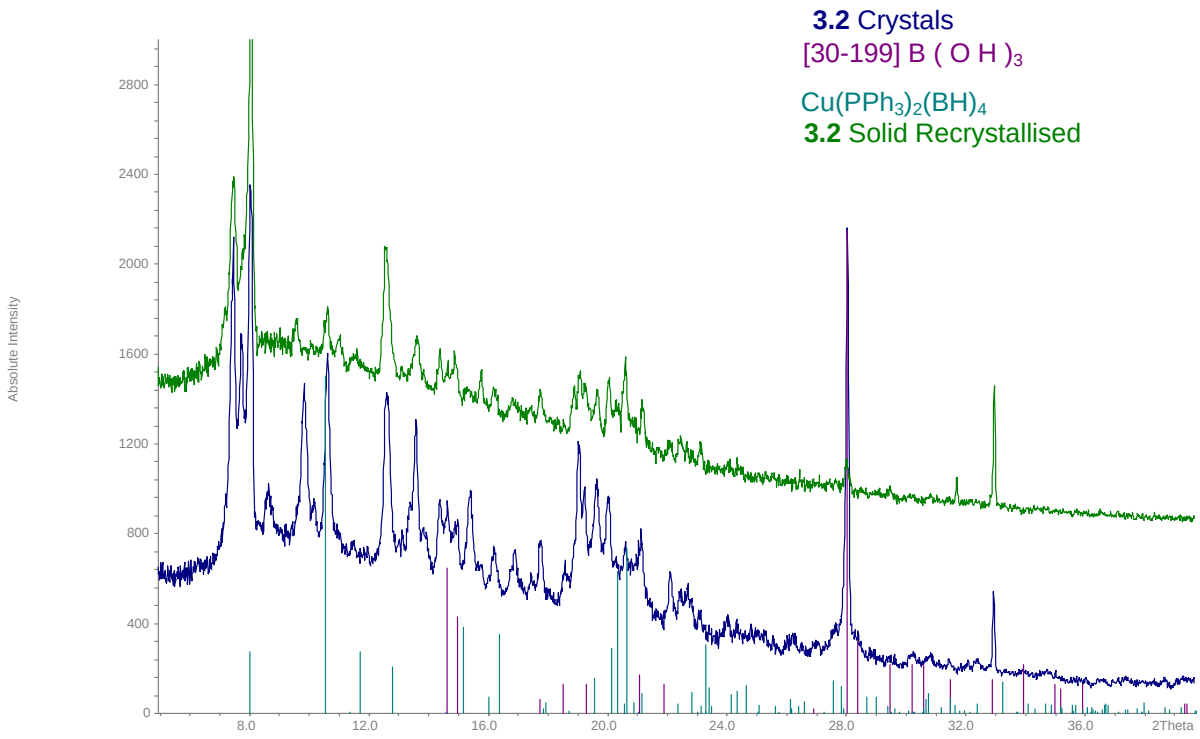

Figure 3.34 Powder diffraction patterns of **3.2**, **3.2** from recrystallisation, $Cu(PPh_3)_2(BH_4)$ and $B(OH)_3$.

The re-crystallisation experiment shows that the amount of $Cu(PPh_3)_2(BH_4)$ and boric acid present in the sample have been reduced dramatically, the diffraction peaks for $Cu(PPh_3)_2(BH_4)$ are shifted slightly due to small changes in the unit cell parameters between that of the standard pattern and the sample present **3.2**. Although there are phases in the diffraction pattern which have not been identified, the reduction in the amount of boric acid indicates that $Cu(PPh_3)_2(BH_4)$ and $B(OH)_3$ are directly related and boric acid may come from two different sources: (i) added as a reagent for the co-crystallisation reactions and (ii) from the hydrolysis of borohydride $[BH_4]^-$.

3.3 Conclusion

Low temperature single X-ray diffraction has enabled the elucidation of eight examples of copper(I)pyridine-/pyrazine-carboxylate complexes with boronic acid co-crystals, which represent novel contributions to the research into the occurrence of the carboxylate-boronic acid motif in co-crystals. Extensive hydrogen bonding exists within the structures, with the heterodimeric boronic···carboxylate $R^2_2(8)$ ring motif present in all cases. Therefore, the family of co-crystals presented in this chapter provide some insight on the supramolecular behaviour of these systems. Boronic···carboxylate $R^2_2(8)$ motifs are present in all crystal structures indicating the robust and predictable character of this synthon when using simple boronic acids in combination with carboxylate functional groups. Furthermore all boronic acids studied display a *syn* configuration, which provides a perfect geometric complement with a carboxylate acceptor (Figure 3.35). Compounds **3.1**-**3.4** combine the common boronic···carboxylate $R^2_2(8)$ dimer motif with the boronic acid···boronic acid $R^2_2(8)$ synthon displaying the same type of hydrogen bonding pattern.

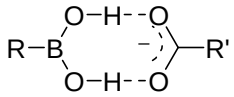

Figure 3.35 Boronic···carboxylate $R^2_2(8)$ motifs with the boronic acid in *syn* configuration.

The co-crystallisation of boronic acids with the copper(I) pyrazine-2,5-dicarboxylate complex studied here (**3.2**, **3.4**, **3.6** and **3.7**) occur in a 1:2 ratio [metal complex:boronic acid] in all cases; exceptions to this trend were observed in compounds **3.5** and **3.9** where the co-crystallisation occurs in a 1:1 ratio. Use of a varied range of solvents and crystallisation conditions has failed to allow the crystallisation of compounds **3.8**, **3.10** and **3.11**. The co-crystallisation of Cu_2(2,5-pzdca)$(PPh_3)_4$ with methylboronic acid has proved to be troublesome with the crystallisation of a second polymorph of compound Cu_2(2,5-pzdca)$(PPh_3)_4 \cdot 2B(OH)_3$ **3.2** instead of the desired co-crystal.

The range of boronic acids discussed in this chapter is somewhat limited in hydrogen bonding potential due to the limited commercial availability of boronic acids bearing, at

most, one extra donor/acceptor hydrogen bonding functionality therefore affording only one-dimensional structures. Only compound **3.9** presents a more extended structure due to the inclusion of water and dichloromethane molecules which help to produce a two-dimensional architecture. The weak hydrogen bond interactions in **3.9** play a very important role in extending the dimensionality of the systems. The co-crystallisation of Cu_2(2,5-pzdca)$(PPh_3)_4$ with boronic acids bearing further hydrogen bonding functionalities other than the $–B(OH)_2$ fails to produce arrays exhibiting higher dimensionality.

Analysis of the powder diffraction data for **3.2** shows the presence of phases other than that identified in the single crystal experiment. Although two phases could be identified, $Cu(PPh_3)_2(BH_4)$ and boric acid, and the sources of boric acid present in the samples could be identified, further investigations to identify the unknown phases in the sample are worthy of study to contribute to the current level of understanding.

3.4 EXPERIMENTAL

Materials

The starting materials pyridine-2-carboxylic acid, pyrazine-2-carboxylic acid, pyrazine-2,5-dicarboxylic acid, $Cu(SO_4)\cdot 6H_2O$, boric acid, phenylboronic acid, 3-aminophenylboronic acid, 2-bromophenylboronic acid, 4-bromophenylboronic acid, 4-carboxyphenylboronic acid, benzene-1,4-diboronic acid and methylboronic acid were purchased from commercial sources Aldrich, Lancaster and Acros. All solvents were purchased from Aldrich, Fisher or Lancaster. CH_2Cl_2 was distilled from CaH_2 under nitrogen.Et_2O was pre-dried using sodium wire before use.

Physical Measurements

Physical measurements were carried out using methods described in the preceding chapter. FT-IR spectra for compounds **3.1**-**3.11** were collected in the range 4000-500 cm^{-1} using a Shimadzu 8400S spectrometer. Powder X-ray measurements were performed using Cu-Kα radiation (λ = 1.5418 Å) on a Bruker D8 diffractometer in reflection geometry and a Braun position sensitive detector. The sample was loaded onto a silicon zero background substrate and the data were collected in the range $5 < 2\theta < 40°$ with a step time of 1 second and step width of 0.014°.

Syntheses

X-ray quality crystals of the desired compounds were obtained in very low yields preventing the acquisition of further data. Compounds **3.8**, **3.10** and **3.11** have not been crystallised and microanalysis and IR spectroscopy data show that the expected compounds have been obtained. Recrystallisation of the bulk material for all the compounds presented in this chapter was done using Et_2O and hexane. In all cases, microanalysis data were collected from the bulk materials which were dried in air before storage in a desiccator containing silica gel.

X-ray quality crystals of compounds **3.1**, **3.3**, **3.5**-**3.7** and **3.9**-**3.10** were obtained by slow evaporation of the dichloromethane saturated solutions at room temperature. For

compounds **3.2** and **3.4**, suitable X-ray quality crystals were obtained by allowing diethyl ether to diffuse into dichloromethane saturated solutions of the respectively compounds.

Characterisation Data

Compound 3.1 $Cu(2\text{-}pyca)(PPh_3)_2 \cdot B(OH)_3$

Colourless crystals.
Analysis calculated for $C_{42}H_{37}NO_5P_2BCu \cdot Et_2O \cdot 0.5CH_2Cl_2 \cdot H_2O$: C, 61.85; H, 5.52; N, 1.53. Found: C, 61.62; H, 5.80; N, 1.24%.
IR υ_{max} (KBr)/cm^{-1} 3215 (br, O-H), 3054 (Ar C-H), 1621 (asymm. CO_2^-), 1434 (C-O) and 1362 (B–O).

Compound 3.2 $Cu_2(2,5\text{-}pzdca)(PPh_3)_4 \cdot 2B(OH)_3$

Orange crystals.
Analysis calculated for $C_{78}H_{65}N_2O_7P_4BCu_2 \cdot 0.5CH_2Cl_2$.: C, 65.35; H, 4.58; N, 1.93. Found: C, 65.37; H, 4.68; N, 2.05%.
IR υ_{max} (KBr)/cm^{-1} 3374 (br, O-H), 3052 (Ar C-H), 1636 (asymm. CO_2^-), 1432 (C-O) and 1366 (B–O).

Compound 3.3 $Cu(2\text{-}pzca)(PPh_3)_2Cl \cdot B(OH)_3 \cdot CH_2Cl_2$

Orange crystals.
Analysis calculated for $C_{41}H_{36}N_2O_5P_2BCu \cdot CH_2Cl_2$.: C, 58.80; H, 4.46; N, 3.27. Found: C, 58.98; H, 4.78; N, 3.23%.
IR υ_{max} (KBr)/cm^{-1} 3215 (br, O-H), 3053 (Ar C-H), 1637 (asymm. CO_2^-), 1434 (C-O) and 1357 (B–O).

Compound 3.4 Cu_2(2,5-pzdca)$(PPh_3)_4 \cdot 2B(OH)_3$

Orange crystals.

Analysis calculated for $C_{78}H_{62}N_2O_4P_4Cu_2 \cdot CH_3B(OH)_2 \cdot B(OH)_3 \cdot C_4H_{10}O$: C, 64.81; H, 5.24; N, 1.82. Found: C, 64.31; H, 5.85; N, 1.81%.

IR υ_{max} (KBr)/cm^{-1} 3226 (br, O-H), 3053 (Ar C-H), 1635 (asymm. CO_2^-), 1433 (C-O) and 1358 (B–O).

Compound 3.5 Cu_2(2,5-pzdca)$(PPh_3)_4 \cdot C_6H_5\{B(OH)_2\}$

Yellow crystals.

Analysis calculated for $C_{47}H_{40}N_2O_4P_2BCu \cdot 0.5CH_2Cl_2 \cdot 0.5C_4H_{10}O$: C, 64.81; H, 5.00; N, 3.02. Found: C, 64.65; H, 5.16; N, 3.06%.

IR υ_{max} (KBr)/cm^{-1} 3421 (br, O-H), 3053 (Ar C-H), 1647 (asymm. CO_2^-), 1435 (C-O), 1368 (B–O), 816 and 743 (Ar C-H).

Compound 3.6 Cu_2(2,5-pzdca)$(PPh_3)_4 \cdot C_6H_4\{1,4\text{-}B(OH)_2\}_2$

Orange crystals.

Analysis calculated for $C_{84}H_{70}N_2O_8P_4B_2Cu_2 \cdot 0.5CH_2Cl_2$: C, 64.36; H, 4.52; N, 1.75. Found: C, 64.72; H, 4.71; N, 2.07%.

IR υ_{max} (KBr)/cm^{-1} 3275 (br, O-H), 3056 (Ar C-H), 1633 (asymm. CO_2^-), 1438 (C-O), 1366 (B–O), 819 and 742 (Ar C-H).

Compound 3.7 Cu_2(2,5-pzdca)$(PPh_3)_4 \cdot 2C_6H_4\{B(OH)_2\}$2-Br

Orange crystals.

Analysis calculated for $C_{84}H_{68}N_2O_6P_4BBrCu_2 \cdot H_2O$: C, 64.63; H, 4.52; N, 1.79. Found: C, 64.83; H, 4.92; N, 1.91%.

IR υ_{max} (KBr)/cm^{-1} 3347 (br, O-H), 3056 (Ar C-H), 1635 (asymm. CO_2^-), 1434 (C-O) and 1380 (br, B–O).

Compound 3.8 Cu_2(2,5-pzdca)$(PPh_3)_4$·C_6H_4{$B(OH)_2$}4-Br

Analysis calculated for $C_{90}H_{74}N_2O_8P_4B_2Br_2Cu_2$·$2CH_2Cl_2$·$H_2O$: C, 57.20; H, 4.17; N, 1.45. Found: C, 57.07; H, 4.35; N, 1.49%.
IR υ_{max} (KBr)/cm^{-1} 3217 (br, O-H), 3054 (Ar C-H), 1637 (asymm. CO_2^-), 1424 (C-O) and 1352 (br, B–O).

Compound 3.9 Cu_2(2,5-pzdca)$(PPh_3)_4$·C_6H_4{$B(OH)_2$}3-NH_2·H_2O·CH_2Cl_2

Red crystals.
Analysis calculated for $C_{84}H_{70}N_3O_6P_4BCu_2$·$0.5CH_2Cl_2$·$2H_2O$.: C, 65.29; H, 4.83; N, 2.69. Found: C, 65.68; H, 4.64; N, 2.33%.
IR υ_{max} (KBr)/cm^{-1} 3372 (br, O-H/N-H), 3055 (Ar C-H), 1631 (asymm. CO_2^-/N-H), 1436 (C-O), 1364 (B–O), 800 and 745 (Ar C-H).

Compound 3.10 Cu_2(2,5-pzdca)$(PPh_3)_4$·C_6H_4{$B(OH)_2$}4-COOH

Analysis calculated for $C_{85}H_{69}N_2O_8P_4BCu_2$·$2CH_2Cl_2$·$2C_4H_{10}O$: C, 62.48; H, 5.13; N, 1.53. Found: C, 62.38; H, 5.38; N, 1.35%.
IR υ_{max} (KBr)/cm^{-1} 3356-3057 (br, O-H), 1687 (C=O, acid), 1633 (asymm. CO_2^-), 1434 (C-O), 1370 (B–O).

Compound 3.11 Cu(2-pzca)$(PPh_3)_2$·C_6H_4{$B(OH)_2$}$_2$

Analysis calculated for $C_{47}H_{40}N_2O_4P_2BCu$: C, 67.76; H, 4.84; N, 3.36. Found: C, 67.38; H, 4.90; N, 3.07%.
IR υ_{max} (KBr)/cm^{-1} 3420 (br, O-H), 3049 (Ar C-H), 1636 (asymm. CO_2^-/N-H), 1436 (C-O), 1354 (br, B–O), 741 and 693 (Ar C-H).

3.5 Crystallographic Experimental

Data for compound **3.1** were collected using a Bruker SMART 1000 CCD diffractometer using graphite-monochromated Mo-K_α radiation (λ = 0.71073 Å). Data for compounds **3.3**, **3.4**, **3.7** and **3.8** were collected using a Bruker APEX 2 CCD diffractometer using graphite-monochromated Mo-K_α radiation (λ = 0.71073 Å). Data for compound **3.5** was collected using a Bruker APEX 2 CCD diffractometer using synchrotron radiation (λ = 0.7848 Å) at Daresbury SRS Station 9.8. Data for compound **3.6** was collected using a Bruker APEX 2 CCD diffractometer using synchrotron radiation (λ = 0.6911 Å) at Daresbury SRS Station 9.8. Data for compound **3.2** was collected using a Bruker-Nonius 95 mm CCD camera on κ-goniostat diffractometer using graphite-monochromated Mo- K_α radiation (λ = 0.71073 Å).

All structures were solved by direct methods (except structures **3.1** and **3.2** which were solved using Patterson synthesis) and refined by full-matrix least-squares methods on F^2. All *H* atoms which were placed in geometrically calculated position were refined using a riding model (aryl C–H 0.95 Å and hydroxyl O–H 0.84 Å). N*H* atoms in compound **3.8** were located in the difference Fourier map and were refined with restraints on the N–H bond length. $U_{iso}(H)$ values were set to be 1.2 times U_{eq} of the carrier atom for aryl and 1.5 times U_{eq} of the carrier atom for O*H*, N*H* and CH_3. Hydrogen atoms were not found on the water molecule in compound **3.8**. The coordinates of O*H* hydrogen atoms in compounds **3.1**, **3.2** and **3.4**-**3.6** were allowed to refine freely.

Unless stated as follows, all structural determinations proceeded without the need for further restraints or disorder modelling. Compound **3.3** was found to contain a disordered phenyl ring, which was modelled with two sets of positions 70.6(15):29.4(15)%, with C(55) and C(56) commons to the two rings. Compound **3.6** also exhibits disorder in two phenyl rings which were modelled over two set of positions [50.2(14):49.8(14)%] and [67.6(9):32.4(9)%] and restraints were placed on the anisotropic displacements parameters of the atoms involved. The coordinates of O*H* hydrogen atoms in compound **3.6** were refined with restraints on the O–H bond length.

Programs used during data collection, refinement and production of graphics were Bruker SMART, Bruker APEX 2, SAINT, SHELXTL, COLLECT, DENZO and local programs.[25,26,28,121-123]

Chapter 4

Synthesis and Supramolecular Coordination Chemistry of Ditertiary Phosphines Containing Nitrogen and Phosphorus Donor Atoms

4. Synthesis and Supramolecular Coordination Chemistry of Ditertiary Phosphines Containing Nitrogen and Phosphorus Donor Atoms

4.1. Introduction

The chemistry of phosphorus(III) compounds is centred on the lone pair and its availability to form new bonds. The geometry of these compounds is pyramidal (Figure 4.1) as would be expected and the pyramidal inversion is slow, with respect to its nitrogen analogues, and therefore they have a fixed pyramidal structure.

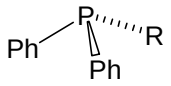

Figure 4.1 The pyramidal geometry of phosphorus(III) compounds [R = alkyl, aryl].

The spatial disposition of substituents around the phosphorus(III) centre plays a crucial role in providing such important properties as chirality and geometric/steric constraints. Therefore, systematic variations of substituents on phosphorus(III) centres are an effective tool for tuning electronic effects in phosphine ligands and their metal complexes.[187-191]

The connectivity between the P(III) atom and the lignad is often readily achieved by either P−C–N or P−C–C bond formation, and therefore a variety of substituents can be introduced at the R position (Figure 4.2).

Figure 4.2 General structure of P−C–N–C–P and P−C–C–C–P containing fragments.

Many ditertiary phosphines containing the P−C–C–C–P fragment have been reported to date,[192-196] with DPPP [DPPP = 1,3-(diphenylphosphino)propane] the simplest example which comprises a C_3-connectivity between the two $–PPh_2$ groups. Although there is

some literature precedence with P−C–C–C–P ligands bearing backbone functionalities [R = $–CH_2NHC_6H_5$, $–CONHC_6H_5$],[197] their multistep synthesis, in moderate yields and/or prior generation of a reactive phosphide intermediate lead us to investigate the use of the more easily prepared P−C–N–C–P ligands. Therefore in order to synthesise suitable new hybrid P−C–N–C–P type ditertiary phosphine ligands bearing backbone functionalities such as [R = $–C_6H_4(OH)(CH_2OH)$, $–C_6H_5(COOH)$],[198,199] simple phosphorus based Mannich condensations have been used.

4.1.1 $Ph_2PCH_2N(R)CH_2PPh_2$ Chemistry

Phosphorus-based Mannich condensation reactions have been used to prepare new ditertiary phosphines, $Ph_2PCH_2N(R)CH_2PPh_2$, from cheap and commercially available starting materials.[198,200] The method used involves the reaction of an appropriate primary amine with Ph_2PCH_2OH, readily preformed from equimolar amounts of $(CH_2O)_n$ and Ph_2PH, in methanol (Equation 4.1).[191,199] This synthetic procedure is versatile and offers many advantages over more classical routes of nucleophilic substitutions using primary/secondary phosphides, palladium catalysed P–C couplings and free radical additions.

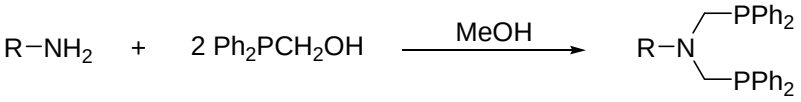

Equation 4.1

Durran *et al.* have applied this method to synthesise a series of ditertiary phosphines **4.1**-**4.3** bearing various functional groups (Equation 4.2).[198] The reactions were completed in short times and no purification steps were required.

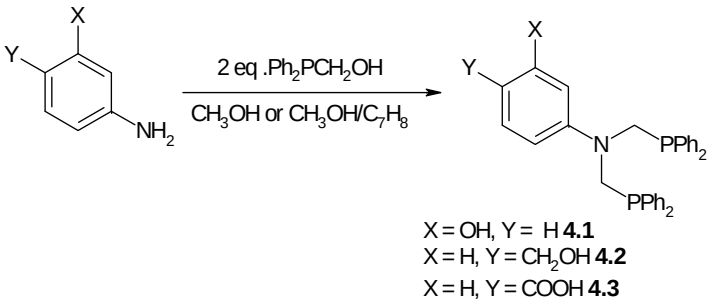

Equation 4.2

The crystal structure of **4.3** shows the Ph_2P– groups to adopt an *anti* configuration with respect to each other (Figure 4.3). Compound **4.3** forms dimers through a strong head-to-tail $R^2_2(8)$ interaction.

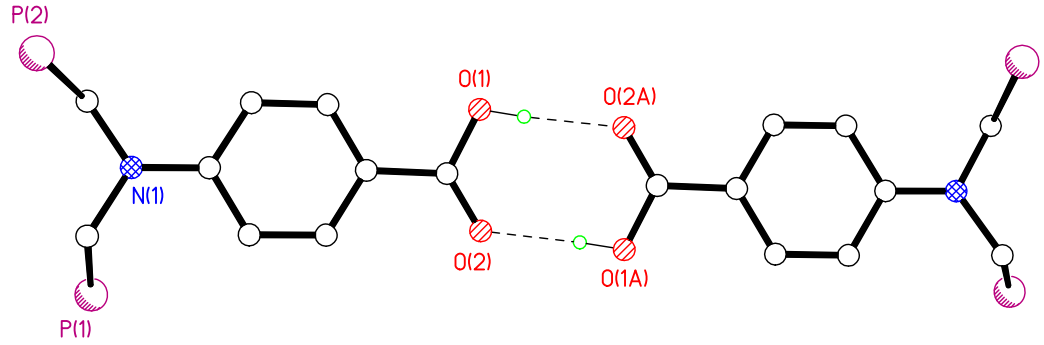

Figure 4.3 Dimers of compound **4.3**. Hydrogen atoms except O*H* and phenyl groups have been omitted for clarity.

Brown and co-workers have been interested in developing novel nonsymmetric ditertiary phosphines, **4.4** and **4.5**, using two consecutive Mannich-based condensation reactions (Equation 4.3).[201]

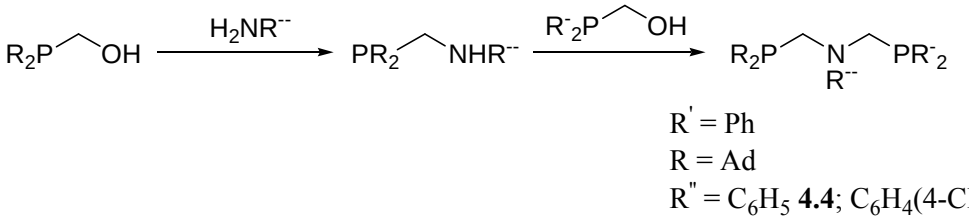

Equation 4.3

Reaction of ligands **4.4** and **4.5** with the corresponding metal(II) complexes [MCl_2(cod)] (M = Pd or Pt) afforded the corresponding Pt(II) and Pd(II) compounds in which the ligands adopt a chelating coordination mode (Figure 4.4).

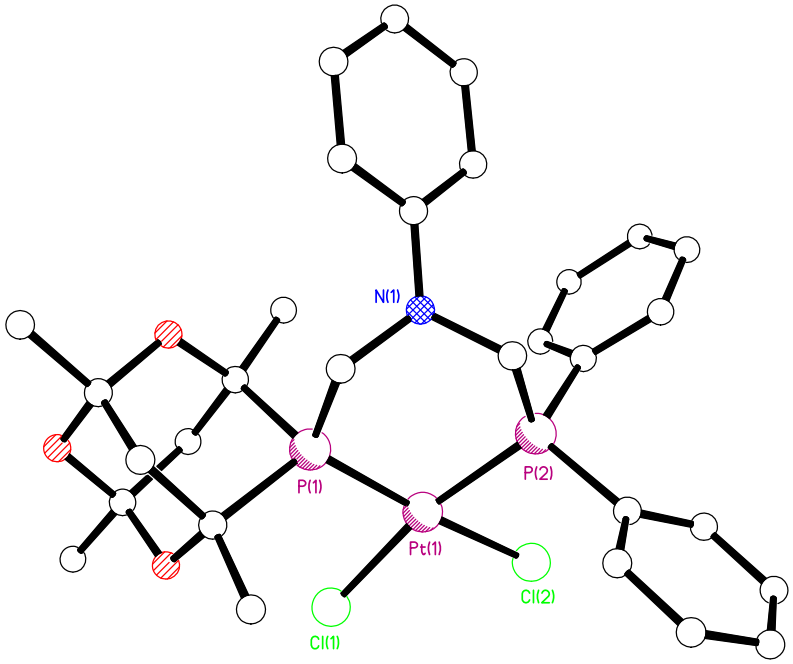

Figure 4.4 Molecular structure of the Pt(II) complex formed with ligand **4.4**. Hydrogen atoms and solvent molecules have been removed for clarity.

The metal centre is square-planar and the P(2)–Pt(1)–Cl(2) bond angle is contracted by 10° with respect to P(1)–Pt(1)–Cl(1) reflecting the different steric effects of phenyl *vs*. adamantane groups.

4.1.2 Coordination Chemistry of Ditertiary and Polytertiary Phosphines

Polydentate phosphine ligands have a number of advantages compared with monodentate systems, including an increased nucleophilicity (or basicity) at the metal centre, more control of the coordination number, stoichiometry and stereochemistry of the resulting metal complexes and useful detailed structural and bonding information from phosphorus-phosphorus and metal-phosphorus coupling constants in NMR

spectroscopy.[202] Numerous tridentate and tetradentate phosphines have been documented,[191,202] these phosphines can be linear, tripodal or branched (Figure 4.5).

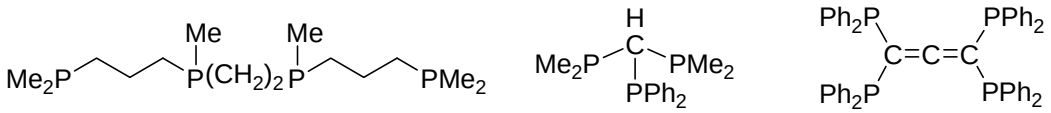

Figure 4.5 Examples of polydentate phosphine ligands.

The phosphine ligands coordinate to various metal centres to afford mononuclear, binuclear or trinuclear complexes with different coordination numbers [four, five and six] and different structures such as, tetrahedral, square planar, square pyramidal or octahedral (Figure 4.6).

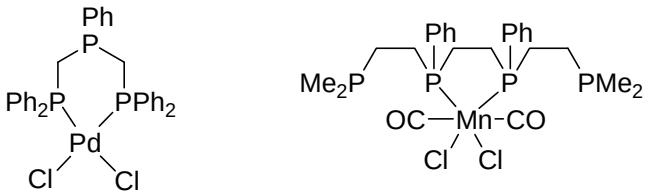

Figure 4.6 Examples of square planar and octahedral complexes.

Fernández and co-workers reported an interesting example of tetranuclear (phosphine)(thiolato)gold(I) compounds (Equation 4.4).[203] The tetradentate ligand $(Ph_2PCH_2)_2NCH_2CH_2N(CH_2PPh_2)_2$ was synthesised following a synthetic method first reported by Grim,[204] by condensation of paraformaldehyde with diphenylphosphine and ethylenediamine.

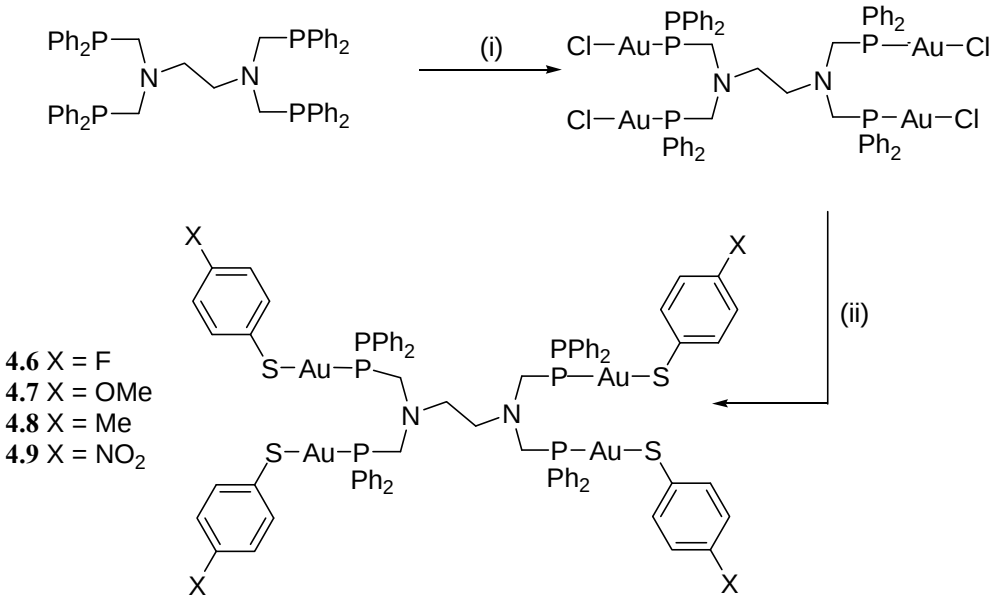

Equation 4.4 (i) $[Au(C_6F_5)(tht)]$; (ii) NaOMe, $SH–C_6H_4–X$ (X = F, OMe, Me or NO_2).

The crystal structure of complex **4.7** shows that the metal centres associate into pairs through weak intramolecular Au···Au interactions [3.1485(4) Å] (Figure 4.7).

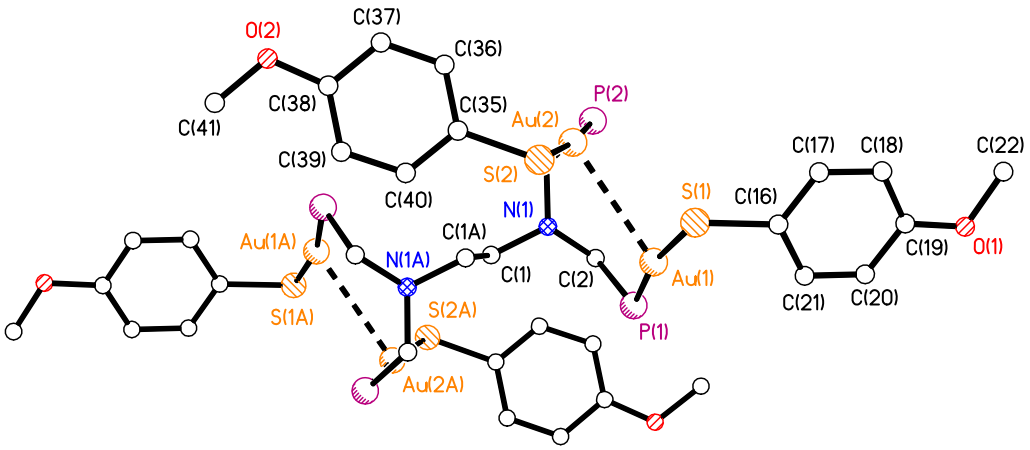

Figure 4.7 Molecular structure of compound **4.7**. Phenyl groups and hydrogen atoms have been omitted for clarity.

Kane and co-workers have described the crystal structure of another class of potentially tetradentate ligand, $[P(Ph)CH_2N(2\text{-pyridyl})CH_2]_2$ **4.10**, first synthesised by Märkl (Figure 4.8).[205,206] The heterocycle adopts a *crown* configuration, with the two phosphorus atoms oriented *syn* to each other, suitable for metal chelation.

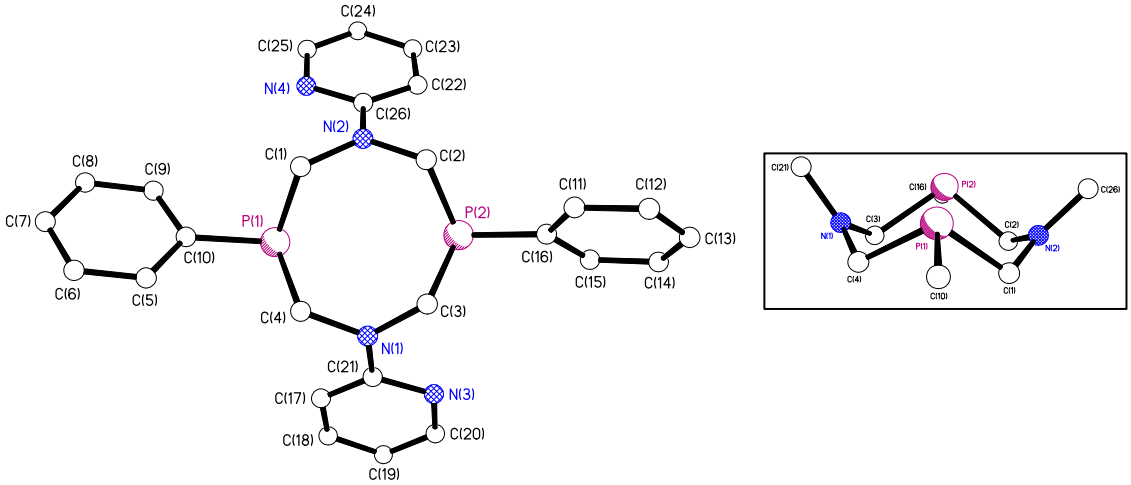

Figure 4.8 Molecular structure and *crown* conformation of ligand **4.10**. Hydrogen atoms have been removed for clarity.

The reaction of **4.10** with $Mo(CO)_4$(nbd) in dichloromethane afforded the complex **4.11** in which the ligand adopts a *chair-boat* conformation (Figure 4.9). Chelation to the $Mo(CO)_4$ moiety led to a closing of the two phosphorus ring atoms compared with the free ligand [3.023(3) Å and 3.750(2) Å respectively].

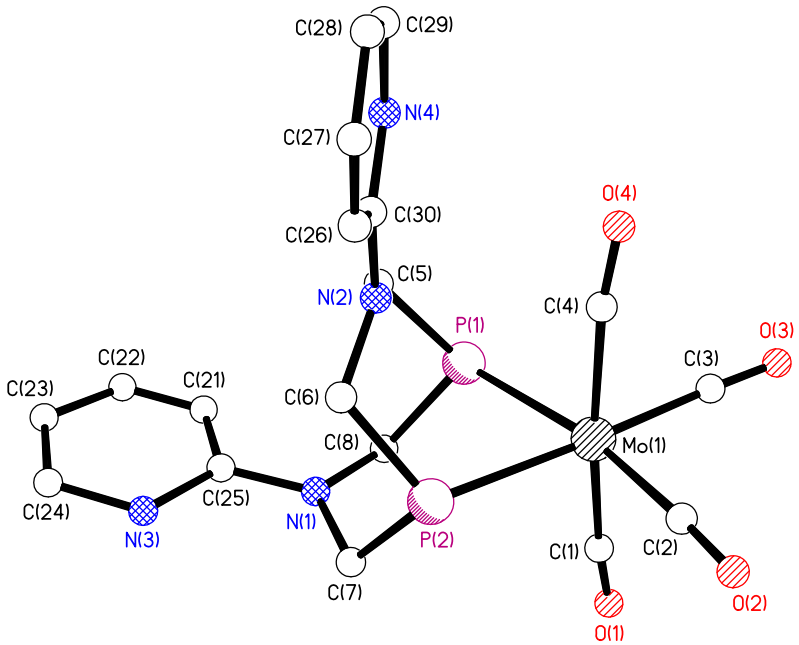

Figure 4.9 View of compound **4.11**. Phenyl groups and hydrogen atoms have been removed for clarity.

Elsegood and co-workers reported the synthesis and coordination studies of a terdentate carboxylic acid ditertiary phosphine $C_6H_4(OCH_3)(COOH)N(CH_2PPh_2)_2$ **4.12** (Equation 4.5).[190]

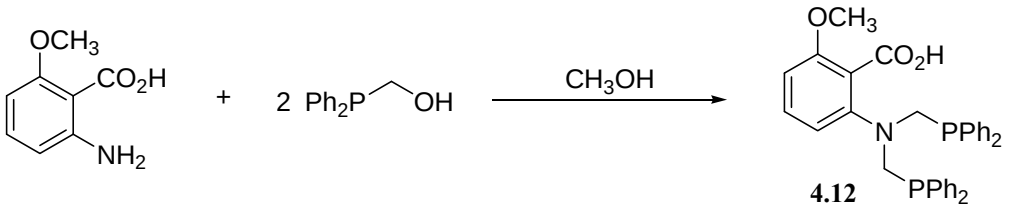

Equation 4.5

Treatment of **4.12** with one equivalent of $Pd(CH_3)Cl(cod)$ in dichloromethane and further metathesis with NaI in acetone afforded the 48-membered hexanuclear Pd_6 metallomacrocycle $[PdI\{2\text{-}\{Ph_2PCH_2)_2N\}\text{-}6\text{-}(OCH_3)C_6H_3CO_2\}]_6$ **4.13** (Figure 4.10). Ligand **4.12** adopts a monoanionic form coordinating one Pd(II) centre through both phosphorus atoms and the second Pd(II) centre *via* a single oxygen-donor centre from the carboxylate group.

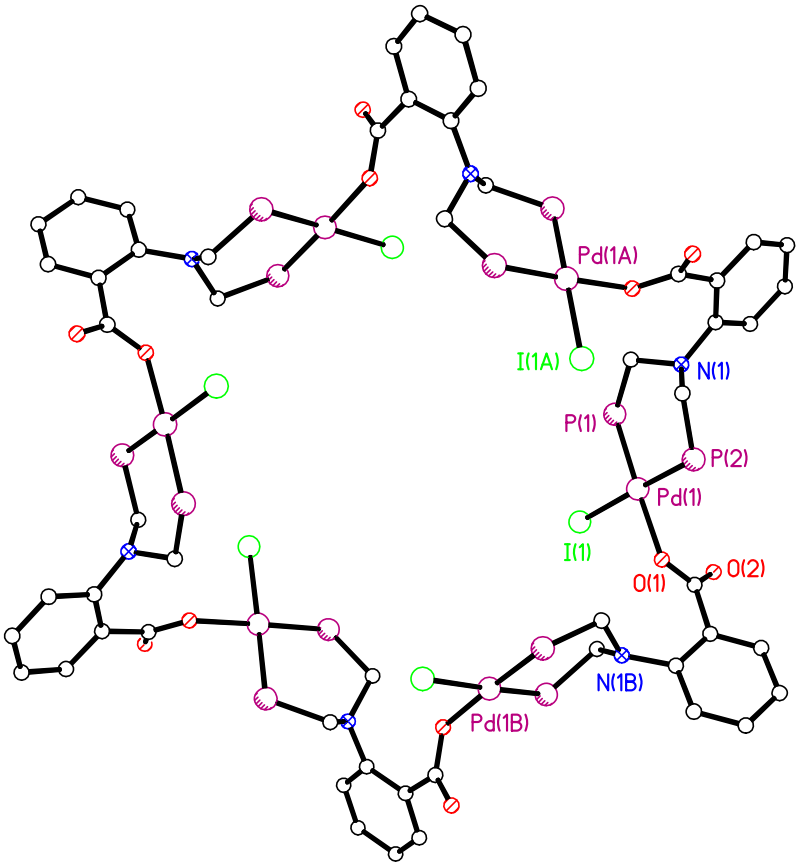

Figure 4.10 Molecular structure of **4.13.** Phenyl groups on each phosphorus atom, all hydrogen atoms, methoxy groups and solvent molecules of crystallisation have been omitted for clarity.

The work of Durran and co-workers aimed at studying the reactivity of an uncommon series of ditertiary phosphine ligands bearing the donor set combination P/N/Se (Equation 4.6) was reported.[207] Compounds **4.14** and **4.15** were found to react with $MCl_2(cod)$ (M = Pt, Pd) to form **4.16-4.19** in good yield.

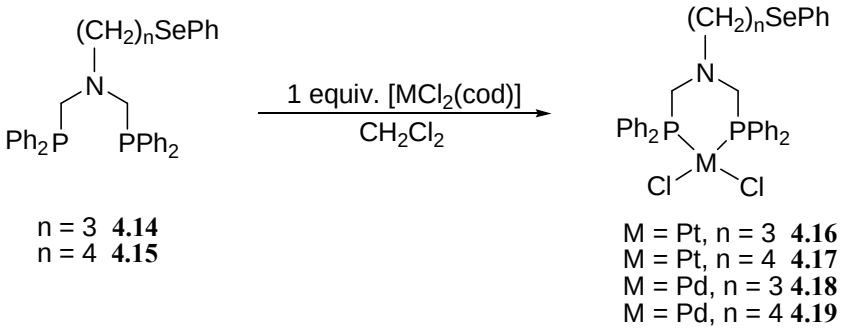

Equation 4.6

The crystal structure of **4.17** shows a *cis* configuration with respect to the two phosphorus donors. The Pt(II) displays a near square-planar coordination environment and the Pt–P–C–N–C–P six-membered ring adopts a boat conformation with the N(1) atom out of the plane [± 0.152 Å] (Figure 4.11). It is interesting to notice that the pendant phenylseleno group is amenable to further coordination chemistry.

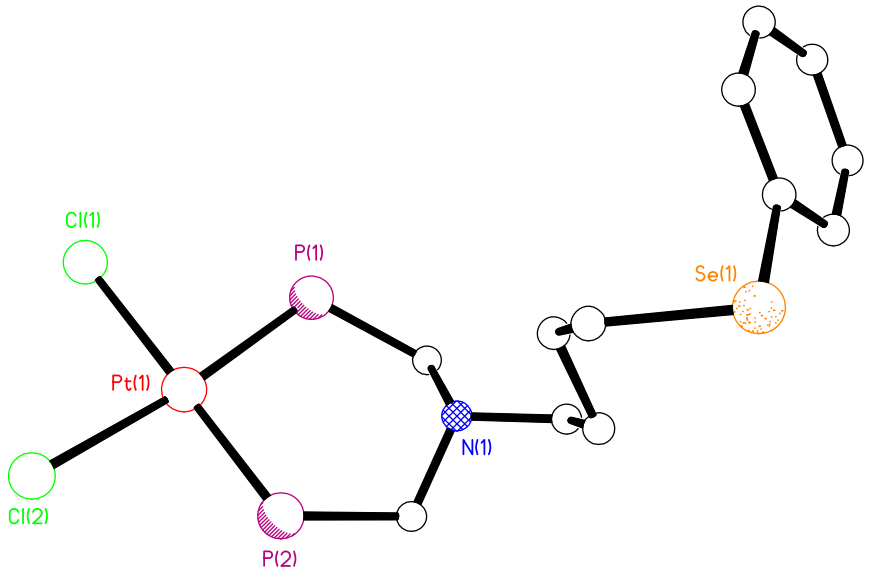

Figure 4.11 View of the asymmetric unit for compound **4.17**. Phenyl groups and hydrogen atoms have been removed for clarity.

Although heterofunctional phosphorus containing ligands bearing a soft phosphorus atom and a hard nitrogen donor atom have found important applications in catalysis and coordination chemistry,[208-215] there is very little documented regarding the use of ditertiary phosphine ligands in supramolecular chemistry. A brief survey of some of these examples is discussed below.

4.1.3 Applications of P–C–N–C–P Based Ligands

Phosphine ligands have seldom been exploited in crystal engineering although they can readily be modified with various functional appendages such as polar carboxylic acid groups.[198,216-218] Recently, Smith and co-workers synthesised and structurally

determined a range of isomeric Au(I) and Pd(II) complexes with ditertiary phosphines containing phenol and carboxylic acid appendages (Equation 4.7).[187,189]

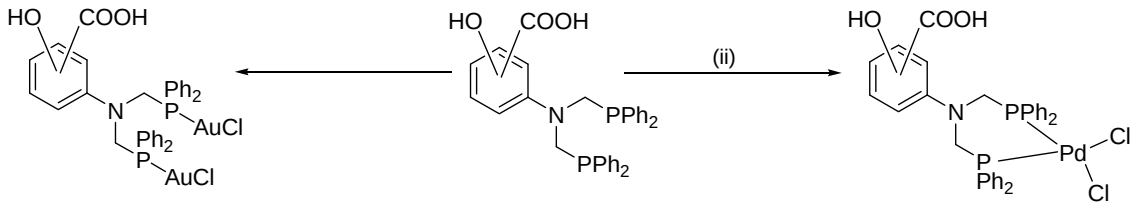

Equation 4.7 (i) 2 equiv. AuCl(tht), CH_2Cl_2; (ii) 1 equiv. $PdCl_2$(cod), CH_2Cl_2.

A range of supramolecular synthons have been observed and dictated by various factors including the nature, predisposition of the –OH and –COOH functional groups, the flexibility about the N–C_{arene} bond and the choice of solvent used in recrystallisation.

The gold(I) complexes crystallise as one-dimensional chain structures when a hydrogen bonding functional group (–COOH or –OH) is located in the 3- or 4-position on the phenyl group with respect to the *N* atom and the second hydrogen bonding functional group is located at least one carbon position away from the –COOH or –OH substituent (Figure 4.12). This example also shows intramolecular Au···Au aurophilic interactions [3.0722(9)].

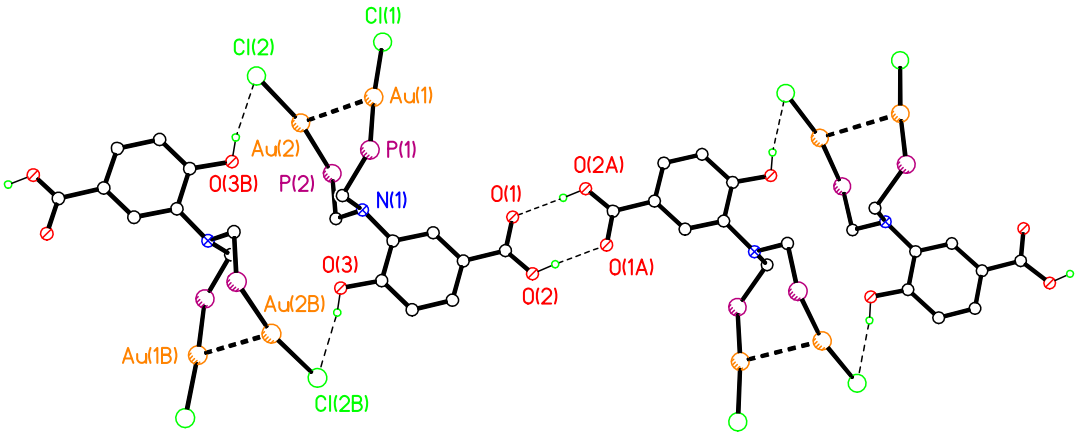

Figure 4.12 Example of one-dimensional polymeric chain. Phenyl groups and hydrogen atoms not involved in hydrogen bonding have been removed for clarity.

In contrast, when the –COOH or –OH functional groups are adjacent to each other on the arene core, dimeric species are preferred (Figure 4.13). This shows that the regioselective incorporation of functional appendages, $–N(CH_2PPh_2)_2$, –COOH and –OH around a central arene core has a pronounced effect on the structural motifs obtained.

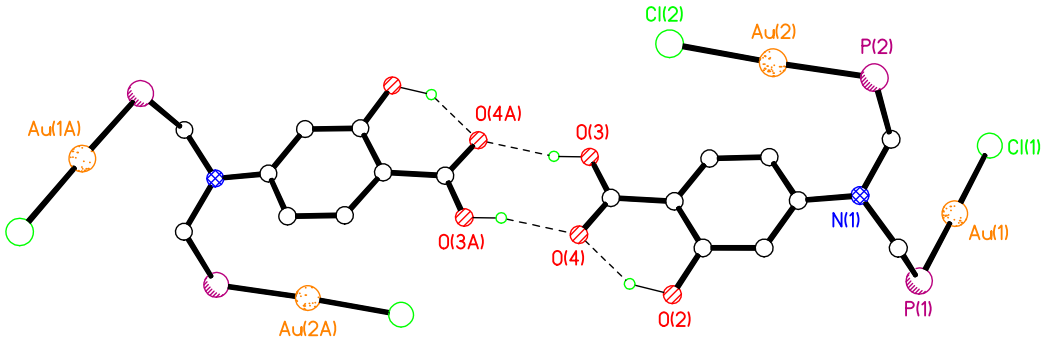

Figure 4.13 Example of dimer formation. Phenyl groups and hydrogen atoms not involved in hydrogen bonding have been omitted for clarity.

Interestingly, for comparison with the gold(I) complex described above which aggregates as a dimer when the –COOH or –OH functional groups are adjacent to each other, the Pd(II) analogue **4.18**, does not present the classic head-to-tail hydrogen bonded carboxylic acid synthon (Figure 4.14). Compound **4.18** crystallises showing the same intramolecular *S*(6) synthon observed above but a one-dimensional chain is formed instead through intermolecular O–H···Cl hydrogen bonding.

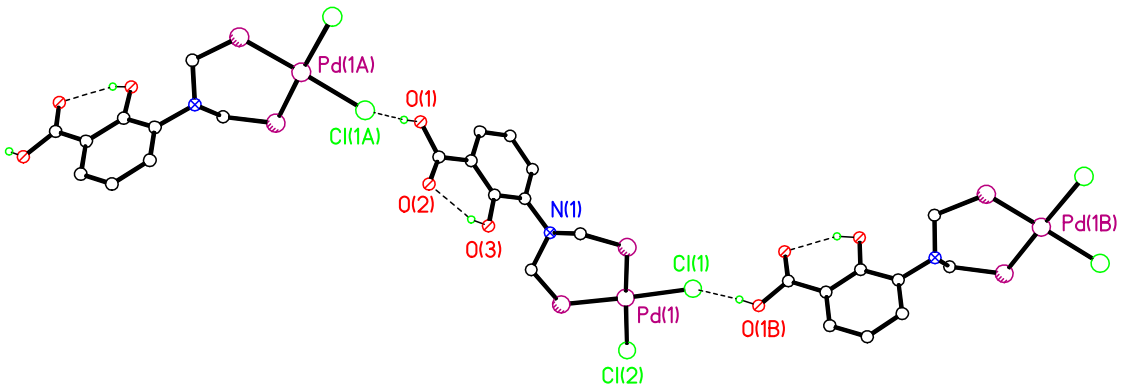

Figure 4.14 View of **4.18** showing a portion of a hydrogen bonded chain. Phenyl groups and hydrogen atoms except O*H* have been omitted for clarity.

Complexes of $(Ph_2PCH_2)_2NC_6H_4X$ ligands with a number of metals such as palladium, rhodium, ruthenium and platinum have exhibited high activity in catalysis.[219] Rhodium complexes were prepared *in-situ* using $Rh(cod)BF_4$ with bis((diphenylphosphino)methyl)aniline ligands and used these in the hydroformylation of 1-octene and 2-vinylnaphthalene. The complexes formed with these ligands were more active than the equivalent complex using bis(diphenylphosphino)propane (4 to 10 times more) (Equation 4.8).

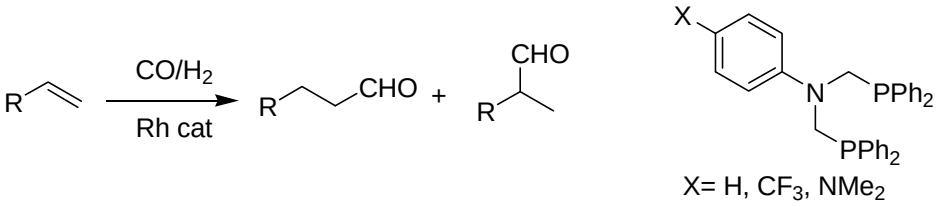

Equation 4.8 Hydroformylation of 1-octene and 2-vinylnaphthalene using P-C-N-C-P ligands.

Heterogeneous catalysis was also investigated; Alper and Bourque studied the use of silica-supported dendritic rhodium complexes in hydroformylation reactions using ligands with a $–N[(CH_2)_nCONHCH_2CH_2N(CH_2PPh_2)_2]_2$ chelating motif where n = 2, 4 and 6.[220] The use of bead-supported and activated carbon-supported catalysts was subsequently reported.[221-223]

Palladium complexes with P-C-N-C-P ligands are versatile coupling reagents. Examples include carbonylation reactions using dendritic palladium(II) complexes immobilized on silica (using ligands with a $–N[(CH_2)_2CONHCH_2CH_2N(CH_2PPh_2)_2]_2$ chelating motif),[224] Heck reaction between aryl halides and methyl acrylate under homogenous conditions using bis((diphenylphosphino)methyl)-alkyl (alkyl= methyl, *tert*-butyl) and -arylamine ligands and a palladium(II) source,[225] Suzuki and Sonogashira coupling using MCM-supported palladium(0) catalysts.[226,227] Recently, Alper and Lu used a solid-supported palladium(II) complex to prepare a series of heterocycles, precursors to enantiomerically enriched lactams.[228]

Del Zotto and co-workers reported the use of complexes of ruthenium(II) with P−C−N−C−P ligands in transfer hydrogenation reactions under homogeneous and heterogeneous conditions (Equation 4.9).[229]

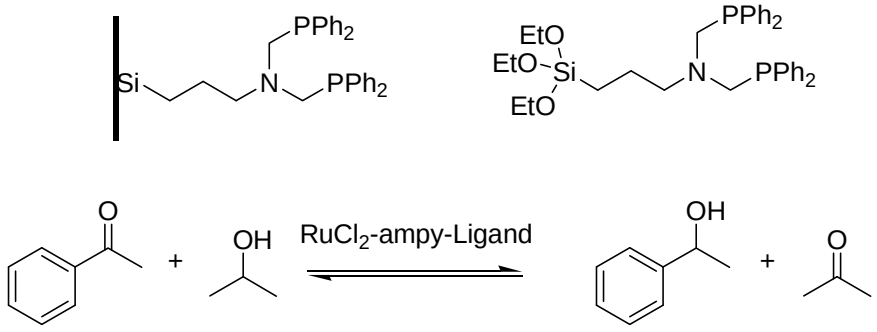

Equation 4.9 Transfer hydrogenation reaction catalysed by Ru(II) complexes [ampy = (2-aminomethyl)pyridine].

Wu and Li used a *N*,*N*-bis((diphenylphosphino)methyl)butan-1-amine ligand complex with platinum(1,3-divinyl-1,1,3,3-tetramethyldisiloxane) to obtain high stereoselectivities and high yields in hydrogenation reactions of a wide range of alkynes.[230]

Phosphines have been shown to play an important role in the design of radiometal-antibody conjugates by their versatile ligating capability with transition metals.[196,231,232] Zhang and co-workers have investigated the cytotoxic activity against murine and human cancer cells of a series of bis(diphenylphosphinomethyl)amine rhenium(I) complexes.[233] These compounds do not show activity against non-cancerous human fibroblast cells which is an important property for any chemotherapeutic agent since harmful side-effects of the treatment will be minimised. The authors also describe a probable mode of action based on ESMS (electrospray mass spectrometry) studies, in which the rhenium(I) complexes described would bind to DNA bases or side-chains of amino acid residues in peptides and proteins after displacement of the bromide ligands.

Curtis, Das and Jacobsen reported independently the synthesis, structural analysis and electrochemical studies of Fe(II) or Ni(II) complexes containing P–C–N–C–R [R = C_6H_6, *n*-Bu, CH_3 or CH_2CH_2OMe] ditertiary ligands with pendant amine bases.[234-237] Some of these complexes have been shown to mimic the active site of hydrogenases.

Dendrimers were originally referred to as cascade molecules and are best described as highly branched regular three dimensional, mono-dispersed macromolecules, with a branch occurring at each monomer unit. They are characterised by the presence of large numbers of functional groups on the surface, which results in solubility, viscosity and thermal behaviours different from more classical polymers. Commercial applications of these dendrimers have been identified and include medical diagnostics and catalysis.[238,239]

Reetz and co-workers reported the synthesis of a dendritic diphosphine and the preparation of corresponding metal and bimetallic complexes.[240] Double phosphinomethylation of each of the 16 primary amino end groups of the DAB-based (DAB = 1,4-diaminobutane) polyamino dendrimer DAB-dendr-$(NH_2)_{16}$ proceeds in essentially quantitative yield to give **4.20** upon use of Ph_2PCH_2OH prepared *in situ* from CH_2O and $HPPh_2$ (Equation 4.10). Dendrimer **4.20** was characterised by elemental analysis, IR and NMR spectroscopy. Compound **4.20** with 16 bidentate ligands on the outer surface, provides a suitable site for complexation to a variety of transition metals such as, Pd(II), Rh(I) and Ir(I).

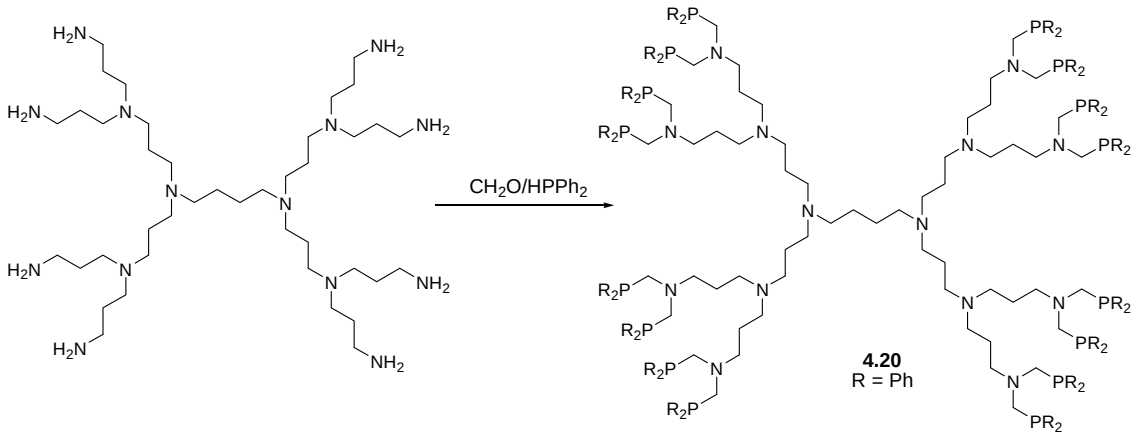

Equation 4.10

The limited previous investigations of isomeric series of ditertary phosphines bearing functional appendages with hydrogen bonding capability have identified them as suitable molecular building blocks for the creation of supramolecular arrays,

particularly those incorporating a combination of coordination and hydrogen bonding interactions.

Analysis of the extensive coordination chemistry, particularly the formation of square planar, linear and octahedral complexes, shows the versatility of these ligands and also that the inclusion of potential hydrogen bonding acceptors such as Cl– and CO– bonded to the metal centre, [$PtCl_2$], [AuCl] and [$Mo(CO)_4$], may allow the extension of the hydrogen bonding arrays in a different manner than the ones observed in the free ligands and between different coordination geometries.

4.2 Results and Discussion

Although phosphine ligands can be readily modified with various functional appendages with hydrogen-bonding capability such as polar carboxylic acid groups,[187,189] they have seldom been exploited in supramolecular chemistry. Therefore, as part of ongoing studies aimed at exploiting highly functionalised phosphorus based ligands in crystal engineering, the synthesis, structural analysis and metal complexation studies with selected transition metals of an isomeric series of functionalised phenols (some of them containing Me or ^{t}Bu groups) ditertiary phosphine ligands, (Figure 4.15), is presented. The structures of the new compounds have been elucidated by a combination of multinuclear NMR spectroscopy, IR spectroscopy, elemental analysis and in several cases, by X-ray crystallography.

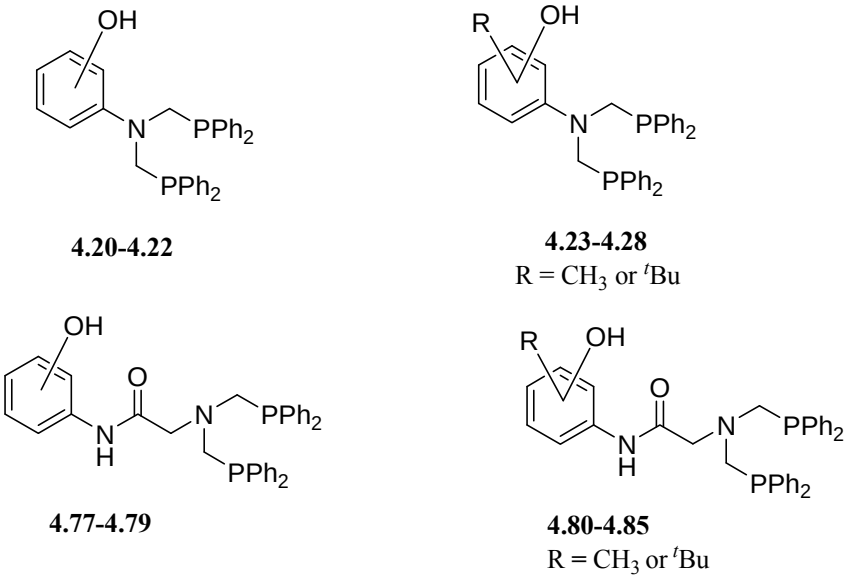

Figure 4.15 Ditertiary functionalised *bis*(phosphino)amines prepared in this study.

4.2.1 Syntheses of $C_6H_4(OH)N(CH_2PPh_2)_2$ 4.20-4.22, $C_6H_3(OH)(CH_3)N(CH_2PPh_2)_2$ 4.23-4.27 and $C_6H_3(OH)(^tBu)N(CH_2PPh_2)_2$ 4.28

The phenol functionalised ditertiary phosphine ligands $C_6H_4(OH)N(CH_2PPh_2)_2$ **4.20–4.22**, $C_6H_3(OH)(CH_3)N(CH_2PPh_2)_2$ **4.23–4.27** and $C_6H_3(OH)(^tBu)N(CH_2PPh_2)_2$ **4.28** were prepared using a Mannich-based condensation reaction which is an efficient and versatile method for the synthesis of novel hybrid phosphine ligands.[43-45] Two

equivalents of Ph_2PCH_2OH were reacted with one equivalent of the primary amine **I-IX** yielding the desired *bis*(phosphino)amine after 24 h at room temperature under N_2 (Equation 4.11).

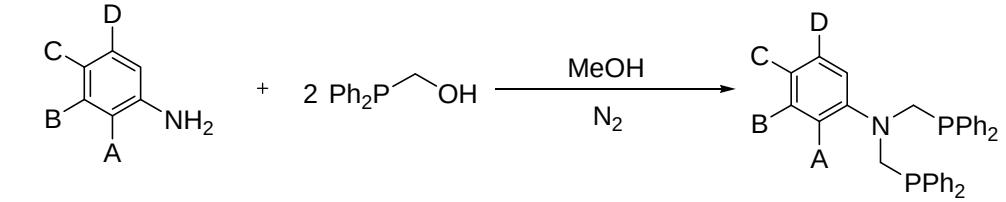

A = OH, B,C,D = H **I**
B = OH, A,C,D = H **II**
C = OH, A,B,D = H **III**
A = OH, D = CH_3, B,C = H **IV**
A = CH_3, C = OH, B,D = H **V**
A = OH, C = CH_3, B,D = H **VI**
B = OH, C = CH_3, A,D = H **VII**
C = OH, B = CH_3, A,D = H **VIII**
A = OH, D = ^{t}Bu, B,C = H **IX**

A = OH, B,C,D = H **4.20**
B = OH, A,C,D = H **4.21**
C = OH, A,B,D = H **4.22**
A = OH, D = CH_3, B,C = H **4.23**
A = CH_3, C = OH, B,D = H **4.24**
A = OH, C = CH_3, B,D = H **4.25**
B = OH, C = CH_3, A,D = H **4.26**
C = OH, B = CH_3, A,D = H **4.27**
A = OH, D = ^{t}Bu, B,C = H **4.28**

Equation 4.11

In all the syntheses, the solution was concentrated under reduced pressure and the white solid **4.20**–**4.28** filtered off. These compounds were found to be air stable in the solid state, but oxidised quickly in solution. Ligands **4.20**–**4.28** were obtained in 58-97% yields. They exhibited a single resonance in their $^{31}P\{^1H\}$ NMR spectra [$(CD_3)_2SO$] in the region of δ(P) −25.32 to −27.63 ppm, indicating the presence of only one phophorus(III) environment. These ligands were also characterised by ^1H NMR spectroscopy. These data supported the double condensation inferred from the absence of an N*H* signal that would be expected if single substitution had occurred.

4.2.1.1 Crystal Structures of Compounds 4.21–4.23

X-ray quality crystals of compounds **4.21-4.23** were obtained by slow evaporation of the methanol filtrate. Structure analysis clearly shows approximate pyramidal geometries about both phosphorus centres (Table 4.1). There is little spread in the P–C and C–N bond lengths in ligands **4.21**–**4.23** and they are consistent with the values reported for other ditertiary phosphine ligands.[190] The P(III) atoms are in the *anti* conformation presumably in order to reduce steric repulsions between the bulky phenyl groups. The geometry about each N(1) centre is approximately pyramidal for ligands

4.22 and **4.23** [Σ(C–N–C) angles about N(1) centre = 335.0(2)° and 337.1(4)° respectively] and approximately trigonal planar for **4.21** [Σ(C–N–C) = 359.03(11)°].

Table 4.1 Selected bond lengths (Å) and angles (°) for compounds **4.21–4.23**.

	4.21	**4.22**	**4.23**
P(1)–C(1)	1.8748(14)	1.870(3)	1.850(5)
P(2)–C(2)	1.8840(14)	1.855(3)	1.841(5)
C(1)–N(1)	1.4517(16)	1.467(4)	1.471(6)
C(2)–N(1)	1.4541(16)	1.469(4)	1.476(6)
P(1)–C(1)–N(1)	113.72(9)	115.9(2)	113.7(3)
P(2)–C(2)–N(1)	112.57(9)	112.3(2)	113.7(3)
C(1)–N(1)–C(2)	117.28(11)	112.1(2)	112.5(3)
C(1)–N(1)–C(3)	120.31(11)	110.3(2)	111.6(4)
C(2)–N(1)–C(3)	121.45(11)	112.6(2)	113.0(4)

Compounds **4.21**–**4.23** contain one molecule in the asymmetric unit, which differs in the disposition of the PCNCP fragment with respect to the functionalised phenyl ring (Figure 4.16). While in compounds **4.22** and **4.23**, the functionalised phenyl rings are twisted almost perpendicular to the C(1)–N(1)–C(2) fragment, 88° and 86° respectively, for compound **4.21**, the twist of the C(1)–N(1)–C(2) fragment lies within 9° of co-planarity with the functionalised phenyl group, apparently as a result of the hydrogen bonding requirements.

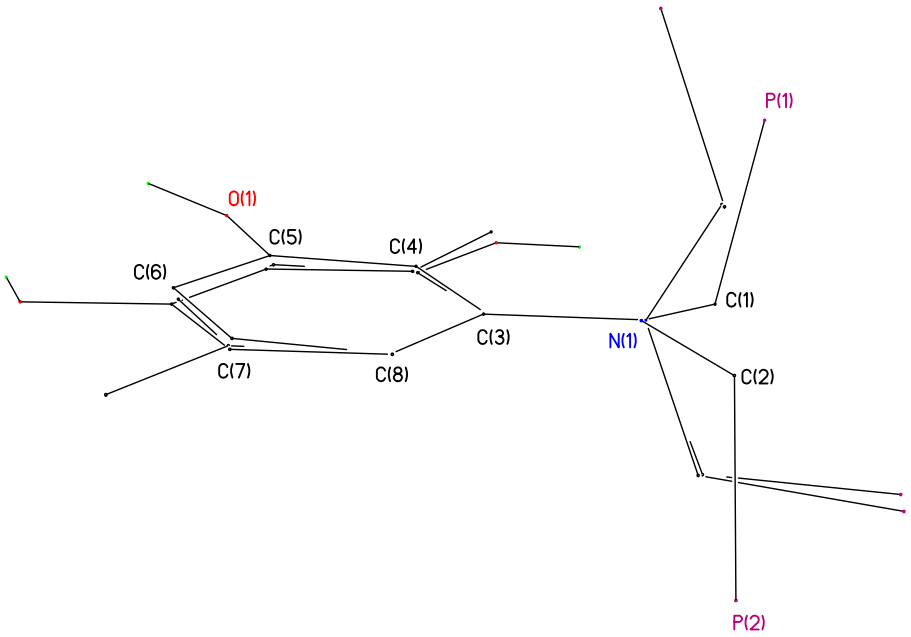

Figure 4.16 Overlay view of structures **4.21**–**4.23**, solvent molecule for compound **4.22** has been omitted for clarity. Phenyl rings and hydrogen atoms except O*H* have been omitted for clarity.

The supramolecular synthons observed in the solid state for these highly modular ligands may be dictated by various factors including the nature of the ligand, the PCNCP fragment flexibility, the predisposition of the OH/CH_3 groups about the N-arene and the solvent used in the crystallisation.

4.2.1.2 Secondary Interactions in Compounds 4.21–4.23

In order to probe the interplay due to the position of the OH/CH_3 groups, the crystal structure of **4.23** with the –OH group in the *ortho* position with respect to the N atom is described first. Ligand **4.23** crystallises with an intramolecular *S*(5) hydrogen bond graph set which is favourable due to the disposition of the hydroxyl functional group (Figure 4.17). The intramolecular hydrogen bonding in **4.23** limits the dimensionality of the packing of the phosphine ligand. Therefore, the structure of **4.23** is essentially zero-dimensional (Table 4.2).

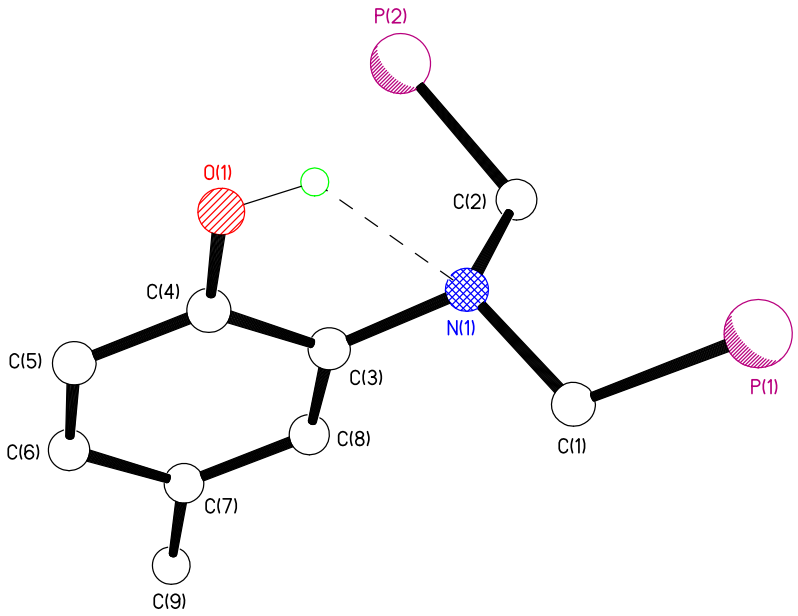

Figure 4.17 View of the asymmetric unit of **4.23**. Phenyl groups and hydrogen atoms except OH have been removed for clarity.

Table 4.2 Selected hydrogen bonding parameters for **4.23**.

D–H···A	D···A/Å	D–H/Å	H···A/Å	D–H···A/º
O(1)–H(1)···N(1)	2.746(5)	0.84	2.27	116.2

Compound **4.21**, where the −OH functional group is in the *meta* position with respect to the tertiary N atom, aggregates in the solid state in such a way that weak hydrogen bonds O−H···P [P···O length 3.46 Å, 166°] form between symmetry related molecules creating dimers in which the two ligands are held in a $R^2_2(16)$ motif (Figure 4.18).[10] The distance between symmetry related nitrogen atoms is 8.26 Å.

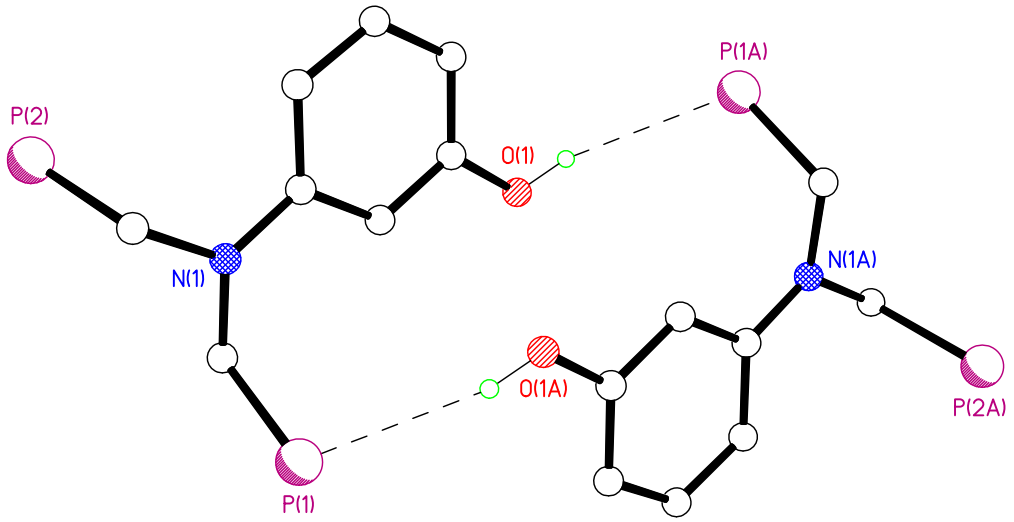

Figure 4.18 Dimers of **4.21**. Phenyl groups and hydrogen atoms not involved in hydrogen bonding have been removed for clarity.

Compound **4.22**, which contains the −OH group in a *para* position with respect to the tertiary N-arene functionality, crystallises with the inclusion of one molecule of methanol per ligand. The methanol molecule was found to be disordered over two sets of positions. This disorder can be explained by the fact that both components are involved in hydrogen bonding. While the first component C(34)–O(2) bonds to the hydroxyl *O* of one **4.22** molecule, the second component C(34X)–O(2X) is involved in a strong (component 2)O–H···O(component 1) interaction with a symmetry related solvent molecule (Figure 4.19). The combination of strong O–H···O and weak (hydroxyl)O−H···P, [P···O bond distance 3.44 Å], hydrogen bonds creates one-dimensional tapes.[10] Selected hydrogen parameters for **4.22** are shown in Table 4.3.

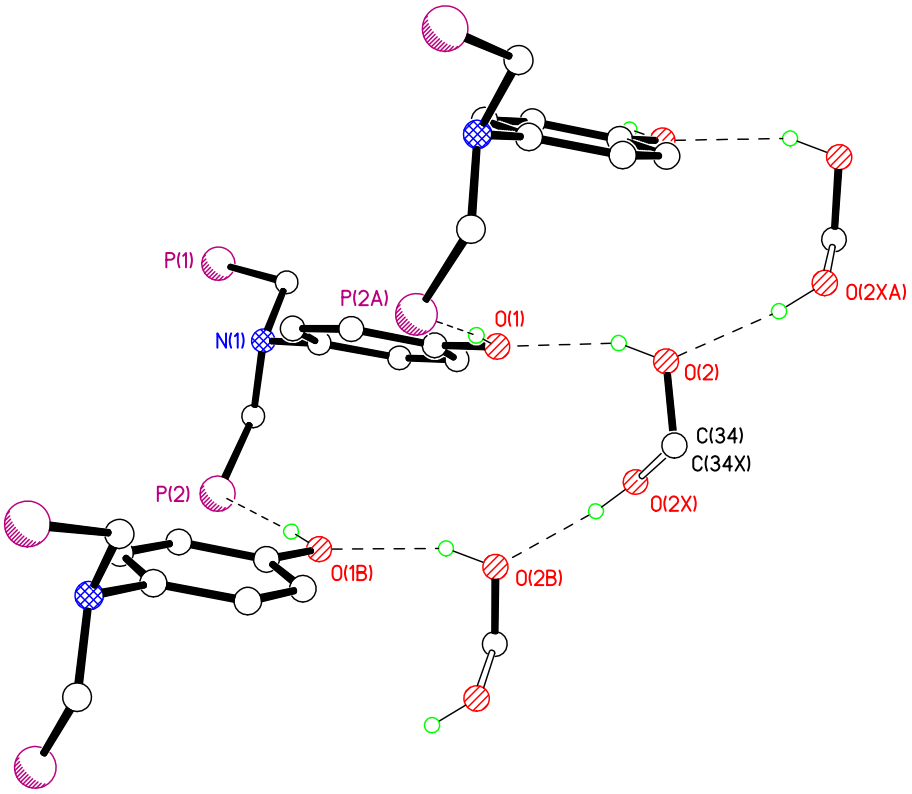

Figure 4.19 View of the hydrogen bonded tapes formed in compound **4.22**. Hydrogen atoms not involved in hydrogen bonding, phenyl and methyl groups have been omitted for clarity.

Table 4.3 Selected hydrogen bonding parameters for **4.22**.

D–H···A	D···A/Å	D–H/Å	H···A/Å	D–H···A/°
O(2)–H(2)···O(1)	2.825(8)	0.84	2.03	158
O(2X)–H(2X)···O(2B)^{i}	2.799(11)	0.84	1.96	172

Symmetry operation: ^{i}x, -y+1/2, z-1/2.

4.2.2 Coordination Chemistry of $C_6H_3(OH)N(CH_2PPh_2)_2$ 4.20–4.22, $C_6H_4(OH)(CH_3)N(CH_2PPh_2)_2$ 4.23–4.27 and $C_6H_3(OH)(^tBu)N(CH_2PPh_2)_2$ 4.28

4.2.2.1 Syntheses of Square Planar Pt(II) Complexes 4.29-4.37

The synthesis of *P*,*P*-chelate complexes $PtCl_2\{P,P\text{-}C_6H_4(OH)N(CH_2PPh_2)_2\}$ **4.29–4.31**, $PtCl_2\{P,P\text{-}C_6H_3(OH)(CH_3)N(CH_2PPh_2)_2\}$ **4.32–4.36** and $PtCl_2\{P,P\text{-}C_6H_3(OH)(^tBu)N(CH_2PPh_2)_2\}$ **4.37** was achieved by stirring the ligands **4.20–4.28** and

$PtCl_2(cod)$ in CH_2Cl_2 for 1.5 h with displacement of the cyclooctadiene ligand (Equation 4.12). The products were isolated in good yields, 66-99%, as white solids obtained upon reduction of the volume of solvent *in vacuo* and addition of Et_2O.

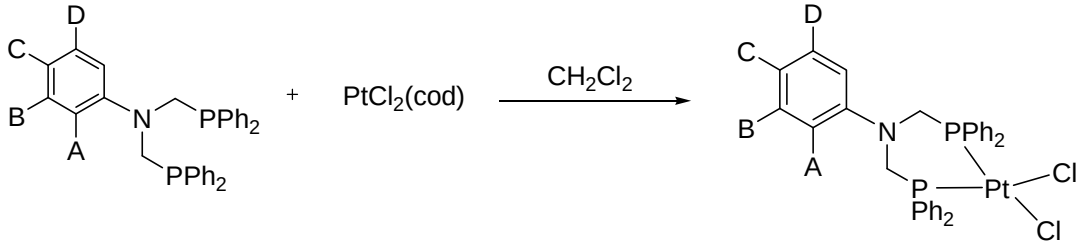

A = OH, B,C,D = H **4.20**
B = OH, A,C,D = H **4.21**
C = OH, A,B,D = H **4.22**
A = OH, D = CH_3, B,C = H **4.23**
A = CH_3, C = OH, B,D = H **4.24**
A = OH, C = CH_3, B,D = H **4.25**
B = OH, C = CH_3, A,D = H **4.26**
C = OH, B = CH_3, A,D = H **4.27**
A = OH, D = ^{t}Bu, B,C = H **4.28**

A = OH, B,C,D = H **4.29**
B = OH, A,C,D = H **4.30**
C = OH, A,B,D = H **4.31**
A = OH, D = CH_3, B,C = H **4.32**
A = CH_3, C = OH, B,D = H **4.33**
A = OH, C = CH_3, B,D = H **4.34**
B = OH, C = CH_3, A,D = H **4.35**
C = OH, B = CH_3, A,D = H **4.36**
A = OH, D = ^{t}Bu, B,C = H **4.37**

Equation 4.12

The complexation of the phosphine ligands was established by ^{31}P NMR spectroscopy. In all cases, the resonance of the free phosphine ligands **4.20–4.28**, observed in the range of δ −25.3 to −27.6 ppm, disappeared and the corresponding coordination-shifted signals were observed in the range of δ –4.0 to –11.7 for the Pt(II) complexes **4.29–4.37**. The coupling constants for **4.29–4.37** were approximately 3400 Hz which indicates that these complexes are in a *cis* conformation. In their infrared spectra, two vibrations in the range of 290-316 cm^{-1} were observed, indicative of ν(PtCl) (Table 4.4). The presence of these two vibrations provides confirmation for the *cis* isomer, as opposed to the *trans* isomer, which would only give one Pt−Cl vibration.

Table 4.4 Selected $^{31}P\{^{1}H\}$ NMR[a] and IR data[b] for **4.29–4.37**.

	δ(P)/ppm	**^{1}J(PtP)/Hz**	**υ(PtCl)/cm^{-1}**
4.29	-8.71	3431	316; 282
4.30	-4.02	3436	311; 289
4.31	-7.93	3424	312; 287
4.32	-9.43	3424	316; 289
4.33	-4.88	3426	315; 282
4.34	-8.55	3436	315; 286
4.35	-11.70	3410	309; 290
4.36	-7.89	3421	314; 290
4.37	-8.54	3450	316; 284

[a] Spectra measured in $(CD_3)_2SO$. [b] Recorded as KBr pellets.

4.2.2.2 Crystal Structures of Compounds 4.30, 4.32, 4.33, 4.35 and 4.36

Structural analysis of complexes **4.30**, **4.32**, **4.33**, **4.35** and **4.36** shows that the geometry about each Pt(II) centre is approximately square planar [P–Pt–P range 94.84(3)-96.41(2)°] (Table 4.5). The Pt–Cl and Pt–P bond lengths are consistent with the values reported in the literature.[189,191]

Table 4.5 Selected bond lengths (Å) and angles (°) for compounds **4.30**, **4.32**, **4.33**, **4.35** and **4.36**.

	4.32	**4.30**	**4.33**	**4.36**	**4.35**[a]
Pt(1)–Cl(1)	2.3624(6)	2.3421(9)	2.359(3)	2.3558(6)	2.3562(18)/[2.3576(17)]
Pt(1)–Cl(2)	2.3484(6)	2.3617(10)	2.357(3)	2.3555(6)	2.3693(18)/[2.3616(18)]
Pt(1)–P(1)	2.2226(6)	2.2220(9)	2.223(3)	2.2256(6)	2.2386(19)/[2.2352(18)]
Pt(1)–P(2)	2.2186(7)	2.2288(9)	2.223(3)	2.2145(6)	2.2474(18)/[2.2465(18)]
P(1)–Pt(1)–P(2)	96.30(3)	94.84(3)	96.29(11)	96.41(2)	96.16(7)/[95.95(7)]
P(1)–Pt(1)–Cl(1)	86.12(2)	88.80(3)	87.91(11)	87.63(2)	87.30(7)/[86.87(7)]
P(2)–Pt(1)–Cl(1)	176.08(3)	173.98(3)	174.95(12)	175.93(2)	176.51(7)/[176.84(7)]
P(1)–Pt(1)–Cl(2)	174.73(2)	174.53(4)	176.45(12)	177.81(2)	169.15(7)/[170.73(7)]
P(2)–Pt(1)–Cl(2)	88.94(2)	87.17(3)	86.70(10)	85.53(2)	88.55(7)/[90.04(7)]
Cl(1)–Pt(1)–Cl(2)	88.68(2)	88.79(4)	89.01(11)	90.43(2)	88.13(7)/[87.34(7)]
P(1)–C(1)–N(1)	111.90(17)	112.5(2)	112.3(7)	112.20(14)	108.6(5)/[110.5(5)]
P(2)–C(2)–N(1)	114.03(17)	112.6(2)	112.6(7)	109.27(15)	107.9(5)/[109.3(5)]
C(1)–N(1)–C(2)	110.0(2)	112.5(3)	111.5(9)	111.19(18)	114.7(6)/[111.2(6)]

[a] Values in square brackets are for the second molecule in the asymmetric unit.

The conformation of the Pt–P–C–N–C–P six-membered ring in each complex is best described as a boat. The dihedral angle measured between the C–N–C and N-arene least-squares planes varies between 55° (in **4.30**) and 88° (in **4.35**), the difference of *ca*. 33° may tentatively be explained by the predisposition of the –OH group about the N-arene group and subsequent hydrogen bonding requirements (Figure 4.20). Upon metal chelation a degree of freedom compared with the free ligands **4.21–4.23** has been removed, as the PCNCP fragment is locked in a specific conformation.

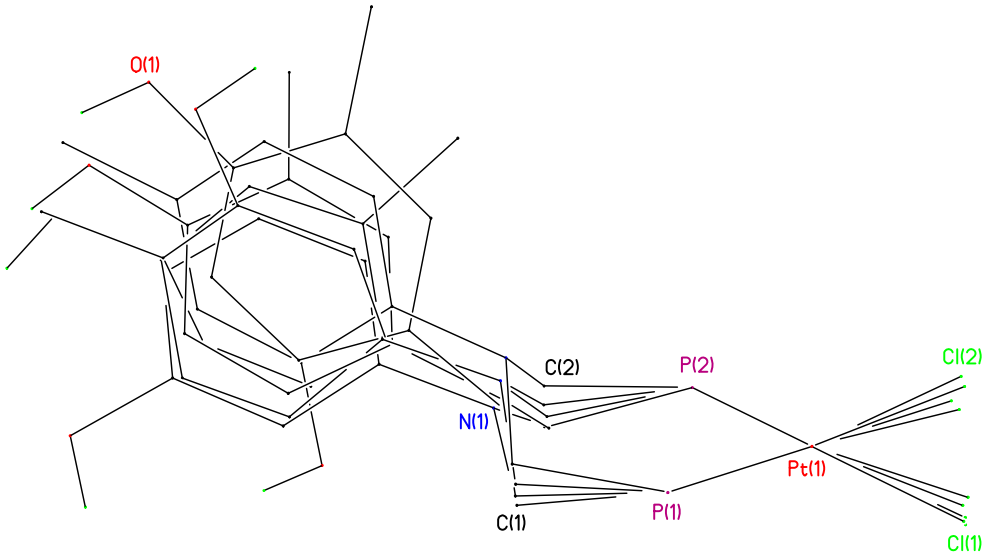

Figure 4.20 Overlay view of **4.30**, **4.32**, **4.33**, **4.35** and **4.36**. Phenyl rings, hydrogen atoms except O*H* and solvent molecules have been omitted for clarity.

4.2.2.3 Secondary Interactions in Compounds 4.30, 4.32, 4.33, 4.35 and 4.36

Suitable crystals of compound **4.32** for X-ray analysis were obtained from a chloroform solution, including one solvent molecule per complex in the structure. The $CHCl_3$ molecule hydrogen bonds to the terminal chlorides of the complex molecule through a weak bifurcated (solvent)C–H···Cl(complex) interaction, [C···Cl 3.66 and 3.86 Å]. Interestingly, despite the –OH group being in an *ortho* position with respect to the N-arene, the intramolecular hydrogen bond seen in **4.23** is prevented by formation of an O–H···Cl hydrogen bond interaction between alternating Pt(II) complex molecules forming chains (Figure 4.21). Selected hydrogen parameters for **4.32** are shown in Table 4.6.

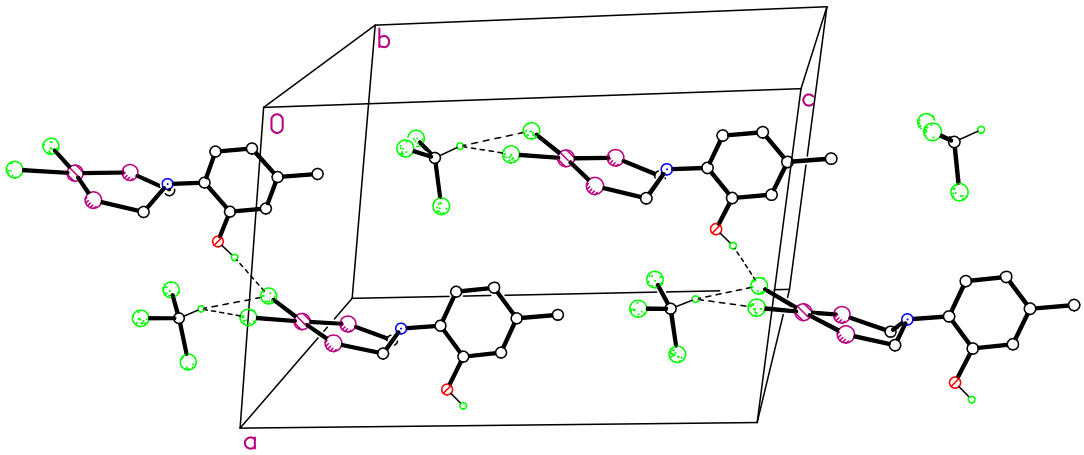

Figure 4.21 View of the chains of **4.32**, propagating in the crystallographic *a* direction. Phenyl groups and hydrogen atoms not involved in hydrogen bonding have been omitted for clarity.

Table 4.6 Selected hydrogen bonding parameters for **4.32**.

D–H···A	D···A/Å	D–H/Å	H···A/Å	D–H···A/º
O(1)–H(1)···Cl(1H)^{i}	3.144(2)	0.84	2.44	143
O(1A)–H(1A)···Cl(2)^{i}	3.360(2)	0.84	2.74	132

Symmetry operation: ^{i}x+1/2, -y+1/2, z+1/2.

Compound **4.30**, in which the –OH group is *meta* to the N-arene backbone, crystallises from vapour diffusion of hexane into a DMSO/$CHCl_3$ solution with the inclusion of a molecule of DMSO per complex, which was found to be disordered over two sets of positions (Figure 4.22). An intermolecular (hydroxyl)O–H···O(solvent) hydrogen bonding interaction with the DMSO molecule effectively precludes any further interactions with other Pt(II) molecules, hence, resulting in a zero-dimensional structure (Table 4.7).

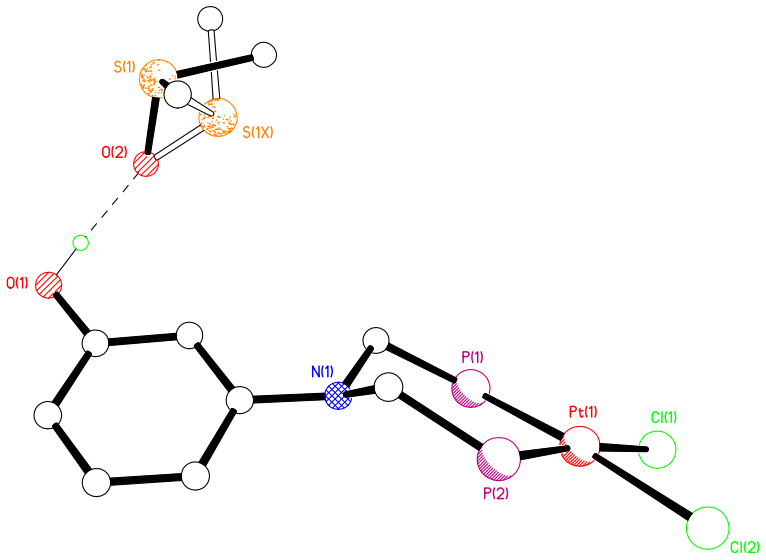

Figure 4.22 View of the asymmetric unit of complex **4.30**. Phenyl groups and hydrogen atoms not involved in hydrogen bonding have been removed for clarity. Minor solvent disorder component shown with open bonds.

Table 4.7 Selected hydrogen bonding parameters for **4.30**.

D–H···A	D···A/Å	D–H/Å	H···A/Å	D–H···A/º
O(1)–H(1)···O(2)	2.620(5)	0.84	1.79	171

Compound **4.36** has been crystallised from the slow evaporation of a CH_2Cl_2/Et_2O/hexane solution including two highly disordered molecules of Et_2O per cell. Compound **4.36** was determined using synchrotron radiation on station 9.8 at the SRS, Daresbury Laboratory, due to the small crystal dimensions. PLATON SQUEEZE was used to determine that 42 electrons were present in the unit cell unaccounted for in the point atom model.[103] This approximated well to two very highly disordered Et_2O molecules per unit cell. The hydroxyl group in the *meta* position to the N-arene moiety was hydrogen bonded to the disordered Et_2O molecules. Therefore, compound **4.36** does not present strong hydrogen bonding. Only weak (aromatic)C−H···Cl [2.852 Å] and (aliphatic)C−H···Cl [2.70 Å and 2.79 Å] interactions have been observed. These interactions are holding the molecules together forming sheets which extend in the *ab* plane, allowing the positioning of the functionalised N-arene groups between layers (Figure 4.23).

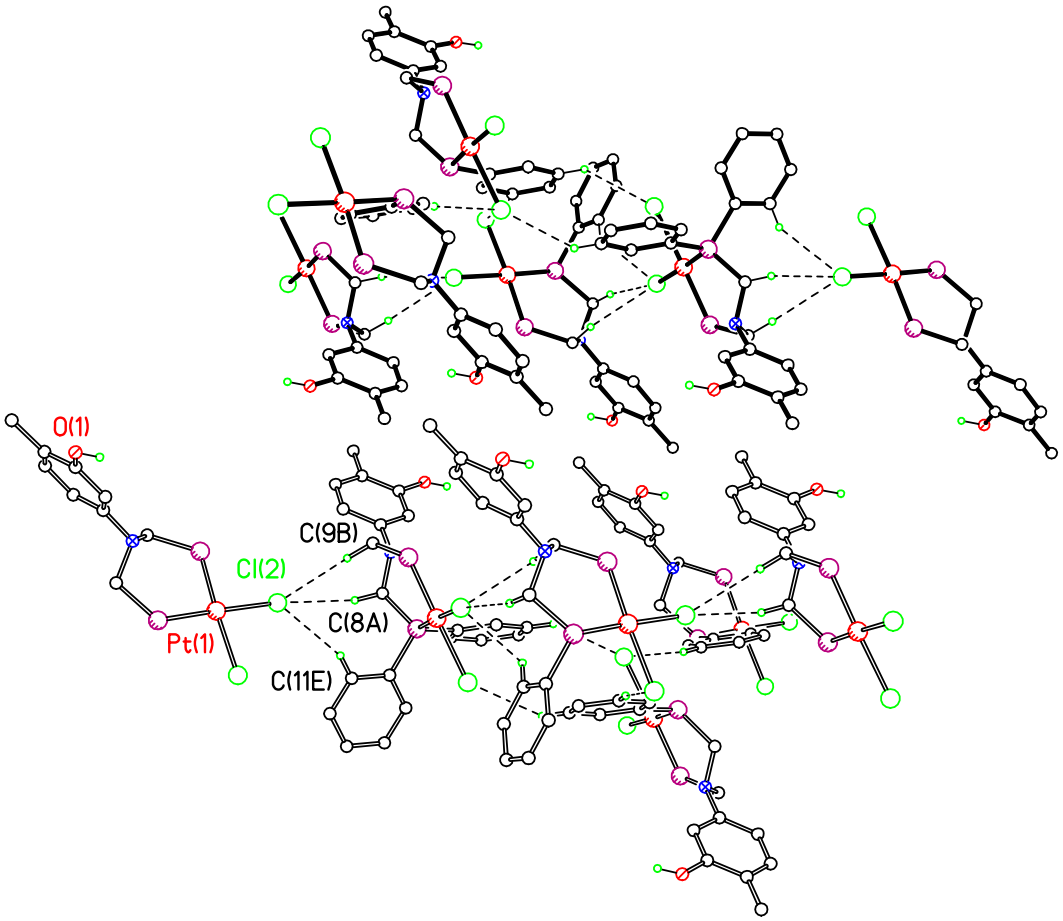

Figure 4.23 View of the hydrogen bonding motifs in **4.36**. Phenyl groups and hydrogen atoms not involved in hydrogen bonding have been omitted for clarity. The molecules in one of the layers are shown using open bonds to show the hydrogen bonding pattern with clarity.

Crystallisation of **4.33** from a DMSO containing solution results in simple hydrogen bonded solvent-complex pairs with no further significant intermolecular interactions due to the same type of hydrogen bonding seen previously for **4.30** (Figure 4.24). Selected hydrogen bonding parameters for **4.33** are shown in Table 4.8.

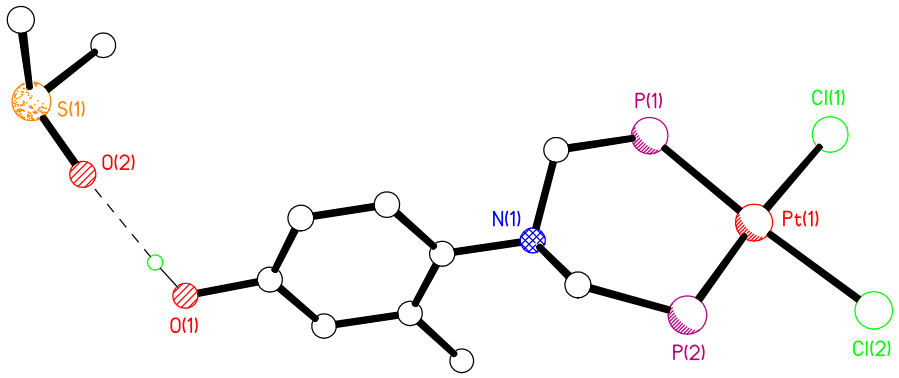

Figure 4.24 View of the asymmetric unit of complex **4.33**. Phenyl groups and hydrogen atoms not involved in hydrogen bonding have been removed for clarity.

Compound **4.33** again illustrates how polar solvents such as DMSO can disrupt any hydrogen bonded supramolecular assemblies as seen above for compound **4.30**.

Table 4.8 Selected hydrogen bonding parameters for **4.33**.

D–H···A	D···A/Å	D–H/Å	H···A/Å	D–H···A/º
O(1)–H(1)···O(2)	2.697(13)	0.84	1.87	169

Compound **4.35** crystallises from the vapour diffusion of Et_2O into a MeOH solution with the inclusion of a molecule of MeOH per two molecules of Pt(II) complex in the asymmetric unit. Careful inspection of the two unique molecules shows that they present different one-dimensional hydrogen bonding patterns (Figure 4.25). While a single (hydroxyl)O–H···Cl hydrogen bond between symmetry related Pt(2) complex molecules creates chains propagating in the *a* direction, the MeOH molecule bridges two Pt(1) complex molecules *via* two strong, crystallographically independent hydrogen bonds, one (hydroxyl)O–H···O(solvent) and one (solvent)O–H···Cl with the metal-bound chloride (Table 4.9). This creates chains of alternating molecules of Pt(1) complex molecules and MeOH anti-parallel to those observed for Pt(2) molecules. Here the inclusion of MeOH facilitates the formation of a supramolecular array, rather than limiting the dimensionality as has been seen in the isomeric DMSO solvates **4.30** and **4.33**.

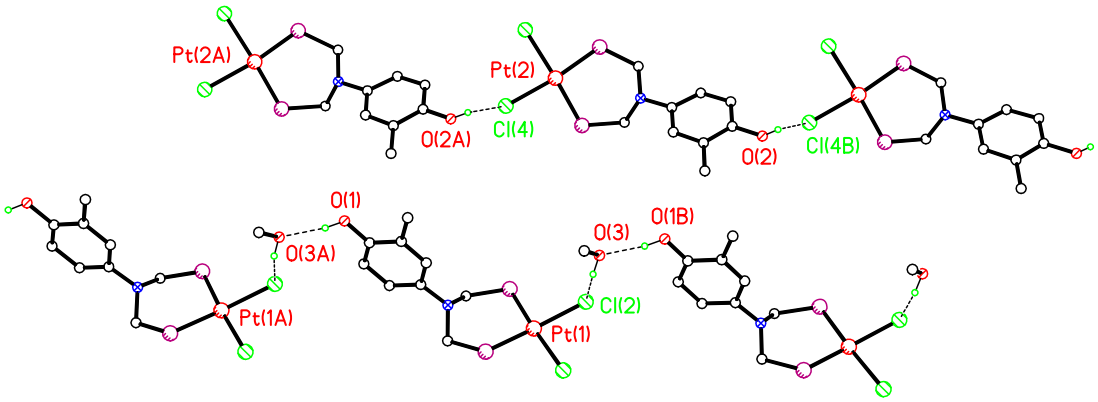

Figure 4.25 View of the two different hydrogen bonding motifs of **4.35**. Phenyl groups and hydrogen atoms not involved in hydrogen bonding have been removed for clarity.

Table 4.9 Selected hydrogen bonding parameters for **4.35**.

D–H···A	D···A/Å	D–H/Å	H···A/Å	D–H···A/°
O(1)–H(1)···O(3A)^{i}	2.624(10)	0.84	1.82	160
O(2)–H(2)···Cl(4B)^{ii}	3.198(6)	0.84	2.40	159
O(3)–H(3)···Cl(2)	3.131(7)	0.84	2.43	141

Symmetry operations: ^{i}x, y-1, z; ^{ii}x, y+1, z.

Therefore, the factors which dictate the solid state architectures for complexes **4.30**, **4.32**, **4.33**, **4.35** and **4.36** are: the configuration of the chelate ring, the N-arene group disposition about the C–N–C plane, the position of the OH/CH_3 groups with respect to the N-arene and the solvent used in the crystallisation.

4.2.2.4 Syntheses of Linear Au(I) Complexes 4.38-4.46

Reaction of ligands **4.20–4.28** with AuCl(tht) in a 1:2 stoichiometry proceeds with displacement of tht to afford the gold(I) complexes $Au_2Cl_2\{P,P\text{-}C_6H_4(OH)N(CH_2PPh_2)_2\}$ **4.38–4.40**, $Au_2Cl_2\{P,P\text{-}C_6H_3(OH)(CH_3)N(CH_2PPh_2)_2\}$ **4.41–4.45** and $Au_2Cl_2\{P,P\text{-}C_6H_3(OH)(^{t}Bu)N(CH_2PPh_2)_2\}$ **4.46** as air stable white solids. Complexes **4.38–4.46** were obtained in 50-94% yields (Equation 4.13).

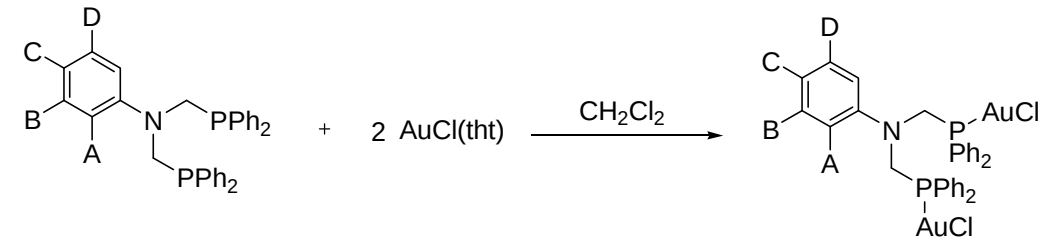

A = OH, B,C,D = H **4.20**
B = OH, A,C,D = H **4.21**
C = OH, A,B,D = H 4.22
A = OH, D = CH_3, B,C = H **4.23**
A = CH_3, C = OH, B,D = H **4.24**
A = OH, C = CH_3, B,D = H **4.25**
B = OH, C = CH_3, A,D = H **4.26**
C = OH, B = CH_3, A,D = H **4.27**
A = OH, D = ^{t}Bu, B,C = H **4.28**

A = OH, B,C,D = H **4.38**
B = OH, A,C,D = H **4.39**
C = OH, A,B,D = H **4.40**
A = OH, D = CH_3, B,C = H **4.41**
A = CH_3, C = OH, B,D = H **4.42**
A = OH, C = CH_3, B,D = H **4.43**
B = OH, C = CH_3, A,D = H **4.44**
C = OH, B = CH_3, A,D = H **4.45**
A = OH, D = ^{t}Bu, B,C = H **4.46**

Equation 4.13

The complexes exhibited the expected spectroscopic and analytical properties. A single, sharp resonance, in their $^{31}P\{^1H\}$ NMR spectra [in $(CD_3)_2SO$] in the region of δ(P) 17.6−24.7 ppm was observed (Table 4.10). From the IR spectra, the ν(AuCl) bands are observed in the range of 324-328 cm^{-1}.

Table 4.10 Selected $^{31}P\{^1H\}$ NMR[a] and IR data[b] for **4.38–4.46**.

	δ(P)/ppm	**ν(AuCl)/cm^{-1}**
4.38	20.02	328
4.39	24.14	326
4.40	22.12	325
4.41	22.18	324
4.42	21.93	328
4.43	22.91	325
4.44	17.59	326
4.45	19.44	328
4.46	24.74	328

[a] Spectra measured in $(CD_3)_2SO$. [b] Recorded as KBr pellets.

Suitable crystals of **4.41** for X-ray analysis were obtained by slow evaporation of the filtrate (CH_2Cl_2/Et_2O/hexane). The X-ray structure of **4.41** showed the geometry about each gold(I) metal centre to be essentially linear [Cl(1)−Au(1)−P(1) 175.22(5)º Cl(2)−Au(2)−P(2) 177.03(5)º] (Figure 4.26). The P–C–N–C–P backbone is sufficiently flexible to promote a strong intramolecular aurophilic Au···Au [3.147 Å] interaction between the two AuCl units.[187] There is also an *S*(5) intramolecular O−H···N hydrogen bond (Table 4.11), as the hydroxyl group is in the *ortho* position with respect to the pyramidal N atom. The same motif was seen in the free ligand **4.41** [O−H···N 2.746(5) Å, 116º].

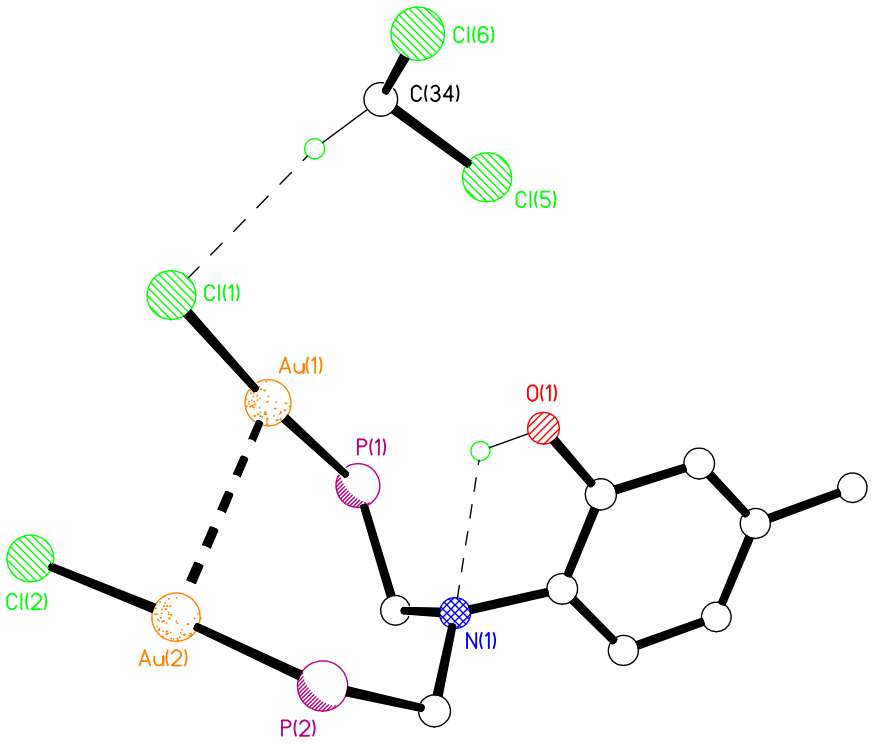

Figure 4.26 View of the asymmetric unit of compound **4.41**. Phenyl groups and hydrogen atoms not involved in hydrogen bonding have been omitted for clarity.

Compound **4.41** crystallises including one molecule of dichloromethane per metal complex, forming a (solvent)C–H···Cl(complex) hydrogen bond [C···Cl 3.675 Å, 108°]. No further hydrogen bonding is observed. Interestingly, the crystal structure of **4.41** represents another contribution to the extremely rare examples reported of crystallographically characterised M–P–C–N–C–P–M metallocycles. The other two examples were reported independently by Johnson and Smith.[187,241]

Table 4.11 Selected hydrogen bonding parameters for **4.41**.

D–H···A	D···A/Å	D–H/Å	H···A/Å	D–H···A/º
O(1)–H(1)···N(1)	2.773(6)	0.84	2.31	115.3

4.2.2.5 Syntheses of Octahedral Mo(0) Complexes 4.48–4.57

In order to investigate the coordination preferences of ligands **4.20–4.28** towards low-valent metal centres, neutral octahedral Mo(0) carbonyl complexes were synthesised under N_2 by ligand displacement of the labile η^4-norbornadiene from $[Mo(CO)_4(nbd)]$ with one equivalent of **4.20–4.28** and $C_6H_5N(CH_2PPh_2)_2$ **4.47** [synthesised by our research group] to afford complexes $Mo(CO)_4\{P,P\text{-}C_6H_4(OH)N(CH_2PPh_2)_2\}$ **4.48–4.50**, $Mo(CO)_4\{P,P\text{-}C_6H_3(OH)(CH_3)N(CH_2PPh_2)_2\}$ **4.51–4.55**, $Mo(CO)_4\{P,P\text{-}C_6H_3(OH)(^t\text{Bu})N(CH_2PPh_2)_2\}$ **4.56** and $Mo(CO)_4\{P,P\text{-}C_6H_5N(CH_2PPh_2)_2\}$ **4.57**, in 26-55% yields, after stiring for 48 h at room temperature (Equation 4.14).

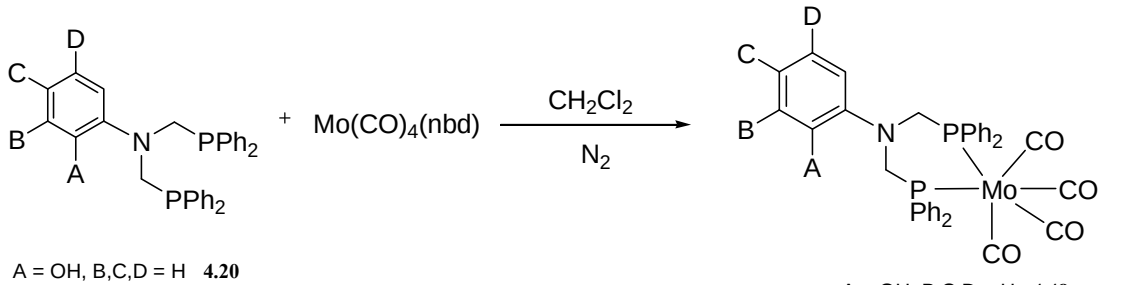

A = OH, B,C,D = H **4.20**
B = OH, A,C,D = H **4.21**
C = OH, A,B,D = H **4.22**
A = OH, D = CH_3, B,C = H **4.23**
A = CH_3, C = OH, B,D = H **4.24**
A = OH, C = CH_3, B,D = H **4.25**
B = OH, C = CH_3, A,D = H **4.26**
C = OH, B = CH_3, A,D = H **4.27**
A = OH, D = ^{t}Bu, B,C = H **4.28**
A,B,C,D = H **4.47**

A = OH, B,C,D = H **4.48**
B = OH, A,C,D = H **4.49**
C = OH, A,B,D = H **4.50**
A = OH, D = CH_3, B,C = H **4.51**
A = CH_3, C = OH, B,D = H **4.52**
A = OH, C = CH_3, B,D = H **4.53**
B = OH, C = CH_3, A,D = H **4.54**
C = OH, B = CH_3, A,D = H **4.55**
A = OH, D = ^{t}Bu, B,C = H **4.56**
A,B,C,D = H **4.57**

Equation 4.14

The $^{31}P\{^1H\}$ NMR spectra show single, sharp resonances, in the region of δ(P) 15.0−20.9 ppm, a downfield shift of approximately 40 ppm with respect to the free phosphine ligands **4.20–4.28**, observed in the range of δ −27.6 to −25.3 ppm. From the IR spectra, while complexes **4.48**, **4.51** and **4.53** display four strong carbonyl absorptions in the region 1878−2020 cm^{-1}, **4.49–4.50**, **4.52**, **4.55–4.57** exhibit only three

absorptions (one of the carbonyl absorptions may be overlapping), consistent with a *cis* tetracarbonyl metal complex (Table 4.12).

Table 4.12 Selected $^{31}P\{^{1}H\}$ NMR[a] and IR data[b] for **4.48–4.56**.

	δ(P)/ppm	**ν(CO)/cm^{-1}**
4.48	15.13	2019; 1926; 1896; 1888
4.49	18.21	2020; 1921; 1897
4.50	18.39	2019; 1919; 1895
4.51	20.85	2018; 1927; 1892; 1888
4.52	18.55	2019; 1917; 1897
4.53	20.11	2020; 1924; 1905; 1878
4.54	n.r.	n.r.
4.55	18.67	2019; 1921; 1898
4.56	14.97	2018; 1921; 1897
4.57	21.14	2020; 1926; 1894

[a] Spectra measured in $CDCl_3$. [b] Recorded as KBr pellets. n.r. = not recorded.

4.2.2.6 Crystal Structures of Compounds 4.50, 4.51, 4.53–4.55 and 4.57

The six-membered chelate ring in compounds **4.50**, **4.51**, **4.53–4.55** and **4.57** adopts a chair conformation with the N atom, above the P_2C_2 plane, in a range of 0.762–0.736 Å and the Mo below the plane in the range 1.251–0.764 Å. The Mo–P–C–N–C–P metallacyclic ring conformation is similar to those M–P–C–N–C–P reported in the literature.[233] The *N*-arene is twisted about the plane C(1)–N–C(2) in the range of 36–83° for hydrogen bonding requirements as seen previously (Figure 4.27).

Structural analysis of complexes **4.50**, **4.51**, **4.53–4.55** and **4.57** shows that the Mo–P and Mo–C distances are consistent with the values reported for related compounds such as the Mo(0) complex $Mo(CO)_4\{P,P\text{-}Ph_2P(CH_2)_3PPh_2\}$ **4.58** structurally reported recently by our research group.[242-244] The Mo–C–O bond angles are all close to linear (Table 4.13). The P–Mo–P bite angles for all the isomers are also similar to **4.58**. As anticipated, this bite angle is enlarged with respect to those found in complexes of the type $Mo(CO)_4\{P,P\text{-}Ph_2PN(R)PPh_2\}$ [R = H, P–Mo–P 65.29(6)°; R = 2-$MeOC_6H_4$, P–

Mo–P 65.78(2)°] in which the chelating $Ph_2PN(R)PPh_2$ ligands adopt near planar four-membered ring conformations.[245,246]

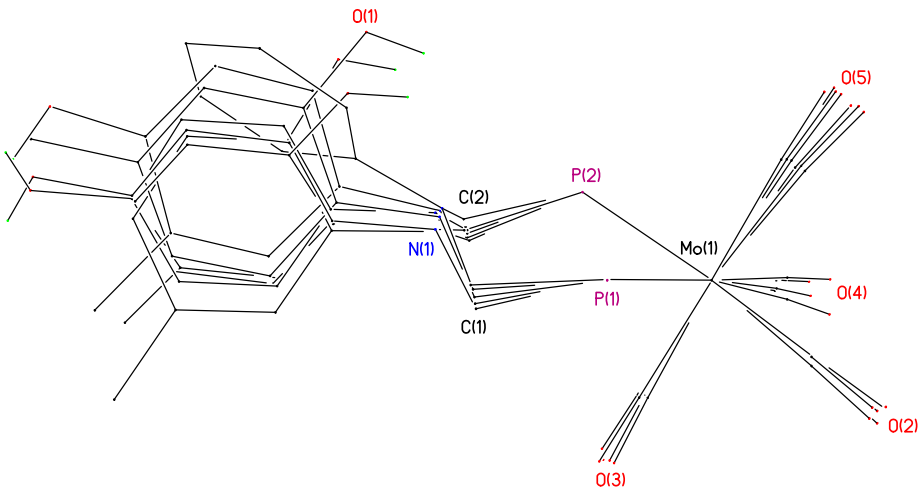

Figure 4.27 Overlay view of **4.50**, **4.51**, **4.53–4.55** and **4.57**, solvent molecule for compound **4.54** has been omitted for clarity. Phenyl rings and hydrogen atoms except O*H* have been omitted for clarity.

Table 4.13 Selected geometric parameters (Å, °) for compounds **4.50**, **4.51**, **4.53–4.55** and **4.57**, **4.58**.

	4.50	**4.51**	**4.53**	**4.54**
Mo–C (*trans* to C)	1.9918(5)/2.0283(5)	2.012(8)/2.024(8)	2.0002(16)/1.9867(16)	2.031(4)/2.041(4)
Mo–C (*trans* to P)	2.0279(5)/2.0010(5)	2.025(8)/2.033(5)	2.0290(15)/2.0500(15)	1.990(3)/1.995(4)
Mo–P	2.4989(11)/2.5096(11)	2.5134(18)/2.5153(19)	2.5155(4)/2.4985(4)	2.4866(9)/2.5090(8)
C–Mo–C (*trans* to C)	176.47(18)/173.77(17)	173.0(3)/173.7(3)	173.46(6)	175.86(14)
C–Mo–C (*cis*, av.)	89.35(17)/88.77(17)	88.2(3)/88.9(3)	88.97(6)	90.12(15)
P–Mo–P	85.32(4)/84.06(4)	84.24(6)/84.72(6)	86.265(11)	87.53(3)
Mo–C–O (av.)	177.2(4)/176.6(4)	177.8(7)/176.5(7)	177.22(15)	176.6(3)

Cont. Table 4.13 Selected geometric parameters (Å, °) for compounds **4.50**, **4.51**, **4.53–4.55** and **4.57**, **4.58**.

	4.55	**4.57**	**4.58**
Mo–C (*trans* to C)	2.019(2)/2.046(2)	2.016(3)/2.043(3)	2.035(4)/2.052(5)
Mo–C (*trans* to P)	1.993(2)/2.004(2)	2.007(3)/1.994(3)	1.995(4)/1.985(5)
Mo–P	2.5227(5)/2.5177(4)	2.5005(8)/2.4986(8)	2.5239(11)/2.5185(11)
C–Mo–C (*trans* to C)	174.40(7)	178.21(12)	177.12(17)
C–Mo–C (*cis*, av.)	88.85(8)	89.72(13)	89.34(18)
P–Mo–P	84.720(14)	86.75(2)	89.30(4)
Mo–C–O (av.)	177.5(2)	178.2(3)	177.4(4)

4.2.2.7 Secondary Interactions in Compounds 4.50, 4.51, 4.53–4.55, 4.57 and 4.58

Compound $Mo(CO)_4\{P,P\text{-}Ph_2P(CH_2)_3PPh_2\}$ **4.58** was obtained as a new polymorphic form differing from the previously reported orthorhombic form **4.58a** described by Ueng and Hwang.[242] Compound **4.58** was obtained by slow evaporation of a concentrated solution of **4.58** in CH_2Cl_2/Et_2O/light petroleum ether and crystallises in the monoclinic space group $P2_1/c$, with one molecule in the asymmetric unit (Figure 4.28).[244] The orthorhombic form crystallises with one half-molecule in the asymmetric unit lying on a mirror plane.

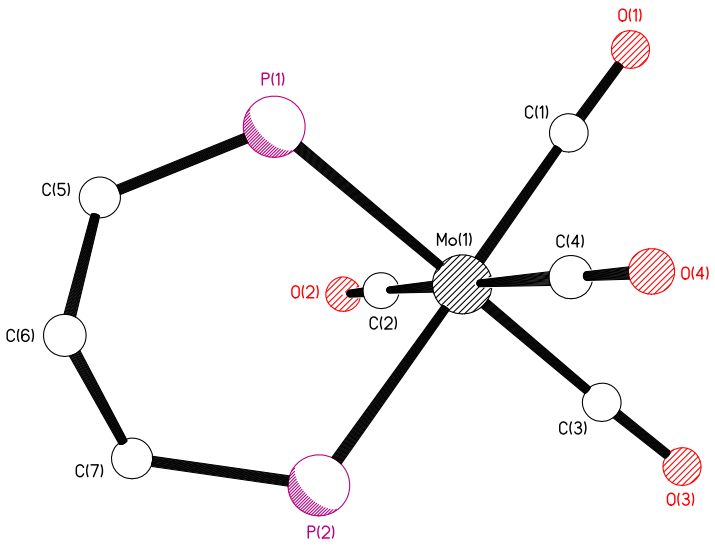

Figure 4.28 View of the asymmetric unit of compound **4.58**. Phenyl groups and hydrogen atoms have been omitted for clarity.

The packing plots of compounds **4.58** and **4.58a** show substantial differences; in **4.58** adjacent molecules are off-set and canted 26° with respect to the *ab* plane. In **4.58a**, molecules lie directly stacked in parallel columns with individual molecules lying on mirror planes (Figure 4.29).

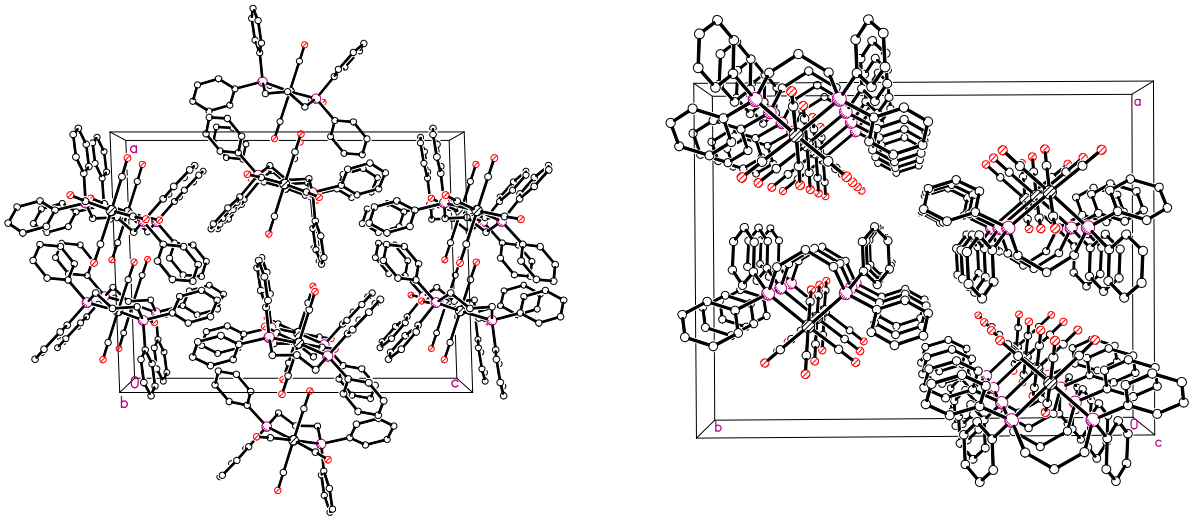

Figure 4.29 Packing plot of **4.58** viewed parallel to the *b* crystallographic axis. Hydrogen atoms have been removed for clarity. Packing plot of **4.58a** viewed parallel to the *c* crystallographic axis. Hydrogen atoms have been omitted for clarity.

X-ray quality crystals of compound **4.57** were obtained as for **4.58** by slow evaporation of a concentrated solution of **4.57** in CH_2Cl_2/Et_2O/light petroleum ether. Compound **4.57** crystallises with one molecule in the asymmetric unit as a zero-dimensional structure due to the lack of potential hydrogen bonding donors (Figure 4.30).[247]

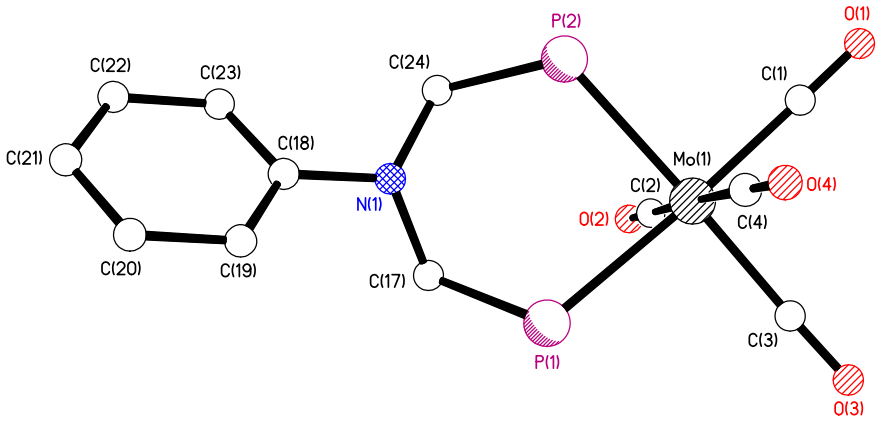

Figure 4.30 View of the asymmetric unit of compound **4.57**. Phenyl groups on phosphorus and hydrogen atoms have been omitted for clarity.

The description of the different structural motifs in four isomeric Mo(0) complexes, obtained by regioselective incorporation of –OH and $–CH_3$ functional groups around the central arene core is described.

Compound **4.53** crystallises with the formation of the same type of *S*(5) intramolecular O–H···N hydrogen bond observed in **4.41** (Table 4.14). Although **4.41** crystallises as a zero-dimensional structure, the carbonyl groups in **4.53** provide additional hydrogen bond acceptors, allowing the formation of weak (aromatic)C–H···O interactions, C···O = 3.527 Å,[10] forming one-dimensional zigzag chains (Figure 4.31).

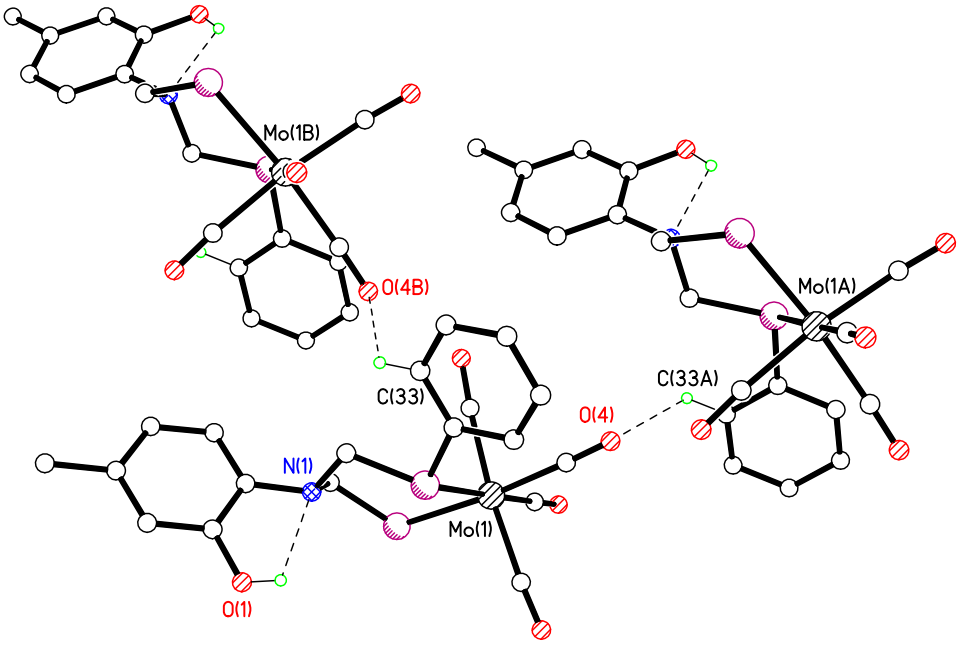

Figure 4.31 View of the hydrogen bonded chains in **4.53**. Phenyl groups and hydrogen atoms not involved in hydrogen bonding have been omitted for clarity.

Table 4.14 Selected hydrogen bonding parameters for **4.53**.

D–H···A	D···A/Å	D–H/Å	H···A/Å	D–H···A/º
O(1)–H(1)···N(1)	2.7661(16)	0.84	2.29	115.9

Compound **4.51** crystallises with two formula units in the asymmetric unit. Although they present similar structural parameters, they differ in their geometrical disposition (Figure 4.32). Both molecules present the same *S*(5) O–H···N intramolecular hydrogen bond as could be predicted from the isomeric structure **4.53** (Figure 4.32, Table 4.15). However a different hydrogen bonding pattern was observed: a combination of weak (aromatic)C–H···O(carbonyl) [C···O 3.44 Å and 3.48 Å] and (aromatic)C–H···O(hydroxyl) [C···O 3.40 Å and 3.39 Å] interactions forming $R^2_2(8)$ ring motifs leads to hydrogen bonding ladders with **4.51** molecules residing in the cavities of the ladder.[10]

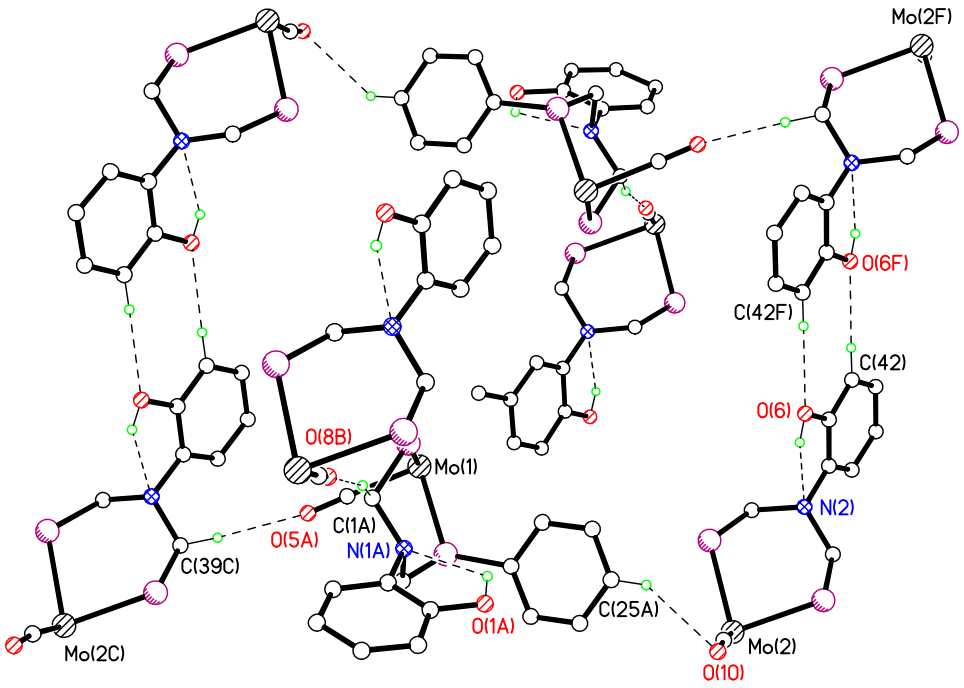

Figure 4.32 View of the hydrogen bonding pattern in **4.51**. Some phenyl groups, carbonyl, methyl groups and hydrogen atoms not involved in hydrogen bonding have been removed for clarity.

Table 4.15 Selected hydrogen bonding parameters for **4.51**.

D–H···A	D···A/Å	D–H/Å	H···A/Å	D–H···A/°
O(1A)–H(1A)···N(1A)	2.780(7)	0.84	2.34	113.4
O(6)–H(6A)···N(2)	2.744(7)	0.84	2.29	114.1

Unfortunately, compound **4.54** was obtained in very low yield (< 5%) and only the crystals obtained by slow evaporation of the methanolic/Et_2O filtrate were analysed by single X-ray diffraction. The low yield did not allow additional analysis by IR, NMR, mass spectrometry and microanalysis methods. Compound **4.54** crystallises as a solvate structure including a half-molecule of Et_2O per Mo(0) complex in the asymmetric unit. The Et_2O molecule lies on a mirror plane and hydrogen bonds to two symmetry related metal complexes through O–H···O hydrogen bonds (Figure 4.33). The included Et_2O molecules in **4.54** prevents any further hydrogen bonding interactions, therefore **4.54** is essentially a zero-dimensional structure. Selected hydrogen bonding parameters for **4.54** are shown in Table 4.16.

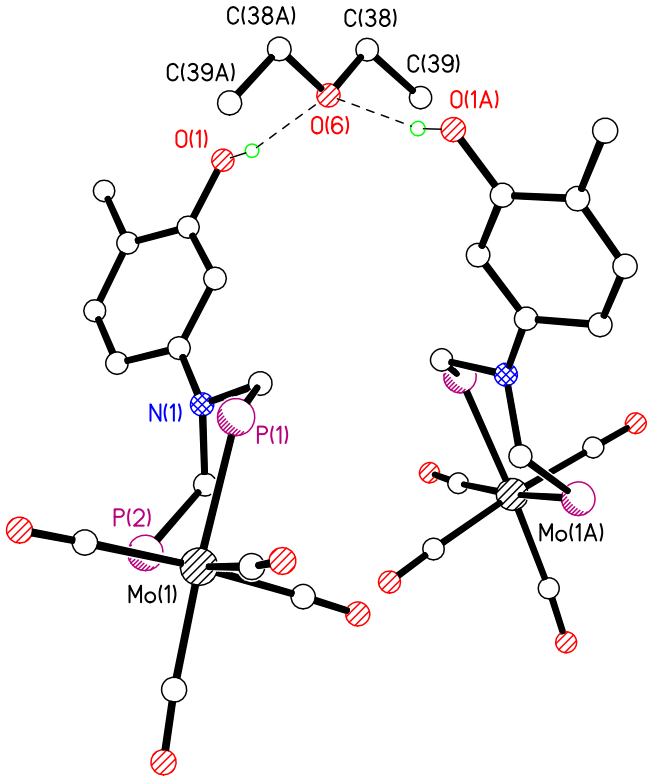

Figure 4.33 Hydrogen bonding pattern in **4.54**. Phenyl groups and hydrogen atoms not involved in hydrogen bonding have been omitted for clarity.

Table 4.16 Selected hydrogen bonding parameters for **4.54**.

D–H···A	D···A/Å	D–H/Å	H···A/Å	D–H···A/°
O(1)–H(1)···O(6)	2.945(3)	0.84	2.13	165

In the X-ray structure of **4.55** (Figure 4.34), in which the –OH group is in an *ortho* position, molecules are arranged in a one-dimensional polymeric chain through (hydroxyl)O–H···O(carbonyl) intermolecular hydrogen bonding showing similarities with those observed for the Pt(2) complex molecules in compound **4.35**.[10] Molecules including Pt(1) also present a one-dimensional pattern due to the inclusion of MeOH molecules in the structure. Selected hydrogen bonding parameters for **4.55** are shown in Table 4.17.

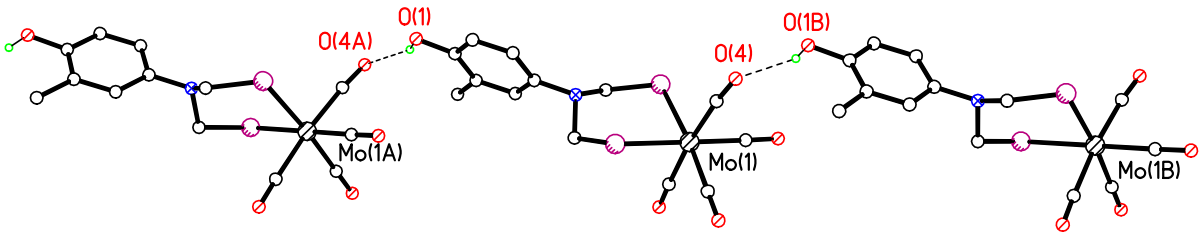

Figure 4.34 View of the hydrogen bonded chains of **4.55**. Phenyl rings and hydrogen atoms except O*H* have been removed for clarity.

Table 4.17 Selected hydrogen bonding parameters for **4.55**.

D–H···A	D···A/Å	D–H/Å	H···A/Å	D–H···A/°
O(1)–H(1)···O(4A)^{i}	3.079(2)	0.89(3)	2.26(3)	151(2)

Symmetry operation: ^{i}x+1, -y+3/2, z+1/2.

Interestingly, compound **4.50** which differs from **4.55** by the absence of the methyl group on the functionalised *N*-phenyl ring, crystallises with two molecules of **4.50** complex in the asymmetric unit producing a completely different hydrogen bonding motif than the one previously observed (Figure 4.35).

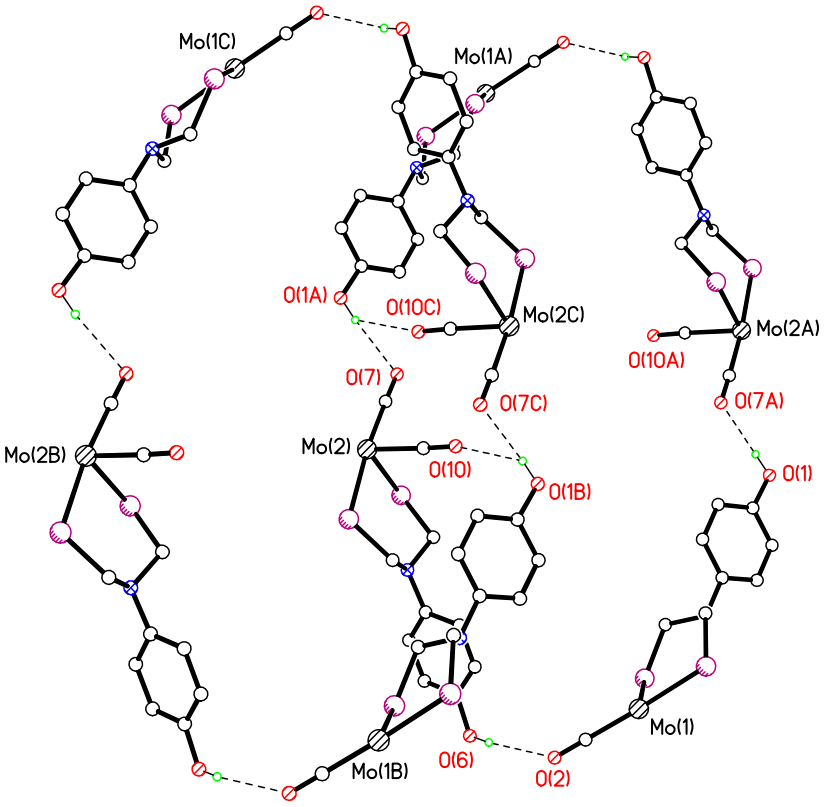

Figure 4.35 View of the hydrogen bonding motifs of **4.50**. Phenyl groups and hydrogen atoms except OH and some carbonyl groups have been omitted for clarity.

The two unique **4.50** molecules hydrogen bond together to form a network of cavities which interpenetrate through two (hydroxyl)O–H···O(carbonyl) interactions between symmetry related molecules forming an $R^4_2(12)$ star-shape motif (Table 4.18).

Table 4.18 Selected hydrogen bonding parameters for **4.50**.

D–H···A	D···A/Å	D–H/Å	H···A/Å	D–H···A/°
O(6)–H(6)···O(2)	2.789(4)	0.84	2.13	136
O(1B)–H(1B)···O(10)^{i}	3.033(5)	0.84	2.49	123
O(1)–H(1)···O(7A)^{ii}	3.283(5)	0.84	2.51	153

Symmetry operations: ^{i}x-1, y, z; ^{ii}-x-1, -y+1, -z+1.

4.2.3 Syntheses of $C_6H_5NHCOCH_2NHCOOCH_2C_6H_4(OH)$ 4.59–4.61, $C_6H_5NHCOCH_2NHCOOCH_2C_6H_3(CH_3)(OH)$ 4.62–4.66 and $C_6H_5NHCOCH_2NHCOOCH_2C_6H_3(^tBu)(OH)$ 4.67

The range of ligands and complexes discussed previously in this chapter is somewhat limited in its hydrogen bonding potential due to the commercial availability of the primary amines bearing a hydroxyl group. The synthesis of ditertiary phosphines containing a flexible backbone, which presents extra potential donor and acceptor atoms with hydrogen bonding capability, in order to facilitate the formation of supramolecular arrays with greater complexity is described above.

The precursors for the synthesis of the desired extended ditertiary phosphines were prepared using one equivalent of the corresponding primary amine **I–IX** with one equivalent of *N*-carbobenzyloxyglycine and one equivalent of dicyclohexylcarbodiimide in tetrahydrofuran yielding the desired products $C_6H_5NHCOCH_2NHCOOCH_2C_6H_4(OH)$ **4.59–4.61**, $C_6H_5NHCOCH_2NHCOOCH_2C_6H_3(CH_3)(OH)$ **4.62–4.66** and $C_6H_5NHCOCH_2NHCOOCH_2C_6H_3(^tBu)(OH)$ **4.67** in 53-91% yields (Equation 4.15).

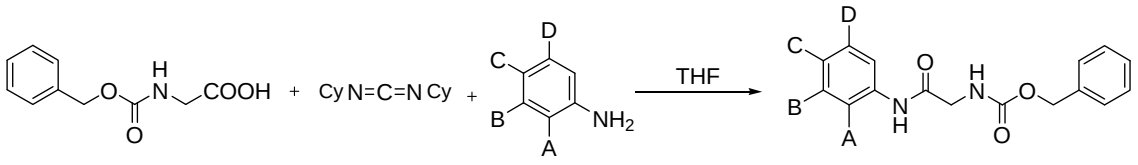

A = OH, B,C,D = H **I**
B = OH, A,C,D = H **II**
C = OH, A,B,D = H **III**
A = OH, D = CH_3, B,C = H **IV**
A = CH_3, C = OH, B,D = H **V**
A = OH, C = CH_3, B,D = H **VI**
B = OH, C = CH_3, A,D = H **VII**
C = OH, B = CH_3, A,D = H **VIII**
A = OH, D = ^{t}Bu, B,C = H **IX**

A = OH, B,C,D = H **4.59**
B = OH, A,C,D = H **4.60**
C = OH, A,B,D = H **4.61**
A = OH, D = CH_3, B,C = H **4.62**
A = CH_3, C = OH, B,D = H **4.63**
A = OH, C = CH_3, B,D = H **4.64**
B = OH, C = CH_3, A,D = H **4.65**
C = OH, B = CH_3, A,D = H **4.66**
A = OH, D = ^{t}Bu, B,C = H **4.67**

Equation 4.15

All of the compounds **4.59–4.67** exhibit the expected spectroscopic and analytical properties. The ^{1}H NMR spectra [in $(CD_3)_2SO$] displayed the anticipated resonances for the aromatic, hydroxy- and amide groups (See Experimental Section) indicating the formation of the desired precursors. The infrared spectra also showed the characteristic absorbing ν(NH) and ν(OH) bands in the range 3200-3400 cm^{-1} and bands in the range

1639-1692 cm^{-1} and 1310-1385 cm^{-1} indicative of ν(C=O amide) and ν(C−O), respectively. Microanalytical data were satisfactory for the new compounds.

4.2.3.1 X-ray Crystal Structures of Compounds 4.59, 4.60, 4.64, 4.65 and 4.67

Compounds **4.59** and **4.64** crystallise presenting the same hydrogen bonding motifs (Figure 4.36). Both present an intramolecular N−H···O hydrogen bond forming a *S*(5) graph set motif. Molecules of **4.59** and **4.64** pack through O–H···O and N–H···O in anti-parallel one-dimensional ladders forming $R^4_4(18)$ and $R^2_2(10)$ alternating hydrogen bond motifs, (Figure 4.36). The presence of an extra $–CH_3$ group did not change the packing of **4.64**. Selected hydrogen bonding parameters for **4.59** and **4.64** are shown in Tables 4.19 and 4.20 respectively.

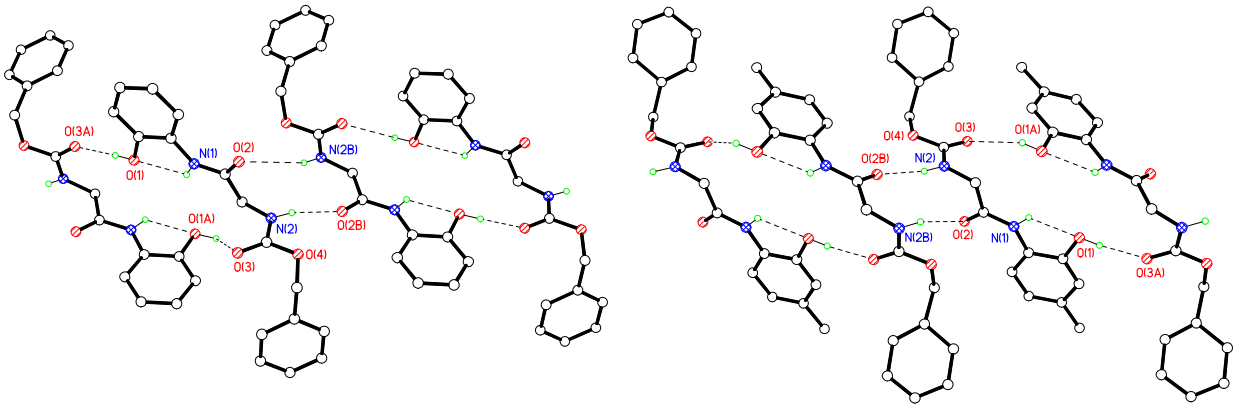

4.59 **4.64**

Figure 4.36 Anti-parallel one-dimensional chains of compounds **4.59** and **4.64**. Hydrogen atoms not involved in hydrogen bonding have been omitted for clarity.

An expansion in the structure due to the incorporation of an extra $–CH_3$ group is not observed when considering the unit cell dimensions of **4.59** and **4.64**.

Table 4.19 Selected hydrogen bonding parameters for **4.59**.

D–H···A	D···A/Å	D–H/Å	H···A/Å	D–H···A/º
N(1)–H(1A)···O(1)	2.6151(17)	0.85(2)	2.189(18)	111.0(15)
O(1)–H(1)···O(3A)^{i}	2.6995(16)	0.89(2)	1.82(2)	173(2)
N(2)–H(2)···O(2B)^{ii}	2.8323(17)	0.86(2)	1.99(2)	164.9(17)

Symmetry operations: ^{i}x+1/2, -y-1/2, -z; ^{ii}x+1/2, -y+1/2, -z.

Table 4.20 Selected hydrogen bonding parameters for **4.64**.

D–H···A	D···A/Å	D–H/Å	H···A/Å	D–H···A/º
N(1)–H(1A)···O(1)	2.625(2)	0.89(2)	2.13(2)	114.0(18)
O(1)–H(1)···O(3A)^{i}	2.7230(19)	0.84	1.90	168
N(2)–H(2)···O(2B)^{ii}	2.826(2)	0.91(2)	1.93(2)	168(2)

Symmetry operations: ^{i}-x-1/2, y+1/2, -z+1/2; ^{ii}-x+1/2, y+1/2, -z+1/2.

Crystals of **4.67** suitable for X-ray crystallography were obtained by slow vapour diffusion of diethyl ether into a solution of **4.67** in THF (Figure 4.37). Compound **4.67** crystallises as a solvent free structure, with the expected intramolecular N−H···O *S*(5) graph set hydrogen bond motif seen previously for compounds **4.59** and **4.64**.[19,20] In contrast with the extended conformation observed in compounds **4.59** and **4.64**, the presence of a bulkier ^{t}Bu group forces the **4.67** molecules to adopt a twisted conformation folding about carbon atoms C(11) and C(12).

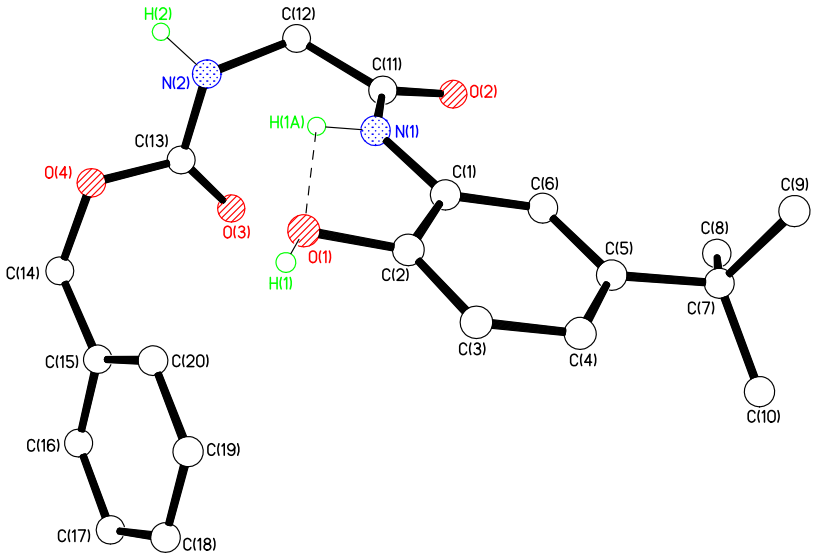

Figure 4.37 View of the asymmetric unit of **4.67**. Hydrogen atoms except N*H* and O*H* have been omitted for clarity.

In order to accommodate the additional steric requirements of the bulky ^{t}Bu functional group, compound **4.67** packs as spirals which propagate in the *a* direction. Strong (amide)N–H···O(amide) and (hydroxyl)O–H···O(amide) interactions between four symmetry related molecules of **4.67** form an $R^4_4(32)$ graph set motif (Figure 4.38). Selected hydrogen bonding parameters for **4.67** are shown in Table 4.21.

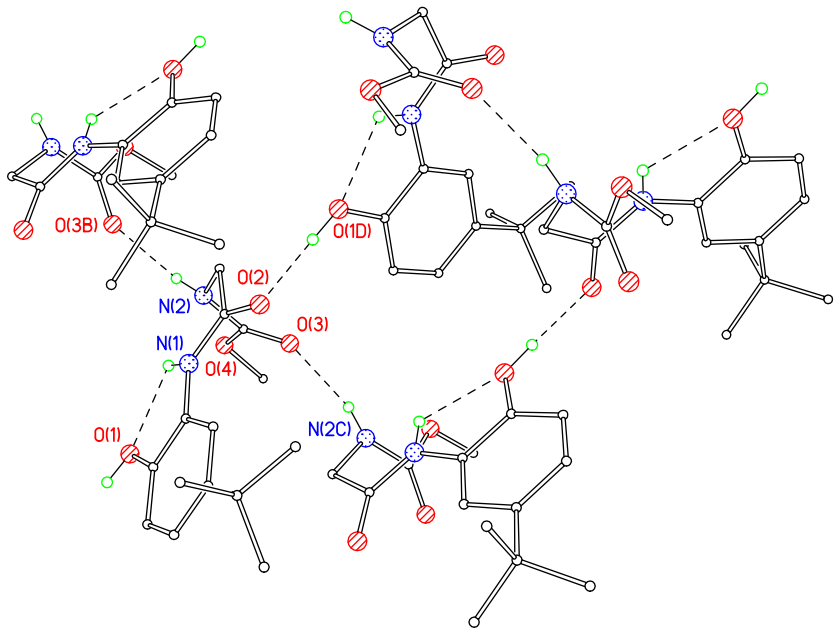

Figure 4.38 View of the hydrogen bonding motifs in **4.67**. Phenyl groups and hydrogen atoms not involved in hydrogen bonding have been removed for clarity.

Table 4.21 Selected hydrogen bonding parameters for **4.67**.

D–H···A	D···A/Å	D–H/Å	H···A/Å	D–H···A/°
O(1)–H(1)···O(2B)[i]	2.6524(15)	0.86(2)	1.80(2)	177(2)
N(2)–H(2)···O(3A)[ii]	2.8744(18)	0.884(18)	2.025(19)	160.8(16)
N(1)–H(1[a])···O(1)	2.5967(18)	0.866(18)	2.156(17)	111.1(14)

Symmetry operations: [i]x+1/2, y, -z+1/2; [ii] -x+1/2, y-1/2, z.

Compound **4.65** has three potential acceptor and donor groups to be involved in hydrogen bonding interactions with symmetry related molecules. Therefore, a combination of strong hydrogen bonding between (amino)N−H···O(amide), (hydroxyl)O−H···O(amide) and weak (amide)N−H···O(hydroxyl) interactions, [3.77 Å], affords a thick, stepped sheet, two-dimensional structure (Figure 4.39). Selected hydrogen bonding parameters for **4.65** are shown in Table 4.22.

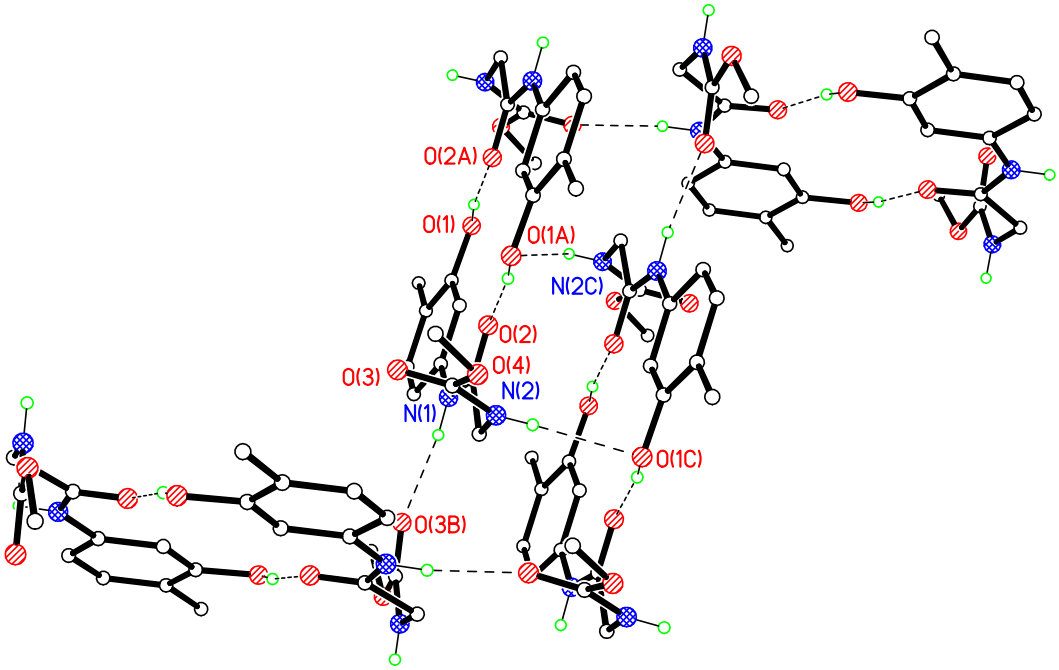

Figure 4.39 View of the hydrogen bonding motifs of **4.65**. Phenyl groups and hydrogen atoms except N*H* and O*H* have been removed for clarity.

Table 4.22 Selected hydrogen bonding parameters for **4.65**.

D–H···A	D···A/Å	D–H/Å	H···A/Å	D–H···A/º
O(1)–H(1)···O(2A)^{i}	2.6887(11)	0.869(17)	1.827(17)	170.7(16)
N(1)–H(1A)···O(3B)^{ii}	2.9358(12)	0.862(15)	2.080(15)	172.4(13)

Symmetry operations: ^{i}-x+1, -y, -z; ^{ii} -x+1, y+1/2, -z+1/2.

Interestingly, in contrast with that observed for compounds **4.59** and **4.64**, where the presence or absence of the methyl group on the functionalised *N*-phenyl group does not affect the supramolecular arrangement obtained, in compounds **4.60** and **4.65** where the –OH functional group is in the *meta* position, the packing obtained is different. While the presence of $–CH_3$ group yields a stepped sheet structure in **4.65**; in the absence of the methyl group, a two-dimensional structure propagating along the *ac* plane was obtained through a combination of strong (amino)N−H···O(amide), (hydroxyl)O−H···O(amide) hydrogen bonding interactions (Figure 4.40). Selected hydrogen bonding parameters for **4.60** are shown in Table 4.23.

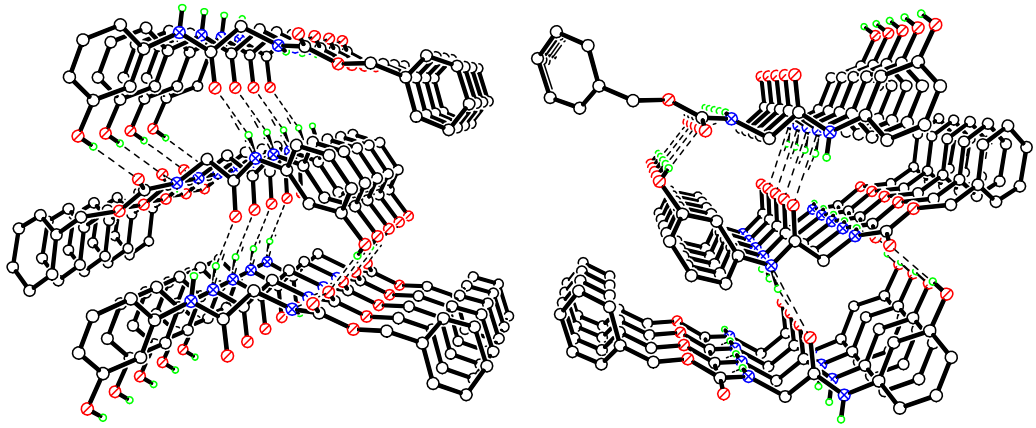

Figure 4.40 View of the hydrogen bonding motifs of **4.60** along the b axis**.** Phenyl groups and hydrogen atoms not involved in hydrogen bonding have been omitted for clarity.

Table 4.23 Selected hydrogen bonding parameters for **4.60**.

D–H···A	D···A/Å	D–H/Å	H···A/Å	D–H···A/º
O(1)–H(1)···O(3)^{i}	2.870(5)	0.83(2)	2.07(3)	162(7)
N(1)–H(1A)···O(2)^{ii}	2.777(5)	0.83(2)	2.00(3)	156(5)
N(2)–H(2)···O(3)^{iii}	2.901(5)	0.83(2)	2.16(3)	149(5)

Symmetry operations: ^{i}x+1/4, -y+1/4, z+1/4; ^{ii}x-1/4, -y+1/4, z-1/4; ^{iii}x, y, z+1.

4.2.4 Syntheses of $C_6H_4(OH)NHCOCH_2NH_2$ 4.68–4.70, $C_6H_3(CH_3)(OH)NHCOCH_2NH_2$ 4.71–4.75 and $C_6H_3(^tBu)(OH)NHCOCH_2NH_2$ 4.76

The functionalised extended primary amines $C_6H_4(OH)NHCOCH_2NH_2$ **4.68–4.70**, $C_6H_3(CH_3)(OH)NHCOCH_2NH_2$ **4.71–4.75** and $C_6H_3(^tBu)(OH)NHCOCH_2NH_2$ **4.76** were obtained after cleavage of the carbamate group in precursors **4.59–4.67** using Pd/C and cyclohexane in ethanol (Equation 4.16). The mixture was heated under reflux for 15-20 min at 110-120 ºC giving **4.68–4.76** in moderate to good yields, 32-99%.

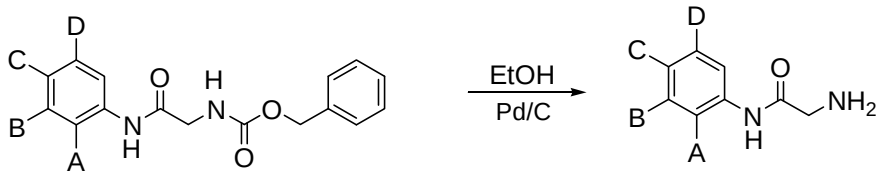

A = OH, B,C,D = H **4.59**
B = OH, A,C,D = H **4.60**
C = OH, A,B,D = H **4.61**
A = OH, D = CH_3, B,C = H **4.62**
A = CH_3, C = OH, B,D = H **4.63**
A = OH, C = CH_3, B,D = H **4.64**
B = OH, C = CH_3, A,D = H **4.65**
C = OH, B = CH_3, A,D = H **4.66**
A = OH, D = ^{t}Bu, B,C = H **4.67**

A = OH, B,C,D = H **4.68**
B = OH, A,C,D = H **4.69**
C = OH, A,B,D = H **4.70**
A = OH, D = CH_3, B,C = H **4.71**
A = CH_3, C = OH, B,D = H **4.72**
A = OH, C = CH_3, B,D = H **4.73**
B = OH, C = CH_3, A,D = H **4.74**
C = OH, B = CH_3, A,D = H **4.75**
A = OH, D = ^{t}Bu, B,C = H **4.76**

Equation 4.16

The new functionalised primary amines were isolated as white or yellow solids, soluble in a range of common organic solvents (*e.g.* MeOH, EtOH, DMSO). The ^{1}H NMR spectra of **4.68–4.76** display a broad singlet around δ(H) 8.01–9.67 ppm assigned to the amide proton. The IR spectra of these compounds show absorptions in the 3300-3400 cm^{-1} region, characteristic of ν(NH) and strong ν(C=O amide) vibration in the range 1642-1675 cm^{-1} (Table 4.24).

Table 4.24 Selected $^{31}P\{^1H\}$ NMR[a] and IR data[b] for **4.68–4.76**.

	δ(H) (NH)/ppm	**ν(C=O amide)/cm^{-1}**	**ν(NH)/cm^{-1}**
4.68	8.18	1648	3420
4.69	9.67	1674	3359
4.70	9.63	1657	3455
4.71	8.01	1648	3421
4.72	9.04	1662	3371
4.73	9.61	1653	3355
4.74	9.57	1655	3375
4.75	9.66	1675	3359
4.76	9.48	1642	3420

[a] Spectra measured in $(CD_3)_2SO$. [b] Recorded as KBr pellets.

4.2.5 Syntheses of $C_6H_4(OH)NHCOCH_2N(CH_2PPh_2)_2$ 4.77–4.79, $C_6H_3(OH)(CH_3)NHCOCH_2N(CH_2PPh_2)_2$ 4.80–4.84 and $C_6H_3(OH)(^tBu)NHCOCH_2N(CH_2PPh_2)_2$ 4.85

The functionalised extended ditertiary phosphines $C_6H_4(OH)NHCOCH_2N(CH_2PPh_2)_2$ **4.77–4.79**, $C_6H_3(OH)(CH_3)NHCOCH_2N(CH_2PPh_2)_2$ **4.80–4.84** and $C_6H_3(OH)(^tBu)NHCOCH_2N(CH_2PPh_2)_2$ **4.85** were prepared by a Mannich-based condensation reaction as described previously for ligands **4.20–4.28**, using one equivalent of the primary amines **4.68–4.76** and two equivalents of diphenylphosphinomethanol (Equation 4.17). The mixture was stirred in methanol at room temperature under nitrogen for 24 h giving the desired ligands **4.77–4.85** in good yields, 70-91%. Concentration of the solution under reduced pressure was sufficient to aid precipitation of the ligands **4.78**, **4.79**, **4.83** and **4.84**, which were filtered and dried *in vacuo*. Compounds **4.77**, **4.80–4.82** and **4.85** required the solvent to be evaporated to dryness, and yellow oils were obtained. The phosphines obtained were sufficiently pure to be used directly in complexation studies with metal precursors. The products obtained by this procedure were found to be air stable in the solid state, but were found to oxidise in solution.

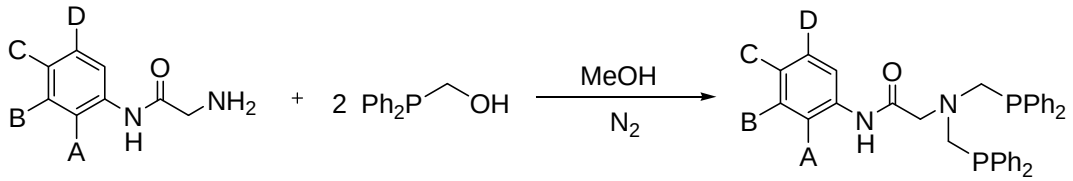

A = OH, B,C,D = H **4.68**
B = OH, A,C,D = H **4.69**
C = OH, A,B,D = H **4.70**
A = OH, D = CH_3, B,C = H **4.71**
A = CH_3, C = OH, B,D = H **4.72**
A = OH, C = CH_3, B,D = H **4.73**
B = OH, C = CH_3, A,D = H **4.74**
C = OH, B = CH_3, A,D = H **4.75**
A = OH, D = ^tBu, B,C = H **4.76**

A = OH, B,C,D = H **4.77**
B = OH, A,C,D = H **4.78**
C = OH, A,B,D = H **4.79**
A = OH, D = CH_3, B,C = H **4.80**
A = CH_3, C = OH, B,D = H **4.81**
A = OH, C = CH_3, B,D = H **4.82**
B = OH, C = CH_3, A,D = H **4.83**
C = OH, B = CH_3, A,D = H **4.84**
A = OH, D = ^tBu, B,C = H **4.85**

Equation 4.17

The infrared spectra for ligands **4.78**, **4.79**, **4.83** and **4.84** showed the characteristic ν(NH) and ν(OH) absorptions in the range 3200-3400 cm^{-1} and also a strong band in the range 1653-1659 cm^{-1} indicative of ν(C=O amide). All compounds exhibited a single

resonance in their $^{31}P\{^{1}H\}$ NMR spectra [$(CD_3)_2SO$] in the region of δ(P) −27.76 to −25.49 ppm, indicating the presence of only one phophorus(III) environment and similar to that previously observed for ligands **4.20–4.28**. Evidently, the inclusion of an amide spacer has negligible effect on δ(P). In the case of **4.78**, **4.79**, **4.83** and **4.84**, infrared spectra and microanalysis were also recorded. The microanalytical data are in good agreement with calculated values.

4.2.5.1 Crystal Structures of Compounds 4.78 and 4.79

X-ray quality crystals of compounds **4.78** and **4.79** were obtained by slow evaporation of the methanol filtrate. Structure analysis clearly shows approximate pyramidal geometries about both phosphorus centres (Table 4.25). As seen previously for ligands **4.21-4.23**, there is little spread in the P–C and C–N bond lengths in compounds **4.78** and **4.79** and they are consistent with the values reported for other ditertiary phosphine ligands.[197] The backbone spacer does not influence the geometric parameters around the pyramidal N atom. The P atoms are in an *anti* conformation as seen previously for **4.21-4.23** in order to presumably reduce the steric repulsions between the bulky phenyl groups.

Table 4.25 Selected geometric parameters (Å, °) for compounds **4.78** and **4.79**.

	4.78[i]	**4.79**
P(1)–C(1)	1.862(3)/[1.867(3)]	1.855(2)
P(2)–C(2)	1.860(3)/[1.856(3)]	1.858(2)
C(1)–N(1)/N(2)	1.467(3)/[1.478(3)]	1.476(3)
C(2)–N(1)/N(2)	1.476(3)/[1.483(4)]	1.466(3)
P(1)–C(1)–N(1)/N(2)	111.36(17)/[108.66(18)]	113.10(14)
P(1)–C(2)–N(1)/N(2)	109.61(18)/[109.77(18)]	113.80(15)
C(1)–N(1)/N(2)–C(2)	110.4(2)/[111.7(2)]	111.19(17)

[i] Values in brackets are for the second molecule in the asymmetric unit for **4.78**.

The presence of the backbone in **4.78** and **4.79** compared with the ligands **4.21-4.23** is expected to increase flexibility and the presence of more potential donor and acceptor atoms with hydrogen bonding capability should facilitate the formation of

supramolecular arrays with increased complexity. Interestingly, even the two molecules of **4.78** in the asymmetric unit differ in the disposition of the PCNCP fragment with respect to the functionalised spacer indicating the degree of flexibility within the backbone (Figure 4.41).

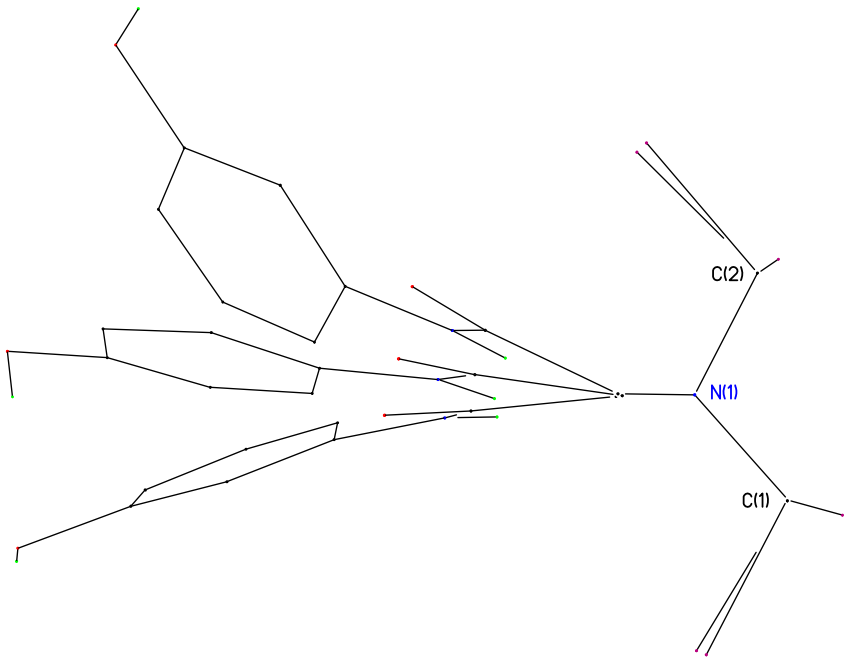

Figure 4.41 Overlay view of **4.78** and **479**. Phenyl rings and hydrogen atoms except O*H* and N*H* have been omitted for clarity.

4.2.5.2 Secondary Interactions in Compounds 4.78 and 4.79

Compound **4.78** crystallises with two molecules in the asymmetric unit which form dimers using (hydroxyl)O–H···O(amide) hydrogen bonds, creating $R^2_2(16)$ ring motifs (Figure 4.42). The distance between symmetry related nitrogen atoms are 6.834 Å and 6.925 Å for N(1) and N(3) respectively, shorter distances than observed in **4.21** which also possesses the –OH functional group in a *meta* position. The NH group from the amide functional group is involved in a *S*(5) N–H···N intramolecular hydrogen bond with the pyramidal N atom (Table 4.26).

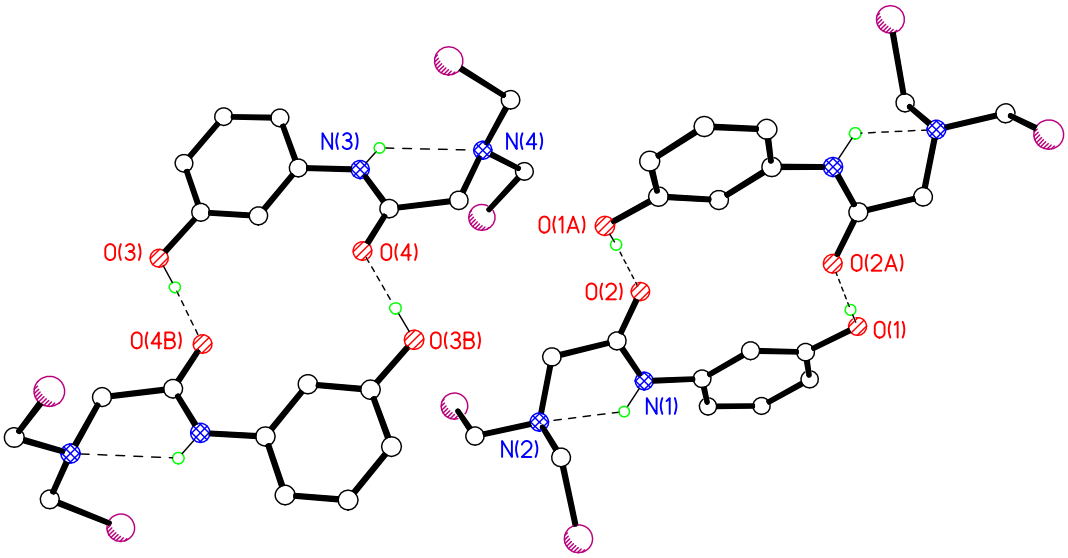

Figure 4.42 Dimers of **4.78** forming $R^2_2(16)$ graph set motifs. Phenyl groups and hydrogen atoms not involved in hydrogen bonding have been omitted for clarity.

Table 4.26 Selected hydrogen bonding parameters for **4.78**.

D–H···A	D···A/Å	D–H/Å	H···A/Å	D–H···A/º
O(1)–H(1)···O(2A)^{i}	2.670(3)	0.84	1.83	174
N(1)–H(1A)···N(2)	2.694(3)	0.83(3)	2.24(3)	115(3)
O(3)–H(3)···O(4B)^{ii}	2.658(3)	0.84	1.83	167
N(3)–H(3A)···N(4)	2.714(3)	0.73(3)	2.30(3)	117(3)

Symmetry operations: ^{i}-x, -y+1, -z+1; ^{ii}-x+1, -y+1, -z.

In preliminary work carried out within the research group, X-ray quality crystals of compound **4.79** were obtained directly from slow evaporation of a methanol filtrate. Compound **4.79** crystallises with one molecule in the asymmetric unit and presents the N–H···N intramolecular *S*(5) graph set hydrogen bond seen above in **4.78**. In this case, the –OH functional group is in the *ortho* position with respect to the N-arene moiety, interacting with the carbonyl(amide) group through (hydroxyl)O–H···O(amide) hydrogen bonds forming one-dimensional chains propagating in the *c* direction (Figure 4.43). Selected hydrogen bonding parameters for **4.79** are shown in Table 4.27.

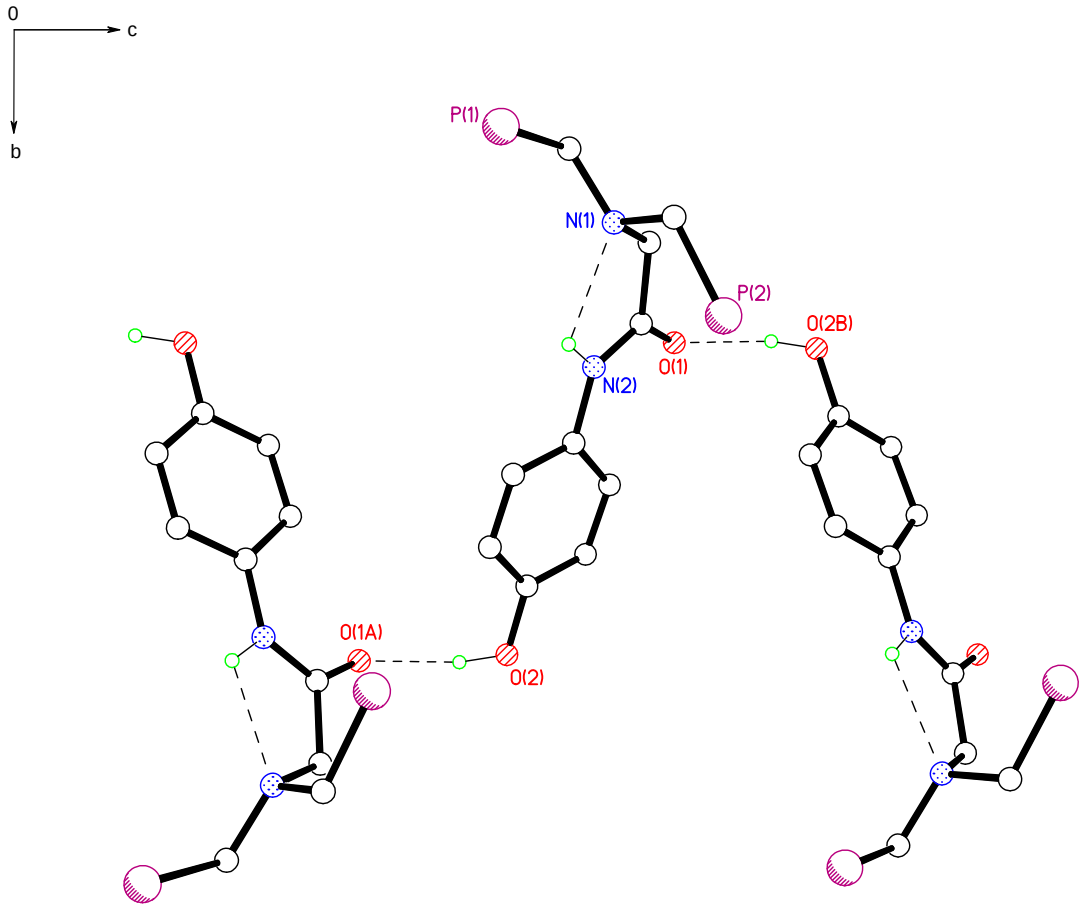

Figure 4.43 Chains of **4.79**. Phenyl groups and hydrogen atoms except O*H* and N*H* have been omitted for clarity.

Table 4.27 Selected hydrogen bonding parameters for **4.79**.

D–H···A	D···A/Å	D–H/Å	H···A/Å	D–H···A/°
N(2)–H(2)···N(1)	2.748(3)	0.85(2)	2.29(2)	114(2)
O(2)–H(2A)···O(1B)^{i}	2.706(3)	0.89(3)	1.83(3)	169(3)

Symmetry operation: ^{i}x, -y+1/2, z-1/2.

4.2.6 Coordination Chemistry of $C_6H_4(OH)NHCOCH_2N(CH_2PPh_2)_2$ 4.86–4.88, $C_6H_3(OH)(CH_3)NHCOCH_2N(CH_2PPh_2)_2$ 4.89–4.93 and $C_6H_3(OH)(^tBu)NHCOCH_2N(CH_2PPh_2)_2$ 4.94

4.2.6.1 Syntheses of Square Planar Pt(II) Complexes 4.86–4.94

The complexes $PtCl_2\{P,P\text{-}C_6H_4(OH)NHCOCH_2N(CH_2PPh_2)_2\}$ **4.86–4.88**, $PtCl_2\{P,P\text{-}C_6H_3(OH)(CH_3)NHCOCH_2N(CH_2PPh_2)_2\}$ **4.89–4.93** and $PtCl_2\{P,P\text{-}C_6H_3(OH)(^tBu)NHCOCH_2N(CH_2PPh_2)_2\}$ **4.94** were prepared following the procedure used for related Pt(II) complexes **4.29–4.37**. Hence addition of the appropriate ligand **4.77–4.85** to a solution containing one equivalent of $PtCl_2(cod)$ in CH_2Cl_2 (Equation 4.18) gave **4.86–4.94**. After stirring for 30 min, the solution was concentrated to approximately 5 ml under reduced pressure and the required products precipitated by addition of Et_2O. Yields for these complexes were in the range 57-99%.

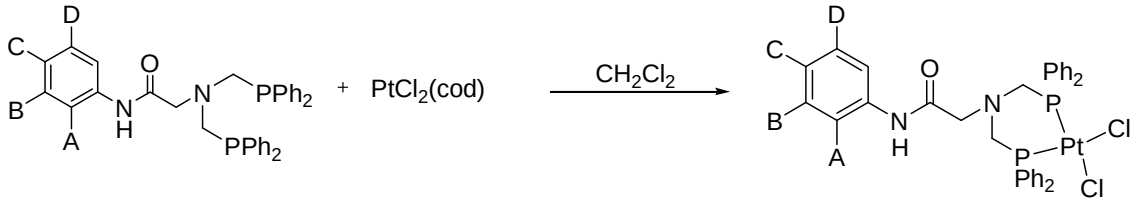

A = OH, B,C,D = H **4.77**
B = OH, A,C,D = H **4.78**
C = OH, A,B,D = H **4.79**
A = OH, D = CH_3, B,C = H **4.80**
A = CH_3, C = OH, B,D = H **4.81**
A = OH, C = CH_3, B,D = H **4.82**
B = OH, C = CH_3, A,D = H **4.83**
C = OH, B = CH_3, A,D = H **4.84**
A = OH, D = ^{t}Bu, B,C = H **4.85**

A = OH, B,C,D = H **4.86**
B = OH, A,C,D = H **4.87**
C = OH, A,B,D = H **4.88**
A = OH, D = CH_3, B,C = H **4.89**
A = CH_3, C = OH, B,D = H **4.90**
A = OH, C = CH_3, B,D = H **4.91**
B = OH, C = CH_3, A,D = H **4.92**
C = OH, B = CH_3, A,D = H **4.93**
A = OH, D = ^{t}Bu, B,C = H **4.94**

Equation 4.18

All of the platinum(II) complexes **4.86–4.94** gave one phosphorus resonance around δ(P) -10 ppm, a downfield shift of approximately 20 ppm with respect to the free ligands and furthermore indicates both the phophorus(III) centres are equivalent. The coupling constants, ^1J(PtP), for **4.86–4.94** are approximately 3400 Hz, which indicates that these complexes are in a *cis* conformation, as expected for this type of *bis*(phosphino)amino ligands. In their infrared spectra, there are two vibrations in the range 290-325 cm^{-1}, indicative of ν(PtCl) (Table 4.28). The presence of these two

vibrations provides confirmation for the *cis* isomers. Compounds **4.86–4.94** present the characteristic ν(NH) and ν(OH) absorptions in the range 3200-3400 cm^{-1} and also a strong band in the range 1653-1675 cm^{-1} indicative of ν(C=O amide).

Table 4.28 Selected $^{31}P\{^{1}H\}$ NMR[a] and IR[b] data for **4.86–4.94**.

	δ(P)/ppm	**^{1}J(PtP)/Hz**	**υ(PtCl)/cm^{-1}**
4.86	-6.89	3422	308; 286
4.87	-9.45	3425	304; 279
4.88	-9.54	3405	311; 287
4.89	-9.83	3398	305; 283
4.90	-11.02	3397	316; 283
4.91	-9.86	3405	315; 290
4.92	-9.79	3398	309; 283
4.93	-9.70	3406	312; 286
4.94	-9.66	3418	309; 283

[a] Spectra measured in $(CD_3)_2SO$. [b] Recorded as KBr pellets.

The solubility of complexes **4.86–4.94** was generally poor in common solvents such as diethyl ether, dichloromethane or chloroform but they are highly soluble in DMSO. Four of the complexes, **4.89–4.92**, afforded crystals from solutions of DMSO/$CHCl_3$/MeOH/diethyl ether and DMSO/$CHCl_3$/MeOH/hexane. Unfortunately the other complexes **4.86–4.88**, **4.93** and **4.94** formed powders under similar experimental conditions.

4.2.6.2 Crystal Structures of Compounds 4.89–4.92

Selected bond distances and angles for **4.89–4.92** are given in Table 4.29. The geometry about each platinum(II) centre is approximately square-planar P−Pt−P [range 91.3-96.5 º], in order to fulfil the constraints imposed by ligand, with Pt−Cl [range 2.343–2.383 Å] and Pt−P [range 2.217–2.233 Å] bond lengths.[248-250] The conformation of the Pt−P−C−N−C−P six-membered ring in each complex is best described as a twisted-chair.

There are close similarities between the solid state structures of **4.89**–**4.92** with all the compounds having the same overall features, a chelating P−C–N–C−P ligand and two chloride ligands forming a square planar geometry.

Table 4.29 Selected geometric parameters (Å, °) for compounds **4.89–4.92**.

	4.89[i]	**4.90**	**4.91**	**4.92**
Pt(1)−P(1)	2.2335(19)/[2.2172(9)]	2.234(2)	2.2263(15)	2.220(3)
Pt(1)−P(2)	2.230(2)/[2.230(2)]	2.2249(9)	2.2200(14)	2.220(3)
Pt(1)−Cl(1)	2.383(2)/[2.378(2)]	2.3685(9)	2.3447(17)	2.348(3)
Pt(1)−Cl(2)	2.361(2)/[2.364(2)]	2.3426(9)	2.3643(15)	2.348(3)
P(1)−Pt(1)−P(2)	95.72(8)/[95.79(8)]	96.52(3)	91.34(5)	92.63(17)
Cl(1)−Pt(1)−Cl(2)	90.23(9)/[90.16(9)]	89.33(3)	88.65(6)	87.39(17)
P(1)−Pt(1)−Cl(1)	86.31(7)/[86.49(7)]	85.73(3)	92.13(6)	89.97(12)
P(2)−Pt(1)−Cl(1)	177.80(9)/[177.51(9)]	176.29(3)	178.73(6)	176.96(13)
P(1)−Pt(1)−Cl(2)	175.76(9)/[175.64(8)]	174.72(3)	171.32(9)	176.96(13)
P(2)−Pt(1)−Cl(2)	87.70(10)/[87.51(10)]	88.31(3)	87.75(5)	89.97(12)
P(1)−C(1)−N(1)	111.5(5)/[112.0(5)]	108.7(2)	105.7(4)	109.1(10)
P(2)−C(2)−N(1)	110.9(5)/[110.8(5)]	113.1(3)	114.9(4)	109.1(10)
C(1)−N(1)−C(2)	112.5(6)/[111.3(7)]	109.7(3)	115.0(5)	113.0(16)

[i] Values in brackets are for the second molecule in the asymmetric unit for **4.89**

4.2.6.3 Secondary Interactions in Compounds 4.89–4.92

Complex **4.89** was crystallised from a diethyl ether solution, including one solvent molecule per complex molecule. Compound **4.89** crystallises with an intramolecular *S*(7) hydrogen bond graph set, a common motif in 1,2-disubstituted phenyl rings.[116,189] The intramolecular hydrogen bonding limits the dimensionality of the packing of the complex, with molecules of **4.89** packing in one-dimensional chains which propagate in the *a* direction through a single weak N−H···Cl interaction (Figure 4.44).[10]

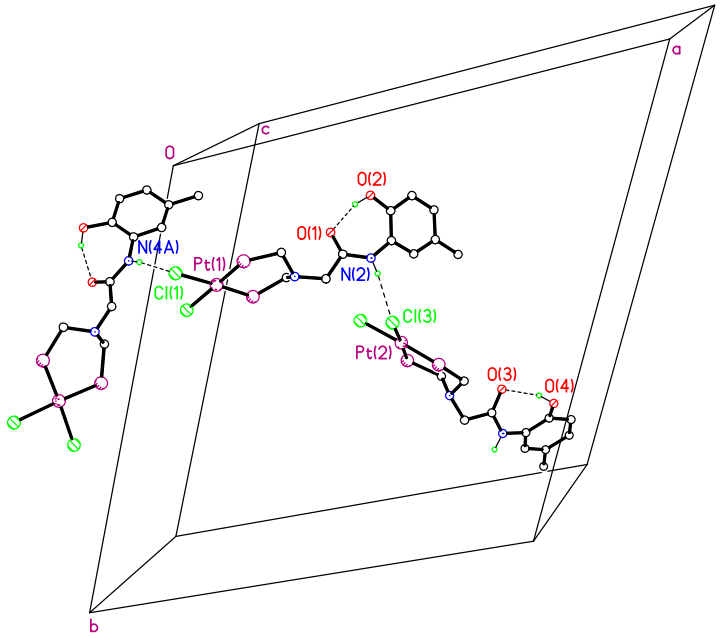

Figure 4.44 One-dimensional chain of **4.89** propagating in the *a* direction. Phenyl groups and hydrogen atoms not involved in hydrogen bonding have been omitted for clarity. Selected hydrogen bonding parameters for **4.89** are shown in Table 4.30.

Table 4.30 Selected hydrogen bonding parameters for **4.89**.

D–H···A	D···A/Å	D–H/Å	H···A/Å	D–H···A/º
N(2)–H(2)···Cl(3)	3.324(8)	0.88	2.46	167.6
O(2)–H(2A)···O(1)	2.596(9)	0.84	1.80	156.4
N(4)–H(4)···Cl(1A)^{i}	3.318(8)	0.88	2.45	167.9
O(4)–H(4A)···O(3)	2.607(9)	0.84	1.82	154.7

Symmetry operations: ^{i}-y+1, x-y+1, z+2/3.

The X-ray structure of **4.91** is shown in Figure 4.45, in which the −OH is in the same *ortho* position as in **4.89**, while the $-CH_3$ group is now in the *para* position. Compound **4.91** presents disorder along the backbone and the functionalised *N*-arene group and has been modelled over two equally-occupied sets of positions with a common C(9) and six-membered chelated ring.

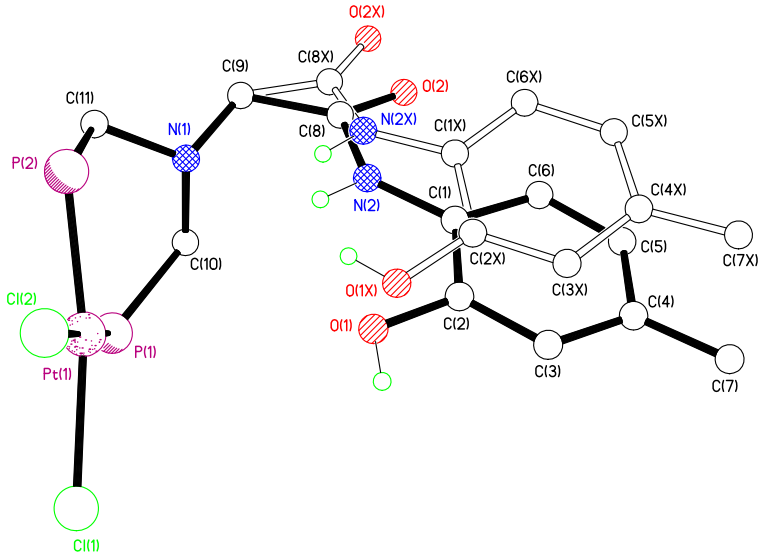

Figure 4.45 View of compound **4.91** showing both components of the disorder. Phenyl groups and hydrogen atoms except N*H* and O*H* have been omitted for clarity.

Compound **4.91** shows an (amide)N−H···N(tertiary) *S*(5) intramolecular hydrogen bond (Figure 4.46). A strong O−H···O interaction links disordered component 1 of **4.91** to disordered component 2 of a symmetry related neighbouring molecule forming a one-dimensional chain. Selected hydrogen bonding parameters for **4.91** are shown in Table 4.31.

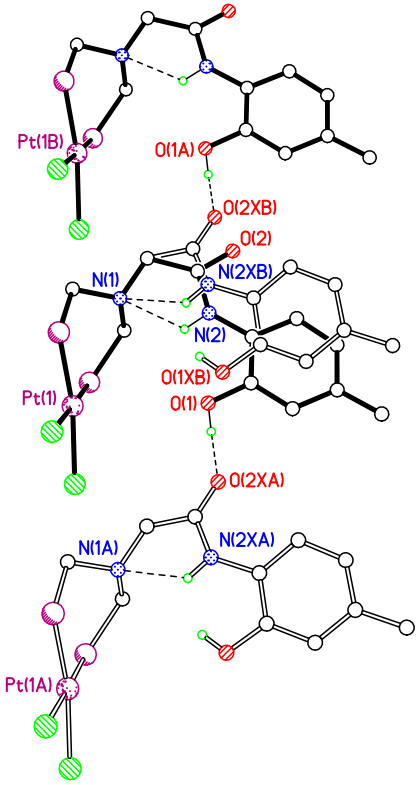

Figure 4.46 View of the one-dimensional chain of **4.91**. Phenyl groups and hydrogen atoms not involved in hydrogen bonding have been omitted for clarity.

Table 4.31 Selected hydrogen bonding parameters for **4.91**.

D–H···A	D···A/Å	D–H/Å	H···A/Å	D–H···A/º
N(2)–H(2)···N(1)	2.755(14)	0.88	2.34	109
O(1)–H(1)···O(2XA)^{i}	2.647(16)	0.84	1.87	154

Symmetry operation: ^{i}x+1, y, z.

Compound **4.92**, in which the $-CH_3$ group is in the *para* position and the –OH group located in the *meta* position with respect to the amide N atom, crystallises with one molecule in the asymmetric unit of Pt(II) complex which lies on a mirror plane. Due to the poor quality of the diffraction data for **4.92**, the −OH hydrogen atom could not be located. The structure of compound **4.92** contains solvent-accessible voids accounting for 3% of the total unit cell volume. The SQUEEZE program within Platon suite identified approximatly 50 unaccounted electrons in the unit cell, and this was assumed to be a diethyl ether molecule (42 electrons per molecule) which were taken into account in the refinement, improving the R1 by 1%.[48] Compound **4.92** packs as a

stepped one-dimensional polymeric chain through a bifurcated intermolecular N−H···Cl hydrogen bonding (Table 4.32).[49,50] This one-dimensional chain is propagating in the *a* direction (Figure 4.47).

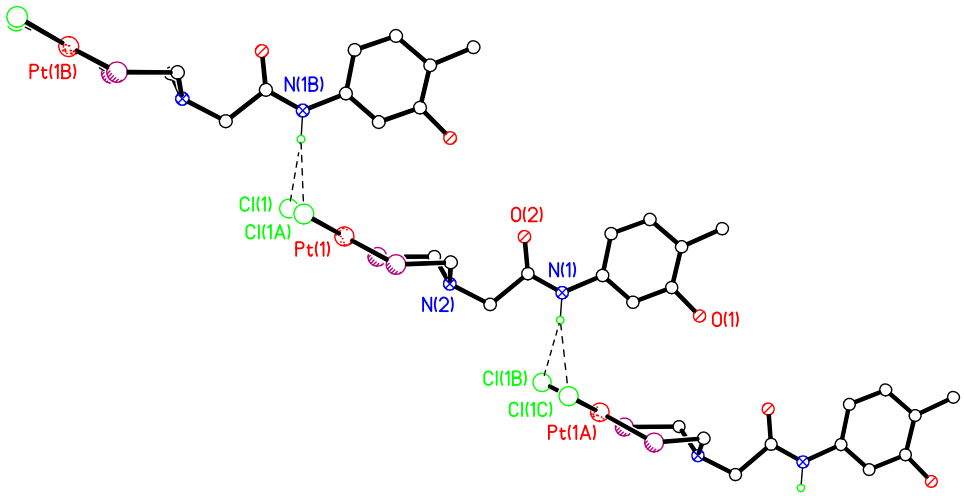

Figure 4.47 View of the one-dimensional stepped chain of **4.92**. Phenyl groups and hydrogen atoms not involved in hydrogen bonding have been omitted for clarity.

Table 4.32 Selected hydrogen bonding parameters for **4.92**.

D–H···A	D···A/Å	D–H/Å	H···A/Å	D–H···A/º
N(1)–H(1A)···Cl(1)^{i}	3.505(14)	0.88	2.76	144

Symmetry operations: ^{i}x-1, y, -z+1/2.

Compound **4.90**, where the −OH and $-CH_3$ functional groups are in *para* and *ortho* positions respectively to the amide N atom reveals an intramolecular *S*(5) (amide)N−H···N(tertiary) hydrogen bonding motif seen previously for **4.91** (Table 4.33). As expected, the (amide)N−H···N(tertiary nitrogen centre) intermolecular hydrogen bond length in both complexes are very similar. The −OH functional group is involved in an intermolecular, single, weak O−H···Cl hydrogen bond that holds the molecules of **4.90** in undulating chains which propagate parallel to the *a* axis (Figure 4.48).

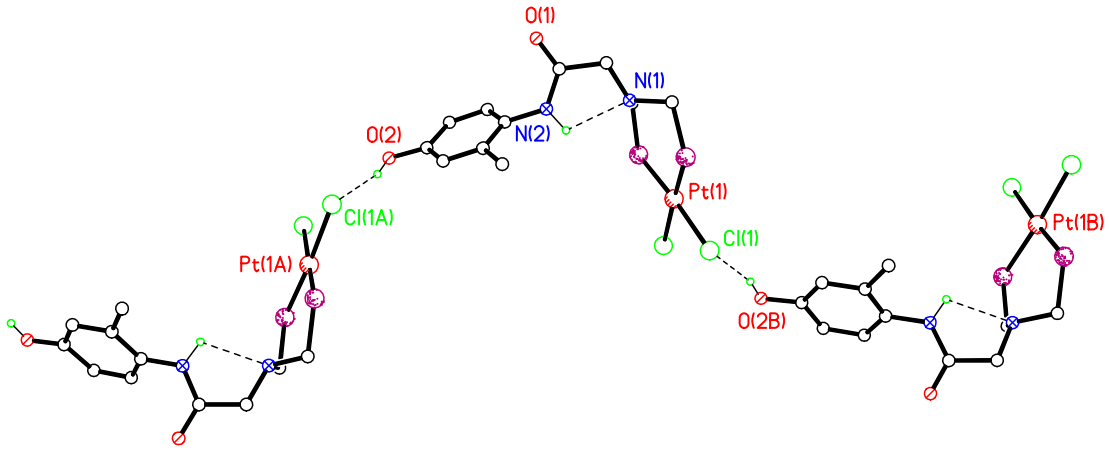

Figure 4.48 View of the undulating chains of **4.90**. Phenyl groups and hydrogen atoms not involved in hydrogen bonding have been omitted for clarity.

The similarities between the structures of **4.90** and **4.91** are obvious, with the common (amide)N−H···N(tertiary) *S*(5) hydrogen bonding motif and the single hydrogen bond holding the molecules in one-dimensional structures. Compounds **4.90** and **4.91** only differ in the nature of the hydrogen bond acceptor (*i.e.* O−H···O in **4.91** compared to O−H···Cl in **4.90**).

Table 4.33 Selected hydrogen bonding parameters for **4.90**.

D–H···A	D···A/Å	D–H/Å	H···A/Å	D–H···A/°
O(2)–H(2)···Cl(1A)^{i}	3.068(3)	0.84	2.25	164
N(2)–H(2A)···N(1)	2.711(5)	0.93(5)	2.29(5)	107(4)

Symmetry operation: ^{i}x-1/2, -y+3/2, z-1/2.

4.2.6.4 Syntheses of Linear Au(I) Complexes 4.95–4.103

Following a similar procedure to that used in the synthesis seen previously for complexes **4.38-4.46**, Au(I) complexes $Au_2Cl_2\{P,P\text{-}C_6H_4(OH)NHCOCH_2N(CH_2PPh_2)_2\}$ **4.95–4.97**, $Au_2Cl_2\{P,P\text{-}C_6H_3(OH)(CH_3)NHCOCH_2N(CH_2PPh_2)_2\}$ **4.98–4.102** and $Au_2Cl_2\{P,P\text{-}C_6H_3(OH)(^{t}Bu)NHCOCH_2N(CH_2PPh_2)_2\}$ **4.103** were synthesised by addition of the appropriate ligand **4.77–4.85** to a solution of AuCl(tht) in CH_2Cl_2. After stirring for 30

min, the solution was concentrated to approximately 5 ml under reduced pressure and the required products precipitated upon addition of Et_2O (Equation 4.19). These complexes were obtained in 50-94% yield.

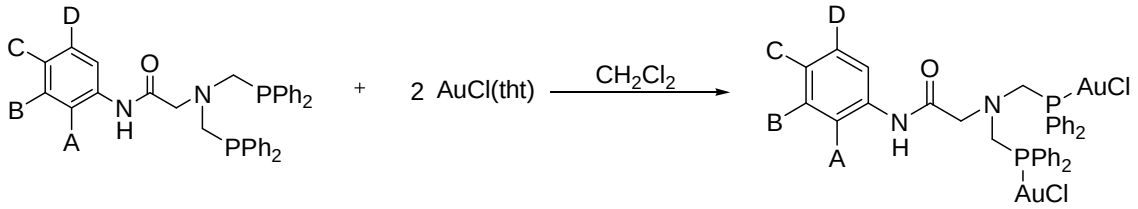

A = OH, B,C,D = H **4.77**
B = OH, A,C,D = H **4.78**
C = OH, A,B,D = H **4.79**
A = OH, D = CH_3, B,C = H **4.80**
A = CH_3, C = OH, B,D = H **4.81**
A = OH, C = CH_3, B,D = H **4.82**
B = OH, C = CH_3, A,D = H **4.83**
C = OH, B = CH_3, A,D = H **4.84**
A = OH, D = ^{t}Bu, B,C = H **4.85**

A = OH, B,C,D = H **4.95**
B = OH, A,C,D = H **4.96**
C = OH, A,B,D = H **4.97**
A = OH, D = CH_3, B,C = H **4.98**
A = CH_3, C = OH, B,D = H **4.99**
A = OH, C = CH_3, B,D = H **4.100**
B = OH, C = CH_3, A,D = H **4.101**
C = OH, B = CH_3, A,D = H **4.102**
A = OH, D = ^{t}Bu, B,C = H **4.103**

Equation 4.19

Compounds **4.95–4.103** were isolated as white or off-white solids, soluble in dimethylsulfoxide but insoluble in chloroform, alcohols or dichloromethane. All the gold complexes display a single phosphorus resonance in the range δ(P) 20.8 – 24.8 ppm, a downfield shift of approximately 40 ppm with respect to the free ligands. The characteristic ν(AuCl) infrared band could be identified in the range of 324-328 cm^{-1} for the complexes **4.95–4.103** (Table 4.34). Compounds **4.95–4.103** showed the characteristic ν(NH) and ν(OH) absorptions in the range 3200-3400 cm^{-1} and also a strong band in the range 1613-1680 cm^{-1} indicative of ν(C=O amide).

Table 4.34 Selected $^{31}P\{^{1}H\}$ NMR[a] and IR data[b] for **4.95–4.103**.

	δ(P)/ppm	ν(AuCl)/cm^{-1}
4.95	22.9	328
4.96	24.2	328
4.97	24.3	325
4.98	21.2	328
4.99	24.8	328
4.100	20.8	328
4.101	24.5	324
4.102	24.1	324
4.103	23.4	328

[a] Spectra measured in $(CD_3)_2SO$. [b] Recorded as KBr pellets.

Numerous attempts have been made to obtain crystals from these gold(I) complexes **4.95-4.103** and only powdered material was isolated.

4.2.6.5 Syntheses of Octahedral Mo(0) Complexes 4.104–4.108

Complexes $Mo(CO)_4\{P,P\text{-}C_6H_4(OH)NHCOCH_2N(CH_2PPh_2)_2\}$ **4.104**, $Mo(CO)_4\{P,P\text{-}C_6H_3(OH)(CH_3)NHCOCH_2N(CH_2PPh_2)_2\}$ **4.105–4.107** and $Mo(CO)_4\{P,P\text{-}C_6H_3(OH)(^{t}Bu)NHCOCH_2N(CH_2PPh_2)_2\}$ **4.108** were synthesised by addition of the appropriate ligand **4.78**, **4.80** or **4.83–4.85** to a solution of $Mo(CO)_4$(nbd) in CH_2Cl_2 under N_2 for 48 h (Equation 4.20). The solution was concentrated to approximately 10 ml under reduced pressure. The required products precipitated upon addition of Et_2O/hexane to give the complexes in good yields, 56-88%.

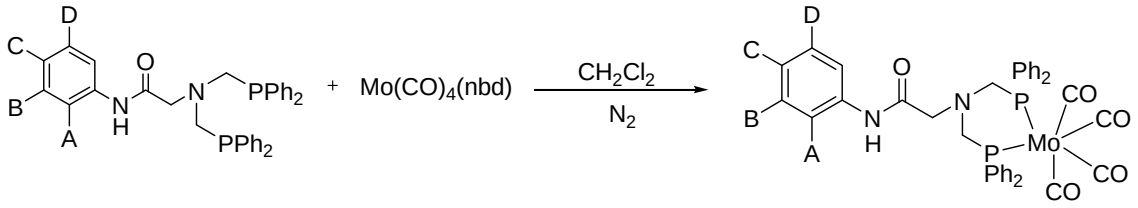

B = OH, A,C,D = H **4.78**
A = OH, D = CH_3, B,C = H **4.80**
C = OH, B = CH_3, A,D = H **4.83**
B = OH, C = CH_3, A,D = H **4.84**
A = OH, D = ^{t}Bu, B,C = H **4.85**

B = OH, A,C,D = H **4.104**
A = OH, D = CH_3, B,C = H **4.105**
C = OH, B = CH_3, A,D = H **4.106**
B = OH, C = CH_3, A,D = H **4.107**
A = OH, D = ^{t}Bu, B,C = H **4.108**

Equation 4.20

The $^{31}P\{^1H\}$ NMR spectra show single, sharp resonances, in the region of δ(P) 13.9 − 20.9 ppm, a downfield shift of approximately 40 ppm with respect to the free phosphine ligands **4.78**, **4.80** and **4.83–4.85**. The OH and NH resonances in the ^1H NMR spectra of **4.78** were not observed. Complexes **4.104–4.108** display three strong carbonyl absorptions in the region 1894-2021 cm^{-1} in the IR spectra consistent with a *cis* tetracarbonyl metal complex (Table 4.35). The infrared spectra for compounds **4.104–4.108** showed the characteristic band for ν(NH) and ν(OH) in the range 3300-3400 cm^{-1} and also a strong band in the range 1654-1669 cm^{-1} indicative of ν(C=O amide). The $^{31}P\{^1H\}$ NMR spectra for **4.108** could not be recorded due to fast oxidation in solution but IR spectroscopy, mass spectrometry and microanalyses all indicate formation of the desired compound.

Table 4.35 Selected $^{31}P\{^1H\}$ NMR[a] and IR data[b] for **4.104–4.108**.[a]

	δ(P)/ppm	**ν(CO)/cm^{-1}**
4.104	20.97	2020; 1921; 1894
4.105	13.93	2020; 1919; 1896
4.106	19.69	2019; 1924; 1896
4.107	19.95	2020; 1919; 1894
4.108	n.r.	2021; 1919; 1902

[a] Spectra measured in $CDCl_3$. [b] Recorded as KBr pellets. n.r. = not recorded.

Numerous attempts have been made to obtain crystals of Mo(0) complexes **4.104–4.108** but only powdered material was isolated.

4.2.7 Novel Ditertiary Phosphines $^{t}BuOC(O)NH(CH_2)_2N(CH_2PPh_2)_2$ 4.109, $HO_2C(CH_2)_2N(CH_2PPh_2)_2$ 4.110, $HO_2CCH_2NHCOCH_2N(CH_2PPh_2)_2$ 4.111 and $HO_2CCH_2NHCOCH_2NHCOCH_2N(CH_2PPh_2)_2$ 4.112

A similar family of ditertiary phosphines containing an amide backbone which is sufficiently flexible to adopt different conformations in order to access different types of supramolecular arrays is presented (Figure 4.49). Instead of a functionalised arene group as seen previously, other functionalities (*e.g.* carboxylic acid groups) were studied on the amide backbone. A CSD search shows that similar compounds to **4.109–4.112** have not been reported, therefore compounds **4.109–4.112** represent first examples of novel highly functionalised phosphorus based ligands which can be exploited as building blocks in crystal engineering. The synthesis, structural analysis and metal complexation studies of **4.109–4.112** with selected transition metals, Pt(II), Ru(II) and Au(I) have been undertaken. The synthesis of compound **4.109** and its complexation studies were carried out by Benoit Genevier and structurally characterised by the Author of this thesis.

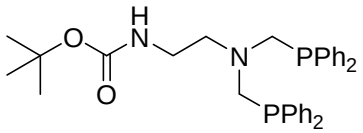

4.109

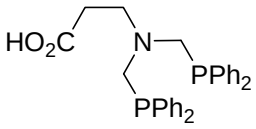

4.110

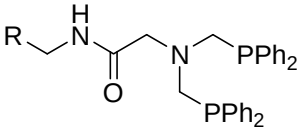

R = CO_2H **4.111**
R = $CONHCH_2CO_2H$ **4.112**

Figure 4.49 Ditertiary functionalised *bis*(phosphino)amines **4.109–4.112** prepared.

4.2.8 Syntheses and Charaterisation of $^{t}BuOC(O)NH(CH_2)_2N(CH_2PPh_2)_2$ 4.109

Ligand $^{t}BuOC(O)NH(CH_2)_2N(CH_2PPh_2)_2$ **4.109** was prepared using a Mannich-based condensation reaction (Equation 4.21). The precursor primary amine, (2-aminoethyl)carbamic acid tert-butyl ester **X**, was synthesised from ethylenediamine and di-*t*-butyl Boc-anhydride following a literature procedure.[251]

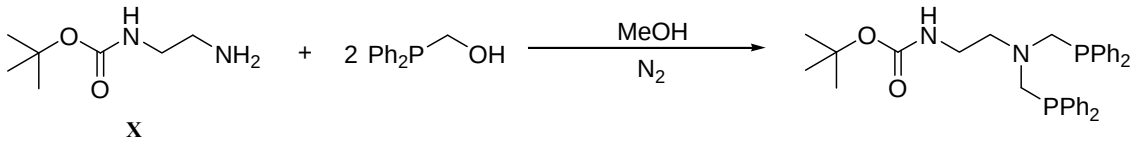

Equation 4.21

Compound **4.109** displays a single phosphorus resonance in the $^{31}P\{^{1}H\}$ NMR spectrum (in $CDCl_3$) at δ(P) -28.8 ppm. An infrared spectrum and microanalysis data were also recorded and are in good agreement with calculated values.

Compound **4.109** represents the simplest example: only the amide group can participate in hydrogen bonding. However, the bulky ^{t}Boc group may interfere in the formation of any supramolecular array. Crystals of **4.109**, suitable for X-ray crystallography, were obtained by slow evaporation of a methanol filtrate. Compound **4.109** crystallises with one molecule in the asymmetric unit (Figure 4.50). Despite **4.109** bearing potential hydrogen bonding donor and acceptor groups, no inter- or intramolecular hydrogen bonding was observed. Hence the structure of **4.109** is essentially zero-dimensional.

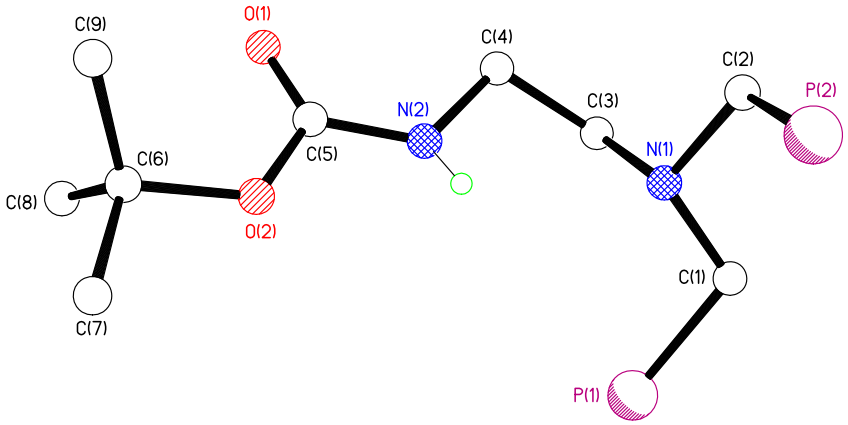

Figure 4.50 View of the asymmetric unit of **4.109**. Phenyl groups and hydrogen atoms except N*H* have been omitted for clarity.

Structure analysis of **4.109** clearly shows approximate pyramidal geometries about the tertiary nitrogen atom [N(1)–C(1)–P(1) 109.08(15)°, N(1)–C(2)–P(2) 112.92(15)° and C(1)–N(1)–C(2) 111.78(18)°]. As seen for ligands **4.77–4.85**, there is little variation in

the P–C and C–N bond lengths [C(1)–N(1) 1.467(3) Å, C(2)–N(1) 1.470(3) Å, C(1)–P(1) 1.859(2) Å and C(2)–P(2) 1.859(2) Å] in **4.109** and they are consistent with the values already described for **4.77–4.85**. Therefore, the geometric parameters around the pyramidal N atom are not influenced by this type of backbone. The phosphorus atoms are in an *anti* conformation presumably in order to reduce steric repulsions between the bulky phenyl groups.

4.2.9 Coordination Chemistry of ^{t}BuOC(O)NH(CH$_2$)$_2$N(CH$_2$PPh$_2$)$_2$ 4.109

Compound **4.109** reacts with $PtCl_2$(cod), AuCl(tht) and [Ru(η^6-*p*-cymene)Cl_2]$_2$ in CH_2Cl_2 to give $PtCl_2$\{^{t}BuOC(O)NH(CH$_2$)$_2$N(CH$_2$PPh$_2$)$_2$\} **4.113**, Au_2Cl_2\{^{t}BuOC(O)NH(CH$_2$)$_2$N(CH$_2$PPh$_2$)$_2$\} **4.114** and [$RuCl_2$(η^6-*p*-cymene)]$_2$\{^{t}BuOC(O)NH(CH$_2$)$_2$N(CH$_2$PPh$_2$)$_2$\} **4.115** as white or red solids in 81%, 77% and 65% yield, respectively (Equation 4.22).

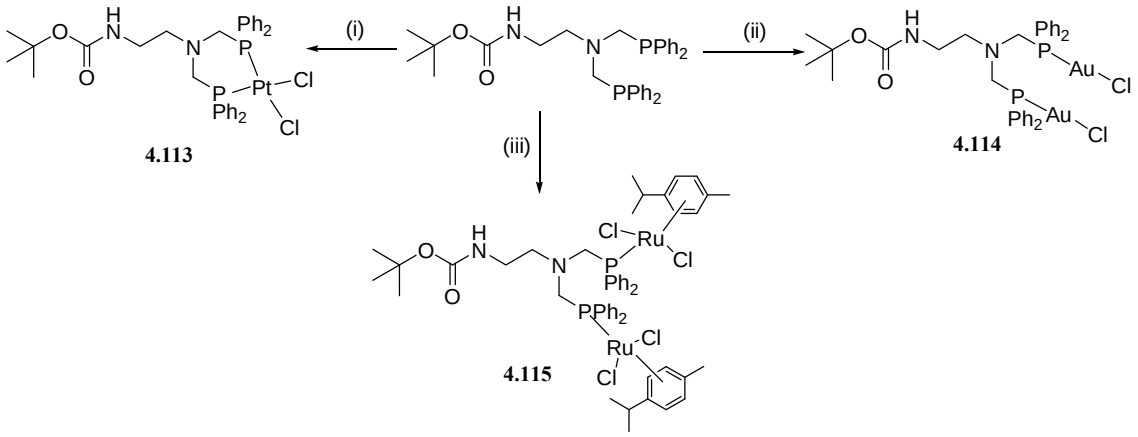

Equation 4.22 (i) $PtCl_2$(cod), CH_2Cl_2, (ii) AuCl(tht), CH_2Cl_2, (iii) [Ru(η^6-*p*-cymene)Cl_2]$_2$, CH_2Cl_2.

The $^{31}P\{^{1}H\}$ NMR spectra (in $CDCl_3$) of the isolated solids **4.113–4.115** showed a single phosphorus resonance at δ(P) -10.1 ppm, 16.5 ppm and 19.2 ppm respectively. The ^{1}J(PtP) coupling constant for **4.113** was *ca*. 3400 Hz suggesting *cis* isomer, similar to those observed for compounds **4.86–4.94**. The IR spectra of **4.113–4.115** also show a characteristic N–H vibration and ν(C=O) stretch around 3400 cm^{-1} and 1700 cm^{-1} respectively.

4.2.9.1 X-ray Crystal Structures of $PtCl_2\{^tBuOC(O)NH(CH_2)_2N(CH_2PPh_2)_2\}$ 4.113 and $[RuCl_2(\eta^6\text{-}p\text{-cymene})]_2\{^tBuOC(O)NH(CH_2)_2N(CH_2PPh_2)_2\}$ 4.115

Crystals of **4.113** suitable for X-ray crystallography were obtained by slow vapour diffusion of Et_2O into a dimethyl sulfoxide/chloroform solution of **4.113**. The X-ray structure of **4.113** revealed an approximate square-planar coordination of the Pt(II) centre [P(1)–Pt(1)–P(2) 95.63(15)°, P(1)–Pt(1)–Cl(1) 88.52(15)°, P(2)–Pt(1)–Cl(2) 86.91(15)° and Cl(1)–Pt(1)–Cl(2) 88.84(14)°] (Figure 4.51). The Pt–Cl and Pt–P bond lengths [Pt(1)–Cl(1) 2.354(4) Å, Pt(1)–Cl(2) 2.366(4) Å, Pt(1)–P(1) 2.231(4) Å and Pt(1)–P(2) 2.234(4) Å] are consistent with values reported in the literature.[189]

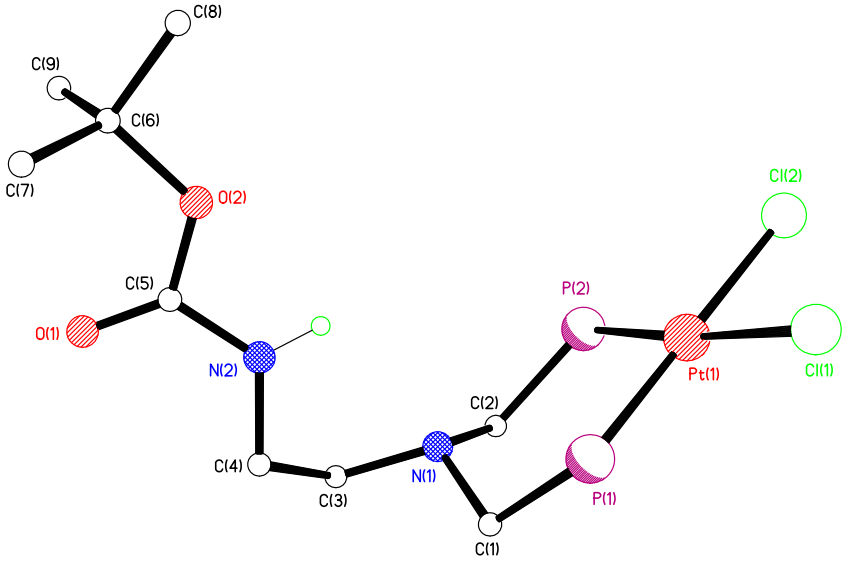

Figure 4.51 View of the asymmetric unit of **4.113**. Phenyl groups and hydrogen atoms have been omitted for clarity.

The conformation of the Pt–P–C–N–C–P six-membered ring in **4.113** is best described as a boat, with the N atom above the P_2C_2 plane by 0.860 Å. As seen for the free ligand **4.109** no intramolecular hydrogen bonding between (amide)N–H···N(tertiary) or intermolecular interactions were observed.

Numerous attempts have been made to obtain crystals of **4.114** without any success affording only powdered material. However, compound **4.115** dimerises through N–H···Cl hydrogen bonds between the amide nitrogen atom and a chloride ligand

coordinated to the ruthenium(II), forming a quadrangular $R^2_2(18)$ motif (Figure 4.52). The distance between symmetry-related ruthenium ions is 9.253 Å. Selected hydrogen bonding parameters for **4.115** are shown in Table 4.36.

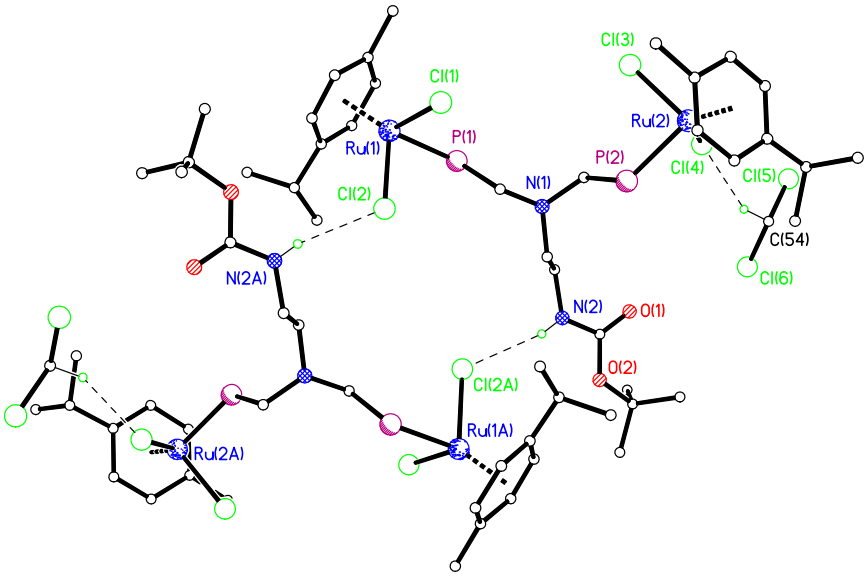

Figure 4.52 Dimers of compound **4.115**. Phenyl groups and hydrogen atoms not involved in hydrogen bonding have been omitted for clarity.

Compound **4.115** includes one molecule of dichloromethane per ruthenium(II) complex. Additional weak (solvent)C–H···Cl, [C···Cl 3.61 Å] hydrogen bonding of two dichloromethane molecules to two of the terminal chlorides within the dimer is observed thereby potentially preventing any further hydrogen bonding associations.

Table 4.36 Selected hydrogen bonding parameters for **4.115**.

D–H···A	D···A/Å	D–H/Å	H···A/Å	D–H···A/°
N(2)–H(2)···Cl(2A)^{i}	3.472(2)	0.80(3)	2.69(3)	166(3)

Symmetry operation: ^{i}-x, -y+1, -z+2.

4.2.10 Syntheses and Characterisation of $HO_2C(CH_2)_2N(CH_2PPh_2)_2$ 4.110, $HO_2CCH_2NHCOCH_2N(CH_2PPh_2)_2$ 4.111 and $HO_2CCH_2NHCOCH_2NHCOCH_2N(CH_2PPh_2)_2$ 4.112

The ligands $HO_2C(CH_2)_2N(CH_2PPh_2)_2$ **4.110**, $HO_2CCH_2NHCOCH_2N(CH_2PPh_2)_2$ **4.111** and $HO_2CCH_2NHCOCH_2NHCOCH_2N(CH_2PPh_2)_2$ **4.112** were prepared by Mannich-based condensation reactions, between the primary amine, glycine, glycylglycine and triglycine, and two equivalents of diphenylphosphinomethanol (Equation 4.23). The mixture was stirred in methanol at room temperature under nitrogen for 24 h giving the desired ligands **4.110–4.112** in good yields 58-99%.

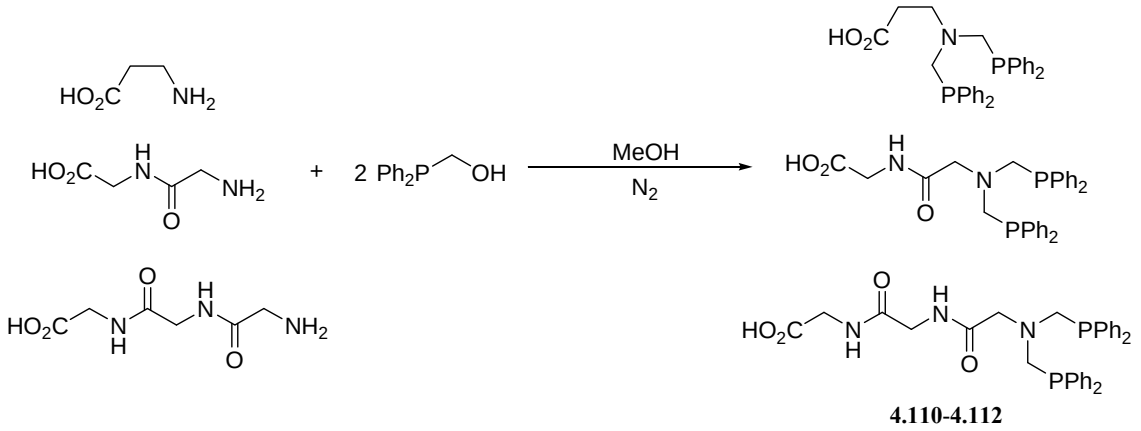

Equation 4.23

The isolation of **4.110–4.112**, as yellow oils, was achieved upon evaporation of the solvent to dryness. Each compound displayed a single phosphorus resonance in the $^{31}P\{^1H\}$ NMR spectra (in $CDCl_3$) around δ(P) -26 – -27 ppm.

4.2.11 Syntheses and Characterisation of $[PtCl_2\{HO_2C(CH_2)_2N(CH_2PPh_2)_2\}]$ 4.116, $[PtCl_2\{HO_2CCH_2NHCOCH_2N(CH_2PPh_2)_2\}]$ 4.117 and $[PtCl_2\{HO_2CCH_2NHCOCH_2NHCOCH_2N(CH_2PPh_2)_2\}]$ 4.118

The complexes $[PtCl_2\{HO_2C(CH_2)_2N(CH_2PPh_2)_2\}]$ **4.116**, $[PtCl_2\{HO_2CCH_2NHCOCH_2N(CH_2PPh_2)_2\}]$ **4.117** and $[PtCl_2\{HO_2CCH_2NHCOCH_2NHCOCH_2N(CH_2PPh_2)_2\}]$ **4.118** were prepared in 90-84% yield by ligand substitution of cod from $PtCl_2$(cod) in an analogous manner to the

synthesis of **4.113**. The $^{31}P\{^{1}H\}$ NMR spectra [in $(CD_3)_2SO$] showed a single resonance around δ(P) -10 ppm with associated ^{195}Pt satellites [^{1}J(PtP) 3400 Hz] (Table 4.37). The IR spectra display bands in the regions 3400 cm^{-1}, 1656-1668 cm^{-1} and 1730 cm^{-1} typical of ν(NH)/ν(OH), ν(C=O amide) and ν(C=O acid) respectively.

Table 4.37 Selected $^{31}P\{^{1}H\}$ NMR data for **4.116–4.118**.[a]

	δ(P)/ppm	**^{1}J(PtP)/Hz**
4.116	-9.91	3411
4.117	-10.64	3393
4.118	-10.41	3474

[a]Spectra measured in $(CD_3)_2SO$.

4.2.11.1 X-ray Crystal Structures of $[PtCl_2\{HO_2CCH_2NHCOCH_2N(CH_2PPh_2)_2\}]$ 4.117 and $[PtCl_2\{HO_2CCH_2NHCOCH_2NHCOCH_2N(CH_2PPh_2)_2\}]$ 4.118

Crystals of $[PtCl_2\{HO_2CCH_2NHCOCH_2N(CH_2PPh_2)_2\}]$ **4.117** were obtained by slow diffusion of Et_2O into a $CHCl_3$/DMSO solution. The addition of an extra carboxylic acid group, compared to **4.113**, provides further hydrogen bonding groups resulting in the extension of the dimensionality of the supramolecular array formed in **4.117** (Figure 4.53). Compound **4.117** forms a two-dimensional structure through a combination of intermolecular weak bifurcated (amide)N–H···Cl and strong (carboxylic acid)O–H···O(amide) interactions (Table 4.38).

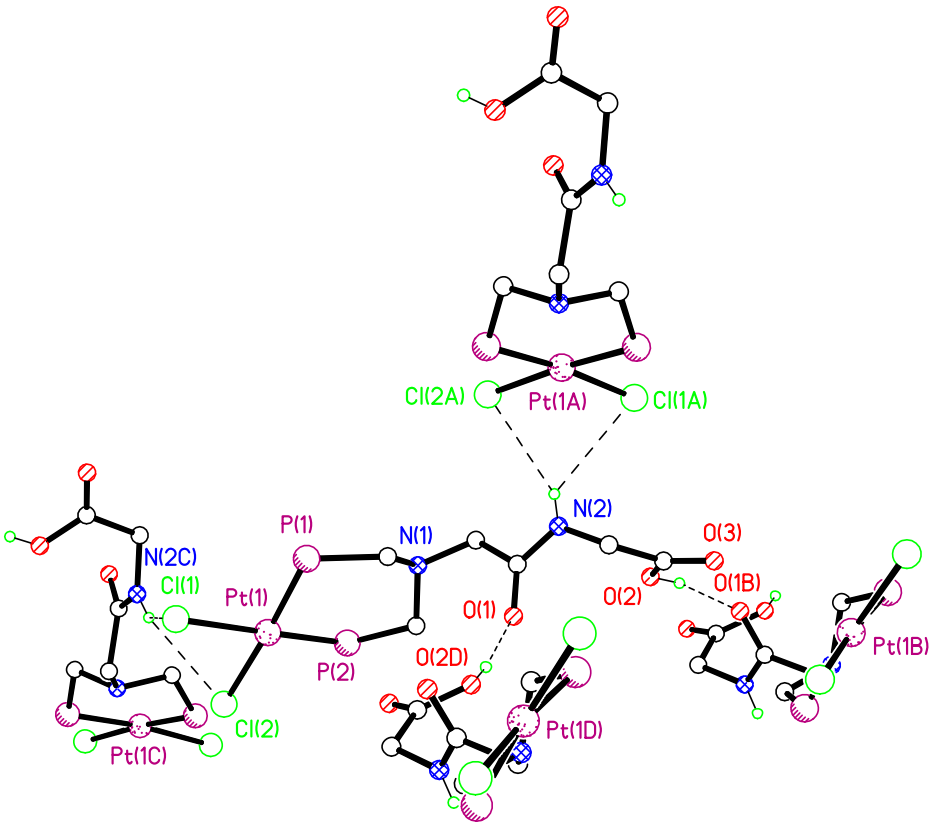

Figure 4.53 Hydrogen bonding motifs for **4.117**. Phenyl groups and hydrogen atoms not involved in hydrogen bonding have been omitted for clarity.

Table 4.38 Selected hydrogen bonding parameters for **4.117**.

D–H···A	D···A/Å	D–H/Å	H···A/Å	D–H···A/°
N(2)–H(2)···Cl(2A)^{i}	3.372(3)	0.76(4)	2.70(4)	150(4)
N(2)–H(2)···Cl(1A)^{i}	3.353(3)	0.76(4)	2.81(4)	130(4)
O(2)–H(2A)···O(1B)^{ii}	2.694(4)	0.84(5)	1.87(5)	169(5)

Symmetry operations: ^{i}-x+1/2, -y+1, z-1/2; ^{ii}x-1/2, -y+1/2, -z.

Although the addition of a second amide group in the backbone in [$PtCl_2${$HO_2CCH_2NHCOCH_2NHCOCH_2N(CH_2PPh_2)_2$}] **4.118** affords more flexibility and potential donor/acceptor groups which can be involved in hydrogen bonding, compound **4.118** crystallises as a one-dimensional chain (Figure 4.54). While one of the amide groups of **4.118** forms a $R^2_2(10)$ dimer motif with a symmetry related molecule *via* strong N–H···O hydrogen bonds, the remaining N*H*(amide) links the dimers into chains through a single N–H···Cl hydrogen bond.[10] Interestingly, the carboxylic acid

group is not involved in hydrogen bonding limiting the dimensionality of the supramolecular array. Selected hydrogen bonding parameters for **4.118** are shown in Table 4.39.

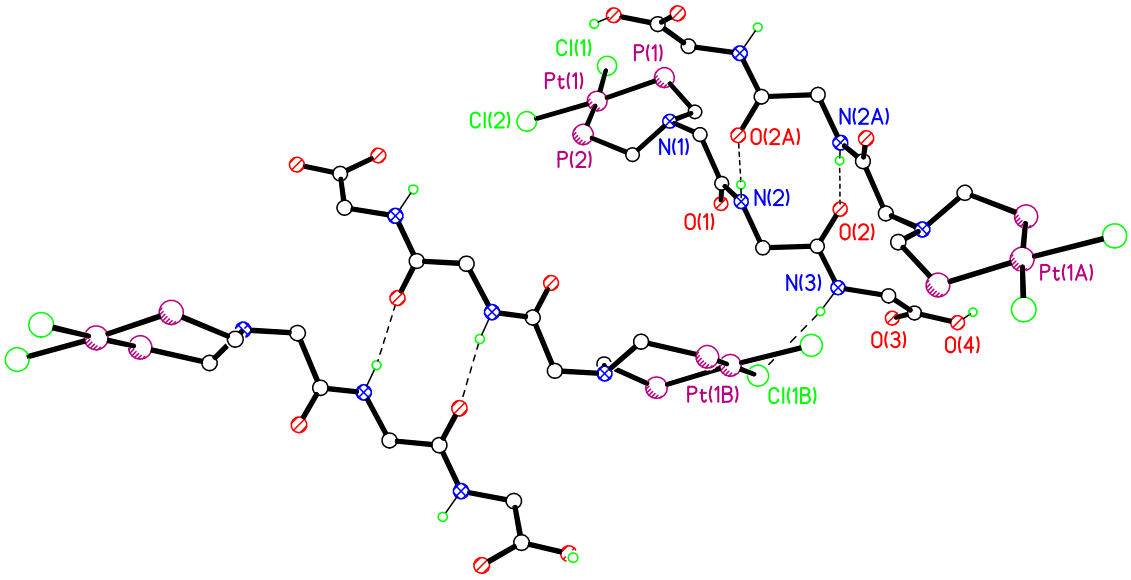

Figure 4.54 Hydrogen bonding motifs for **4.118**. Phenyl groups and hydrogen atoms not involved in hydrogen bonding have been omitted for clarity.

Table 4.39 Selected hydrogen bonding parameters for **4.118**.

D–H···A	D···A/Å	D–H/Å	H···A/Å	D–H···A/°
N(2)–H(2)···O(2A)^{i}	3.859(4)	0.88	1.99	170
N(3)–H(3)···Cl(1B)^{ii}	3.359(3)	0.88	2.55	154

Symmetry operations: ^{i}-x+3/2, -y+1/2, -z+2; ^{ii}-x+3/2, y-1/2, -z+3/2.

Complexes **4.117** and **4.118** show an approximate square-planar coordination of the Pt(II) centre [P(1)–Pt(1)–P(2) 92.76(3)-92.89(3)°, P(1)–Pt(1)–Cl(1) 89.82(3)-89.97(3)°, P(2)–Pt(1)–Cl(2) 88.51(3)-88.93(3)° and Cl(1)–Pt(1)–Cl(2) 88.65(3)-88.93°, respectively]. Analysis of the Pt–Cl and Pt–P bond lengths [Pt(1)–Cl(1) 2.3618(9)-2.3689(8) Å, Pt(1)–Cl(2) 2.3593(7)-2.3520(9) Å, Pt(1)–P(1) 2.2248(7)-2.2293(9) Å and Pt(1)–P(2) 2.2283(8)-2.2210(8) Å] are consistent with values reported in the literature.[189]

4.2.11.2 Syntheses and Characterisation of $[Au_2Cl_2\{HO_2C(CH_2)_2N(CH_2PPh_2)_2\}]$ 4.119, $[Au_2Cl_2\{HO_2CCH_2NHCOCH_2N(CH_2PPh_2)_2\}$ 4.120 and $[Au_2Cl_2\{HO_2CCH_2NHCOCH_2NHCOCH_2N(CH_2PPh_2)_2\}$ 4.121

Reaction of ligands **4.110-4.112** with AuCl(tht) in a 1:2 stoichiometry proceeds with displacement of tht to afford the gold(I) compounds $[Au_2Cl_2\{HO_2C(CH_2)_2N(CH_2PPh_2)_2\}]$ **4.119**, $[Au_2Cl_2\{HO_2CCH_2NHCOCH_2N(CH_2PPh_2)_2\}$ **4.120** and $[Au_2Cl_2\{HO_2CCH_2NHCOCH_2NHCOCH_2N(CH_2PPh_2)_2\}$ **4.121** as air stable white solids in 60-95% yield. The complexes exhibit the expected spectroscopic and analytical properties. Hence, a single sharp resonance, in their $^{31}P\{^1H\}$ NMR spectra [in $(CD_3)_2SO$] around δ(P) 23 ppm was observed in all cases. In the IR spectra, ν(NH) and ν(OH) bands and ν(C=O amide) are observed in the range of 3300-3400 cm^{-1} and 1658-1670 cm^{-1} respectively. In addition a strong band around 1700 cm^{-1} was indicative of ν(C=O acid).

Numerous attempts have been made to obtain crystals of these gold(I) complexes **4.119–4.121** without any success, affording only powdered material.

4.2.11.3 Syntheses and Characterisation of $[RuCl_2(\eta^6\text{-}p\text{-cymene})]_2\{HO_2C(CH_2)_2N(CH_2PPh_2)_2\}$ 4.122, $[RuCl_2(\eta^6\text{-}p\text{-cymene})]_2\{HO_2CCH_2NHCOCH_2N(CH_2PPh_2)_2\}$ 4.123 and $[RuCl_2(\eta^6\text{-}p\text{-cymene})]_2\{HO_2CCH_2NHCOCH_2NHCOCH_2N(CH_2PPh_2)_2\}$ 4.124

Complexes $[RuCl_2(\eta^6\text{-}p\text{-cymene})]_2\{HO_2C(CH_2)_2N(CH_2PPh_2)_2\}$ **4.122**, $[RuCl_2(\eta^6\text{-}p\text{-cymene})]_2\{HO_2CCH_2NHCOCH_2N(CH_2PPh_2)_2\}$ **4.123** and $[RuCl_2(\eta^6\text{-}p\text{-cymene})]_2\{HO_2CCH_2NHCOCH_2NHCOCH_2N(CH_2PPh_2)_2\}$ **4.124** were obtained by reaction of ligands **4.110–4.112** with $[Ru(\eta^6\text{-}p\text{-cymene})Cl_2]_2$, 1:1 stoichiometry respectively, in dichloromethane. After stirring for 30 min, the solution was concentrated to approximately 5 ml under reduced pressure and the required orange products precipitated upon addition of Et_2O. These complexes were obtained in good yields 63-88%. All the ruthenium complexes display a single phosphorus resonance around δ(P) 15-18 ppm, a downfield shift of approximately 40 ppm with respect to the free ligands. The ^1H NMR spectra of **4.122–4.124** show well resolved, distinct

resonances for the η^6-*p*-cymene ancillary ligand. The infrared spectra for compounds **4.122–4.124** showed the characteristic ν(NH) and ν(OH) and ν(C=O amide) absorbances in the range 3300-3400 cm^{-1} and 1664-1673 cm^{-1} respectively; also a strong band around 1700 cm^{-1} indicative of ν(C=O acid) (Table 4.40).

Table 4.40 Selected $^{31}P\{^1H\}$ NMR[a] and IR data[b] for **4.122–4.124**.

	δ(P)/ppm	**ν(CO)/cm^{-1}**
4.122	19.60	1708
4.123	15.69	1735
4.124	18.24	1737

[a] Spectra measured in $(CD_3)_2SO$. [b] Recorded as KBr pellets.

4.2.11.4 X-ray Crystal Structures of 4.122 and 4.124

The X-ray crystal structure of **4.122** has been determined within the group although not published. Compound **4.122** displays the classic "piano-stool" geometry formed by the η^6-*p*-cymene ancillary ligand and the three "legs" being the two chlorides and the phosphorus donor atom of the P–C–N–C–P ligand. Molecules of **4.122** are associated in dimers through classic intermolecular carboxylic acid-carboxylic acid head-to-tail O–H···O hydrogen bonding (Table 4.41) with the formation of the typical $R^2_2(8)$ graph set motif (Figure 4.55).[252]

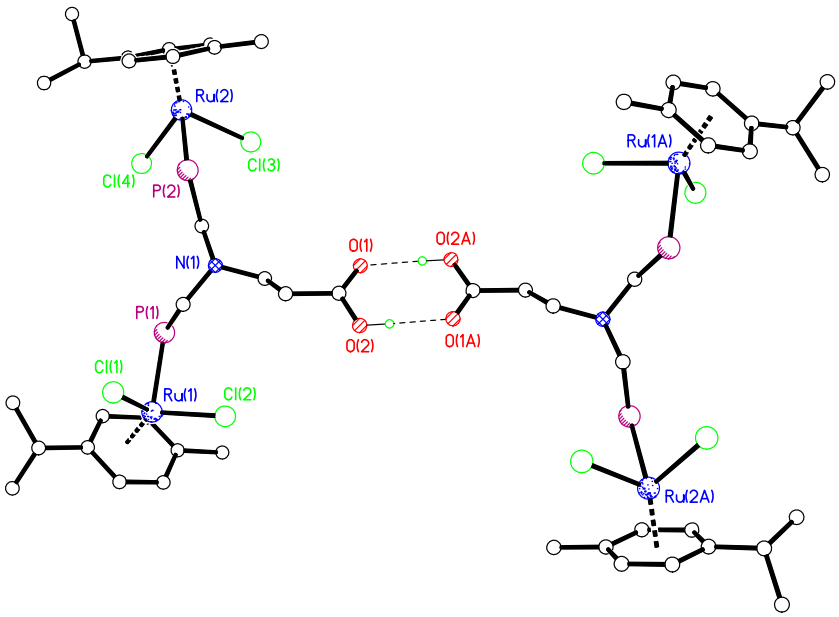

Figure 4.55 View of the head-to-tail arrangement for compound **4.122**. Phenyl groups and hydrogen atoms not involved in hydrogen bonding have been omitted for clarity.

Table 4.41 Selected hydrogen bonding parameters for **4.122**.

D–H···A	D···A/Å	D–H/Å	H···A/Å	D–H···A/º
O(2)–H(2)···O(1A)^{i}	2.630(3)	0.84	1.79	178

Symmetry operation: ^{i}-x, -y+1, -z+1.

Compound **4.124** adopts an identical hydrogen bonding pattern to that found in **4.122** with the carboxylic acid group forming head-to-tail $R^2_2(8)$ rings and arranging molecules of **4.124** into dimers (Figure 4.56). In contrast to **4.122**, complex **4.124** possesses two additional amide functional groups which are involved in two intramolecular N–H···Cl hydrogen bonds with two chlorides ligands forming S(9) and S(12) graph set hydrogen bond motifs (Table 4.42).

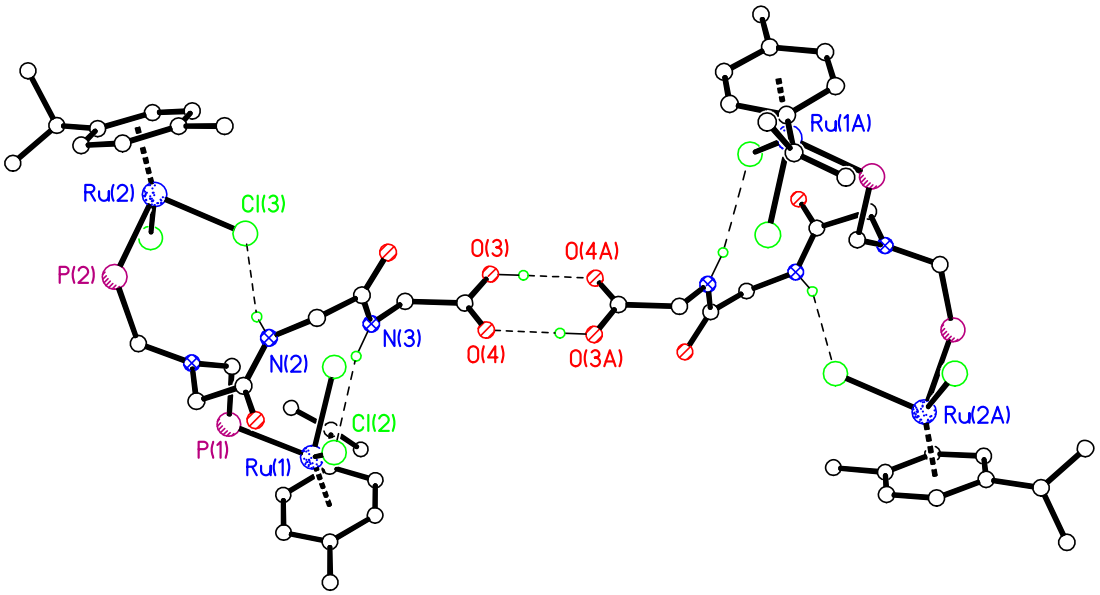

Figure 4.56 Hydrogen bonding motifs for **4.124**. Phenyl groups and hydrogen atoms not involved in hydrogen bonding have been omitted for clarity.

Interestingly, while in compound **4.117** the incorporation along the backbone of additional functional groups with potential hydrogen bonding capability allowed the extension of the dimensionality of the supramolecular array obtained, for compound **4.124** a zero-dimensional structure was found. Instead of the common $R^2_2(8)$ motif observed in **4.124**, compound **4.117** extends the dimensionality through a combination of intermolecular (amide)N–H···Cl and single (carboxylic acid)O–H···O(amide) interactions.

Table 4.42 Selected hydrogen bonding parameters for **4.124**.

D–H···A	D···A/Å	D–H/Å	H···A/Å	D–H···A/º
N(2)–H(2)···Cl(3)	3.306(9)	0.88	2.48	157
N(3)–H(3A)···Cl(2)	3.464(7)	0.88	2.61	163
O(3)–H(3)···O(4A)^{i}	2.638(9)	0.84	1.80	175

Symmetry operation: ^{i}-x-1, -y+1, -z.

4.3 Conclusions

A range of new isomeric ditertiary phosphino(amines) **4.20**–**4.28** and **4.77**–**4.85** has been prepared either *via* a three-step or single step synthetic route which involves a well known method of reductive amination followed by an efficient Mannich-based condensation. Furthermore, the ditertiary phosphines **4.20**–**4.28** and **4.77**–**4.85** synthesised in this Chapter act as *cis*-chelating *P*,*P*-bidentate ligands and have the ability to chelate to various transition metal centres such as Pt(II) and Mo(0), they can also act as bridging ligands for Ru(II) and Au(I).

The regioselective incorporation of functional groups with potential hydrogen bonding capability such as hydroxyl and amide around a central arene core has been demonstrated to have a pronounced effect on the structural motifs observed in the isomeric series. In the isomeric series of compounds **4.20**–**4.57**, while the *S*(5) intramolecular motif is observed in **4.41**, **4.51** and **4.53** when the –OH functional group is located in the *ortho*-position on the arene ring with respect to $–N(CH_2PPh_2)_2$, it is absent in **4.32** where an alternative O–H···Cl hydrogen bond interaction is formed extending the dimensionality of the supramolecular array from zero-dimensional discrete units to one-dimensional chains. When the –OH functional group is located in *para*-position on the arene ring with respect to $–N(CH_2PPh_2)_2$, one-dimensional chain structures were adopted in **4.22**, **4.35** and **4.55**. Interestingly, compound **4.50**, which differs from **4.55** only by the absence of a methyl group on the functionalised arene ring, crystallises with a different trend forming a network of cavities which interpenetrate through (hydroxyl)O–H···O(carbonyl) interactions forming $R^4_2(12)$ star-shape motifs. The structures obtained with the –OH positioned in the *meta*-position on the arene ring with respect to $–N(CH_2PPh_2)_2$ show a range of hydrogen bonded supramolecular structures with varying dimensionalities.

The inclusion of polar DMSO molecules into the structures of **4.30** and **4.33** show that it can limit the dimensionality of the resulting solid-state structure compared with **4.35**, where the inclusion of methanol molecules produced a more extended structure. Therefore the dimensionality of these systems will also depend on the nature of any co-crystallised species.

For compounds **4.77**–**4.108** the incorporation of the amide-backbone is observed to increase the flexibility of the system compared with the ligands **4.21-4.57**. Interestingly, in **4.90** where the –OH functional groups is located in *para*-position on the arene ring with respect to $–NHCOCH_2N(CH_2PPh_2)_2$, a one-dimensional chain is observed as seen for compounds **4.22**, **4.35** and **4.55**. The presence of the amide group in the backbone failed to extend the dimensionality of these systems. Although a Pt(II) complex with the –OH positioned in the *meta*-position on the arene ring with respect to $–NHCOCH_2N(CH_2PPh_2)_2$ was successfully crystallised, due to the poor quality of the diffraction data for **4.92**; the −OH hydrogen atom could not be located.

Interestingly, while the common carboxylic acid $R^2_2(8)$ head-to-tail ring motif is observed in the Ru(II) complexes **4.122** and **4.124**, it is absent in the Pt(II) complexes **4.117** and **4.118**. Instead a series of motifs in which strong hydrogen bonds (O–H···O) combine with weaker interactions (N–H···Cl and N–H···O) extending the dimensionality from zero-dimensional, observed in Ru(II) complexes **4.122** and **4.124**, to one- and two-dimensional, observed in Pt(II) complexes **4.117** and **4.118**. This perhaps indicates a weakness in the predictability of the $R^2_2(8)$ synthon which is well known to be either disrupted or fail to form in competition with other hydrogen bonding possibilities.[253]

4.4 EXPERIMENTAL

Materials

Unless otherwise stated, all reactions were performed in air. Standard Schlenk techniques were used for experiments carried out under an oxygen-free nitrogen atmosphere. The starting materials 2-hydroxyaniline, 3-hydroxyaniline, 4-hydroxyaniline, 2-amino-4-methylphenol, 4-amino-3-methylphenol, 2-amino-5-methylphenol, 4-amino-2-methylphenol, 3-amino-2-methylphenol, 2-amino-4-tertbuthylphenol, dicyclohexylcarbodiimide, N-carbobenzyloxyglycine, cyclohexene, palladium/Carbon, di-*t*-butyl Boc-anhydridre, $RuCl_3 \cdot xH_2O$, glycine, glycylglycine and triglycine were purchased from Aldrich, Lancaster, Avocado or Acros. All solvents were purchased from Aldrich, Fisher or Lancaster. CH_2Cl_2 was distilled from CaH_2 under nitrogen, and diethyl ether distilled from Na under nitrogen. The transition metal precursors, $PtCl_2(COD)$, AuCl(tht) and $[Ru(\eta^6\text{-}p\text{-cymene})Cl_2]_2$ were prepared according to literature methods.[254-256] The tertiary phosphine Ph_2PCH_2OH used in these reactions was readily preformed from equimol amounts of Ph_2PH and $(CH_2O)_n$.[198] Physical measurements were carried out using methods described in the preceding chapter.

4.4.1 Characterisation Data

The following general method was used for the synthesis of compounds **4.20**–**4.28**: The mixture of hydroxymethyldiphenylphosphine (2 eq) and the primary amine **I**–**IX** (1 eq) in methanol (20 ml) was stirred under N_2 for 24 h. In all the cases, except for compound **4.28**, the volume of the solution obtained was evaporated to *ca*. 2-3 ml under reduced pressure and a solid was obtained. The suspension was stirred for 10 min. The white solids obtained were collected by suction filtration and dried *in vacuo*. In the case of **4.28**, the solution was evaporated to dryness under reduced pressure yielding a yellow oil.

Compound 4.20

Yield: 0.553 g, 97%.

IR υ_{max} (KBr)/cm^{-1} 3364.1 (O−H), 746.4, 716.4 and 697.0 (Ar C−H).

^{1}H NMR (400 MHz, $(CD_3)_2SO$) δ 8.93 (1H, s, O−H), 7.39-7.29 (20H, m, Ar C−H), 6.98 (1H, d, Ar C−H, *J* 7.6 Hz), 6.86 (1H, dd, Ar C−H, *J* 1.6 and 15.2 Hz), 6.83-6.65 (2H, m, Ar C−H), 4.27 (4H, d, CH_2, *J* 3.2 Hz) ppm.

^{31}P NMR data: δ -27.63 ppm.

Analysis calculated for $C_{32}H_{29}ONP_2$: C, 76.03; H, 5.78; N, 2.77. Found: C, 75.67; H, 5.74; N, 2.83%.

m/z 504 $[C_{32}H_{29}ONP_2]^+$.

Compound 4.21

Yield: 0.718 g, 53%.

IR υ_{max} (KBr)/cm^{-1} 3376.0 (O−H), 742.4, 695.7 and 683.6 (Ar C−H).

^{1}H NMR (400 MHz, $(CD_3)_2SO$) δ 9.12 (1H, s, O−H), 7.38-7.31 (21H, m, Ar C−H), 6.92 (1H, s, Ar C−H), 6.30 (2H, d, Ar C−H, *J* 16.8 Hz), 6.13 (1H, s, Ar C−H), 3.85 (4H, s, CH_2) ppm.

^{31}P NMR data: δ -27.57 ppm.

Analysis calculated for $C_{32}H_{29}ONP_2$: C, 76.03; H, 5.78; N, 2.77. Found: C, 75.67; H, 5.71; N, 2.74%.

m/z 504 $[C_{32}H_{29}ONP_2]^+$.

Compound 4.22

Yield: 0.534 g, 95%.

IR υ_{max} (KBr)/cm^{-1} 3256.8 (O−H), 749.5, 732.3 and 696.5 (Ar C−H).

^{1}H NMR (400 MHz, $(CD_3)_2SO$) δ 8.81 (1H, s, O−H), 7.49-7.29 (21H, m, Ar C−H), 6.76 (2H, d, Ar C−H, *J* 9.2 Hz), 6.59 (2H, d, Ar C−H, *J* 6.8 Hz), 4.01 (4H, d, CH_2, *J* 3.6 Hz) ppm.

^{31}P NMR data: δ -27.41 ppm.

Analysis calculated for $C_{32}H_{29}ONP_2$: C, 76.03; H, 5.78; N, 2.77. Found: C, 75.43; H, 5.71; N, 2.84%.

m/z 504 $[C_{32}H_{29}ONP_2]^+$.

Compound 4.23

Yield: 0.464 g, 79%.

IR υ_{max} (KBr)/cm^{-1} 3398.2 (O−H), 744.8, 715.9 and 699.1 (Ar C−H).

^{1}H NMR (400 MHz, $(CD_3)_2SO$) δ 8.62 (1H, s, O−H), 7.37-7.23 (20H, m, Ar C−H), 6.76 (1H, s, Ar C−H), 6.69-6.57 (2H, m, Ar C−H), 4.15 (4H, d, CH_2, *J* 2.4 Hz), 2.10 (3H, s, CH_3) ppm.

^{31}P NMR data: δ -27.50 ppm.

Analysis calculated for $C_{33}H_{31}ONP_2$: C, 76.29; H, 6.01; N, 2.70. Found: C, 76.07; H, 6.13; N, 2.78%.

m/z 518 $[C_{33}H_{31}ONP_2]^+$.

Compound 4.24

Yield: 0.323 g, 56%.

IR υ_{max} (KBr)/cm^{-1} 3281.5 (O−H), 2920.3 (sp^3 C−H), 740.7 and 694.2 (Ar C−H).

^{1}H NMR (400 MHz, $(CD_3)_2SO$) δ 9.06 (1H, s, O−H), 7.36-7.26 (20H, m, Ar C−H), 7.15 (1H, d, Ar C−H, *J* 8.5 Hz), 6.50 (1H, dd, Ar C−H, *J* 2.4 and 8.4 Hz), 6.44 (1H, d, Ar C−H, *J* 2.4 Hz), 3.96 (4H, d, CH_2, *J* 5.6 Hz), 1.74 (3H, s, CH_3) ppm.

^{31}P NMR data: δ -27.30 ppm.

Analysis calculated for $C_{33}H_{31}ONP_2 \cdot 2CH_3OH$: C, 72.03; H, 6.74; N, 2.40. Found: C, 72.45; H, 6.04; N, 2.58%.

m/z 518 $[C_{33}H_{31}ONP_2]^+$.

Compound 4.25

Yield: 0.559 g, 97%.

IR υ_{max} (KBr)/cm^{-1} 3389.3 (O−H), 2917.3 (sp^3 C−H), 767.3, 748.6, 732.9 and 696.9 (Ar C−H).

^{1}H NMR (400 MHz, $(CD_3)_2SO$) δ 8.77 (1H, s, O−H), 7.44-7.22 (20H, m, Ar C−H), 6.86 (1H, d, Ar C−H, *J* 8 Hz), 6.54 (1H, s, Ar C−H), 6.48 (1H, d, Ar C−H, *J* 8 Hz), 4.09 (4H, d, CH_2, *J* 3.4 Hz), 2.12 (3H, s, CH_3) ppm.

^{31}P NMR data: δ -27.48 ppm.

Analysis calculated for $C_{33}H_{31}ONP_2$: C, 76.29; H, 6.01; N, 2.70. Found: C, 75.99; H, 6.00; N, 2.76%.

m/z 518 $[C_{33}H_{31}ONP_2]^+$.

Compound 4.26

Yield: 0.339 g, 38%.

IR υ_{max} (KBr)/cm^{-1} 3431.9 (O−H), 736.7 and 691.9 (Ar C−H).

^{1}H NMR (400 MHz, $(CD_3)_2SO$) δ 8.63 (1H, s, O−H), 7.40-7.30 (21H, m, Ar C−H), 6.55 (2H, m, Ar C−H), 4.02 (4H, d, CH_2, *J* 3.2 Hz), 1.96 (3H, s, CH_3) ppm.

^{31}P NMR data: δ -26.68 ppm.

Analysis calculated for $C_{33}H_{31}ONP_2$: C, 76.29; H, 6.01; N, 2.70. Found: C, 75.53; H, 6.05; N, 2.74%.

m/z 518 $[C_{33}H_{31}ONP_2]^+$.

Compound 4.27

Yield: 0.587 g, 96%.

IR υ_{max} (KBr)/cm^{-1} 3386.5 (O−H), 738.9 and 693.6 (Ar C−H).

^{1}H NMR (400 MHz, $(CD_3)_2SO$) δ 9.06 (1H, s, O−H), 7.49-7.33 (20H, m, Ar C−H), 6.85 (1H, d, Ar C−H, *J* 8 Hz), 6.50 (1H, d, Ar C−H, *J* 2 Hz), 6.27 (1H, dd, Ar C−H, *J* 2.4 and 8.4 Hz), 3.88 (4H, d, CH_2, *J* 3.6 Hz), 2.08 (3H, s, CH_3) ppm.

^{31}P NMR data: δ -26.41 ppm.

Analysis calculated for $C_{33}H_{31}ONP_2$·MeOH: C, 74.03; H, 6.40; N, 2.54. Found: C, 74.81; H, 5.93; N, 2.61%.

m/z 518 $[C_{33}H_{31}ONP_2]^+$.

Compound 4.28

Yield: 0.556 g, 93%.

^{1}H NMR (400 MHz, $(CD_3)_2SO$) δ 8.77 (1H, s, O−H), 7.48-7.28 (20H, m, Ar C−H), 6.90-6.87 (2H, m, Ar C−H), 6.66 (1H, dd, Ar C−H, *J* 3.2 and 5.6 Hz), 4.17 (4H, d, CH_2, *J* 3.6 Hz), 2.56 (9H, s, CH_3) ppm.

^{31}P NMR data: δ -25.32 ppm.

The following general method was used for the synthesis of compounds **4.29**–**4.37**: To a solution of $PtCl_2$(COD) in dichloromethane (5 ml) was added a solution of **4.20**–**4.28** (1 eq) in dichloromethane (5 ml). The pale yellow/colourless solutions obtained were stirred for 30 min at r.t., the solution was evaporated to *ca*. 2-3 ml under reduced pressure and diethyl ether (10 ml) added. The suspension was stirred for 10 min. The white solids obtained were collected by suction filtration and dried *in vacuo*.

Compound 4.29

Yield: 0.097 g, 99%.

IR υ_{max} (KBr)/cm^{-1} 3441.1 (O−H), 739.1 and 690.4 (Ar C−H), 315.8 and 281.9 (Pt−Cl).

^{1}H NMR (400 MHz, $(CD_3)_2SO$) δ 9.65 (1H, s, O−H), 7.99-7.94 (8H, m, Ar C−H), 7.66-7.52 (12H, m, Ar C−H), 7.04 (1H, m, Ar C−H), 6.87 (1H, dd, Ar C−H, *J* 0.8 and 8 Hz), 6.57 (1H, m, Ar C−H), 6.30 (1H, dd, Ar C−H, *J* 1.6 and 8 Hz), 4.29 (4H, s, CH_2) ppm.

Analysis calculated for $C_{32}H_{29}ONP_2Cl_2Pt$: C, 49.82; H, 3.79; N, 1.82. Found: C, 49.61; H, 3.47; N, 1.82%.

m/z 770 $[C_{32}H_{29}ONP_2Cl_2Pt]^+$, 734 $[M\text{-}Cl]^+$, 699 $[M\text{-}2Cl]^+$.

Compound 4.30

Yield: 0.115 g, 89%.

IR υ_{max} (KBr)/cm^{-1} 3355.5 (O−H), 735.8 and 689.3 (Ar C−H), 310.7 and 288.8 (Pt−Cl).

^{1}H NMR (400 MHz, $(CD_3)_2SO$) δ 8.45 (1H, s, O−H), 7.45-7.05 (10H, m, Ar C−H), 6.89-6.76 (14H, m, Ar C−H), 6.31 (1H, t, Ar C−H), 4.31 (4H, s, CH_2) ppm.

Analysis calculated for $C_{32}H_{29}ONP_2Cl_2Pt$: C, 49.82; H, 3.79; N, 1.82. Found: C, 49.31; H, 3.58; N, 1.79%.

m/z 771 $[C_{32}H_{29}ONP_2Cl_2Pt]^+$, 735 $[M^+\text{-}Cl]$, 700 $[M^+\text{-}2Cl]$.

Compound 4.31

Yield: 0.089 g, 78%.

IR υ_{max} (KBr)/cm^{-1} 3374.9 (O−H), 735.6 and 689.4 (Ar C−H), 312.2 and 286.5 (Pt−Cl).

^{1}H NMR (400 MHz, $(CD_3)_2SO$) δ 9.11 (1H, s, O−H), 7.91-7.84 (8H, m, Ar C−H), 7.59-7.44 (12H, m, Ar C−H), 6.50 (4H, m, Ar C−H), 4.28 (4H, s, CH_2) ppm.

Analysis calculated for $C_{32}H_{29}ONP_2Cl_2Pt$: C, 49.82; H, 3.79; N, 1.82. Found: C, 49.64; H, 3.74; N, 1.86%.

Accurate mass for $[C_{32}H_{29}ONP_2Cl_2Pt]^+$ 771.5828, requires 769.0885. m/z 771 $[C_{32}H_{29}ONP_2Cl_2Pt]^+$, 735 $[M\text{-}Cl]^+$, 700 $[M\text{-}2Cl]^+$.

Compound 4.32

Yield: 0.111 g, 98%.

IR υ_{max} (KBr)/cm^{-1} 3313.9 (O−H), 741.8, 726.4 and 693.1 (Ar C−H), 316.1 and 288.8 (Pt−Cl).

^{1}H NMR (400 MHz, $(CD_3)_2SO$) δ 9.25 (1H, s, O−H), 7.89-7.80 (8H, m, Ar C−H), 7.64-7.46 (12H, m, Ar C−H), 6.68 (2H, dd, Ar C−H, *J* 8 and 29.2 Hz), 5.90 (1H, s, Ar C−H), 4.21 (4H, bs, CH_2), 1.92 (3H, s, CH_3) ppm.

Analysis calculated for $C_{33}H_{31}ONP_2Cl_2Pt{\cdot}CH_2Cl_2$: C, 46.91; H, 3.82; N, 1.61. Found: C, 47.07; H, 3.77; N, 1.69%.

m/z 784 $[C_{33}H_{31}ONP_2Cl_2Pt]^+$, 749 $[M^+$-Cl].

Compound 4.33

Yield: 0.097 g, 81%.

IR υ_{max} (KBr)/cm^{-1} 3373.1 (O−H), 734.0, 694.9 and 686.7 (Ar C−H), 314.9 and 282.4 (Pt−Cl).

^{1}H NMR (400 MHz, $(CD_3)_2SO$) δ 9.22 (1H, s, O−H), 7.96-7.53 (20H, m, Ar C−H), 6.96 (1H, d, Ar C−H, *J* 8.8 Hz), 6.49 (1H, dd, Ar C−H, *J* 2.8 and 8.4 Hz), 6.33 (1H, d, Ar C−H, *J* 2.8 Hz), 4.19 (4H, bs, CH_2), 1.29 (3H, s, CH_3) ppm.

Analysis calculated for $C_{33}H_{31}ONP_2Cl_2Pt$: C, 50.46; H, 3.98; N, 1.78. Found: C, 50.51; H, 4.13; N, 1.83%.

m/z 785 $[C_{33}H_{31}ONP_2Cl_2Pt]^+$, 750 $[M^+$-Cl], 714 $[M^+$-2Cl].

Compound 4.34

Yield: 0.093 g, 78%.

IR υ_{max} (KBr)/cm^{-1} 3432.5 (O−H), 739.1 and 690.5 (Ar C−H), 315.1 and 285.9 (Pt−Cl).

^{1}H NMR (400 MHz, $(CD_3)_2SO$) δ 9.42 (1H, s, O−H), 7.89-7.84 (8H, m, Ar C−H), 7.56-7.43 (12H, m, Ar C−H), 6.59 (1H, s, Ar C−H), 6.30 (1H, d, Ar C−H, *J* 8 Hz), 6.05 (1H, d, Ar C−H, *J* 8 Hz), 4.16 (4H, s, CH_2), 2.06 (3H, s, CH_3) ppm.

Analysis calculated for $C_{33}H_{31}ONP_2Cl_2Pt{\cdot}0.5CH_2Cl_2$: C, 48.96; H, 3.87; N, 1.68. Found: C, 49.42; H, 3.96; N, 1.73%.

m/z 784 $[C_{33}H_{31}ONP_2Cl_2Pt]^+$, 749 $[M\text{-}Cl]^+$, 713 $[M\text{-}2Cl]^+$.

Compound 4.35

Yield: 0.097 g, 99%.

IR υ_{max} (KBr)/cm^{-1} 3420.5 (O−H), 743.9, 724.9 and 688.1 (Ar C−H), 308.9 and 289.9 (Pt−Cl).

^{1}H NMR (400 MHz, $(CD_3)_2SO$) δ 8.44 (1H, s, O−H), 7.94-7.87 (8H, m, Ar C−H), 7.78-7.62 (12H, m, Ar C−H), 6.86 (1H, d, Ar C−H, J 8.4 Hz), 6.47 (2H, m, Ar C−H), 4.43 (4H, s, CH_2), 2.02 (3H, s, CH_3) ppm.

Analysis calculated for $C_{33}H_{31}ONP_2Cl_2Pt$: C, 50.46; H, 3.98; N, 1.78. Found: C, 50.24; H, 3.98; N, 1.85%.

m/z $[C_{33}H_{31}ONP_2Cl_2Pt]^+$: 749 $[M^+$-Cl], 713 $[M^+$-2Cl].

Compound 4.36

Yield: 0.081 g, 67%.

IR υ_{max} (KBr)/cm^{-1} 3415.9 (O−H), 735.7 and 692.3 (Ar C−H), 314.0 and 289.6 (Pt−Cl).

^{1}H NMR (400 MHz, $(CD_3)_2SO$) δ 9.01 (1H, s, O−H), 7.96-7.85 (8H, m, Ar C−H), 7.59-7.45 (12H, m, Ar C−H), 6.75 (1H, d, Ar C−H, *J* 8.4 Hz), 6.27 (1H, d, Ar C−H, *J* 2.4 Hz), 6.03 (1H, dd, Ar C−H, *J* 2.4 and 8.4 Hz), 4.33 (4H, s, CH_2), 2.09 (3H, s, CH_3), ppm.

Analysis calculated for $C_{33}H_{31}ONP_2Cl_2Pt$: C, 50.46; H, 3.98; N, 1.78. Found: C, 50.66; H, 4.61; N, 1.70%.

m/z 785 $[C_{33}H_{31}ONP_2Cl_2Pt]^+$, 750 $[M^+$-Cl], 714 $[M^+$-2Cl].

Compound 4.37

Yield: 0.083 g, 66%.

IR υ_{max} (KBr)/cm^{-1} 3284.6 (O−H), 736.8, 710.4 and 689.4 (Ar C−H), 316.3 and 284.0 (Pt−Cl).

^{1}H NMR (400 MHz, $(CD_3)_2SO$) δ 9.48 (1H, s, O−H), 8.01-7.92 (8H, m, Ar C−H), 7.67-7.52 (12H, m, Ar C−H), 7.03 (1H, d, Ar C−H, *J* 2.4 Hz), 6.76 (1H, d, Ar C−H, *J* 8.4 Hz), 6.07 (1H, s, Ar C−H), 4.01 (4H, s, CH_2), 1.09 (9H, s, CH_3) ppm.

Analysis calculated for $C_{36}H_{37}ONP_2Cl_2Pt{\cdot}0.5CH_2Cl_2$: C, 50.73; H, 4.37; N, 1.60. Found: C, 50.44; H, 4.40; N, 1.69%.

m/z 826 $[C_{36}H_{37}ONP_2Cl_2Pt]^+$, 790 $[M^+$-Cl], 755 $[M^+$-2Cl].

The following general method was used for the synthesis of compounds **4.38**–**4.46**: To a stirring solution of AuCl(tht) in dichloromethane (5 ml) solution of AuCl(tht) was added a solution of **4.20**–**4.28** (0.5 eq) in dichloromethane (5 ml). The pale yellow/colourless solutions obtained were stirred for 30 min at rt. The volume was evaporated to *ca*. 2-3 ml under reduced pressure and diethyl ether (10 ml) added. The suspension was stirred for 10 min. The white solids obtained were collected by suction filtration and dried *in vacuo*.

Compound 4.38

Yield: 0.077 g, 79%.

IR υ_{max} (KBr)/cm^{-1} 3419.9.6 (O−H), 743.5 and 690.9 (Ar C−H), 328.1 (Au−Cl).

^{1}H NMR (400 MHz, $CDCl_3$) δ 7.76-7.14 (20H, m, Ar C−H), 6.84 (2H, bs, Ar C−H), 6.73 (2H, bs, Ar C−H), 4.54 (4H, s, CH_2) ppm.

Analysis calculated for $C_{32}H_{29}NOP_2Cl_2Au_2$: C, 39.61; H, 3.01; N, 1.44. Found: C, 40.79; H, 2.85; N, 1.49%.

m/z $[C_{32}H_{29}ONP_2Cl_2Au_2]^+$: 934 $[M^+$-Cl], 898 $[M^+$-2Cl].

Compound 4.39

Yield: 0.056 g, 70%.

IR υ_{max} (KBr)/cm^{-1} 3326.5 (O−H), 743.0 and 691.2 (Ar C−H), 326.4 (Au−Cl).

^{1}H NMR (400 MHz, $CDCl_3$) δ 9.28 (1H, s, O−H), 7.88-7.82 (8H, m, Ar C−H), 7.57-7.46 (13H, m, Ar C−H), 7.14 (1H, d, Ar C−H, *J* 8.1 Hz), 6.86 (1H, d, Ar C−H, *J* 16.4 Hz), 6.63 (1H, dd, Ar C−H, *J* 8.4 and 16.2 Hz), 4.75 (4H, s, CH_2) ppm.

Analysis calculated for $C_{32}H_{29}NOP_2Cl_2Au_2$: C, 39.61; H, 3.01; N, 1.44. Found: C, 39.52; H, 3.21; N, 2.52%.

m/z 968 $[C_{32}H_{29}ONP_2Cl_2Au_2]^+$.

Compound 4.40

Yield: 0.055 g, 69%.

IR υ_{max} (KBr)/cm^{-1} 3394.6 (O−H), 743.1 and 690.6 (Ar C−H), 324.8 (Au−Cl).

^{1}H NMR (400 MHz, $CDCl_3$) δ 8.97 (1H, s, O−H), 7.73-7.69 (8H, m, Ar C−H), 7.60-7.45 (12H, m, Ar C−H), 7.67 (2H, d, Ar C−H, *J* 8.8 Hz), 6.30 (2H, d, Ar C−H, *J* 8.4 Hz), 4.84 (4H, s, CH_2) ppm.

Analysis calculated for $C_{32}H_{29}NOP_2Cl_2Au_2 \cdot 0.5Et_2O$: C, 40.22; H, 3.37; N, 1.38. Found: C, 40.54; H, 3.10; N, 1.53%.

m/z $[C_{32}H_{29}ONP_2Cl_2Au_2]^+$: 934 $[M^+-Cl]$, 898 $[M^+-2Cl]$.

Compound 4.41

Yield: 0.079 g, 79%.

IR υ_{max} (KBr)/cm^{-1} 3384.6 (O−H), 2965.3 (sp^3 C−H), 741.9 and 690.1 (Ar C−H), 323.9 (Au−Cl).

^{1}H NMR (400 MHz, $CDCl_3$) δ 9.35 (1H, s, O−H), 7.73-7.68 (8H, m, Ar C−H), 7.54-7.32 (13H, m, Ar C−H), 7.47 (1H, dd, Ar C−H, *J* 7.2 Hz, *J* 20.4 Hz), 6.12 (1H, s, Ar C−H), 4.80 (4H, s, CH_2), 1.78 (3H, s, CH_3) ppm.

Analysis calculated for $C_{33}H_{31}NOP_2Cl_2Au_2 \cdot Et_2O$: C, 41.40; H, 3.76; N, 1.34. Found: C, 41.34; H, 3.62; N, 1.45%.

m/z $[Au2C_{33}H_{31}ONP_2Cl_2]^+$: 948 $[M^+-Cl]$, 912 $[M^+-2Cl]$.

Compound 4.42

Yield: 0.068 g, 74%.

IR υ_{max} (KBr)/cm^{-1} 3422.0 (O−H), 2940.2 (sp^3 C−H), 743.3 and 690.9 (Ar C−H), 328.1 (Au−Cl).

^{1}H NMR (400 MHz, $CDCl_3$) δ 8.79 (1H, s, O−H), 7.58-7.53 (8H, m, Ar C−H), 7.36-7.24 (12H, m, Ar C−H), 6.64 (1H, d, Ar C−H, *J* 8.4 Hz), 5.96-5.92 (2H, m, Ar C−H), 4.64 (4H, s, CH_2), 1.40 (3H, s, CH_3) ppm.

Analysis calculated for $C_{33}H_{31}NOP_2Cl_2Au_2$: C, 40.26; H, 3.17; N, 1.42. Found: C, 39.76; H, 3.32; N, 1.32%.

m/z 983 $[C_{33}H_{31}ONP_2Cl_2Au_2]^+$, 948 $[M^+-Cl]$.

Compound 4.43

Yield: 0.077 g, 79%.

IR υ_{max} (KBr)/cm^{-1} 3411.7 (O−H), 741.9 and 690.0 (Ar C−H), 324.8 (Au−Cl).

^{1}H NMR (400 MHz, $CDCl_3$) δ 9.59 (1H, s, O−H), 7.87-7.77 (8H, m, Ar C−H), 7.64-7.48 (12H, m, Ar C−H), 6.44 (1H, s, Ar C−H), 6.26 (1H, d, Ar C−H, *J* 8 Hz), 6.06 (1H, d, Ar C−H, *J* 6.4 Hz, *J* 7.6 Hz), 4.87 (4H, s, CH_2), 2.09 (3H, s, CH_3) ppm.

Analysis calculated for $C_{33}H_{31}NOP_2Cl_2Au_2$: C, 40.26; H, 3.17; N, 1.42. Found: C, 40.40; H, 3.41; N, 1.47%. m/z $[C_{33}H_{31}ONP_2Cl_2Au_2]^+$: 948 $[M^+-Cl]$, 912 $[M^+-2Cl]$.

Compound 4.44

Yield: 0.067 g, 78%.

IR υ_{max} (KBr)/cm^{-1} 3396.9 (O−H), 742.5 and 690.3 (Ar C−H), 325.5 (Au−Cl).

^{1}H NMR (400 MHz, $CDCl_3$) δ 7.57-7.52 (8H, m, Ar C−H), 7.43-7.31 (13H, m, Ar C−H), 6.42 (2H, m, Ar C−H), 4.62 (4H, s, CH_2), 1.98 (3H, s, CH_3) ppm.

Analysis calculated for $C_{33}H_{31}NOP_2Cl_2Au_2 \cdot CH_2Cl_2$: C, 38.19; H, 3.11; N, 1.31. Found: C, 38.69; H, 3.22; N, 1.37%.

m/z 983 $[C_{33}H_{31}ONP_2Cl_2Au_2]^+$, 948 $[M^+$-Cl], 912 $[M^+$-2Cl].

Compound 4.45

Yield: 0.048 g, 57%.

IR υ_{max} (KBr)/cm^{-1} 3420.2 (O−H), 743.2 and 690.9 (Ar C−H), 328.0 (Au−Cl).

^{1}H NMR (400 MHz, $CDCl_3$) δ 8.86 (1H, s, O−H), 7.78-7.10 (20H, m, Ar C−H), 6.58 (1H, bs, Ar C−H), 6.40 (1H, s, Ar C−H), 6.29 (1H, dd, Ar C−H, *J* 6.4 Hz, *J* 8.4 Hz), 4.69 (4H, s, CH_2), 1.96 (3H, s, CH_3) ppm.

Analysis calculated for $C_{33}H_{31}NOP_2Cl_2Au_2 \cdot Et_2O$: C, 41.98; H, 3.90; N, 1.32. Found: C, 42.66; H, 3.42; N, 1.57%.

m/z $[C_{33}H_{31}ONP_2Cl_2Au_2]^+$: 948 $[M^+$-Cl], 912 $[M^+$-2Cl].

Compound 4.46

Yield: 0.029 g, 45%.

IR υ_{max} (KBr)/cm^{-1} 3420.1 (O−H), 2957.2 (sp^3 C−H), 743.8 and 691.3 (Ar C−H), 328.1 (Au−Cl).

^{1}H NMR (400 MHz, $CDCl_3$) δ 9.58 (1H, s, O−H), 7.73-7.16 (20H, m, Ar C−H), 6.68 (1H, m, Ar C−H), 6.46 (2H, m, Ar C−H), 4.78 (4H, s, CH_2), 1.98 (3H, s, CH_3) ppm.

Analysis calculated for $C_{36}H_{37}NOP_2Cl_2Au_2$: C, 42.12; H, 3.63; N, 1.36. Found: C, 42.92; H, 3.85; N, 1.53%.

m/z $[C_{36}H_{37}ONP_2Cl_2Au_2]^+$: 990 $[M^+$-Cl], 954 $[M^+$-2Cl].

The following general method was used for the synthesis of compounds **4.48**–**4.57**: To a solution of $[Mo(CO)_4(nbd)]$ in dichloromethane (5 ml) was added a solution of **4.20**–**4.28** (1 eq) in dichloromethane (5 ml). The pale yellow solutions obtained were stirred for 24 h at r.t. under N_2, the solution was evaporated to *ca*. 2-3 ml under reduced

pressure and diethyl ether (10 ml) added. The suspension was stirred for 10 min. The yellow/brown solids obtained were collected by suction filtration and dried *in vacuo*.

Compound 4.48

Yield: 0.045 g, 39%.

IR υ_{max} (KBr)/cm^{-1} 3436.1 (O−H), 2018.8, 1926.4, 1896.3 and 1887.9 (CO), 736.2 and 694.2 (Ar C−H).

^{1}H NMR (400 MHz, $CDCl_3$) δ 9.71 (1H, s, O−H), 7.58-7.48 (20H, m, Ar C−H), 7.07 (1H, m, Ar C−H), 6.92 (1H, d, Ar C−H, *J* 8.8 Hz), 6.65 (1H, m, Ar C−H), 6.42 (1H, dd, Ar C−H, *J* 2.4 Hz, *J* 6.8 Hz), 4.11 (4H, s, CH_2) ppm.

^{31}P NMR data: δ 15.13 ppm.

Analysis calculated for $C_{36}H_{29}NO_5P_2Mo$: C, 60.60; H, 4.10; N, 1.96. Found: C, 59.52; H, 4.42; N, 1.92%.

m/z 715 $[C_{36}H_{29}O_5NP_2Mo]^+$, 687 $[M^+$-CO], 659 $[M^+$-2CO], 631 $[M^+$-3CO] and 603 $[M^+$-4CO].

Compound 4.49

Yield: 0.048 g, 35%.

IR υ_{max} (KBr)/cm^{-1} 3411.9 (O−H), 2019.7, 1920.5 and 1896.9 (CO), 741.4 and 693.8 (Ar C−H).

^{1}H NMR (400 MHz, $CDCl_3$) δ 7.79-6.88 (24H, m, Ar C−H, O−H), 6.72 (1H, s, Ar C−H), 6.34 (1H, d, Ar C−H, *J* 8.4 Hz), 6.02 (1H, d, Ar C−H, *J* 8.4 Hz), 4.09 (4H, s, CH_2) ppm.

^{31}P NMR data: δ 18.21 ppm.

Analysis calculated for $C_{36}H_{29}NO_5P_2Mo$: C, 60.60; H, 4.10; N, 1.96. Found: C, 61.10; H, 4.10; N, 1.40%.

m/z 715 $[C_{36}H_{29}O_5NP_2Mo]^+$, 687 $[M^+$-CO], 659 $[M^+$-2CO], 631 $[M^+$-3CO] and 603 $[M^+$-4CO].

Compound 4.50

Yield: 0.036 g, 30%.

IR υ_{max} (KBr)/cm^{-1} 3385.8 (O−H), 2019.1, 1919.1 and 1894.5 (CO), 740.8 and 694.1 (Ar C−H).

^{1}H NMR (400 MHz, $CDCl_3$) δ 9.23 (1H, s, O−H), 7.68-7.24 (21H, m, Ar C−H), 6.83 (1H, m, Ar C−H), 6.57 (2H, m, Ar C−H), 4.12 (4H, s, CH_2) ppm.

^{31}P NMR data: δ 18.39 ppm.

Analysis calculated for $C_{36}H_{29}NO_5P_2Mo{\cdot}CH_2Cl_2$: C, 55.66; H, 3.91; N, 1.75. Found: C, 55.21; H, 4.19; N, 1.34%.

m/z 715 $[C_{36}H_{29}O_5NP_2Mo]^+$, 687 $[M^+$-CO], 659 $[M^+$-2CO], 631 $[M^+$-3CO] and 603 $[M^+$-4CO].

Compound 4.51

Yield: 0.025 g, 26%.

IR υ_{max} (KBr)/cm^{-1} 3450.8 (O−H), 2017.8, 1926.7, 1892.4 and 1888.1 (CO), 736.4 and 694.4 (Ar C−H).

^{1}H NMR (400 MHz, $CDCl_3$) δ 7.39-7.19 (20H, m, Ar C−H), 6.90 (1H, s, Ar C−H), 6.78 (1H, d, Ar C−H, *J* 8.4 Hz), 6.57 (1H, d, Ar C−H, *J* 8.4 Hz), 4.65 (4H, s, CH_2), 2.20 (3H, s, CH_3) ppm.

^{31}P NMR data: δ 20.85 ppm.

Analysis calculated for $C_{37}H_{31}NO_5P_2Mo{\cdot}CH_2Cl_2$: C, 56.18; H, 4.09; N, 1.72. Found: C, 55.71; H, 4.25; N, 1.66%.

Compound 4.52

Yield: 0.043 g, 40%.

IR υ_{max} (KBr)/cm^{-1} 3384.9 (O−H), 2018.8, 1916.5 and 1897.2 (CO), 741.2 and 693.6 (Ar C−H).

^{1}H NMR (400 MHz, $CDCl_3$) δ 7.42-7.16 (20H, m, Ar C−H), 6.37 (2H, m, Ar C−H), 6.28 (1H, s, Ar C−H), 3.65 (4H, s, CH_2), 2.32 (3H, s, CH_3) ppm.

^{31}P NMR data: δ 18.55 ppm.

Analysis calculated for $C_{37}H_{31}NO_5P_2Mo{\cdot}0.5Et_2O$: C, 60.63; H, 4.70; N, 1.81. Found: C, 59.57; H, 5.01; N, 1.93%.

m/z 727 $[C_{37}H_{31}O_5NP_2Mo]^+$, 701 $[M^+$-CO], 674 $[M^+$-2CO], 645 $[M^+$-3CO].

Compound 4.53

Yield: 0.048 g, 38%.

IR υ_{max} (KBr)/cm^{-1} 3432.0 (O−H), 2019.9, 1924.4, 1904.5 and 1878.2 (CO), 736.4 and 693.7 (Ar C−H).

^{1}H NMR (400 MHz, $CDCl_3$) δ 9.50 (1H, s, O−H), 7.52-7.42 (20H, m, Ar C−H), 6.66 (1H, s, Ar C−H), 6.41 (1H, d, Ar C−H, *J* 7.6 Hz), 6.25 (1H, d, Ar C−H, *J* 6.8 Hz), 4.03 (4H, s, CH_2), 2.16 (3H, s, CH_3) ppm.

^{31}P NMR data: δ 20.11 ppm.

Analysis calculated for $C_{37}H_{31}NO_5P_2Mo$: C, 61.08; H, 4.29; N, 1.93. Found: C, 60.81; H, 4.67; N, 1.98%.

m/z 727 $[C_{37}H_{31}O_5NP_2Mo]^+$, 673 $[M^+$-2CO], 645 $[M^+$-3CO].

Compound 4.54

Yield: 0.049 g, 33%.

IR υ_{max} (KBr)/cm^{-1} 3397.1 (O−H), 2018.7, 1920.5 and 1897.7 (CO), 741.4 and 693.9 (Ar C−H).

^{1}H NMR (400 MHz, $CDCl_3$) δ 7.49-7.38 (20H, m, Ar C−H), 6.45 (1H, s, Ar C−H), 6.26 (2H, m, Ar C−H), 3.54 (4H, s, CH_2), 2.19 (3H, s, CH_3) ppm.

^{31}P NMR data: δ 18.67 ppm.

Analysis calculated for $C_{37}H_{31}NO_5P_2Mo{\cdot}CH_2Cl_2$: C, 56.18; H, 4.09; N, 1.72. Found: C, 56.88; H, 4.63; N, 1.73%.

m/z 728 $[C_{37}H_{31}O_5NP_2Mo]^+$, 701 $[M^+$-CO], 672 $[M^+$-2CO], 645 $[M^+$-3CO] and 617 $[M^+$-4CO].

Compound 4.55

Yield: 0.089 g, 55%.

IR υ_{max} (KBr)/cm^{-1} 3422.3 (O−H), 2018.3, 1920.6 and 1897.3 (CO), 741.7 and 694.1 (Ar C−H).

^{1}H NMR (400 MHz, $(CD_3)_2SO$) δ 7.98-7.57 (20H, m, Ar C−H), 6.98 (1H, d, Ar C−H, *J* 2.4 Hz), 6.67 (1H, d, Ar C−H, *J* 8.4 Hz), 6.12 (1H, s, Ar C−H), 4.12 (4H, s, CH_2), 2.09 (9H, s, CH_3) ppm.

^{31}P NMR data: δ 14.97 ppm.

Analysis calculated for $C_{40}H_{37}NO_5P_2Mo$: C, 62.42; H, 4.85; N, 1.82. Found: C, 61.58; H, 5.26; N, 1.80%.

m/z $[C_{40}H_{37}O_5NP_2Mo]^+$: 741 $[M^+$-CO], 713 $[M^+$-2CO], 687 $[M^+$-3CO] and 658 $[M^+$-4CO].

Compound 4.56

Yield: 0.071 g, 50%.

IR υ_{max} (KBr)/cm^{-1} 2020.4, 1926.1 and 1893.8 (CO), 742.7 and 694.4 (Ar C−H).

^{1}H NMR (400 MHz, $CDCl_3$) δ 7.59-7.28 (20H, m, Ar C−H), 7.05 (2H, m, Ar C−H), 6.56 (3H, m, Ar C−H), 3.98 (4H, s, CH_2) ppm.

^{31}P NMR data: δ 21.14 ppm.

Analysis calculated for $C_{36}H_{29}NO_4P_2Mo$: C, 63.25; H, 4.90; N, 1.89. Found: C, 63.09; H, 4.75; N, 1.87%.

The following general method was used for the synthesis of compounds **4.59**–**4.67**: To a stirring solution of *N*-carbobenzyloxyglycine in THF (60 ml), primary amines **I**–**IX** and dicyclohexylcarbodiimide were added respectively. The solution was stirred for 4 h at room temperature. The unwanted by-product was filtered and the solution obtained evaporated to dryness and a brown/white residue obtained. The residue was treated with ethyl acetate (50 ml) and petroleum ether b.p. 40-60 (50 ml) and left stirring for 1 h at room temperature. The solid obtained was filtered and dried under vacuum yielding a pale brown/white solid.

Compound 4.59

Yield: 2.265 g, 63%.

IR υ_{max} (KBr)/cm^{-1} 3254.7 (O−H), 3391.6 (N−H), 2927.7 (sp^3 C−H), 1663.5, 1661.9 (C=O amide), 1323.1 (C−O), 900.3-690.7 (Ar C−H).

^{1}H NMR (400 MHz, $(CD_3)_2SO$) δ 9.87 (1H, s, O−H), 9.10 (1H, s, N−H), 7.90 (1H, d, Ar C−H), 7.58 (1H, s, N−H), 7.40-7.23 (5H, m, Ar C−H), 6.92 (1H, t, Ar C−H), 6.87 (1H, d, Ar C−H), 6.77 (1H, t, Ar C−H), 5.07 (2H, s, CH_2), 3.85 (2H, d, *J* 3.4 Hz, CH_2) ppm.

Analysis calculated for $C_{16}H_{16}O_4N_2$: C, 63.99; H, 5.37; N, 9.33. Found: C, 64.10; H, 5.71; N, 9.45%.

m/z 300 $[C_{16}H_{16}O_4N_2]^+$.

Compound 4.60

Yield: 2.849 g, 80%.

IR υ_{max} (KBr)/cm^{-1} 3312.3 (O−H), 3392.5 (N−H), 2934.7 (sp^3 C−H), 1678.8, 1674.4 (C=O amide), 1385.1 (C−O), 775.0, 732.2, 693.9 and 683.1 (Ar C−H).

^{1}H NMR (400 MHz, $(CD_3)_2SO$) δ 9.87 (1H, s, O−H), 9.43 (1H, s, N−H), 7.48-6.99 (8H, m, Ar C−H), 6.50 (1H, d, Ar C−H, *J* 7.6 Hz), 5.11 (4H, s, CH_2), 4.10 (1H, bs, N−H), 3.83 (2H, d, CH_2, *J* 3.2 Hz) ppm.

Analysis calculated for $C_{16}H_{16}O_4N_2$: C, 63.99; H, 5.37; N, 9.33. Found: C, 64.23; H, 5.66; N, 9.48%.

m/z 300 $[C_{16}H_{16}O_4N_2]^+$.

Compound 4.61

Yield: 2.753 g, 77%.

IR υ_{max} (KBr)/cm^{-1} 3331.5 (O−H), 2928.5 (sp^3 C−H), 1691.7, 1668.1 (C=O amide), 1374.8 (C−O), 831.4, 788.4, 736.6, 697.3 and 641.2 (Ar C−H).

^{1}H NMR (400 MHz, $(CD_3)_2SO$) δ 9.69 (1H, s, O−H), 9.18 (1H, s, N−H), 7.27-7.52 (5H, m, Ar C−H), 6.70 (4H, d, *J* 10 Hz, Ar C−H), 5.05 (2H, s, CH_2), 3.75 (2H, d, *J* 6 Hz, CH_2) ppm.

Analysis calculated for $C_{16}H_{16}O_4N_2$: C, 63.99; H, 5.37; N, 9.33. Found: C, 64.40; H, 5.85; N, 9.32%.

Accurate mass for $[C_{16}H_{16}O_4N_2]^+$ 300.1110, requires 300.1110. m/z 300 $[C_{16}H_{16}O_4N_2]^+$.

Compound 4.62

Yield: 1.780 g, 53%.

IR υ_{max} (KBr)/cm^{-1} 3266.2 (O−H), 3330.9 (N−H), 2924.8 (sp^3 C−H), 1669.3, 1664.3 (C=O amide), 1309.6 (C−O), 912.3-697.2 (Ar C−H).

^{1}H NMR (400 MHz, $(CD_3)_2SO$) δ 9.62 (1H, s, N−H), 9.05 (1H, s, O−H), 7.70 (1H, s, NH−C=O), 7.41-7.25 (5H, m, Ar C−H), 6.77-6.70 (3H, m, Ar C−H), 5.05 (2H, s, CH_2), 3.83 (2H, d, *J* 2.4 Hz, CH_2), 2.14 (3H, s, CH_3) ppm.

Analysis calculated for $C_{17}H_{18}O_4N_2$: C, 64.96; H, 5.77; N, 8.91. Found: C, 65.07; H, 5.95; N, 8.96%.

m/z 314 $[C_{17}H_{18}O_4N_2]^+$.

Compound 4.63

Yield: 2.003 g, 60%.

IR υ_{max} (KBr)/cm^{-1} 3286.5 (O−H), 3343.4 (N−H), 2943.2 (sp^3 C−H), 1669.4, 1652.9 (C=O amide), 1352.0 (C−O), 872.4, 781.6, 693.7 (Ar C−H).

^{1}H NMR (400 MHz, $(CD_3)_2SO$) δ 9.21 (1H, s, O−H), 9.10 (1H, s, N−H), 7.51 (1H, s, N−H), 7.40-7.27 (5H, m, Ar C−H), 7.05 (1H, d, Ar C−H), 6.60 (1H, s, Ar C−H), 6.55 (1H, d, Ar C−H), 5.05 (2H, s, CH_2), 3.77 (2H, d, CH_2) 2.07 (3H, s, CH_3) ppm.

Analysis calculated for $C_{17}H_{18}O_4N_2$: C, 64.96; H, 5.77; N, 8.91. Found: C, 64.99; H, 5.76; N, 9.06%.

m/z 314 $[C_{17}H_{18}O_4N_2]^+$.

Compound 4.64

Yield: 2.177 g, 66%.

IR υ_{max} (KBr)/cm^{-1} 3292.3 (O−H), 3373.3 (N−H), 2900.1 (sp^3 C−H), 1667.5, 1664.6 (C=O amide), 1319.6 (C−O), 858.3-769.5 (Ar C−H).

^{1}H NMR (400 MHz, $(CD_3)_2SO$) δ 9.71 (1H, s, O−H), 9.05 (1H, s, N−H), 7.70 (1H, s, C−H), 7.67 (1H, s, NH−C=O), 7.40-7.25 (5H, m, Ar C−H), 6.70 (1H, s, Ar C−H), 6.58 (1H, d, C−H), 5.05 (2H, s, CH_2), 3.85 (2H, d, CH_2), 2.20 (3H, s, CH_3) ppm.

Analysis calculated for $C_{17}H_{18}O_4N_2$: C, 64.96; H, 5.77; N, 8.91. Found: C, 65.07; H, 5.94; N, 8.98%.

m/z 314 $[C_{17}H_{18}O_4N_2]^+$.

Compound 4.65

Yield: 2.263 g, 69%.

IR υ_{max} (KBr)/cm^{-1} 3271.2 (O−H), 3365.9 (N−H), 1708.7, 1639.3 (C=O amide), 1363.7 (C−O), 748.4, 696.6 and 594.2 (Ar C−H).

^{1}H NMR (400 MHz, $(CD_3)_2SO$) δ 9.69 (1H, s, N−H), 9.24 (1H, s, O−H), 7.54-7.17 (8H, m, Ar C−H), 6.69 (1H, d, Ar C−H, *J* 8.4 Hz), 5.05 (2H, s, CH_2), 3.75 (2H, d, CH_2, *J* 6 Hz), 2.09 (3H, s, CH_3) ppm.

Analysis calculated for $C_{17}H_{18}N_2O_4$: C, 64.96; H, 5.77; N, 8.91. Found: C, 65.13; H, 6.06; N, 9.02%.

Accurate mass for $[C_{17}H_{18}O_4N_2]^+$ 314.1267, requires 314.1263. m/z 314 $[C_{17}H_{18}O_4N_2]^+$.

Compound 4.66

Yield: 2.104 g, 64%.

IR υ_{max} (KBr)/cm^{-1} 3316.0 (O−H), 3401.8 (N−H), 1695.1, 1673.8 (C=O amide), 1382.1 (C−O), 779.5, 727.9 and 693.4 (Ar C−H).

^{1}H NMR (400 MHz, $(CD_3)_2SO$) δ 9.64 (1H, s, N−H), 9.27 (1H, s, O−H), 7.47-7.11 (6H, m, Ar C−H), 6.89 (1H, d, Ar C−H, *J* 16.4 Hz), 6.76 (1H, dd, Ar C−H, *J* 1.7, 9.7 Hz), 4.96 (2H, s, CH_2), 3.68 (2H, d, CH_2, *J* 6.4 Hz), 2.00 (3H, s, CH_3) ppm.
Analysis calculated for $C_{17}H_{18}N_2O_4$: C, 64.96; H, 5.77; N, 8.91. Found: C, 65.09; H, 6.09; N, 9.01%.
Accurate mass for $[C_{17}H_{18}O_4N_2]^+$ 314.1267, requires 314.1266. m/z 314 $[C_{17}H_{18}O_4N_2]^+$.

Compound 4.67

Yield: 3.894 g, 91%.
IR υ_{max} (KBr)/cm^{-1} 3322.1 (O−H), 3431.2 (N−H), 2936.0 (sp^3 C−H), 1776.2, 1663.0 (C=O amide), 1356.8 (C−O), 737.6, 715.7 and 696.3 (Ar C−H).
^{1}H NMR (400 MHz, $(CD_3)_2SO$) δ9.64 (1H, bs, N−H), 9.14 (1H, s, O−H), 7.92 (1H, s, N−H), 7.74-7.26 (6H, m, Ar C−H), 6.96 (1H, dd, Ar C−H, *J* 8.4, 2.3 Hz), 6.87 (1H, d, Ar C−H, *J* 6.5 Hz), 5.07 (2H, s, CH_2), 3.85 (2H, d, CH_2, *J* 6 Hz), 1.23 (9H, s, ^{t}Bu) ppm.
Analysis calculated for $C_{20}H_{24}N_2O_4$: C, 67.40; H, 6.79; N, 7.86. Found: C, 67.43; H, 7.14; N, 8.05%.
Accurate mass for $[C_{20}H_{24}O_4N_2]^+$ 356.4212, requires 356.4221. m/z 356 $[C_{20}H_{24}O_4N_2]^+$.

The following general method was used for the synthesis of compounds **4.68**–**4.76**: To a solution of compounds **4.59**–**4.67** in absolute ethanol (60 ml) were added cyclohexene (2.5 ml) and Pd/C (1.5 g). The solution was refluxed for 15 min (110-120 ºC). The Pd/C was filtered and the solution obtained was evaporated to dryness yielding the desired product.

Compound 4.68

Yield: 0.407 g, 73%.
IR υ_{max} (KBr)/cm^{-1} 3419.6 (N−H), 3296.7 (O−H), 1648.1 (C=O amide), 902.6-760.9 (Ar C−H).
^{1}H NMR (400 MHz, $(CD_3)_2SO$) δ 8.18 (1H, s, O−H), 6.95 (1H, s, NH−C=O), 6.80-6.73 (4H, m, Ar C−H), 5.57 (2H, d, CH_2, *J* 8 Hz).
Analysis calculated for $C_8H_{10}N_2O_2$: C, 57.82; H, 6.07; N, 16.86. Found: C, 57.59; H, 6.40; N, 15.83%.
m/z 167 $[C_8H_{10}O_2N_2]^+$, 136 $[C_7H_6O_2N]^+$.

Compound 4.69

Yield: 0.177 g, 32%.

IR υ_{max} (KBr)/cm^{-1} 3358.8 (N−H), 3312.7 (O−H), 1674.1 (C=O amide), 775.1, 762.3 and 679.7 (Ar C−H).

^{1}H NMR (400 MHz, $(CD_3)_2SO$) δ 9.67 (1H, bs, N−H), 7.20 (1H, s, Ar C−H), 7.09-7.05 (1H, m, Ar C−H), 6.98 (1H, d, Ar C−H, *J* 11.2 Hz), 6.45 (1H, dd, Ar C−H, *J* 1.2 and 8 Hz), 5.56 (2H, d, CH_2, *J* 10 Hz) ppm.

Analysis calculated for $C_8H_{10}N_2O_2$: C, 57.82; H, 6.07; N, 16.86. Found: C, 57.26; H, 6.37; N, 15.29%.

m/z 167 $[C_8H_{10}O_2N_2]^+$, 136 $[C_7H_6O_2N]^+$.

Compound 4.70

Yield: 0.494 g, 87%.

IR υ_{max} (KBr)/cm^{-1} 3455.3 (N−H), 3291.5 (O−H), 1656.9 (C=O amide), 856.9 and 830.8 (Ar C−H).

^{1}H NMR (400 MHz, $(CD_3)_2SO$) δ 9.63 (1H, s, N−H), 9.22 (1H, s, O−H), 7.47-7.43 (2H, m, C−H), 6.93-6.75 (2H, m, Ar C−H), 7.24 (1H, s, NH−C=O), 5.63 (2H, d, CH_2, *J* 8 Hz) ppm.

Analysis calculated for $C_8H_{10}N_2O_2$: C, 57.82; H, 6.07; N, 16.86. Found: C, 57.70; H, 6.48; N, 16.60%.

m/z 167 $[C_8H_{10}O_2N_2]^+$, 136 $[C_7H_6O_2N]^+$.

Compound 4.71

Yield: 0.450 g, 78%.

IR υ_{max} (KBr)/cm^{-1} 3420.5 (N−H), 3254.7 (O−H), 2924.8 (sp^3 C−H), 1648.1 (C=O amide), 937.3-722.3 (Ar C−H).

^{1}H NMR (400 MHz, $(CD_3)_2SO$) δ 8.01 (1H, s, O−H), 6.76 (1H, s, NH−C=O), 6.74-6.67 (3H, m, Ar C−H), 5.57 (2H, d, CH_2, *J* 8 Hz), 1.99 (3H, s, CH_3) ppm.

Analysis calculated for $C_9H_{12}O_2N_2$: C, 59.99; H, 6.71; N, 15.55. Found: C, 59.64; H, 6.77; N, 14.35%.

m/z 181 $[C_9H_{12}O_2N_2]^+$.

Compound 4.72

Yield: 0.570 g, 99%.

IR υ_{max} (KBr)/cm^{-1} 3371.1 (N−H), 3269.1 (O−H), 2900.2 (sp^3 C−H), 1661.6 (C=O amide), 889.7-668.3 (Ar C−H).

^{1}H NMR (400 MHz, $(CD_3)_2SO$) δ 9.04 (1H, s, O−H), 7.13-6.24 (3H, m, C−H), 7.15 (1H, s, NH−C=O), 5.34 (2H, d, CH_2, *J* 7.6 Hz), 4.01 (3H, s, CH_3) ppm.

Analysis calculated for $C_9H_{12}O_2N_2$: C, 59.98; H, 6.71; N, 15.55. Found: C, 58.32; H, 6.97; N, 13.35%.

m/z 181 $[C_9H_{12}O_2N_2]^+$.

Compound 4.73

Yield: 0.410 g, 71%.

IR υ_{max} (KBr)/cm^{-1} 3354.9 (N−H), 3276.8 (O−H), 2915.2 (sp^3 C−H), 1652.9 (C=O amide), 928.7-668.3 (Ar C−H).

^{1}H NMR (400 MHz, $(CD_3)_2SO$) δ 9.61 (1H, s, O−H), 7.83 (1H, s, Ar C−H), 7.75 (1H, s, NH−C=O), 6.60-6.32 (2H, m, Ar C−H), 5.34 (2H, d, CH_2, *J* 8 Hz), 2.26 (3H, s, CH_3) ppm.

Analysis calculated for $C_9H_{12}O_2N_2$: C, 59.98; H, 6.71; N, 15.55. Found: C, 59.77; H, 6.74; N, 14.92%.

m/z 181 $[C_9H_{12}O_2N_2]^+$.

Compound 4.74

Yield: 0.472 g, 82%.

IR υ_{max} (KBr)/cm^{-1} 3374.7 (N−H), 3280.2 (O−H), 2926.3 (sp^3 C−H), 1654.5 (C=O amide), 916.9, 868.8, 821.8, 747.5 and 697.3 (Ar C−H).

^{1}H NMR (400 MHz, $(CD_3)_2SO$) δ 9.57 (1H, bs, N−H), 9.11 (1H, bs, O−H), 7.35 (1H, d, Ar C−H, *J* 2 Hz), 7.27 (1H, dd, Ar C−H, *J* 2.8 Hz, *J* 8.8 Hz), 6.74 (1H, d, Ar C−H, *J* 8.4 Hz), 3.48 (2H, s, CH_2), 2.19 (3H, s, CH_3) ppm.

Analysis calculated for $C_9H_{12}N_2O_2$: C, 59.99; H, 6.71; N, 15.55. Found: C, 60.08; H, 7.06; N, 14.29%.

m/z 180 $[C_9H_{12}O_2N_2]^+$.

Compound 4.75

Yield: 0.451 g, 78%.

IR υ_{max} (KBr)/cm^{-1} 3359.1 (N−H), 3197.0 (O−H), 2917.2 (sp^3 C−H), 1674.9 (C=O amide), 799.1, 768.9, 752.4 and 692.5 (Ar C−H).

^{1}H NMR (400 MHz, $(CD_3)_2SO$) δ 9.66 (1H, bs, N−H), 9.35 (1H, bs, O−H), 7.33 (1H, d, Ar C−H, *J* 2 Hz), 7.00 (1H, d, Ar C−H, *J* 8 Hz), 6.89 (1H, dd, Ar C−H, *J* 2 Hz, *J* 8.4 Hz), 3.23 (2H, s, CH_2), 2.11 (3H, s, CH_3) ppm.

Analysis calculated for $C_9H_{12}N_2O_2$: C, 59.99; H, 6.71; N, 15.55. Found: C, 59.98; H, 7.18; N, 14.05%.

m/z 180 $[C_9H_{12}O_2N_2]^+$.

Compound 4.76

Yield: 0.552 g, 93%.

IR υ_{max} (KBr)/cm^{-1} 3419.7 (N−H), 3072.7 (O−H), 2953.1 (sp^3 C−H), 1642.4 (C=O amide), 819.8, 773.9 and 642.1 (Ar C−H).

^{1}H NMR (400 MHz, $(CD_3)_2SO$) δ 9.48 (1H, bs, N−H), 8.30 (1H, d, O−H, *J* 2.4 Hz), 6.96 (2H, dd, Ar C−H, *J* 2.4 and 8.4 Hz), 6.83 (1H, d, Ar C−H, *J* 2 and 8.4 Hz), 3.18 (2H, s, CH_2), 2.15 (9H, s, CH_3) ppm.

Analysis calculated for $C_{12}H_{18}N_2O_2$: C, 64.82; H, 8.16; N, 12.60. Found: C, 64.32; H, 8.18; N, 11.78%.

m/z 210 $[C_{11}H_{18}O_2N_2]^+$.

The following general method was used for the synthesis of compounds **4.77**–**4.85**: The mixture of hydroxymethyldiphenylphosphine (2 eq) and the primary amine **4.68**–**4.76** (1 eq) in methanol (20 ml) was stirred under N_2 for 24 h. In all the cases, except for compound **4.78**, **4.79**, **4.83**, **4.84**, the solution was evaporated to dryness under reduced pressure yielding yellow/white oils. In the case of **4.78**, **4.79**, **4.83**, **4.84**, the volume of the solution obtained was evaporated to *ca*. 2-3 ml under reduced pressure and a solid was obtained. The suspension was stirred for 10 min. The white solids obtained were collected by suction filtration and dried *in vacuo*.

Compound 4.77

Yield: 0.502, 82%.

^{1}H NMR (400 MHz, $(CD_3)_2SO$) δ 9.37 (1H, s, O−H), 8.48 (1H, s, N−H) 7.96-7.85 (8H, m, Ar C−H), 7.54-7.46 (12H, m, Ar C−H), 7.04-6.99 (1H, m, Ar C−H), 6.84 (1H, dd, Ar C−H, *J* 1.2 Hz, *J* 8 Hz), 6.76-6.73 (1H, m, Ar C−H), 3.76 (4H, s, CH_2), 3.46 (2H, s, CH_2) ppm.

^{31}P NMR data: δ -25.77 ppm.

Compound 4.78

Yield: 0.391, 70%.

IR υ_{max} (KBr)/cm^{-1} 3283.4 (N−H), 3162.6 (O−H), 1653.2 (C=O amide), 741.9 and 694.9 (Ar C−H).

^{1}H NMR (400 MHz, $(CD_3)_2SO$) δ 9.31 (1H, s, O−H), 9.07 (1H, s, N−H), 7.41-7.03 (21H, m, Ar C−H), 6.94 (1H, t, Ar C−H), 6.40 (1H, dd, Ar C−H, *J* 2 and 8.4 Hz), 6.30 (1H, dd, Ar C−H, *J* 0.8 and 8 Hz), 3.77 (4H, d, CH_2, *J* 4.4 Hz), 3.69 (2H, s, CH_2) ppm.

^{31}P NMR data: δ -27.51 ppm.

Analysis calculated for $C_{34}H_{32}O_2N_2P_2$: C, 72.59; H, 5.73; N, 4.98. Found: C, 72.10; H, 5.80; N, 4.95%.

m/z 561 $[C_{34}H_{32}O_2N_2P_2]^+$.

Compound 4.79

Yield: 0.521, 85%.

IR υ_{max} (KBr)/cm^{-1} 3294.3 (N−H), 3176.3 (O−H), 1667.1 (C=O amide), 745.9 and 696.3 (Ar C−H).

^{1}H NMR (400 MHz, $(CD_3)_2SO$) δ 9.14 (1H, s, O−H), 8.83 (1H, s, N−H), 7.50-7.29 (20H, m, Ar C−H), 6.88 (2H, d, Ar C−H, *J* 9.2 Hz), 6.56 (2H, d, Ar C−H, *J* 12 Hz), 6.30 (1H, dd, Ar C−H, *J* 0.8 and 8 Hz), 3.77 (4H, d, CH_2, *J* 4.4 Hz), 3.69 (2H, s, CH_2) ppm.

^{31}P NMR data: δ -27.38 ppm.

Analysis calculated for $C_{34}H_{32}O_2N_2P_2$: C, 72.59; H, 5.73; N, 4.98. Found: C, 72.15; H, 5.72; N, 4.95%.

m/z 561 $[C_{34}H_{32}O_2N_2P_2]^+$.

Compound 4.80

Yield: 0.521 g, 81%.

^{1}H NMR (400 MHz, DMSO) δ 8.15 (1H, s, O−H), 7.19-7.77 (23H, m, Ar C−H), 5.06 (2H, s, CH_2), 1.19 (3H, s, CH_3), 3.62 (4H, d, CH_2 *J* 8 Hz) ppm.

^{31}P NMR data: δ -25.99 ppm.

Compound 4.81

Yield: 0.554 g, 89%.

^{1}H NMR (400 MHz, $(CD_3)_2SO$) δ 7.83 (1H, s, O−H), 7.60-7.21 (23H, m, Ar C−H), 5.07 (2H, s, CH_2), 1.63 (3H, s, CH_3), 3.69 (4H, d, CH_2 *J* 3.6 Hz) ppm.

^{31}P NMR data: δ -25.49 ppm.

Compound 4.82

Yield: 0.547 g, 88%.

^{1}H NMR (400 MHz, $CDCl_3$) δ 9.34 (1H, s, O−H), 8.17 (1H, s, N−H), 7.19-7.71 (23H, m, Ar C−H), 5.27 (4H, d, CH_2, *J* 8 Hz), 1.63 (3H, s, CH_3), 3.61 (2H, d, CH_2, *J* 4.8 Hz) ppm.

^{31}P NMR data: δ -26.46 ppm.

Compound 4.83

Yield: 0.422 g, 65%.

IR υ_{max} (KBr)/cm^{-1} 3228.3 (N−H), 3047.2 (O−H), 2938.7 (sp^3 C−H), 1645.2 (C=O amide), 742.2, 734.7 and 692.7 (Ar C−H).

^{1}H NMR (400 MHz, $(CD_3)_2SO$) δ 9.05 (1H, s, O−H), 8.68 (1H, s, N−H), 7.55-7.32 (20H, m, Ar C−H), 6.95 (1H, dd, Ar C−H, *J* 2.4 Hz, *J* 8.4 Hz), 6.61 (1H, d, Ar C−H, *J* 8.8 Hz), 6.41 (1H, d, Ar C−H, *J* 2.4 Hz), 3.81 (4H, d, CH_2, *J* 4.8 Hz), 3.69 (2H, s, CH_2), 2.04 (3H, s, CH_3) ppm.

^{31}P NMR data: δ -27.13 ppm.

Analysis calculated for $C_{35}H_{34}O_2N_2P_2$: C, 72.91; H, 5.94; N, 4.86. Found: C, 72.72; H, 5.95; N, 4.88%.

Accurate mass for $[C_{35}H_{34}O_2N_2P_2]^+$ 576.2096, requires 577.2179. m/z 576 $[C_{20}H_{24}O_4N_2]^+$.

Compound 4.84

Yield: 0.537 g, 80%.

IR υ_{max} (KBr)/cm^{-1} 3316.9 (N−H), 3178.1 (O−H), 2918.7 (sp^3 C−H), 1659.5 (C=O amide), 753.3, 743.1 and 696.5 (Ar C−H).

^{1}H NMR (400 MHz, $(CD_3)_2SO$) δ 9.29 (1H, s, O−H), 9.08 (1H, s, N−H), 7.46-7.35 (20H, m, Ar C−H), 7.29 (1H, d, Ar C−H, *J* 2 Hz), 6.86 (1H, d, Ar C−H, *J* 8.8 Hz), 6.15 (1H, dd, Ar C−H, *J* 1.6 Hz, *J* 8 Hz), 3.82 (4H, d, CH_2, *J* 4.4 Hz), 3.73 (2H, s, CH_2), 2.08 (3H, s, CH_3) ppm.

^{31}P NMR data: δ -27.52 ppm.

Analysis calculated for $C_{35}H_{34}O_2N_2P_2$: C, 72.91; H, 5.94; N, 4.86. Found: C, 72.71; H, 5.94; N, 4.82%.

m/z 575 $[C_{35}H_{34}O_2N_2P_2]^+$.

Compound 4.85

Yield: 0.645 g, 91%.

^{1}H NMR (400 MHz, $(CD_3)_2SO$) δ 9.52 (1H, s, O−H), 9.03 (1H, s, N−H), 7.83-7.28 (21H, m, Ar C−H), 6.94 (1H, dd, Ar C−H, *J* 7.6 and 10 Hz), 6.77 (1H, d, Ar C−H, *J* 6.8 Hz), 3.73 (4H, d, CH_2, *J* 2 Hz), 3.68 (2H, s, CH_2), 1.22 (9H, s, CH_3) ppm.

^{31}P NMR data: δ -27.76 ppm.

The following general method was used for the synthesis of compounds **4.86**–**4.94**: To a stirring solution of $PtCl_2$(COD) in dichloromethane (5 ml) was added a solution of **4.77**–**4.85** (1 eq) in dichloromethane (5 ml). The pale yellow/colourless solutions obtained were stirred for 30 min. The volume was evaporated to *ca*. 2-3 ml under reduced pressure and diethyl ether (10 ml) added. The suspension was stirred for 10 min. The white solids obtained were collected by suction filtration and dried *in vacuo*.

Compound 4.86

Yield: 0.086 g, 57%.

IR υ_{max} (KBr)/cm^{-1} 3243.5 (N−H), 3051.6 (O−H), 1653.0 (C=O amide), 743.9 and 688.7 (Ar C−H), 307.6 and 285.8 (Pt−Cl).

^{1}H NMR (400 MHz, $CDCl_3$) δ 9.35 (1H, s, O−H), 8.50 (1H, s, N−H) 7.87-7.82 (8H, m, Ar C−H), 7.50-7.41 (12H, m, Ar C−H), 7.01-6.97 (1H, m, Ar C−H), 6.87 (1H, dd, Ar

C−H, *J* 1.2 Hz, *J* 8 Hz), 6.78-6.75 (1H, m, Ar C−H), 3.72 (4H, s, CH_2), 3.42 (2H, s, CH_2) ppm.

^{31}P NMR data: δ -6.89 ppm, $^{1}J_{PtP}$ 3422 Hz.

Analysis calculated for $C_{34}H_{30}N_2O_2P_2Cl_2Pt{\cdot}0.5CH_2Cl_2$: C, 48.63; H, 3.74; N, 3.15. Found: C, 48.87; H, 3.90; N, 3.26%.

m/z $[C_{34}H_{30}O_2N_2P_2Cl_2Pt]^+$: 791 $[M^+$-Cl], 756 $[M^+$-2Cl].

Compound 4.87

Yield: 0.102 g, 85%.

IR υ_{max} (KBr)/cm^{-1} 3311.5 (N−H), 3052.5 (O−H), 1679.5 (C=O amide), 740.4 and 688.8 (Ar C−H), 303.5 and 279.3 (Pt−Cl).

^{1}H NMR (400 MHz, $CDCl_3$) δ 9.62 (1H, s, O−H), 9.36 (1H, s, N−H) 7.91-7.86 (8H, m, Ar C−H), 7.60-7.42 (12H, m, Ar C−H), 7.05 (2H, m, Ar C−H), 6.83 (1H, d, Ar C−H, *J* 8.4 Hz), 6.45 (1H, dd, Ar C−H, *J* 1.6 Hz, *J* 8 Hz), 4.18 (4H, s, CH_2), 3.47 (2H, s, CH_2) ppm.

^{31}P NMR data: δ -9.45 ppm, $^{1}J_{PtP}$ 3425 Hz.

Analysis calculated for $C_{34}H_{32}N_2O_2P_2Cl_2Pt$: C, 49.29; H, 3.89; N, 3.38. Found: C, 48.98; H, 3.68; N, 3.37%.

m/z 827 $[C_{34}H_{32}O_2N_2P_2Cl_2Pt]^+$, 792 $[M^+$-Cl], 757 $[M^+$-2Cl].

Compound 4.88

Yield: 0.104 g, 84%.

IR υ_{max} (KBr)/cm^{-1} 3325.1 (N−H), 3053.7 (O−H), 1672.3 (C=O amide), 739.1 and 695.5 (Ar C−H), 310.7 and 287.1 (Pt−Cl).

^{1}H NMR (400 MHz, $CDCl_3$) δ 9.52 (1H, s, O−H), 9.31 (1H, s, N−H) 8.01-7.97 (8H, m, Ar C−H), 7.70-7.61 (12H, m, Ar C−H), 7.34 (2H, d, Ar C−H, *J* 8.8 Hz), 6.78 (2H, d, Ar C−H, *J* 9.2 Hz), 4.26 (4H, s, CH_2), 3.49 (2H, s, CH_2) ppm.

^{31}P NMR data: δ -9.54 ppm, $^{1}J_{PtP}$ 3405 Hz.

Analysis calculated for $C_{34}H_{32}N_2O_2P_2Cl_2Pt$: C, 49.29; H, 3.89; N, 3.38. Found: C, 48.72; H, 3.66; N, 3.33%.

m/z 827 $[C_{34}H_{32}O_2N_2P_2Cl_2Pt]^+$, 792 $[M\text{-}Cl]^+$.

Compound 4.89

Yield: 0.115 g, 89%.

IR υ_{max} (KBr)/cm^{-1} 3248.5 (N−H), 3051.4 (O−H), 1654.6 (C=O amide), 739.3 and 688.4 (Ar C−H), 305.4 and 283.0 (Pt−Cl).

^{1}H NMR (400 MHz, $CDCl_3/CD_3OD$) δ 9.45 (1H, s, O−H), 8.91 (1H, s, N−H) 7.84-7.80 (8H, m, Ar C−H), 7.53-7.44 (13H, m, Ar C−H), 6.69 (2H, s, Ar C−H), 4.05 (4H, s, CH_2), 3.49 (2H, s, CH_2), 2.22 (3H, s, CH_3) ppm.

^{31}P NMR data: δ -9.83 ppm, $^{1}J_{PtP}$ 3398 Hz.

Analysis calculated for $C_{35}H_{34}O_2N_2P_2Cl_2Pt{\cdot}0.5CH_2Cl_2$: C, 48.63; H, 3.74; N, 3.15. Found: C, 49.00; H, 4.07; N, 3.13%.

m/z 841 $[C_{35}H_{34}O_2N_2P_2Cl_2Pt]^+$, 806 $[M\text{-}Cl]^+$, 771 $[M\text{-}2Cl]^+$.

Compound 4.90

Yield: 0.092 g, 65%.

IR υ_{max} (KBr)/cm^{-1} 3349.6 (N−H), 3049.7 (O−H), 1679.8 (C=O amide), 739.2 and 691.2 (Ar C−H), 316.2 and 283.3 (Pt−Cl).

^{1}H NMR (400 MHz, $(CD_3)_2SO$) δ 9.16 (1H, s, O−H), 8.61 (1H, s, N−H) 7.83-7.80 (8H, m, Ar C−H), 7.57-7.41 (13H, m, Ar C−H), 7.05 (1H, d, Ar C−H, *J* 8.4 Hz), 6.48 (1H, dd, Ar C−H, *J* 2.4 Hz, *J* 11.2 Hz), 4.03 (6H, s, CH_2), 1.80 (3H, s, CH_3) ppm.

^{31}P NMR data: δ -11.02 ppm, $^{1}J_{PtP}$ 3397 Hz.

Analysis calculated for $C_{35}H_{34}N_2O_2P_2Cl_2Pt$: C, 49.89; H, 4.07; N, 3.32. Found: C, 49.32; H, 4.17; N, 3.25%.

m/z 842 $[C_{35}H_{34}O_2N_2P_2Cl_2Pt]^+$, 807 $[M^+\text{-}Cl]$.

Compound 4.91

Yield: 0.098 g, 73%.

IR υ_{max} (KBr)/cm^{-1} 3346.5 (N−H), 3075.1 (O−H), 1654.1 (C=O amide), 738.7 and 696.9 (Ar C−H), 315.0 and 290.0 (Pt−Cl).

^{1}H NMR (400 MHz, $(CD_3)_2SO$) δ 9.56 (1H, s, O−H), 8.94 (1H, s, N−H) 7.85-7.77 (8H, m, Ar C−H), 7.59-7.38 (13H, m, Ar C−H), 6.63 (1H, d, Ar C−H, *J* 1.2 Hz), 6.51 (1H, dd, Ar C−H, *J* 1.4 Hz, *J* 8.4 Hz), 4.05 (4H, s, CH_2), 3.17 (2H, s, CH_2), 2.17 (3H, s, CH_3) ppm.

^{31}P NMR data: δ -9.86 ppm, $^{1}J_{PtP}$ 3405 Hz.

Analysis calculated for $C_{35}H_{34}N_2O_2P_2Cl_2Pt$: C, 49.89; H, 4.07; N, 3.32. Found: C, 49.28; H, 4.05; N, 2.91%.

m/z 841 $[C_{35}H_{34}O_2N_2P_2Cl_2Pt]^+$, 807 $[M^+\text{-Cl}]$, 771 $[M^+\text{-2Cl}]$.

Compound 4.92

Yield: 0.137 g, 99%.

IR υ_{max} (KBr)/cm^{-1} 3465.3 (N−H), 3323.0 (O−H), 1674.8 (C=O amide), 740.9 and 695.9 (Ar C−H), 309.4 and 282.8 (Pt−Cl).

^{1}H NMR (400 MHz, $CDCl_3$) δ 9.17 (1H, s, O−H), 8.90 (1H, s, N−H), 7.98-7.50 (20H, m, Ar C−H), 6.97-6.84 (2H, m, Ar C−H), 6.68 (1H, d, Ar C−H, *J* 8 Hz), 4.66 (4H, s, CH_2), 3.20 (2H, s, CH_2), 2.13 (3H, s, CH_3) ppm.

^{31}P NMR data: δ -9.79 ppm, $^1J_{PtP}$ 3398 Hz.

Analysis calculated for $C_{35}H_{34}N_2O_2P_2Cl_2Pt{\cdot}0.5C_4H_{10}O$: C, 50.52; H, 4.47; N, 3.19. Found: C, 50.91; H, 4.53; N, 3.61%.

m/z 806 $[M\text{-Cl}]^+$, 770 $[M\text{-2Cl}]^+$.

Compound 4.93

Yield: 0.120 g, 90%.

IR υ_{max} (KBr)/cm^{-1} 3439.0 (N−H), 3286.9 (O−H), 1612.6 (C=O amide), 734.9, 708.5 and 688.4 (Ar C−H), 311.9 and 285.9 (Pt−Cl).

^{1}H NMR (400 MHz, $CDCl_3$) δ 9.46 (1H, s, O−H), 9.21 (1H, s, N−H) 7.94-7.78 (8H, m, Ar C−H), 7.54-7.42 (12H, m, Ar C−H), 7.09 (1H, d, Ar C−H, *J* 2 Hz), 6.87 (1H, d, Ar C−H, *J* 8 Hz), 6.69 (1H, dd, Ar C−H, *J* 2 Hz, *J* 8 Hz), 4.12 (4H, s, CH_2), 3.43 (2H, s, CH_2), 2.02 (3H, s, CH_3) ppm.

^{31}P NMR data: δ -9.7 ppm, $^1J_{PtP}$ 3406 Hz.

Analysis calculated for $C_{35}H_{34}N_2O_2P_2Cl_2Pt$: C, 49.89; H, 4.07; N, 3.32. Found: C, 49.77; H, 3.95; N, 3.38%.

m/z 806 $[M\text{-Cl}]^+$, 771$[M\text{-2Cl}]^+$.

Compound 4.94

Yield: 0.112 g, 81%.

IR υ_{max} (KBr)/cm^{-1} 3479.7 (N−H), 3312.4 (O−H), 2950.0 (sp^3 C−H), 1653.3 (C=O amide), 738.6, 698.9 and 688.9 (Ar C−H), 308.9 and 283.1 (Pt−Cl).

^{1}H NMR (400 MHz, $CDCl_3$) δ 9.44 (1H, s, O−H), 8.95 (1H, s, N−H) 7.86-7.81 (8H, m, Ar C−H), 7.54-7.45 (13H, m, Ar C−H), 6.91 (1H, dd, Ar C−H, *J* 2.4 Hz, *J* 8.4 Hz), 6.73 (1H, d, Ar C−H, *J* 8.4 Hz), 4.09 (4H, bs, CH_2), 3.50 (2H, s, CH_2), 2.00 (9H, s, CH_3) ppm.

^{31}P NMR data: δ -9.66 ppm, $^{1}J_{PtP}$ 3418 Hz.

Analysis calculated for $C_{39}H_{42}N_2O_2P_2Cl_2Pt{\cdot}CH_2Cl_2$: C, 51.34; H, 4.52; N, 2.92. Found: C, 51.14; H, 4.63; N, 3.10%.

m/z 847 $[M\text{-}Cl]^+$.

The following general method was used for the synthesis of compounds **4.95**–**4.103**: To a stirring solution of AuCl(tht) in dichloromethane (5 ml) was added a solution of **4.77**–**4.85** (0.5 eq) in dichloromethane (5 ml). The pale yellow/colourless solutions obtained were stirred for 30 min. The volume was evaporated to *ca*. 2-3 ml under reduced pressure and diethyl ether (10 ml) added. The suspension was stirred for 10 min. The white solids obtained were collected by suction filtration and dried *in vacuo*.

Compound 4.95

Yield: 0.066 g, 62%.

IR υ_{max} (KBr)/cm^{-1} 3344.7 (N−H), 3002.2 (O−H), 2958.9 (sp^3 C−H), 1654.9 (C=O amide), 744.6 and 690.5 (Ar C−H), 328.4 (Au−Cl).

^{1}H NMR (400 MHz, $CDCl_3$) δ 9.62 (1H, s, O−H), 8.81 (1H, s, N−H), 7.97-7.53 (21H, m, Ar C−H), 6.96 (1H, t, Ar C−H), 6.87 (1H, d, Ar C−H, *J* 8 Hz), 6.78 (1H, t, Ar C−H), 4.70 (4H, s, CH_2), 2.72 (2H, s, CH_2) ppm.

^{31}P NMR data: δ 22.9 ppm.

Analysis calculated for $C_{34}H_{32}N_2O_2P_2Cl_2Au_2{\cdot}CH_2Cl_2$: C, 37.79; H, 3.08; N, 2.52. Found: C, 38.13; H, 3.22; N, 2.38%.

m/z $[C_{34}H_{32}O_2N_2P_2Cl_2Au_2]^+$: 991 $[M^+\text{-}Cl]$, 955 $[M^+\text{-}2Cl]$.

Compound 4.96

Yield: 0.085 g, 81%.

IR υ_{max} (KBr)/cm^{-1} 3326.7 (N−H), 3052.4 (O−H), 2959.3 (sp^3 C−H), 1675.2 (C=O amide), 742.5 and 689.9 (Ar C−H), 328.0 (Au−Cl).

^{1}H NMR (400 MHz, $CDCl_3$) δ 9.30 (1H, s, O−H), 9.13 (1H, s, N−H), 7.89-7.84 (8H, m, Ar C−H), 7.58-7.38 (12H, m, Ar C−H), 6.99 (2H, m, Ar C−H), 6.71 (1H, d, Ar C−H, *J* 8 Hz), 6.41 (1H, dd, Ar C−H, *J* 1.6 Hz, *J* 8 Hz), 4.64 (4H, s, CH_2), 3.10 (2H, s, CH_2) ppm.

^{31}P NMR data: δ 24.2 ppm.

Analysis calculated for $C_{34}H_{32}N_2O_2P_2Cl_2Au_2 \cdot 0.5CH_2Cl_2$: C, 39.07; H, 3.09; N, 2.60. Found: C, 38.65; H, 2.87; N, 2.64%.

m/z $[C_{34}H_{32}O_2N_2P_2Cl_2Au_2]^+$: 991 [$M^+$-Cl], 955 [$M^+$-2Cl].

Compound 4.97

Yield: 0.093 g, 96%.

IR υ_{max} (KBr)/cm^{-1} 3326.7 (N−H), 3329.0 (O−H), 2965.1 (sp^3 C−H), 1664.1 (C=O amide), 742.9 and 691.1 (Ar C−H), 325.3 (Au−Cl).

^{1}H NMR (400 MHz, $CDCl_3$) δ 9.12 (1H, s, O−H), 8.92 (1H, s, N−H), 7.87-7.81 (8H, m, Ar C−H), 7.55-7.46 (12H, m, Ar C−H), 7.07 (2H, d, Ar C−H, *J* 12.4 Hz), 6.60 (2H, d, Ar C−H, *J* 10 Hz), 4.61 (4H, s, CH_2), 3.07 (2H, s, CH_2) ppm.

^{31}P NMR data: δ 24.3 ppm.

Analysis calculated for $C_{34}H_{32}N_2O_2P_2Cl_2Au_2$: C, 39.75; H, 3.14; N, 2.73. Found: C, 39.55; H, 2.98; N, 2.65%.

m/z $[C_{34}H_{32}O_2N_2P_2Cl_2Au_2]^+$: 991 [$M^+$-Cl], 955 [$M^+$-2Cl].

Compound 4.98

Yield: 0.059 g, 63%.

IR υ_{max} (KBr)/cm^{-1} 3447.2 (N−H), 3113.8 (O−H), 2923.1 (sp^3 C−H), 1653.2 (C=O amide), 744.2 and 691.7 (Ar C−H), 328.1 (Au−Cl).

^{1}H NMR (400 MHz, $CDCl_3$) δ 8.29 (1H, s, O−H), 7.42-7.85 (23H, m, Ar C−H), 3.35 (4H, d, CH_2, *J* 3.2 Hz), 3.45 (2H, s, CH_2), 2.27 (3H, s, CH_3) ppm.

^{31}P NMR data: δ 21.21 ppm.

Analysis calculated for $C_{35}H_{34}N_2O_2P_2Cl_2Au_2 \cdot CH_2Cl_2$: C, 38.39; H, 3.22; N, 2.49. Found: C, 38.60; H, 3.27; N, 2.41%.

m/z $[C_{35}H_{34}O_2N_2P_2Cl_2Au_2]^+$: 1005 [$M^+$-Cl], 969 [$M^+$-2Cl].

Compound 4.99

Yield: 0.056 g, 60%.

IR υ_{max} (KBr)/cm^{-1} 3358.2 (N−H), 3052.9 (O−H), 2951.2 (sp^3 C−H), 1669.3 (C=O amide), 743.9 and 691.2 (Ar C−H), 328.3 (Au−Cl).

^{1}H NMR (400 MHz, $CDCl_3$) δ 9.16 (1H, s, O−H), 8.54 (1H, s, N−H), 7.90-7.85 (8H, m, Ar C−H), 7.60-7.52 (12H, m, Ar C−H), 7.02 (1H, d, Ar C−H, *J* 8.4 Hz), 6.52 (2H, m, Ar C−H), 4.75 (4H, s, CH_2), 3.67 (2H, s, CH_2), 1.93 (3H, s, CH_3) ppm.

^{31}P NMR data: δ 24.84 ppm.

Analysis calculated for $C_{35}H_{34}N_2O_2P_2Cl_2Au_2 \cdot 0.5CH_2Cl_2$: C, 39.67; H, 3.24; N, 2.57. Found: C, 39.15; H, 3.38; N, 2.51%.

m/z 1041 $[C_{35}H_{34}O_2N_2P_2Cl_2Au_2]^+$, 1005 $[M^+$-Cl], 970 $[M^+$-2Cl].

Compound 4.100

Yield: 0.065 g, 58%.

IR υ_{max} (KBr)/cm^{-1} 3383.9 (N−H), 3051.3 (O−H), 2918.6 (sp^3 C−H), 1653.1 (C=O amide), 742.3 and 690.7 (Ar C−H), 327.9 (Au−Cl).

^{1}H NMR (400 MHz, $CDCl_3$) δ 8.13 (1H, s, O−H), 8.10 (1H, s, N−H), 7.42-7.76 (23H, m, Ar C−H), 4.36 (2H, d, CH_2, *J* 3.2 Hz), 3.47 (4H, s, CH_2), 2.29 (3H, s, CH_3) ppm.

^{31}P NMR data: δ 20.76 ppm.

Analysis calculated for $C_{35}H_{34}N_2O_2P_2Cl_2Au_2 \cdot 0.5CH_2Cl_2$: C, 39.67; H, 3.24; N, 2.57. Found: C, 39.20; H, 3.32; N, 2.47%.

m/z $[C_{35}H_{34}O_2N_2P_2Cl_2Au_2]^+$: 1005 $[M^+$-Cl], 970 $[M^+$-2Cl].

Compound 4.101

Yield: 0.114 g, 94%.

IR υ_{max} (KBr)/cm^{-1} 3398.4 (N−H), 3052.8 (O−H), 2961.3 (sp^3 C−H), 1669.1 (C=O amide), 742.7 and 690.8 (Ar C−H), 324.2 (Au−Cl).

^{1}H NMR (400 MHz, $CDCl_3$) δ 9.07 (1H, s, O−H), 8.90 (1H, s, N−H), 7.96-7.91 (8H, m, Ar C−H), 7.65-7.49 (12H, m, Ar C−H), 7.02-6.97 (2H, m, Ar C−H), 6.67 (1H, d, Ar C−H, *J* 8.4 Hz), 4.65 (4H, s, CH_2), 3.17 (2H, s, CH_2), 2.13 (3H, s, CH_3) ppm.

^{31}P NMR data: δ 24.46 ppm.

Analysis calculated for $C_{35}H_{34}N_2O_2P_2Cl_2Au_2$: C, 40.36; H, 3.29; N, 2.69. Found: C, 40.13; H, 3.37; N, 2.60%.

m/z $[C_{35}H_{34}O_2N_2P_2Cl_2Au_2]^+$: 1005 $[M^+$-Cl], 969 $[M^+$-2Cl].

Compound 4.102

Yield: 0.111 g, 50%.

IR υ_{max} (KBr)/cm^{-1} 3446.2 (N−H), 3048.8 (O−H), 2963.9 (sp^3 C−H), 1675.2 (C=O amide), 743.1 and 690.8 (Ar C−H), 324.0 (Au−Cl).

^{1}H NMR (400 MHz, $CDCl_3$) δ 9.21 (1H, s, O−H), 9.05 (1H, s, N−H), 7.94-7.44 (20H, m, Ar C−H), 7.05 (1H, d, Ar C−H, *J* 1.6 Hz), 6.89 (1H, d, Ar C−H, *J* 8.4 Hz), 6.62 (1H, dd, Ar C−H, *J* 1.6 Hz, *J* 7.6 Hz), 4.64 (2H, s, CH_2), 3.09 (4H, s, CH_2), 2.09 (3H, s, CH_3) ppm.

^{31}P NMR data: δ 24.14 ppm.

Analysis calculated for $C_{35}H_{34}N_2O_2P_2Cl_2Au_2$: C, 39.82; H, 2.95; N, 2.73. Found: C, 39.93; H, 3.31; N, 2.67%.

m/z $[C_{35}H_{34}O_2N_2P_2Cl_2Au_2]^+$: 1005 [$M^+$-Cl].

Compound 4.103

Yield: 0.046 g, 52%.

IR υ_{max} (KBr)/cm^{-1} 3455.3 (N−H), 3053.8 (O−H), 2955.5 (sp^3 C−H), 1653.2 (C=O amide), 742.1 and 690.9 (Ar C−H), 328.1 (Au−Cl).

^{1}H NMR (400 MHz, $CDCl_3$) δ 9.40 (1H, s, O−H), 8.76 (1H, s, N−H), 7.95-7.84 (8H, m, Ar C−H), 7.61-7.50 (13H, m, Ar C−H), 6.94 (1H, dd, Ar C−H, *J* 2.4 and 8.4 Hz), 6.73 (1H, d, Ar C−H, *J* 8.4 Hz), 4.64 (4H, s, CH_2), 4.04 (2H, s, CH_2), 1.23 (3H, s, CH_3) ppm.

^{31}P NMR data: δ 23.40 ppm.

Analysis calculated for $C_{38}H_{39}N_2O_2P_2Cl_2Au_2$: C, 42.16; H, 3.63; N, 2.59. Found: C, 42.18; H, 3.92; N, 2.48%.

m/z $[C_{38}H_{40}O_2N_2P_2Cl_2Au_2]^+$: 1047 [$M^+$-Cl], 1011 [$M^+$-2Cl].

The following general method was used for the synthesis of compounds **4.104**–**4.108**: To a solution of $[Mo(CO)_4(nbd)]$ in dichloromethane (5 ml) was added a solution of **4.78**, **4.80** and **4.83**–**4.85** (1 eq) in dichloromethane (5 ml). The pale yellow solutions obtained were stirred for 24 h at r.t. under N_2, the solution was evaporated to *ca*. 2-3 ml under reduced pressure and diethyl ether (10 ml) added. The suspension was stirred for 10 min. The yellow/brown solids obtained were collected by suction filtration and dried *in vacuo*.

Compound 4.104

Yield: 0.065 g, 56%.

IR υ_{max} (KBr)/cm^{-1} 3335.1 (O−H), 2019.4, 1924.4 and 1895.6 (CO), 1663.1 (C=O amide), 741.2 and 694.2 (Ar C−H).

^{1}H NMR (400 MHz, $CDCl_3$) δ 9.72 (1H, s, O−H), 9.26 (1H, s, N–H), 7.60-7.21 (21H, m, Ar C−H), 6.95 (1H, d, Ar C−H, *J* 8 Hz), 6.85 (1H, dd, Ar C−H, *J* 3.2 Hz, *J* 9.2 Hz), 3.99 (4H, s, CH_2), 3.79 (2H, s, CH_2), 2.07 (3H, s, CH_3) ppm.

^{31}P NMR data: δ 19.69 ppm.

Analysis calculated for $C_{39}H_{34}N_2O_6P_2Mo$: C, 59.70; H, 4.37; N, 3.57. Found: C, 58.86; H, 4.58; N, 3.65%.

m/z 758 [M^+-CO], 730 [M^+-2CO], 702 [M^+-3CO], 674 [M^+-4CO].

Compound 4.105

Yield: 0.098 g, 88%.

IR υ_{max} (KBr)/cm^{-1} 3332.5 (O−H), 2019.8, 1920.5 and 1894.1 (CO), 1669.6 (C=O amide), 741.6 and 694.3 (Ar C−H).

^{1}H NMR (400 MHz, $CDCl_3$) δ 7.48-6.98 (20H, m, Ar C−H), 6.53 (1H, d, Ar C−H, *J* 4 Hz), 6.35 (1H, Ar C−H), 5.94 (1H, d, Ar C−H, *J* 8 Hz), 3.63 (4H, s, CH_2), 3.33 (2H, s, CH_2) ppm.

^{31}P NMR data: δ 20.97 ppm.

Analysis calculated for $C_{38}H_{32}N_2O_6P_2Mo{\cdot}0.5CH_2Cl_2$: C, 57.19; H, 4.06; N, 3.42. Found: C, 57.41; H, 4.37; N, 3.53%.

m/z 773 [$C_{38}H_{32}O_6N_2P_2Mo]^+$, 744 [$M^+$-CO], 716 [$M^+$-2CO], 688 [$M^+$-3CO] and 660 [$M^+$-4CO].

Compound 4.106

Yield: 0.084 g, 84%.

IR υ_{max} (KBr)/cm^{-1} 3328.0 (O−H), 2019.7, 1919.1 and 1893.9 (CO), 1657.1 (C=O amide), 741.3 and 694.5 (Ar C−H).

^{1}H NMR (400 MHz, $(CD_3)_2SO$) δ 9.56 (1H, s, O−H), 9.49 (1H, s, N–H), 7.57-7.16 (21H, m, Ar C−H), 7.08 (1H, dd, Ar C−H, *J* 4 Hz, *J* 12 Hz), 6.63 (1H, d, Ar C−H, *J* 12 Hz), 3.92 (4H, s, CH_2), 3.73 (2H, s, CH_2), 2.10 (3H, s, CH_3) ppm.

^{31}P NMR data: δ 19.95 ppm.

Analysis calculated for $C_{39}H_{34}N_2O_6P_2Mo$: C, 59.70; H, 4.37; N, 3.57. Found: C, 59.85; H, 4.86; N, 3.16%.

m/z 786 $[MoC_{39}H_{34}O_6N_2P_2]^+$, 758 $[M^+-CO]$, 730 $[M^+-2CO]$, 702 $[M^+-3CO]$ and 674 $[M^+-4CO]$.

Compound 4.107

Yield: 0.088 g, 86%.

IR υ_{max} (KBr)/cm^{-1} 3332.5 (O−H), 2019.8, 1919.1 and 1895.9 (CO), 1663.8 (C=O amide), 741.3 and 694.8 (Ar C−H).

^1H NMR (400 MHz, $(CD_3)_2SO$) δ 9.75 (1H, s, O−H), 9.29 (1H, s, N–H), 7.63-7.21 (20H, m, Ar C−H), 6.98 (1H, Ar C−H), 6.94 (1H, Ar C−H), 6.85 (1H, dd, Ar C−H, *J* 4 Hz, *J* 8 Hz), 3.97 (4H, s, CH_2), 3.76 (2H, s, CH_2), 2.09 (3H, s, CH_3) ppm.

^{31}P NMR data: δ 13.93 ppm.

Analysis calculated for $C_{39}H_{34}N_2O_6P_2Mo$: C, 59.70; H, 4.37; N, 3.57. Found: C, 60.52; H, 4.66; N, 3.64%.

m/z 758 $[M^+-CO]$, 730 $[M^+-2CO]$, 702 $[M^+-3CO]$ and 674 $[M^+-4CO]$.

Compound 4.108

Yield: 0.054 g, 61%.

IR υ_{max} (KBr)/cm^{-1} 3330.6 (O−H), 2020.8, 1919.1 and 1901.5 (CO), 1654.4 (C=O amide), 741.4 and 694.2 (Ar C−H).

Analysis calculated for $C_{42}H_{40}N_2O_6P_2Mo$: C, 61.02; H, 4.88; N, 3.39. Found: C, 60.41; H, 5.37; N, 2.99%.

m/z 828 $[C_{42}H_{40}O_6N_2P_2Mo]^+$, 800 $[M^+-CO]$, 772 $[M^+-2CO]$, 744 $[M^+-3CO]$ and 716 $[M^+-4CO]$.

The following general method was used for the synthesis of compounds **4.109**–**4.112**: The mixture of hydroxymethyldiphenylphosphine (2 eq) and the primary amine (2-aminoethyl)carbamic acid tert-butyl ester **X**, glycine, glycylglycine and triglycine(1 eq) in methanol (20 ml) respectively, was stirred under N_2 for 24 h. In all the cases, except for compound **4.109**, the solution was evaporated to dryness under reduced pressure yielding yellow/white oils. In the case of **4.109**, the volume of the solution obtained was evaporated to *ca*. 2-3 ml under reduced pressure and a solid was obtained. The

suspension was stirred for 10 min. The white solid obtained was collected by suction filtration and dried *in vacuo*.

Compound 4.109

Yield: 0.336 g, 48%.

IR υ_{max} (KBr)/cm^{-1} 3417.9 (N−H), 2785.3 (sp^3 C–H), 1701.3 (C=O), 735.4 and 686.3 (Ar C−H).

^{1}H NMR (400 MHz, $CDCl_3$) δ 7.40-7.18 (20H, m, Ar C−H), 4.30 (1H, s, N−H), 3.49 (4H, m, CH_2), 2.87 (2H, s, CH_2), 1.65 (2H, s, CH_2), 1.36 (9H, s, CH_3) ppm.

^{31}P NMR data: δ -28.80 ppm.

Analysis calculated for $C_{33}H_{38}O_2N_2P_2$: C, 71.21; H, 6.88; N, 5.03. Found: C, 71.09; H, 6.78; N, 5.60%.

m/z 555 $[C_{33}H_{38}O_2N_2P_2]^+$.

Compound 4.110

Yield: 0.415 g, 94%.

^{1}H NMR (400 MHz, $CDCl_3$) δ 10.82 (1H, s, O−H), 7.40-7.32 (20H, m, Ar C−H), 2.69 (2H, s, CH_2), 2.44 (4H, s, CH_2), 2.32 (4H, s, CH_2) ppm.

^{31}P NMR data: δ -27.26 ppm.

Compound 4.111

Yield: 0.331 g, 58%.

^{1}H NMR (400 MHz, $CDCl_3$) δ 10.76 (1H, s, O−H), 8.07 (1H, s, N–H), 7.39-7.34 (20H, m, Ar C−H), 4.16 (2H, s, CH_2), 3.29 (2H, s, CH_2), 2.17 (4H, s, CH_2) ppm.

^{31}P NMR data: δ -26.75 ppm.

Compound 4.112

Yield: 0.436 g, 99%.

^{1}H NMR (400 MHz, $CDCl_3$) δ 10.64 (1H, s, O−H), 8.12 (1H, s, N–H), 8.23 (1H, s, N–H), 7.42-7.31 (20H, m, Ar C−H), 4.19 (2H, s, CH_2), 3.98 (2H, s, CH_2), 3.27 (2H, s, CH_2), 2.38 (4H, s, CH_2) ppm.

^{31}P NMR data: δ -26.81 ppm.

The following general method was used for the synthesis of compounds **4.113**–**4.124**: To a stirring solution of $PtCl_2$(COD) (1 eq), AuCl(tht) (2 eq) or [Ru(η^6-*p*-cymene)Cl_2]$_2$ (2 eq), in dichloromethane (5 ml) was added a solution of **4.110**–**4.112** (1 eq) respectively, in dichloromethane (5 ml). The pale solutions obtained were stirred for 30 min. The volume was evaporated to *ca*. 2-3 ml under reduced pressure and diethyl ether (10 ml) added. The suspension was stirred for 10 min. The solids obtained were collected by suction filtration and dried *in vacuo*.

Compound 4.113

Yield: 0.094 g, 82%.

IR υ_{max} (KBr)/cm^{-1} 3429.6 (N−H), 2862.5 (*sp*^{3} C–H), 1701.3 (C=O), 734.6 and 688.4 (Ar C−H).

^{1}H NMR (400 MHz, $CDCl_3$) δ 7.83-7.47 (20H, m, Ar C−H), 6.25 (1H, s, N−H), 3.83 (4H, s, CH_2), 2.87 (2H, s, CH_2), 2.65 (2H, s, CH_2), 1.26 (9H, s, CH_3) ppm.

^{31}P NMR data: δ -10.14 ppm, $^1J_{PtP}$ 3400 Hz.

Analysis calculated for $C_{33}H_{38}O_2N_2P_2Cl_2Pt{\cdot}1.5Et_2O$: C, 50.60; H, 5.77; N, 3.03. Found: C, 50.17; H, 5.51; N, 2.94%.

m/z $[C_{33}H_{38}O_2N_2P_2Cl_2Pt]^+$: 787 [$M^+$-Cl], 731 [$M^+$-2Cl].

Compound 4.114

Yield: 0.059 g, 77%.

IR υ_{max} (KBr)/cm^{-1} 3427.6 (N−H), 1705.1 (C=O), 736.3 and 688.4 (Ar C−H).

^{1}H NMR (400 MHz, $CDCl_3$) δ 7.66-7.19 (20H, m, Ar C−H), 5.23 (1H, s, N−H), 4.23 (4H, s, CH_2), 1.54-1.20 (9H, m, CH_3) ppm.

^{31}P NMR data: δ 16.45 ppm.

Analysis calculated for $C_{33}H_{37}O_2N_2P_2Cl_2Au_2{\cdot}CH_2Cl_2$: C, 36.94; H, 3.56; N, 2.53. Found: C, 36.60; H, 3.32; N, 2.49%.

m/z $[C_{33}H_{37}O_2N_2P_2Cl_2Au_2]^+$: 985 [$M^+$-Cl].

Compound 4.115

Yield: 0.091 g, 65%.

IR υ_{max} (KBr)/cm^{-1} 3344.7 (N−H), 2870.2 (*sp*^{3} C–H), 1705.1 (C=O), 735.4 and 688.2 (Ar C−H).

^{1}H NMR (400 MHz, $CDCl_3$) δ 7.79-7.35 (28H, m, Ar C−H), 3.90 (1H, s, N−H), 3.57 (4H, s, CH_2), 2.87 (2H, s, CH_2), 2.30 (2H, s, CH_2), 2.09 (2H, m, CH_2), 1.54 (18H, s, CH_3), 1.22 (9H, s, CH_3) ppm.

^{31}P NMR data: δ 19.16 ppm.

Analysis calculated for $C_{53}H_{70}O_2N_2P_2Cl_4Ru_2 \cdot CH_2Cl_2$: C, 51.56; H, 5.77; N, 2.23. Found: C, 52.00; H, 5.63; N, 2.31%.

m/z $[C_{53}H_{70}O_2N_2P_2Cl_4Ru_2]^+$: 1103 [$M^+$-2Cl].

Compound 4.116

Yield: 0.102 g, 90%.

IR υ_{max} (KBr)/cm^{-1} 3387.1 (N−H), 3054.4 (O−H), 1730.2 (C=O, acid), 738.8 and 691.5 (Ar C−H).

^{1}H NMR (400 MHz, $(CD_3)_2SO$) δ 12.55 (1H, s, O−H), 7.88-7.36 (20H, m, Ar C−H), 2.51 (6H, s, CH_2), 2.09 (2H, s, CH_2) ppm.

^{31}P NMR data: δ -9.91 ppm, $^{1}J_{PtP}$ 3411 Hz.

Analysis calculated for $C_{29}H_{29}O_2NP_2Cl_2Pt \cdot 0.5CH_2Cl_2$: C, 45.04; H, 3.78; N, 1.75. Found: C, 45.33; H, 3.98; N, 1.85%.

Compound 4.117

Yield: 0.090 g, 85%.

IR υ_{max} (KBr)/cm^{-1} 3312.9 (N−H), 3023.5 (O−H), 1661.6 (C=O, amide), 1739.4 (C=O, acid), 1655.9 (C=O amide), 743.6 and 695.4 (Ar C−H).

^{1}H NMR (400 MHz, $(CD_3)_2SO$) δ 12.63 (1H, s, O−H), 8.12 (1H, s, N–H), 7.84-7.41 (20H, m, Ar C−H), 4.01 (2H, s, CH_2), 3.70 (2H, s, CH_2), 2.53 (4H, s, CH_2) ppm.

^{31}P NMR data: δ -10.64 ppm, $^{1}J_{PtP}$ 3393 Hz.

Analysis calculated for $C_{30}H_{30}O_3N_2P_2Cl_2Pt$: C, 45.35; H, 3.81; N, 3.53. Found: C, 45.82; H, 3.99; N, 3.63%.

m/z $[C_{30}H_{30}O_3N_2P_2Cl_2Pt]^+$: 759 [$M^+$-Cl], 723 [$M^+$-2Cl].

Compound 4.118

Yield: 0.091 g, 84%.

IR υ_{max} (KBr)/cm^{-1} 3328.2 (N−H), 3054.4 (O−H), 1672.1 (C=O, amide), 1737.9 (C=O, acid), 1667.5 (C=O amide), 741.7 and 691.5 (Ar C−H).

^{1}H NMR (400 MHz, $(CD_3)_2SO$) δ 12.69 (1H, s, O−H), 8.21 (1H, s, N–H), 8.09 (1H, s, N–H), 7.90-7.44 (20H, m, Ar C−H), 4.04 (2H, s, CH_2), 3.79 (2H, s, CH_2), 3.66 (2H, s, CH_2), 2.34 (4H, s, CH_2) ppm.

^{31}P NMR data: δ -10.41 ppm, $^{1}J_{PtP}$ 3474 Hz.

Analysis calculated for $C_{32}H_{33}O_4N_3P_2Cl_2Pt$: C, 45.90; H, 4.28; N, 4.46. Found: C, 45.50; H, 4.30; N, 4.69%.

m/z $[C_{32}H_{33}O_4N_3P_2Cl_2Pt]^+$: 816 $[M^+$-Cl].

Compound 4.119

Yield: 0.124 g, 60%.

IR υ_{max} (KBr)/cm^{-1} 3483.6 (O−H), 1716.7 (C=O, acid), 744.6 and 694.4 (Ar C−H).

^{1}H NMR (400 MHz, $(CD_3)_2SO$) δ 7.89-7.45 (20H, m, Ar C−H), 2.93 (6H, s, CH_2), 2.09 (2H, s, CH_2) ppm.

^{31}P NMR data: δ 23.79 ppm.

Analysis calculated for $C_{29}H_{29}O_2NP_2Cl_2Au_2 \cdot 0.5CH_2Cl_2$: C, 35.69; H, 3.05; N, 1.41. Found: C, 35.59; H, 3.02; N, 1.32%.

Compound 4.120

Yield: 0.180 g, 95%.

IR υ_{max} (KBr)/cm^{-1} 3387.1 (N−H), 3055.4 (O−H), 1732.1 (C=O, acid), 1670.4 (C=O amide), 744.6 and 694.4 (Ar C−H).

^{1}H NMR (400 MHz, $(CD_3)_2SO$) δ 12.61 (1H, s, O−H), 7.96-7.22 (21H, m, Ar C−H, N–H), 4.62 (2H, s, CH_2), 3.23 (2H, s, CH_2), 2.52 (4H, s, CH_2) ppm.

^{31}P NMR data: δ 23.05 ppm.

Analysis calculated for $C_{30}H_{30}O_3N_2P_2Cl_2Au_2 \cdot C_4H_{10}O$: C, 38.27; H, 3.78; N, 2.62. Found: C, 38.51; H, 3.51; N, 2.55%.

m/z $[C_{30}H_{30}O_3N_2P_2Cl_2Au_2]^+$: 957 $[M^+$-Cl].

Compound 4.121

Yield: 0.078 g, 64%.

IR υ_{max} (KBr)/cm^{-1} 3325.4 (N−H), 3055.4 (O−H), 1728.3 (C=O, acid), 1662.1 (C=O amide), 744.6 and 694.4 (Ar C−H).

^{1}H NMR (400 MHz, $(CD_3)_2SO$) δ 12.69 (1H, s, O−H), 8.19 (1H, s, N–H), 8.03 (1H, s, N–H), 7.83-7.41 (20H, m, Ar C−H), 4.53 (2H, s, CH_2), 3.77 (2H, s, CH_2), 3.61 (2H, s, CH_2), 2.46 (4H, s, CH_2) ppm.

^{31}P NMR data: δ 23.40 ppm.

Analysis calculated for $C_{32}H_{33}O_4N_3P_2Cl_2Au_2 \cdot C_4H_{10}O$: C, 38.45; H, 3.85; N, 3.74. Found: C, 38.17; H, 3.44; N, 4.17%.

m/z $[C_{32}H_{33}O_4N_3P_2Cl_2Au_2]^+$: 1014 $[M^+$-Cl], 978 $[M^+$-2Cl].

Compound 4.122

IR υ_{max} (KBr)/cm^{-1} 3484.5 (N−H), 3054.2 (O−H), 2960.8 and 2923.9 (sp^3 C–H), 1707.6 (C=O, acid), 746.5 and 696.5 (Ar C−H), 290.8 (Ru−Cl).

^{31}P NMR (400 MHz, $CDCl_3$) data: δ 19.60 ppm.

Analysis calculated for $C_{49}H_{57}O_2NP_2Cl_4Ru_2$: C, 53.60; H, 5.24; N, 1.28. Found: C, 52.96; H, 5.64; N, 1.32%.

m/z 1098 $[C_{49}H_{57}O_2NP_2Cl_4Ru_2]^+$, 1063 $[M^+$-Cl], 1027 $[M^+$-2Cl].

Compound 4.123

Yield: 0.088 g, 88%.

IR υ_{max} (KBr)/cm^{-1} 3387.1 (N−H), 3056.3 (O−H), 2960.8, 2925.1 and 2871.1 (sp^3 C–H), 1736.9 (C=O, acid), 1663.7 (C=O amide), 745.5 and 696.3 (Ar C−H).

^{1}H NMR (400 MHz, $CDCl_3$) δ 7.84-7.33 (20H, m, Ar C−H), 5.44-5.41 (2H, m, CH), 5.19 (1H, s, CH), 5.01 (1H, s, CH), 2.55 (2H, s, CH_2), 2.24 (9H, s, CH_3), 2.03 (2H, s, CH_2), 1.64 (18H, s, CH_3) ppm.

^{31}P NMR data: δ 15.69 ppm.

Analysis calculated for $C_{50}H_{58}O_3N_2P_2Cl_4Ru_2 \cdot 0.5CH_2Cl_2$: C, 51.26; H, 5.03; N, 2.37. Found: C, 51.36; H, 5.31; N, 2.42%.

m/z $[C_{50}H_{58}O_3N_2P_2Cl_4Ru_2]^+$: 1104 $[M^+$-Cl].

Compound 4.124

Yield: 0.041 g, 63%.

IR υ_{max} (KBr)/cm^{-1} 3374.6 (N−H), 3056.3 (O−H), 2960.8, 2927.1 and 2871.1 (sp^3 C–H), 1737.0 (C=O, acid), 1673.3 (C=O amide), 747.4 and 697.3 (Ar C−H).

^{1}H NMR (400 MHz, $CDCl_3$) δ 7.92-7.20 (20H, m, Ar C−H), 5.42 (2H, d, CH, *J* 16 Hz), 5.28 (2H, d, CH, *J* 9.2 Hz), 4.95 (2H, d, CH_2, *J* 14 Hz), 3.82 (4H, s, CH_2), 2.82 (2H, s, CH_2), 2.24 (9H, s, CH_3), 1.61 (18H, s, CH_3) ppm.

^{31}P NMR data: δ 18.24 ppm.

Analysis calculated for $C_{52}H_{61}O_4N_3P_2Cl_4Ru_2 \cdot CH_2Cl_2$: C, 49.62; H, 4.95; N, 3.28. Found: C, 49.68; H, 5.21; N, 3.29%.

m/z $[C_{52}H_{61}O_4N_3P_2Cl_4Ru_2]^+$, 1162 $[M^+$-Cl], 1125 $[M^+$-2Cl].

4.5 Crystallographic Experimental

Data for compounds **4.21**, **4.23**, **4.30**, **4.32**, **4.33**, **4.50**, **4.53**–**4.55**, **4.60**, **4.64**, **4.65**, **4.67**, **4.92**, **4.109** and **4.118** were collected using a Bruker APEX 2 CCD diffractometer using graphite-monochromated Mo-K_α radiation (λ = 0.71073 Å). Data for compounds **4.36**, **4.41**, **4.57**, **4.90** and **4.91** were collected using a Bruker APEX 2 CCD diffractometer using synchrotron radiation (λ = 0.6710 Å) at Daresbury SRS Station 9.8. Data for compounds **4.113**, **4.115** and **4.117** were collected using a Bruker APEX 2 CCD diffractometer using synchrotron radiation (λ = 0.6943 Å) at Daresbury SRS Station 9.8. Data for compound **4.51** and **4.124** were collected using a Bruker APEX 2 CCD diffractometer using synchrotron radiation (λ = 0.6884 Å or 0.6939 Å respectively) at Daresbury SRS Station 9.8. Data for compounds **4.89** was collected using a Bruker APEX 2 CCD diffractometer using synchrotron radiation (λ = 0.7848 Å) at Daresbury SRS Station 16.2 SMX. Data for compounds **4.58** was collected using a Bruker-Nonius 95 mm CCD camera on κ-goniostat diffractometer using graphite-monochromated Mo-K_α radiation (λ = 0.71073 Å). Data for compounds **4.22**, **4.35** and **4.78** were collected using a Bruker-Nonius Apex 2 CCD camera on κ-goniostat diffractometer using graphite-monochromated Mo-K_α radiation (λ = 0.71073 Å). Data for compounds **4.59**, **4.79** and **4.122** were collected using a Bruker SMART 1000 CCD diffractometer using graphite-monochromated Mo-K_α radiation (λ = 0.71073 Å).

All structures were solved by direct methods (except structures **4.33**, **4.89**, **4.90** and **4.113** which were solved using Patterson synthesis) and refined by full-matrix least-squares methods on F^2. All *H* atoms were placed in geometrically calculated positions and were refined using a riding model (aryl C–H 0.95 Å, methyl C–H 0.98 Å, methylene C–H 0.99 Å and hydroxyl O–H 0.84 Å). $U_{iso}(H)$ values were set to be 1.2 times U_{eq} of the carrier atom for aryl C*H* and N*H*, and 1.5 times U_{eq} of the carrier atom for O*H* and CH_3. The hydroxyl hydrogen atom in compound **4.92** could not be located due to the poor quality of the diffraction data. The coordinates of O*H* and NH hydrogen atoms in compounds **4.55**, **4.59**, **4.60**, **4.65**, **4.67**, **4.79**, **4.109**, **4.115** and **4.117** were allowed to refine freely.

Unless stated below, all structural determinations proceeded without the need for restraints or disorder modelling. Compound **4.22** was found to contain a disordered methanol and was modelled over two sets of positions, each at half weight. Methanolic H(2) and H(2X) atoms in **4.22** were located in the difference Fourier map and the coordinates allowed to freely refine. The remaining O*H* hydrogen atoms were placed in geometric positions.

Compound **4.30** was modelled with disorder in the DMSO molecule with atoms split over two sets of positions [72.6(6):27.4(6)%] with the C(33) coincident for both components and restraints were placed on the geometry and the anisotropic displacement parameters of the atoms involved.

Compounds **4.41** and **4.64** were found to contain a disordered phenyl ring which was modelled with atoms split over two sets of positions [major occupancy 50.4(4)%] and [56.5(17)%] respectively and restraints were placed on the geometry and the anisotropic displacements parameters of the atoms involved.

Compounds **4.35** and **4.118** were found to contain disorder in one chloroform molecule, while in **4.118** the Cl_3H_2 fragment was modelled split over two sets of positions, with refined occupancies 85.4(4):14.6(4)% with C(33) coincident to the two fragments; in **4.35** the solvent molecule was modelled across two alternative positions without any coincident atoms [56.9(7):43.1(7)%].

Compound **4.91** was found to be highly disordered; the backbone and functionalised methyl-/hydroxyl- arene group were modelled with atoms split over two sets of positions, with refined occupancies 51.1(7):48.9(7)% without any coincident atoms across the two alternative positions.

Compound **4.89** contained three disordered phenyl groups; one modelled with three consecutive coincident atoms across the two sets of positions [major occupancy 51.1(12)%] and two with only two C atoms coincident [major occupancy 53.4(12) and 52.2(2)%] respectively. Restraints on the geometric and anisotropic displacement parameters were used on the three phenyl rings. The refinement of **4.122** led to the

modelling of two of the three chloroform molecules as disordered, the Cl_3H_2 fragment was modelled over two sets of positions, with major occupancies 85.1(4) and 63.8(5)% with C(50) and C(51) coincident to the two fragments, respectively.

The structure of compound **4.124** contains solvent-accessible voids accounting for 9.5% of the total unit cell volume. The SQUEEZE program within Platon suite identified approximatly 70 unaccounted electrons in the unit cell, and this was assumed to be four methanol molecules per cell (18 electrons per molecule) which were taken into account in the refinement.[48]

Programs used during data collection, refinement and production of graphics were Bruker SMART, Bruker APEX 2, SAINT, SHELXTL, COLLECT, DENZO and local programs.[25,26,28,121-123]

Chapter 5

Synthesis and Supramolecular Coordination Chemistry of New H-bonded Functionalised Phosphines

5. Synthesis and Supramolecular Coordination Chemistry of New H-bonded Functionalised Phosphines

5.1 Introduction

The process of catalyst discovery and development is the most important tool to obtain effective transition-metal catalysis. However, this process has suffered from the difficult access to structurally diverse and large libraries of ligands. A new approach to this problem has been the use of structurally less complicated monodentate ligands that self-assemble in the coordination sphere of the metal centre through non-covalent attractive ligand-ligand interactions to generate bidentate, chelating ligands.[257-260] Irrespective of the strength of the ligand-ligand interaction, from weak van der Waals, π stacking, charge-transfer, and dipole-dipole interactions to hydrogen bonding, the specific formation of heterodimeric ligands requires two different sets of monodentate ligands with complementary binding sites.[261] A brief survey of monodentate phosphine ligands used in homogeneous catalysis is discussed below.

5.1.1 Weak Ligand-Ligand Interactions: van der Waals, π Stacking and Dipole-Dipole Interactions

Reetz and co-workers reported a Pt(II) complex with a binol-derived phosphonite ligand. Interestingly, the two monodentate phosphorus ligands coordinated in a *cis* orientation around the Pt(II) centre, which is supposed to be sterically less favourable than the alternative *trans* orientation. The formation of the *cis* complex may be explained by the establishment of weak attractive ligand-ligand interactions based on van der Waals, π stacking, and/or dipole-dipole interactions of the P–O bond dipoles. As a consequence of the *cis* coordination mode, a conformational locking of the two monodentate ligands is achieved mimicking the conformational properties of a bidentate ligand. Reetz and co-workers have reported the asymmetric hydrogenation of *N*-acyl enamines using the homocombination of two monodentate ligands **5.1–5.4** (Equation 5.1).[262-265]

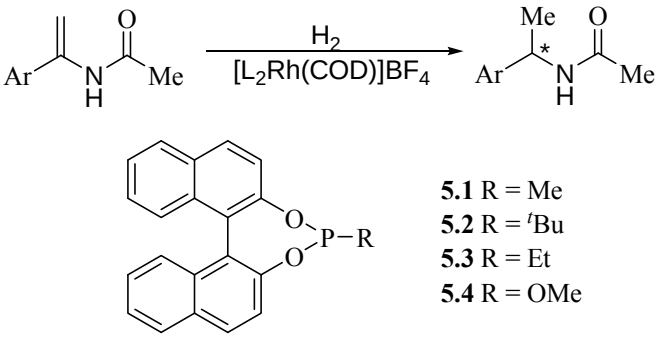

Equation 5.1

5.1.2 Attractive Ligand-Ligand Interactions through Hydrogen Bonding

Breit and Seiche described the *in situ* generation of bidentate ligands based on self-assembly through hydrogen bonding of monodentate ligands in the coordination sphere of a Rh(I) centre.[266] The Rh(I) catalyst displayed the behaviour of a bidentate ligand in the hydroformylation of terminal alkenes (Equation 5.2).

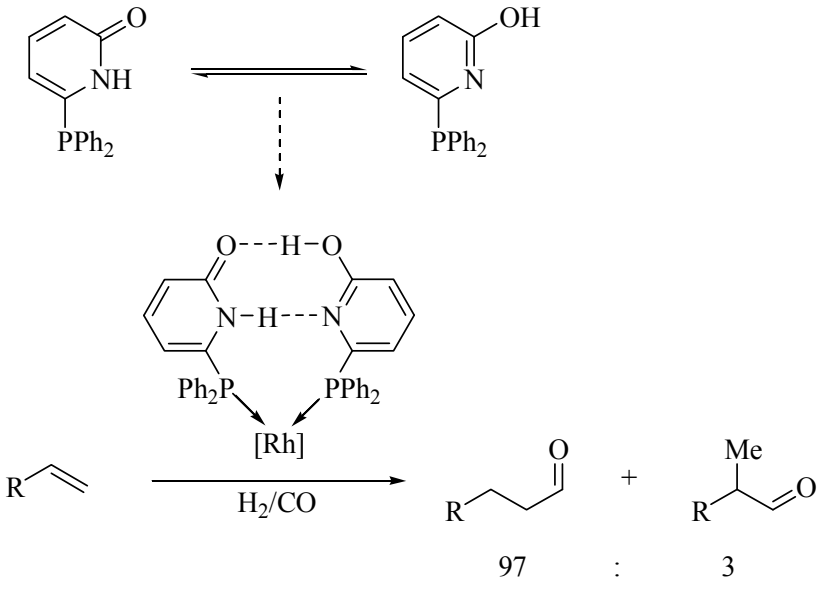

Equation 5.2

Excellent regioselectivity in favour of the linear aldehyde was obtained for hydroformylation of a range of functionalised terminal alkenes such as R = $Br(CH_2)_3$–, $AcO(CH_2)_3$–, $MeO_2C(CH_2)_7$–, $MeCO(CH_2)$–, $HO(CH_2)$–, $HO(CH_2)_8$–. The hydrogen-

bonding network in the ligands and thus the chelating binding mode can be disrupted by employing either temperatures above 110°C or protic solvents such as methanol and acetic acid resulting in lower regioselectivities.

5.1.3 Attractive Ligand-Ligand Interactions through Coordinative Bonding

Reek and van Leeuwen used Zn(II) porphyrin complexes for the supramolecular construction of bidentate ligands (Figure 5.1).[267]

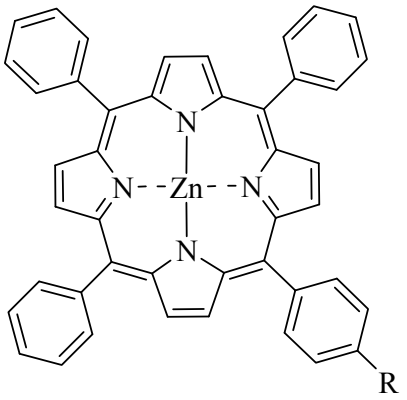

Figure 5.1 Zn(II) porphyrin complexes.

A set of Zn(II) porphyrin functionalised phosphites, **5.13**-**5.18**, and eight monodentate phosphorus donor ligands equipped with N-donor functions, **5.5**-**5.12**, were used by Slagt and co-workers to generate a library of chelating ligands (Figure 5.2).[268]

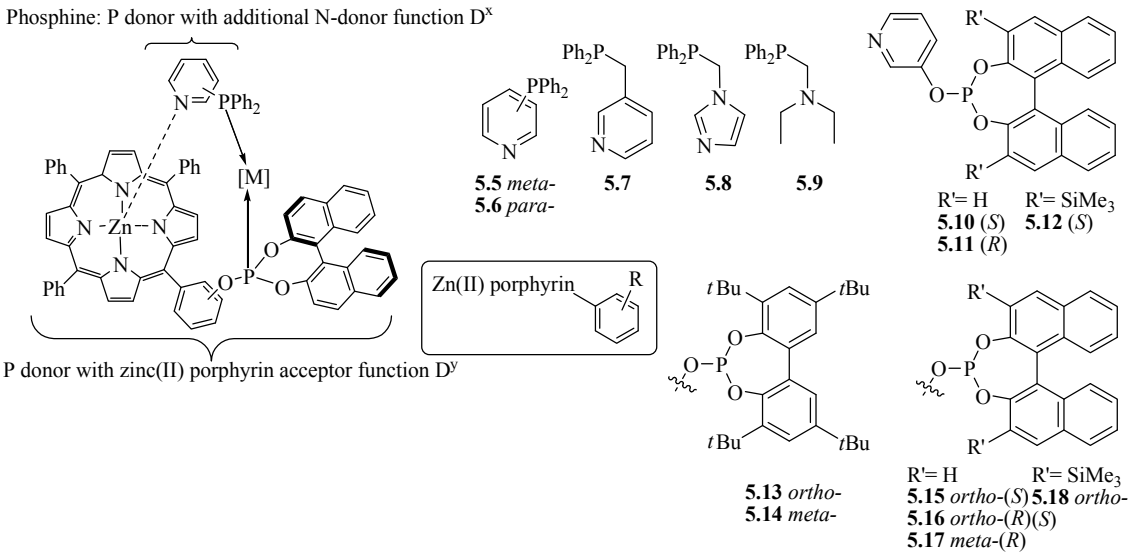

Figure 5.2 Library of heterodimeric bidentate ligands.

These combinations were tested by application to the asymmetric allylic alkylation of 1,3-diphenylallyl acetate (Equation 5.3).

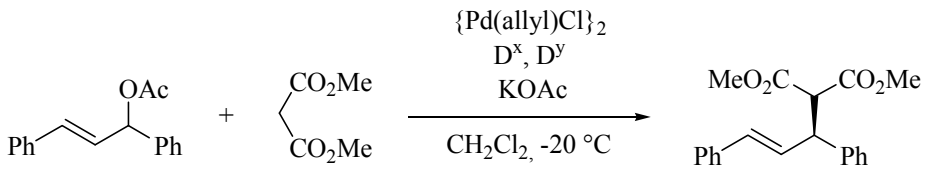

Equation 5.3

The best heterodimer combinations were **5.5**·**5.15** and **5.5**·**5.16** which gave up to 60% *ee* of either the *R* or *S* product depending on the absolute configuration of the ligand employed. Optimal enantioselectivities (96-97% *ee*) were obtained for the monodentate Zn(II)-porphyrin substituted phosphite ligands **5.15** and **5.16**.

The chemistry in Chapter V explores the synthesis of new phosphorus donor ligands and their coordination studies with a range of metal centres such as Pt(II) and Cu(I). This work and any future phosphorus donor ligands generated by this approach may have important uses in coordination chemistry and in supramolecular based homogeneous catalysis.

5.2 Test Reactions Leading to Ideas for Future Work

The unexpected monodentate phosphine ligand 2-amino-3-CH_2PPh_2-4-1*H*-quinolinone **5.19** was synthesised using a Mannich-based condensation reaction which is an efficient and versatile method for the synthesis of phosphine ligands. One equivalent of Ph_2PCH_2OH was reacted with one equivalent of 2-amino-4-1*H*-quinolinone in MeOH yielding the mono(phosphino) ligand after 3 h under reflux and N_2 (Equation 5.4). The solution was concentrated under reduced pressure and a white crystalline solid **5.19** was filtered off. This compound was found to be air stable in the solid state, but oxidised quickly in solution. Interestingly, the expected Mannich condensation proceeding at the primary amine group yielding the mono(phosphino) ligand **5.20** was not observed here.

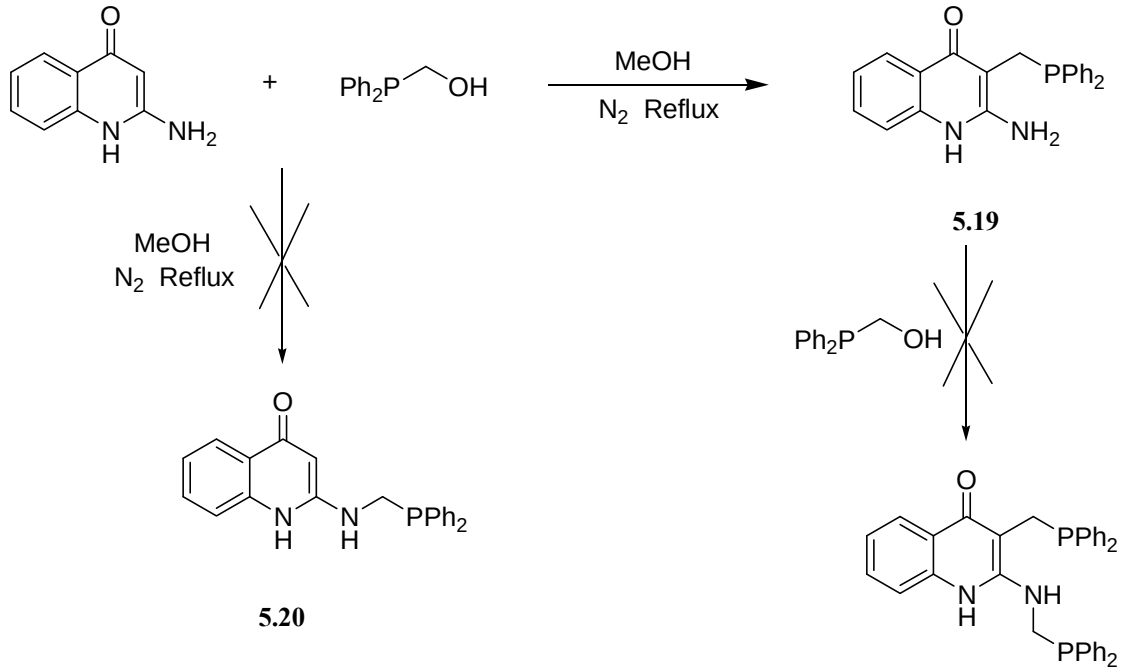

Equation 5.4

Compound **5.19** was obtained in a 70% yield and exhibits a single resonance in its $^{31}P\{^1H\}$ NMR spectrum ($(CD_3)_2SO$) at δ(P) −19.05 ppm. This ligand was also characterised by ^1H NMR spectroscopy, data obtained supporting the condensation at the 3-position of the quinolinone ring as inferred from the presence of an N*H* signal from the primary amine (Experimental Section).

Condensation of a second Ph_2PCH_2OH (1eq) on the free primary amine site in **5.19** failed to produced the desired phosphine ligand yielding only starting material (Equation 5.4).

5.2.1 Crystal Structure of Compound 5.19

X-ray quality crystals for compound **5.19** were obtained by slow evaporation of the methanol filtrate and included one methanol solvent molecule per ligand in the structure (Figure 5.3). The two ligand molecules in the asymmetric unit crystallise in two different conformations.

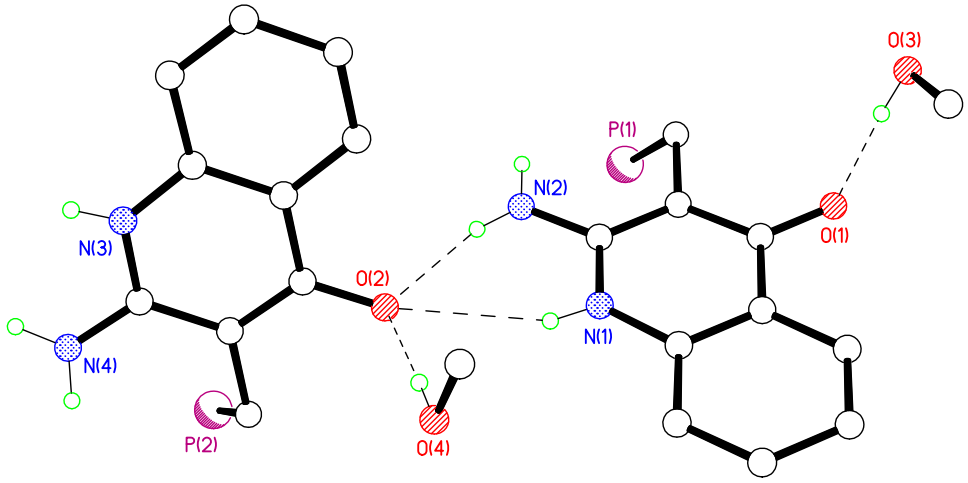

Figure 5.3 View of the asymmetric unit of **5.19**. Phenyl groups and hydrogen atoms except N*H* and O*H* have been omitted for clarity.

Each molecule of **5.19** is hydrogen bonded to two symmetry related molecules through N–H···O interactions forming perpendicular stacked layers. Neighbouring layers close-pack to form cavities within which the solvent molecules reside (Figure 5.4). Selected hydrogen bonding parameters for **5.19** are shown in Table 5.1.

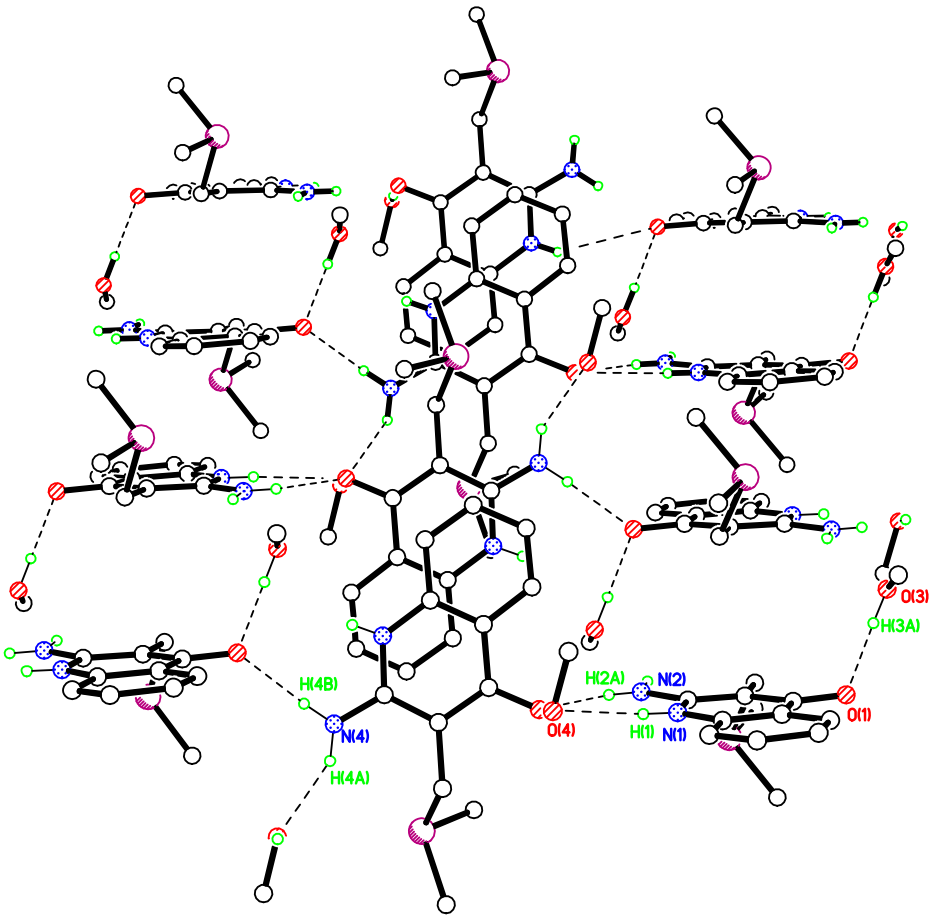

Figure 5.4 View of the hydrogen bonding motifs in compound **5.19**. Phenyl groups and hydrogen atoms except O*H* and N*H* have been removed for clarity.

Table 5.1 Selected hydrogen bonding parameters for **5.19**.

D–H···A	D···A/Å	D–H/Å	H···A/Å	D–H···A/°
N(1)–H(1)···O(2)	3.178(3)	0.793(17)	2.46(2)	150(3)
N(2)–H(2A)···O(2)	2.823(3)	0.82(3)	2.02(3)	167(3)
N(2)–H(2B)···O(3)^{i}	3.026(4)	0.84(3)	2.39(3)	134(3)
N(3)–H(3)···O(3)^{ii}	3.176(4)	0.757(18)	2.48(2)	154(3)
N(4)–H(4B)···O(1)^{ii}	2.848(3)	0.84(4)	2.01(4)	174(3)
O(4)–H(4A)···O(4)^{iii}	2.935(4)	0.87(3)	2.14(4)	152(3)
O(3)–H(3^{a})···O(1)	2.590(3)	0.84	1.75	175.1
O(4)–H(4)···O(2)	2.667(3)	0.84	1.83	178.3

Symmetry operations: ^{i}-x+1, -y+1, -z+1, ^{ii}x, y, z+1, ^{iii} –x, -y+1, -z+2.

5.2.2 Coordination Chemistry of 2-amino-3-CH_2PPh_2-4-1*H*-quinolinone 5.19

5.n Syntheses of Square Planar Pt(II) Complexes 5.21 and 5.22

The synthesis of complex Pt(**5.19**)$_2Cl_2$ **5.21** was achieved by stirring a suspension of **5.19** and $PtCl_2$(COD) in CH_2Cl_2 for 1.5 h, to displace the cyclooctadiene ligand (Equation 5.5). The product was isolated in 73% yield, as a white precipitate obtained upon reduction of the volume of solvent *in vacuo* and addition of Et_2O. The isolated product **5.21** was treated with ^{t}BuOK in MeOH for 1 h under reflux yielding the *P*,*N*-bidentate chelate complex **5.22** as colourless crystals after cooling the solution.

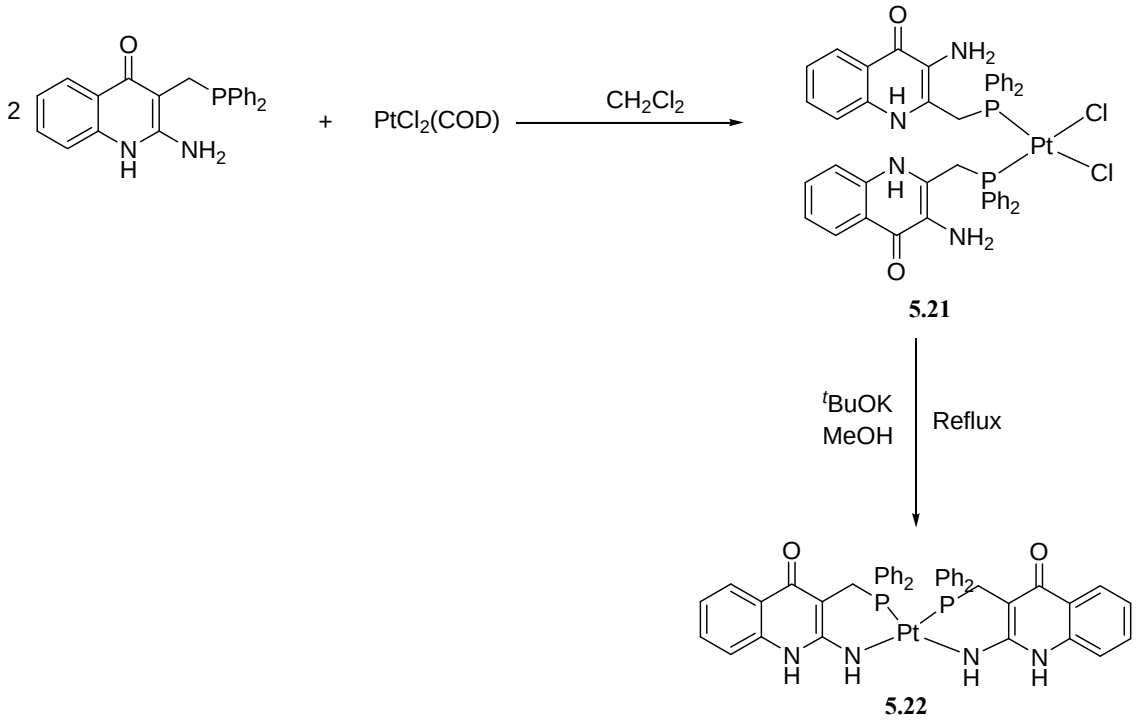

Equation 5.5

The coupling constant ^1J(PtP) for **5.21** is approximately 3300 Hz, which indicates that this complex is in a *cis* conformation. Compound **5.21** exhibits the characteristic strong ν(NH) absorption in the range 3350-2800 cm^{-1} and also a strong band at 1633 cm^{-1} indicative of ν(C=O). Crystals of **5.22** were obtained by slow evaporation of the methanolic solution and analysed by single X-ray diffraction. Further work would

clearly be required in order to obtain the characterisation of **5.22** by IR, NMR, mass spectrometry and microanalysis methods.

Compound **5.22** crystallised from the slow evaporation of a methanolic solution including one water molecule per complex. The diffraction data was collected using synchrotron radiation on station 9.8 at the SRS, Daresbury Laboratory, due to the small crystal dimensions. PLATON SQUEEZE was used to determine that 74 electrons were present in the unit cell unaccounted for in the point atom model.[103] This approximated well to four very highly disordered MeOH molecules per unit cell. Ligand **5.22** acts as a bidentate ligand through the amino-N and the P atoms (Figure 5.5). The two phosphorus atoms are *cis* coordinated at the Pt(II) centre, which is supposed to be a sterically less favourable arrangement than the alternative *trans* orientation.

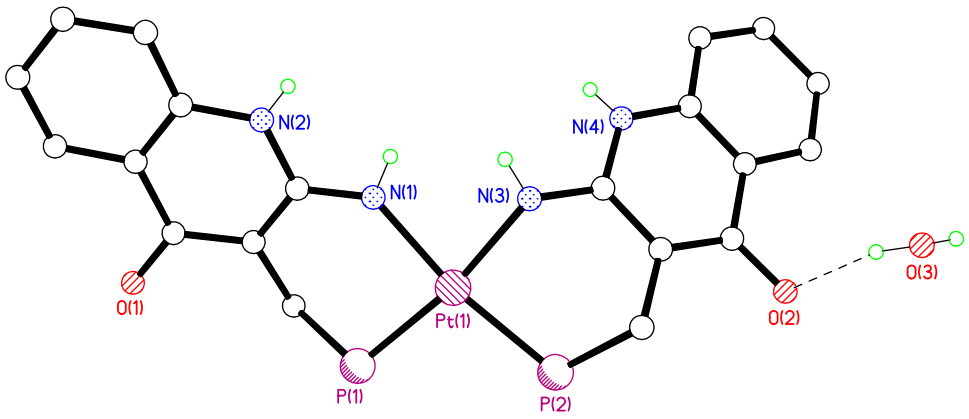

Figure 5.5 View of the asymmetric unit of **5.22**. Phenyl groups and hydrogen atoms except N*H* and O*H* have been omitted for clarity.

Each **5.22** molecule forms a trifurcated N–H···O hydrogen bond with a symmetry related Pt(II) complex (Figure 5.6). The water molecules extend the dimensionality of the structure by linking **5.22** into a three-dimensional supramolecular array through N–H···O(water) and (water)O–H···O hydrogen bonds (Table 5.2).

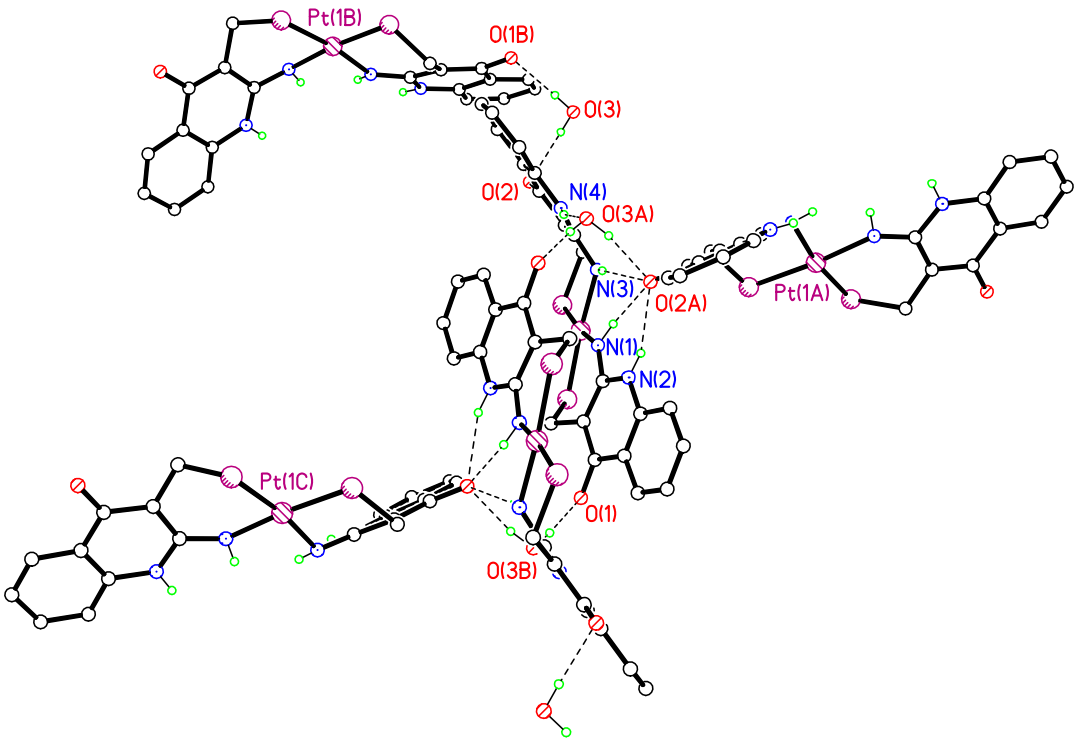

Figure 5.6 View of the hydrogen bonding motifs in compound **5.22**. Phenyl groups and hydrogen atoms except O*H* and N*H* have been removed for clarity.

Table 5.2 Selected hydrogen bonding parameters for **5.22**.

D–H···A	D···A/Å	D–H/Å	H···A/Å	D–H···A/°
N(1)–H(1)···O(2A)^{i}	2.874(3)	0.88(3)	2.01(3)	170(3)
N(3)–H(3)···O(2A)^{i}	3.204(3)	0.77(3)	2.48(3)	156(3)
N(2)–H(2)···O(2A)^{i}	3.001(4)	0.84(3)	2.26(3)	148(3)
N(4)–H(4)···O(3A)^{i}	2.790(3)	0.74(3)	2.08(3)	163(4)
O(3)–H(3A)···O(1B)^{ii}	2.715(3)	0.83(4)	1.89(4)	174(4)
O(3)–H(3B)···O(2)	2.775(3)	0.85(4)	1.94(4)	167(4)

Symmetry operations: ^{i}y-1/4, -x+3/4, z-1/4, ^{ii}y-1/4, -x+1/4, -z+1/4.

5.3 Further Investigation of Copper(I) Complexes

Preliminary investigations have been carried out into the coordination of the mono(phosphine) ligand **5.23**, synthesised within the Smith group, to the $[Cu(PPh_3)_2]^+$ fragment. One equivalent of **5.23** was reacted with one equivalent of $Cu(PPh_3)_2(BH_4)$.

The reaction was performed at r.t. in CH_2Cl_2 and under N_2 because **5.23** is air-sensitive (Equation 5.6).

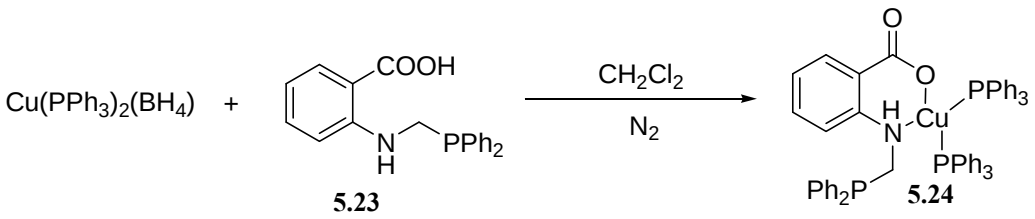

Equation 5.6

It was anticipated that **5.23** would adopt a similar coordination mode to that observed in Chapter II for the range of pyridine- and pyrazine-carboxylic acids studied. Therefore in the expected compound **5.24** the copper(II) ion is bonded to two triphenylphosphine ligands and chelated to one **5.23** ligand through the amine nitrogen and carboxylate oxygen atoms.

Interestingly, crystals obtained from slow vapour diffusion of diethyl ether into a methanol/dichloromethane solution of the solid obtained in Equation 5.6, exhibit an unexpected dimeric crystal structure **5.25** (Figure 5.7). Two deprotonated $[Ph_2PCH_2NHC_6H_4(2\text{-}CO_2)]^-$ ligands bridge two copper(I) ions, with a distance of 5.087 Å between symmetry-related copper ions, forming a fourteen-membered metallomacrocycle. The two carboxylate oxygen atoms act as a bidentate ligand being coordinated to the metal forming a four-membered chelated ring. The dimer is stabilised by two strong N–H···O(carboxylate) hydrogen bonds, one within each ligand (Table 5.3).

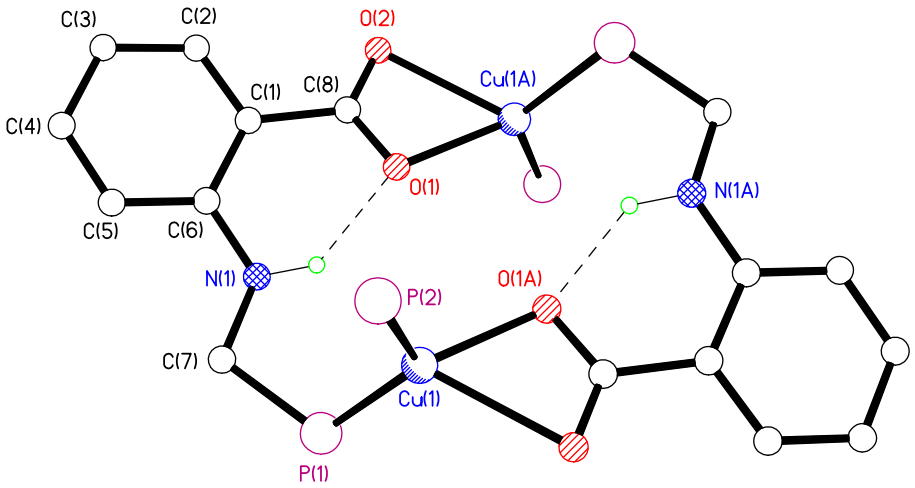

Figure 5.7 View of $(PPh_3)_2Cu_2\{Ph_2PCH_2NHC_6H_4(2\text{-}CO_2)\}_2$ **5.25**.
Phenyl groups and hydrogen atoms except N*H* have been removed for clarity.

Table 5.3 Selected hydrogen bonding parameters for **5.25**.

D–H···A	D···A/Å	D–H/Å	H···A/Å	D–H···A/º
N(1)–H(1)···O(1)	2.667(3)	0.91(3)	1.91(3)	140(3)

A selection of key bond lengths is given in Table 5.4. The Cu–P interatomic distances and P–Cu–P angle [125.16(3)º] are similar to those previously seen for almost all the complexes of copper(I) with pyridine and pyrazine carboxylic acids studied. The different Cu–O bonds lengths for the chelate ring suggest that the carboxylate group is not delocalised. The ligand O(1)–Cu(1)–O(2) bite angle is 57.82(8)º, smaller than previously found in Chapter II, (79.77-80.16º), in accord with the formation of a four-membered ring.

Table 5.4 Selected bond lengths (Å) for **5.25**.

	Cu(1)–P(1)	Cu(1)–P(2)	Cu(1)–O(1)	Cu(1)–O(2)
5.25	2.2278(8)	2.2533(8)	2.069(2)	2.414(2)

The crystal structure of the compound reveals that one molecule of triphenylphosphine per metal centre has been displaced by a carboxylate moiety leading to the formation of the dimer. The crystals of **5.25** were obtained only once; in several other attempts, the crystals obtained were of triphenylphosphine alone. The crude material was cleaned several times with diethyl ether, but the crystallisation of **5.25** failed to give any further crystals. Characterisation of the crude material also failed to show which products were obtained in this reaction showing a mixture of non-identified by-products. Further work would clearly be required in order to fully understand the chemistry presented here.

5.4 Experimental

5.4.1 Characterisation Data

Compound 5.19

A mixture of hydroxymethyldiphenylphosphine (1 eq, 0.466 g) and 2-amino-4-1*H*-quinolinone (1 eq, 0.347 g) in methanol (20 ml) was refluxed under N_2 for 3 h. The volume of the solution obtained was evaporated to *ca*. 10 ml under reduced pressure and a white crystalline solid was obtained. The suspension was stirred for 10 min. The white solid obtained was collected by suction filtration and dried *in vacuo*.

Yield: 0.539 g, 70%.

IR υ_{max} (KBr)/cm^{-1} 3345.2–2870.2 (N−H), 1634.6 (C=O), 740.9 and 692.3 (Ar C−H).

^{1}H NMR (400 MHz, $CDCl_3$) δ 7.32-7.19 (12H, m, Ar C−H), 6.24 (2H, bs, Ar C−H), 3.42 (1H, s, NH), 2.84 (2H, s, NH_2), 2.50 (2H, s, CH_2) ppm.

^{31}P NMR data: δ -19.05 ppm.

Analysis calculated for $C_{22}H_{18}N_2OP$: C, 73.73; H, 5.34; N, 7.82. Found: C, 73.94; H, 5.08; N, 7.84%.

m/z 359 $[C_{22}H_{18}ON_2P]^+$.

Compound 5.21

To a solution of $PtCl_2$(COD) (0.053 g) in dichloromethane (5 ml) was added a solution of **5.19** (0.102 g) in dichloromethane (5 ml). The pale colourless solution was stirred for 1.5 h at r.t., the solution was evaporated to *ca*. 2-3 ml under reduced pressure and diethyl ether (10 ml) added. The suspension was stirred for 10 min. The white solid obtained was collected by suction filtration and dried *in vacuo*.

Yield: 0.122 g, 73%.

IR υ_{max} (KBr)/cm^{-1} 3353.4–2863.2 (N−H), 1632.8 (C=O), 740.7 and 690.5 (Ar C−H).

^{1}H NMR (400 MHz, $(CD_3)_2SO$) δ 12.73 (2H, s, NH), 7.57-7.25 (28H, m, Ar C−H), 5.46 (2H, s, NH), 2.51 (4H, s, CH_2) ppm.

^{31}P NMR data: δ 20.57 ppm, $^1J_{PtP}$ 3297.8 Hz.

Analysis calculated for $C_{44}H_{38}N_4O_2P_2Cl_2Pt{\cdot}CH_2Cl_2$: C, 50.62; H, 3.78; N, 5.25. Found: C, 51.02; H, 3.92; N, 5.29%.
m/z $[PtC_{44}H_{38}O_2N_4P_2Cl_2]^+$: 910 $[M^+$-2Cl].

Compound 5.22

The isolated product **5.21** (0.043 g) was then treated with ^{t}BuOK (2.5 eq, 0.016 g) in MeOH (10 ml). The solution obtained was refluxed for 1 h yielding **5.22** as white crystals after cooling the solution.
Yield: 0.029 g, 87%.

Compound 5.25

Under nitrogen, a solution of $Ph_2PCH_2NHC_6H_4(2\text{-}CO_2H)$ **5.23** (1 eq, 0.048 g) and $Cu(PPh_3)_2(BH_4)$ (1 eq, 0.087 g) in dichloromethane (10 ml) was stirred for 24 h. The solvent was evaporated to dryness under reduced pressure to give a crystalline yellow solid. Diethyl ether (20 ml) was added to the solid and the mixture was stirred at room temperature for 30 min. The solid was filtered and dried yielding a yellow solid. Yield 0.087 g, 66%.

X-ray quality crystals of **5.25** were grown by the vapour diffusion of diethyl ether into a methanol/dichloromethane solution of the yellow solid obtained in the synthesis described above.

5.5 Crystallographic Experimental

Data for compound **5.19** was collected using a Bruker APEX 2 CCD diffractometer using graphite-monochromated Mo-K_α radiation (λ = 0.71073 Å). Data for compound **5.22** was collected using a Bruker APEX 2 CCD diffractometer using synchrotron radiation (λ = 0.6943 Å) at Daresbury SRS Station 9.8. Data for compound **5.25** was collected using a Bruker-Nonius 95 mm CCD camera on κ-goniostat diffractometer using graphite-monochromated Mo-K_α radiation (λ = 0.71073 Å).

All the structures were solved by direct methods and refined by full-matrix least-squares methods on F^2. All *H* atoms were placed in geometrically calculated positions and were refined using a riding model (aryl C–H 0.95 Å). $U_{iso}(H)$ values were set to be 1.2 times U_{eq} of the carrier atom for aryl and 1.5 times U_{eq} of the carrier atom for CH_3. The coordinates of O*H* and N*H* hydrogen atoms in all compounds were allowed to refine freely apart from O3 and O4 coordinates of O*H* hydrogen atoms in **5.19** which were placed in geometrically calculated positions and were refined using a riding model (hydroxyl O–H 0.84 Å). $U_{iso}(H)$ values were set to be 1.5 times U_{eq} of the carrier atom for O*H*.

Compound **5.19** was found to contain a disordered phenyl ring, and was modelled over two sets of positions 75.5(12):24.5(12)% with C(11) and C(14) common for both rings.

Programs used during data collection, data reduction, refinement and production of graphics were Bruker SMART, Bruker APEX 2, SAINT, SHELXTL, COLLECT, DENZO and local programs.[25,26,28,121-123]

References

[1] J.-M. Lehn, *Angew. Chem. Int. Ed. Engl.*, 1988, **27**, 89-112.

[2] J.-M. Lehn, M. Mascal, A. Decian and J. Fischer, *J. Chem. Soc., Chem. Commun.*, 1990, 479-481.

[3] C.L.D. Gibb and B.C. Gibb, *J. Supramol. Chem.*, 2001, **1**, 39-52.

[4] J.W. Steed and J.L. Atwood, Supramolecular Chemistry, Wiley, 2000.

[5] G.R. Desiraju, *Angew. Chem. Int. Ed. Engl.*, 1995, **34**, 2311-2327.

[6] P. Vishweshwar, A. Nangia and V.M. Lynch, *J. Org. Chem.*, 2002, **67**, 556-565.

[7] G.A. Jaffrey, An Introduction to Hydrogen Bonding, OUP, New York, 1997.

[8] S. Subramanian and M.J. Zaworotko, *Coord. Chem. Rev.*, 1994, **137**, 357-401.

[9] C.B. Aakeröy, and K.R. Seddon, *Chem. Soc. Rev.*, 1993, 397-407.

[10] G.R. Desiraju and T. Steiner, The Weak Hydrogen Bond, OUP, Oxford, 1999.

[11] G. Gilli and P. Gilli, *J. Mol. Struct.*, 2000, **552**, 1-15.

[12] F.H. Allen, W.D.S. Motherwell, P.R. Raithby, G.P. Shields and R. Taylor, *New J. Chem.*, 1999, **23**, 25-34.

[13] G.R. Desiraju, *Chem. Commun.*, 1997, 1475-1482.

[14] M.J. Zaworotko, *Angew. Chem. Int. Ed. Engl.*, 2000, **39**, 3052-3054.

[15] A. Gavezzotti, *Acc. Chem. Res.*, 1994, **27**, 309-314.

[16] R.W. Lancaster, P.G. Karamertzanis, A.T. Hulme, D.A. Tocher, D.F. Corey and S.L. Price, *Chem. Commun.*, 2006, 4921-4923.

[17] A.T. Hulme, A. Johnston, A.J. Florence, P. Fernandes, K. Shankland, C.T. Bedford, G.W.A. Welch, G. Sadiq, D.A. Haynes, W.D.S. Motherwell, D.A. Tocher and S.L. Price, *J. Am. Chem. Soc.*, 2007, **129**, 3649-3657.

[18] M.C. Etter, J.C. McDonald and J. Bernstein, *Acta Cryst.*, 1990, **B46**, 256-262.

[19] M.C. Etter, *Acc. Chem. Res.*, 1990, **23**, 120-126.

[20] G.M. Frankenbach and M.C. Etter, *Chem. Mater.*, 1992, **4**, 272-278.

[21] F. Allen, *Cryst. Rev.*, 2004, **10**, 3-15.

[22] The United Kingdom Chemical Database Service: D.A. Fletcher, R.F. McMeeking and D. Parkin, *J. Chem. Inf. Comput. Sci.*, 1996, **36**, 746-749.

[23] A.D. Bond, *CrystEngComm*, 2007, **9**, 833-834.

[24] M.J. Zaworotko, *Cryst. Growth Des.*, 2007, **7**, 4-9.

[25] Bruker SMART Version 5.611. Bruker AXS Inc., Wisconsin, USA, 2001.

[26] Bruker-Nonius, Wiscosin, USA, Area-Detector Integration Software, APEX-II, Version V1, 2004.

[27] B. McMeeking, and D. Fletcher, *The CrystalWeb database interface*, http://cds.dl.ac.uk/report/res_high2002_2003/McMeeking_and_Fletcher.pdf.

[28] SAINT Version 6.02a. Bruker AXS Inc., Wisconsin, USA, 2001.

[29] G.M. Sheldrick, *SADABS*, 2004, Version 2004/2001. University of Göttingen, Germany.

[30] G.M. Sheldrick, *Acta Cryst. A*, 2008, 112-120.

[31] G.M. Sheldrick, *SHELXTL user manual*, 2000, **version 6.10**, Bruker AXS Inc. Madison, WI.

[32] S.-I. Noro, H. Miyasaka, S. Kitagawa, T. Wada, T. Okubo, M. Yamashita and T. Mitani, *Inorg. Chem.*, 2005, **44**, 133-146.

[33] R. Clérac, H. Miyasaka, M. Yamashita and C. Coulon, *J. Am. Chem. Soc.*, 2002, **124**, 12837-12844.

[34] H. Kitagawa, N. Onodera, T. Sonoyama, M. Yamamoto, T. Fukawa, T. Mitani, M. Seto and Y. Maeda, *J. Am. Chem. Soc.*, 1999, **121**, 10068-10080.

[35] D. Braga, F. Grepioni and G.R. Desiraju, *Chem. Rev.*, 1998, **98**, 1375-1406.

[36] M. Fujita, Y.J. Kwon, S. Washizu and K. Ogura, *J. Am. Chem. Soc.*, 1994, **116**, 1151-1152.

[37] B.F. Abrahams, S.R. Batten, H. Hamit, B.F. Hoskins and R. Robson, *Angew. Chem. Int. Ed. Engl.*, 1996, **35**, 1690-1692.

[38] A.M. Beatty, *CrystEngComm*, 2001, **51**, 1-13.

[39] M.J. Zaworotko, *Chem. Commun.*, 2001, 1-9.

[40] G. Beobide, O. Castillo, U. García-Couceiro, J.P. García-Terán, A. Luque, M. Martínez-Ripoll and P. Román, *Eur. J. Inorg. Chem.*, 2005, 2586-2589.

[41] G. Beobide, O. Castillo, U. García-Couceiro, J.P. García-Terán, A. Luque and P. Román, *Inorg. Chem.*, 2006, **45**, 5367-5382.

[42] J. Luo, B. Alexander, T.R. Wagner and P.A. Maggard, *Inorg. Chem.*, 2004, **43**, 5537-5542.

[43] H. Yin and S.-X. Liu, *Polyhedron*, 2007, **26**, 3103-3111.

[44] B.O. Patrick, C.L. Stevens, A. Storr and R.C. Thompson, *Polyhedron*, 2005, **24**, 2242-2249.

[45] B.O. Patrick, C.L. Stevens, A. Storr and R.C. Thomson, *Polyhedron*, 2003, **22**, 3025-3035.

[46] F.H. Allen, *Cryst. Rev.*, 2004, **10**, 3-15.

[47] W. Yang, H. He and D.G. Drueckhammer, *Angew. Chem. Int. Ed. Engl.*, 2001, **40**, 1714-1718.

[48] W. Lin, M.E. Chapman, Z. Wang, and G.T. Yee, *Inorg. Chem.*, 2000, **39**, 4169-4173.

[49] L.-M. Zheng, X. Wang and A.J. Jacobson, *J. Solid State Chem.*, 2000, **152**, 174-182.

[50] F. Cariati, L. Naldini and A. Panzanelli, *Inorg. Chim. Acta*, 1983, **69**, 117-122.

[51] M.A.S. Goher and T.C.W. Mak, *Inorg. Chim. Acta*, 1985, **101**, L27-L30.

[52] M.A.S. Goher and T.C.W. Mak, *Inorg. Chim. Acta*, 1987, **127**, L13-L16.

[53] F. Bottomley, E. Hahn, J. Pickardt, H. Schumann, M. Mukaida and H. Kakihana, *J. Chem. Soc., Dalton Trans.*, 1985, 2427-2431.

[54] M.C. Barral, R. Jimenez-Aparicio, E.C. Poyer, M.J. Saucedo, F.A. Urbanos, E. Gutiérrez-Puebla and C. Ruíz-Valero, *J. Chem. Soc., Dalton Trans.*, 1991, 1609-1613.

[55] A.-Q. Wu, G.-H. Guo, C. Yang, F.-K. Zheng, X. Liu, G.-C. Guo, J.-S. Huang, Z.-C. Dong and Y. Takano, *Eur. J. Inorg. Chem.*, 2005, 1947-1954.

[56] D. Min, S.S. Yoon, D.-Y. Jung, C.Y. Lee, Y. Kim, W.S. Han and S.W. Lee, *Inorg. Chim. Acta*, 2001, **324**, 293-299.

[57] J.W. Moore, M.D. Glick, and J. W. A. Baker, *J. Am. Chem. Soc.*, 1972, **94**, 1858-1865.

[58] G. Smith, A.N. Reddy, K.A. Byriel and C.H. Kennard, *Polyhedron*, 1994, **13**, 2425-2430.

[59] A.D. Burrows, M.F. Mahon and M.T. Palmer, *J. Chem. Soc., Dalton Trans.*, 1998, 1941-1942.

[60] O.R. Evans, R.-G. Xiong, Z. Wang, G.K. Wong and W. Lin, *Angew. Chem. Int. Ed. Engl.*, 1999, **38**, 536-538.

[61] W. Lin, O.R. Evans, R.-G. Xiong and Z. Wang, *J. Am. Chem. Soc.*, 1998, **120**, 13272-13273.

[62] O.R. Evans, Z. Wang, R.-G. Xiong, B.M. Foxman and W. Lin, *Inorg. Chem.*, 1999, **38**, 2969-2973.

[63] C.-W. Yeh, M.-C. Suen, H.-L. Hu, J.-D. Chen and J.-C. Wang, *Polyhedron*, 2004, **23**, 1947-1952.

[64] M.E. Chapman, P. Ayyappan, B.M. Foxman, G.T. Yee and W. Lin, *Cryst. Growth Des.*, 2001, **1**, 159-163.

[65] H.S. Huh and S.W. Lee, *J. Mol. Struct.*, 2007, **829**, 44-50.

[66] M.A.S. Goher and T.C.W. Mak, *Inorg. Chim. Acta*, 1988, **141**, 323.

[67] P. Naumov, G. Jovanovski, M.G.B. Drew and S.W. Ng, *Inorg. Chim. Acta*, 2001, **314**, 154-162.

[68] J.-H. Yu, J.-Q. Xu, L. Ye, H. Ding, W.-J. Jing, T.-G. Wang, J.-N. Xu, H.-B. Jia, Z.-C. Mu and G.-D. Yang, *Inorg. Chem. Commun.*, 2002, **5**, 572-576.

[69] R.K. Barman, S.K. Singh and B.K. Das, *J. Chem. Cryst.*, 2002, **32**, 369-375.

[70] W. Feng, Y. Xu, G. Zhou, C. Zhang and X. Zheng, *Inorg. Chem. Commun.*, 2007, **10**, 49-52.

[71] K. Pavani, A. Ramanan and M.S. Whittingham, *J. Mol. Struct.*, 2006, **796**, 179-186.

[72] M.-L. Tong, J. Wang, S. Hu and S.R. Batten, *Inorg. Chem. Commun.*, 2005, **8**, 48-51.

[73] P. Wang, C.N. Moorefield, M. Panzner and G.R. Newkome, *Cryst. Growth Des.*, 2006, **6**, 1563-1565.

[74] P. Wang, C.N. Moorefield, M. Panzner and G.R. Newkome, *Chem. Commun.*, 2005, 4405-4407.

[75] C.L. Klein, R.J. Majeste, L.M. Trefonas and C.J. O'Connor, *Inorg. Chem.*, 1982, **21**, 1891-1897.

[76] L.-M. Zheng, Y. Wang, X. Wang, J.D. Korp and A.J. Jacobson, *Inorg. Chem.*, 2001, **40**, 1380-1385.

[77] D.M. Ciurtin, M.D. Smith and H.-C.z. Loye, *Dalton Trans.*, 2003, 1245-1250.

[78] X.-M. Zhang and R.-Q. Fang, *Inorg. Chem.*, 2005, **44**, 3955-3959.

[79] C.-M. Liu, D.-Q. Zhang, J.-L. Luo, N.-L. Wang, H.-M. Hu and D.-B. Zhu, *Eur. J. Inorg. Chem.*, 2003, 3618-3622.

[80] F.-C. Liu, Y.-F. Zeng, J.-P. Zhao, B.-W. Hu, X.-H. Bu, J. Ribas and S.R. Batten, *Inorg. Chem. Commun.*, 2007, **10**, 129-132.

[81] L. Mao, S.J. Rettig, R.C. Thompson, J. Trotter and S.-H. Xia, *Can. J. Chem.*, 1996, **74**, 433-444.

[82] C.J. O'Connor, C.L. Klein, R.J. Majeste and L.M. Trefonas, *Inorg. Chem.*, 1982, **21**, 64-.

[83] M. Kondo, T. Okubo, A. Asami, S.-I. Noro, T. Yoshitomi, S. Kitagawa, T. Ishii, H. Matsuzaka and K. Seki, *Angew. Chem. Int. Ed. Engl.*, 1999, **38**, 140-143.

[84] X.-H. Li, Q. Shi, M.-L. Hu and H.-P. Xiao, *Inorg. Chem. Commun.*, 2004, **7**, 912-914.

[85] J.-Z. Zou, Z. Xu, W. Chen, K.M. Lo and X.-Z. You, *Polyhedron*, 1999, **18**, 1507-1512.

[86] R. Matsuda, R. Kitaura, S. Kitagawa, Y. Kubota, T.C. Kobayashi, S. Horike and M. Takata, *J. Am. Chem. Soc.*, 2004, **126**, 14063-14070.

[87] R. Kitaura, K. Fujimoto, S.-I. Noro, M. Kondo and S. Kitagawa, *Angew. Chem. Int. Ed. Engl.*, 2002, **41**, 133-135.

[88] T.K. Maji, K. Uemura, H.-C. Chang, R. Matsuda and S. Kitagawa, *Angew. Chem. Int. Ed. Engl.*, 2004, **43**, 3269-3272.

[89] J.-H. Yang, S.-L. Zheng, X.-L. Yu and X.-M. Chen, *Cryst. Growth Des.*, 2004, **4**, 831-836.

[90] G. Smith, A.N. Reddy, K.A. Byriel and C.H.L. Kennard, *J. Chem. Soc., Dalton Trans.*, 1995, 3565-3570.

[91] F. Jaber, F. Charbonnier and R. Faure, *J. Chem. Cryst.*, 1994, **24**, 681-684.

[92] G.-Q. Xiang, N.-W. Zhu, M.-L. Hu, H.-P. Xiao and X.-X. Chen, *Acta Cryst.*, 2004, **E60**, m647-m649.

[93] S. Konar, S.C. Manna, E. Zangrando and N.R. Chaudhuri, *Inorg. Chim. Acta*, 2004, **357**, 1593-1597.

[94] R.L. Harlow and S.H. Simonsen, *Acta Cryst.*, 1974, **B30**, 1370-1372.

[95] H. Ptasiewicz-Bak and J. Leciejewicz, *J. Coord. Chem.*, 1998, **44**, 299-309.

[96] F. Cariati and L. Naldini, *Gazz. Chim. Ital.*, 1965, **95**, 3-7.

[97] S.J. Lippard and D.A. Ucko, *Inorg. Chem.*, 1968, **7**, 1051-1056.

[98] S.J. Lippard and K.M. Melmed, *J. Am. Chem. Soc.*, 1967, **89**, 3929-3930.

[99] S.J. Lippard and K.M. Melmed, *Inorg. Chem.*, 1967, **6**, 2223-2228.

[100] B. Zurowska, J. Ochocki, J. Mrozinski, Z. Ciunik and J. Reedijk, *Inorg. Chim. Acta*, 2004, **357**, 755-763.

[101] M. Palicová, P. Segl'a, D. Miklós, M. Kopcová, M. Melník, B. Dudová, D. Hudecová and T. Glowiak, *Polyhedron*, 2000, **19**, 2689-2695.

[102] G.B. Deacon and R.J. Phillips, *Coord. Chem. Rev.*, 1980, **33**, 227-250.

[103] A.L. Spek, *Acta Cryst. Sect. A*, 1990, **46**, C34.

[104] A.A.D. Tulloch, A.A. Danopoulos, S. Kleinhenz, M.E. Light, M.B. Hursthouseand G. Eastham, *Organometallics*, 2001, **20**, 2027-2031.

[105] E. Balogh-Hergovich, J. Kaizer, G. Speier, V. Fülöp and L. Párkányi, *Inorg. Chem.*, 1999, **38**, 3787-3795.

[106] F. Jian, F. Bei, L. Lu, X. Yang, X. Wang, I.A. Razak, S.S. Raj and H.-K. Fun, *Acta Cryst.*, 2000, **56**, e288-e289.

[107] T.C. Deivaraj and J.J. Vittal, *Acta Cryst.*, 2001, **E57**, m566-m567.

[108] A.Y. Verat, F.D. Sokolov, N.G. Zabirov, M.G. Babashkina, D.B. Krivolapov, V.V. Brusko and I.A. Litvinov, *Inorg. Chim. Acta*, 2006, **359**, 475-483.

[109] I. García-Orozco, M.C. Ortega-Alfaro, J.G. López-Cortés, R.A. Toscano and C. Alvarez-Toledano, *Inorg. Chem.*, 2006, **45**, 1766-1773.

[110] R.-Q. Zau, X.-H. Bu, M. Du and Y.-X. Sui, *J. Mol. Struct.*, 2004, **707**, 11-15.

[111] G.R. Newkome, D.K. Kohli, F.R. Fronczek, B.J. Hales, E.E. Case and G. Chiari, *J. Am. Chem. Soc.*, 1980, **102**, 7608-7610.

[112] M. Du, X.-H. Bu, M. Shioroya and M. Shiro, *J. Mol. Struct.*, 2002, **607**, 155-161.

[113] E.J. O'Reilly, G. Smith, C.H.L. Kennard and A.H. White, *Aust. J. Chem.*, 1983, **36**, 183-190.

[114] J.-F. Xiang, M. Li, S.-M. Wu, L.-J. Yuan and J.-T. Sun, *Acta Cryst.*, 2006, **E62**, m1122-m1123.

[115] S. Martínez-Vargas, R.A. Toscano and J. Valdés-Martínez, *Acta Cryst.*, 2007, **E63**, m1975-m1976.

[116] L. Leiserowitz, *Acta Cryst.*, 1976, **B32**, 775-802.

[117] F. Takusagawa and T.F. Koetzle, *Acta Cryst.*, 1978, **B34**, 1149-1154.

[118] K. Biradha and M.J. Zaworotko, *Crystal Engineering*, 1998, **1**, 67-78.

[119] J.Y. Lu and V. Schauss, *CrystEngComm*, 2001, **26**, 1-3.

[120] J.M. Ellsworth and H.-C.z. Loye, *Dalton Trans.*, 2008, 5823-5835.

[121] SHELXTL Version 6.10. G. M. Sheldrick, Madison, Wisconsin, USA, 2000.

[122] DENZO, Z. Otwinowski, W. Minor, in: C.W.C. Jr and R.M.S. (Eds.), *Academic Press*, 1997, **276**, 307-326.

[123] COLLECT: Data Collection Software, R. Hooft, and B.V. Nonius, 1998.

[124] S. Liu, Y. Yu and L.S. Liebeskind, *Org. Lett.*, 2007, **9**, 1947-1950.

[125] Z. Zhang, Y. Yu and L.S. Liebeskind, *Org. Lett.*, 2008, **10**, 3005-3008.

[126] C.G. Frost, S.D. Penrose, K. Lambshead, P.R. Raithby, J.E. Warren and R. Gleave, *Org. Lett.*, 2007, **9**, 2119-2122.

[127] D. Naskar, A. Roy, W.L. Seibel and D.E. Portlock, *Tetrahedron Lett.*, 2003, **44**, 5819-5821.

[128] A.H. Soloway, W. Tjarks, B.A. Barnum, F.G. Rong, R.F. Barth, I.M. Codogni and J.G. Wilson, *Chem. Rev.*, 1998, **98**, 1515-1562.

[129] M.F. Hawthorne, *Angew. Chem. Int. Ed. Engl.*, 1993, **32**, 950-984.

[130] W. Wu, H. Zhu, L. Fan, D. Liu, R. Renneberg and S. Yang, *Chem. Commun.*, 2007, 2345-2347.

[131] A. Schiller, R.A. Wessling and B. Singaram, *Angew. Chem. Int. Ed. Engl.*, 2007, **46**, 6457-6459.

[132] H.Y.V. Ching, J.K. Clegg and L.M. Rendina, *Dalton Trans.*, 2007, 2121-2126.

[133] C. He, C. Cheng, J. Cheng, C. Liu, Q. Li and A. Lei, *Angew. Chem. Int. Ed. Engl.*, 2008, **47**, 6414-6417.

[134] J. Fournier, T. Maris, J.D. Wuest, W. Guo and E. Galoppini, *J. Am. Chem. Soc.*, 2003, **125**, 1002-1006.

[135] V.R. Pedireddi and N. SeethaLekshmi, *Tetrahedron Lett.*, 2004, **45**, 1903-1906.

[136] R.W. Tilford, W.R. Gemmill, H.-C.z. Loye and J.J. Lavigne, *Chem. Mater.*, 2006, **18**, 5296-5301.

[137] P. Rodríguez-Cuamatzi, O.I. Arillo-Flores, M.I. Bernal-Uruchurtu and H. Höpfl, *Cryst. Growth Des.*, 2005, **5**, 167-175.

[138] M. Filthaus, I.M. Oppel and H.F. Bettinger, *Org. Biomol. Chem.*, 2008, **6**, 1201-1207.

[139] N. SeethaLekshmi and V.R. Pedireddi, *Cryst. Growth Des.*, 2007, **7**, 944-949.

[140] C.B. Aakeröy, J. Desper and B. Levin, *CrystEngComm*, 2005, **7**, 102-107.

[141] P. Rogowska, M.K. Cyranski, A. Sporzynski and A. Ciesielski, *Tetrahedron Lett.*, 2006, **47**, 1389-1393.

[142] M.T. Reetz, J. Huff, J. Rudolph, K. Töllner, A. Deege and R. Goddard, *J. Am. Chem. Soc.*, 1994, **116**, 11588-11589.

[143] P. Rodríguez-Cuamatzi, G. Vargas-Díaz and H. Höpfl, *Angew. Chem. Int. Ed. Engl.*, 2004, **43**, 3041-3044.

[144] D. Braga, M. Polito, M. Bracaccini, D. D'Addario, E. Tagliavini and L. Sturba, *Organometallics*, 2003, **22**, 2142-2150.

[145] R. Knapp and M. Rehahn, *J. Organomet. Chem.*, 1993, **452**, 235-240.

[146] A.S. Batsanov, D. Hérault, J.A.K. Howard, L.G.F. Patrick, M.R. Probert and A. Whiting, *Organometallics*, 2007, **26**, 2414-2419.

[147] J.C. Norrild and I. Sotofte, *J. Chem. Soc., Perkin Trans. 2*, 2001, **2**, 727-732.

[148] K. Arnold, B. Davies, R.L. Giles, C. Grosjean, G.E. Smith and A. Whiting, *Adv. Synth. Catal.*, 2006, **348**, 813-820.

[149] N. SeethaLekshmi and V.R. Pedireddi, *Inorg. Chem.*, 2006, **45**, 2400-2402.

[150] H. Kara, C.J. Adams, G. Orpen and T.J. Podesta, *New J. Chem.*, 2006, **30**, 1461-1469.

[151] Y.-J. Zhong, Y.-M. Chen, Y.-Q. Sun and G.-Y. Yang, *CrystEngComm*, 2005, **7**, 237-242.

[152] M. Wiebcke, *J. Mater. Chem.*, 2002, **12**, 143-147.

[153] W. Tjarks, *J. Organomet. Chem.*, 2000, **614-615**, 37-47.

[154] J. Myung, K.B. Kim, and C.M. Crews, *Med. Res. Rev.*, 2001, **21**, 245-273.

[155] A. Sugasaki, K. Sugiyasu, M. Ikeda, M. Takeuchi and S. Shinkai, *J. Am. Chem. Soc.*, 2001, **123**, 10239-10244.

[156] G.S. Weston, J. Blázquez, F. Baquero and B.K. Shoichet, *J. Med. Chem.*, 1998, **41**, 4577-4586.

[157] W.J. Bodell, A.P. Bodell and D.D. Giannini, *Neuro-Oncol*, 2007, **9**, 12-19.

[158] J.P. Lorand and J.O. Edwards, *J. Org. Chem.*, 1959, **24**, 769-774.

[159] S. Gamsey, A. Miller, M.M. Olmstead, C.M. Beavers, L.C. Hirayama, S. Pradhan, R.A. Wessling and B. Singaram, *J. Am. Chem. Soc.*, 2007, **129**, 1278-1286.

[160] J. Zhao, M.G. Davidson, M.F. Mahon, G. Kociok-Köhn and T.D. James, *J. Am. Chem. Soc.*, 2004, **126**, 16179-16186.

[161] L. Chi, J. Zhao and T.D. James, *J. Org. Chem.*, 2008, **73**, 4684-4687.

[162] D.B. Cordes, S. Gamsey, Z. Sharrett, A. Miller, P. Thoniyot, R.A. Wessling and B. Singaram, *Langmuir*, 2005, **21**, 6540-6547.

[163] S. Gamsey, N.A. Baxter, Z. Sharrett, D.B. Cordes, M.M. Olmstead, R.A. Wessling and B. Singaram, *Tetrahedron*, 2006, **62**, 6321-6331.

[164] N.A. Petasis and I.A. Zavialov, *J. Am. Chem. Soc.*, 1998, **120**, 11798-11799.

[165] K. Ishihara and H. Yamamoto, *Eur. J. Org. Chem.*, 1999, 527-538.

[166] J.-P. Corbet and G. Mignani, *Chem. Rev.*, 2006, **106**, 2651-2710.

[167] N. Miyaura and A. Suzuki, *Chem. Rev.*, 1995, **95**, 2457-2483.

[168] P.R. Parry, C. Wang, A.S. Batsanov, M.R. Bryce and B. Tarbit, *J. Org. Chem.*, 2002, **67**, 7541-7543.

[169] L.S. Liebeskind and J. Srogl, *J. Am. Chem. Soc.*, 2000, **122**, 11260-11261.

[170] L.S. Liebeskind and J. Srogl, *J. Org. Lett.*, 2002, **4**, 979-981.

[171] H. Yang, H. Li, R. Wittenberg, M. Egi, W. Huang and L.S. Liebeskind, *J. Am. Chem. Soc.*, 2007, **129**, 1132-1140.

[172] H. Prokopcová and C.O. Kappe, *J. Org. Chem.*, 2007, **72**, 4440-4448.

[173] K. Billingsley and S.L. Buchwald, *J. Am. Chem. Soc.*, 2007, **129**, 3358-3366.

[174] R.R. Shuvalov and P.C. Burns, *Acta Cryst.*, 2003, **C59**, i47-i49.

[175] P. Metrangolo, H. Neukirch, T. Pilati and G. Resnati, *Acc. Chem. Res.*, 2005, **38**, 386-395.

[176] T. Caronna, R. Liantonio, T.A. Logothetis, P. Metrangolo and G. Resnati, *J. Am. Chem. Soc.*, 2004, **126**, 4500-4501.

[177] E. Corradi, S.V. Meille, M.T. Messina, P. Metrangolo and G. Resnati, *Angew. Chem. Int. Ed. Engl.*, 2000, **39**, 1782-1786.

[178] T. Klis and J. Serwatowski, *Acta Cryst.*, 2008, **E64**, o1054.

[179] J.-M. Lo, S.-M. Chen, M.-H. Chen, Y.-J. Chen, F.-L. Liao and T.-H. Lu, *Acta Cryst.*, 2004, **E60**, o1851-o1853.

[180] P. Rodríguez-Cuamatzi, G. Vargas-Díaz, T. Maris, J.D. Wuest and H. Höpfl, *Acta Cryst.*, 2004, **E60**, o1316-o1318.

[181] J.A. Swift, R. Pal, and J.M. McBride, *J. Am. Chem. Soc.*, 1998, **20**, 96-104.

[182] P. Kirsop, J.M.D. Storey and W.T.A. Harrison, *Acta Cryst.*, 2006, **E60**, o222-o224.

[183] M.R. Shimpi, N. SeethaLekshmi and V.R. Pedireddi, *Cryst. Growth Des.*, 2007, **7**, 1958-1963.

[184] N.S.P. Bhuvanesh, and J.H. Reibenspies, *Acta Cryst.*, 2005, **E61**, o362-o364.

[185] L.M. Wilson and A.C. Griffin, *J. Mater. Chem.*, 1993, **3**, 991-994.

[186] J.D. Larkin, K.L. Bhat, G.D. Markham, B.R. Brooks, H.F. Schaefer and C.W. Bock, *J. Phys. Chem. A*, 2006, **110**, 10633-10642.

[187] M.B. Smith, S.H. Dale, S.J. Coles, T. Gelbrich, M.B. Hursthouse and M.E. Light, *CrystEngComm*, 2006, **8**, 140-149.

[188] S.E. Dann, S.E. Durran, M.R.J. Elsegood, M.B. Smith, P.M. Staniland, S. Talib and S.H. Dale, *J. Organomet. Chem.*, 2006, **691**, 4829-4842.

[189] M.B. Smith, S.H. Dale, S.J. Coles, T. Gelbrich, M.B. Hursthouse, M.E. Light and P.N. Horton, *CrystEngComm*, 2007, **9**, 165-175.

[190] M.R.J. Elsegood, M.B. Smith and P.M. Staniland, *Inorg. Chem.*, 2006, **45**, 6761-6770.

[191] A.L. Balch, M.M. Olmstead and S.P. Rowley, *Inorg. Chim. Acta*, 1990, **168**, 255-264.

[192] D.J. Darensbourg, P. Ganguly and D.R. Billodeaux, *Organometallics*, 2004, **23**, 6025-6030.

[193] W.L. Steffen and G.J. Palenik, *Inorg. Chem.*, 1976, **15**, 2432-2439.

[194] J. Cook, A. Hicks, T. Frazier, D.M. Kimari, T.A. Budzichowski, J.A.K. Bauer and S.K. Mandal, *J. Chem. Cryst.*, 2003, **33**, 481-489.

[195] B.L. Shaw and S.D. Perera, *Chem. Commun.*, 1998, 1863-1864.

[196] D.E. Berning, K.V. Katti, C.L. Barnes and W.A. Volkert, *J. Am. Chem. Soc.*, 1999, **121**, 1658-1664.

[197] N. Pillarsetty, K. Raghuraman, C.L. Barnes and K.V. Katti, *J. Am. Chem. Soc.*, 2005, **127**, 331-336.

[198] S.E. Durran, M.R.J. Elsegood, N. Hawkins, M.B. Smith and S. Talib, *Tetrahedron Lett.*, 2003, **44**, 5255-5257.

[199] M.B. Smith and M.R.J. Elsegood, *Tetrahedron Lett.*, 2002, **43**, 1299-1301.

[200] J. Fawcett, P.A.T. Hoye, R.D.W. Kemmitt, D.J.K. Law and D.R. Russell, *J. Chem. Soc., Dalton Trans.*, 1993, 2563-2568.

[201] G.M. Brown, M.R.J. Elsegood, A.J. Lake, N.M. Sanchez-Ballester, M.B. Smith, T.S. Varley and K. Blann, *Eur. J. Inorg. Chem.*, 2007, 1405-1414.

[202] F.A. Cotton and B. Hong, *Prog. Inorg. Chem.*, 1992, **40**, 179.

[203] E.J. Fernández, A. Laguna, J.M. López-de-Luzuriaga, M. Monge, M. Montiel, M.E. Olmos, R.C. Puelles and E. Sánchez-Forcada, *Eur. J. Inorg. Chem.*, 2007, 4001-4005.

[204] S.O. Grim and L.J. Matienzo, *Tetrahedron Lett.*, 1973, **14**, 2951-2953.

[205] G. Märkl, G.Y. Jin and C. Schoerner, *Tetrahedron Lett.*, 1980, **21**, 1409-1412.

[206] J.C. Kane, E.H. Wong, G.P.A. Yap and A.L. Rheingold, *Polyhedron*, 1999, **18**, 1183-1188.

[207] S.E. Durran, M.R.J. Elsegood and M.B. Smith, *New J. Chem.*, 2002, **26**, 1402-1408.

[208] D.A. Clarke, P.W. Miller, N.J. Long and A.J.P. White, *Dalton Trans.*, 2007, 4556-4564.

[209] E. Shirakaw and T. Hiyama, *J. Organomet. Chem.*, 1999, **576**, 169-178.

[210] K.R. Reddy, K. Surekha, G.-H. Lee, S.-M. Peng and S.-T. Liu, *Organometallics*, 2000, **19**, 2637-2639.

[211] E.K.v.d. Beuken, W.J.J. Smeets, A.L. Spek and B.L. Feringa, *Chem. Commun.*, 1998, 223-224.

[212] R.E. Rülke, V.E. Kaasjager, P. Wehman, C.J. Elsevier, P.W.N.M.v. Leeuwen, K. Vrieze, J. Fraanje, K. Goubitz and A.L. Spek, *Organometallics*, 1996, **15**, 3022-3031.

[213] P. Pelagatti, A. Bacchi, M. Carcelli, M. Costa, A. Fochi, P. Ghidini, E. Leporati, M. Masi, C. Pelizzi and G. Pelizzi, *J. Organomet. Chem.*, 1999, **583**, 94-105.

[214] T. Fukuda, A. Takeharà and M. Iwao, *Tetrahedron: Asymmetry*, 2001, **12**, 2793-2799.

[215] H. Yoshida, Y. Honda, E. Shirakawa and T. Hiyama, *Chem. Commun.*, 2001, 1880-1881.

[216] P.P. Phadnis, S. Dey, V.K. Jain, M. Nethaji and R.J. Butcher, *Polyhedron*, 2006, **25**, 87-94.

[217] P. Stepnicka, *Eur. J. Inorg. Chem.*, 2005, 3787-3803.

[218] A.D. Burrows, R.W. Harrington, M.F. Mahon and S.J. Teat, *Eur. J. Inorg. Chem.*, 2003, 1433-1439.

[219] M.T. Reetz, S.R. Waldvogel and R. Goddard, *Tetrahedron Lett.*, 1997, **38**, 5967-5970.

[220] S.C. Bourque and H. Alper, *J. Am. Chem. Soc.*, 2000, **122**, 956-957.

[221] M.C. Róman-Martínez, J.A. Díaz-Auñon, C.S.-M.d. Lecea and H. Alper, *J. Mol. Catal.*, 2004, **213**, 177-182.

[222] P. Arya, N.V. Rao and J. Singkhonrat, *J. Org. Chem.*, 2000, **65**, 1881-1885.

[223] P. Arya, G. Panda, N.V. Rao, H. Alper, S.C. Bourque and L.E. Manzer, *J. Am. Chem. Soc.*, 2001, **123**, 2889-2890.

[224] S. Antebi, P. Arya, L.E. Manzer and H. Alper, *J. Org. Chem.*, 2002, **67**, 6623-6631.

[225] M. Keles, Z. Aydin and O. Serindag, *J. Organomet. Chem.*, 2007, **692**, 1951-1955.

[226] M. Cai, J. Sha and Q. Xu, *Tetrahedron*, 2007, **63**, 4642-4647.

[227] M. Cai, J. Sha and Q. Xu, *J. Mol. Catal.*, 2007, **268**, 82-86.

[228] S.-M. Lu and H. Alper, *J. Am. Chem. Soc.*, 2008, **130**, 6451-6455.

[229] A.D. Zotto, C. Greco, W. Baratta, K. Siega and P. Rigo, *Eur. J. Inorg. Chem.*, 2007, 2909-2916.

[230] W. Wu and C.-J. Li, *Chem. Commun.*, 2003, 1668-1669.

[231] S. Liu and D.S. Edwards, *Chem. Rev.*, 1999, **99**, 2235-2268.

[232] R. Schibli, K.V. Katti, W.A. Volkert and C.L. Barnes, *Inorg. Chem.*, 2001, **40**, 2358-2362.

[233] J. Zhang, J.J. Vittal, W. Henderson, J.R. Wheaton, I.H. Hall, T.S.A. Hor and Y.K. Yan, *J. Organomet. Chem.*, 2002, **650**, 123-132.

[234] G.M. Jacobsen, R.K. Shoemaker, M.J. McNevin, M. Rakowski and D.L. DuBois, *Organometallics*, 2007, **26**, 5003-5009.

[235] R.M. Henry, R.K. Shoemaker, R.H. Newell, G.M. Jacobsen, D.L. DuBois and M.R. DuBois, *Organometallics*, 2005, **24**, 2481-2491.

[236] P. Das, J.-F. Capon, F. Gloaguen, F.Y. Pétillon, P. Schollhammer and J. Talarmin, *Inorg. Chem.*, 2004, **43**, 8203-8205.

[237] C.J. Curtis, A. Miedaner, R. Ciancanelli, W.W. Ellis, B.C. Noll, M.R. DuBois and D.L. DuBois, *Inorg. Chem.*, 2003, **42**, 216-227.

[238] M. Fischer and F. Vögtle, *Angew. Chem. Int. Ed. Engl.*, 1999, **38**, 884-905.

[239] S. Gatard, S. Nlate, E. Cloutet, G. Bravic, J.-C. Blais and D. Astruc, *Angew. Chem. Int. Ed. Engl.*, 2003, **42**, 452-456.

[240] M.T. Reetz, G. Lohmer and R. Schwichardi, *Angew. Chem. Int. Ed. Engl.*, 1997, **36**, 1526-1529.

[241] N. Feeder, J. Geng, P.G. Goh, B.F.G. Johnson, C.M. Martin, D.S. Shephard and W. Zhou, *Angew. Chem. Int. Ed. Engl.*, 2000, 1661-1664.

[242] C.-H. Ueng and G.-Y. Hwang, *Acta Cryst.*, 1991, **C47**, 522-525.

[243] J.L. Bookham, W. Clegg, W. McFarlane and E.S. Raper, *J. Chem. Soc., Dalton Trans.*, 1993, 3567-3573.

[244] N.M. Sanchez-Ballester, M.R.J. Elsegood and M.B. Smith, *Acta Cryst.*, 2007, **E63**, m1638.

[245] K.G. Gaw, M.B. Smith and A.M.Z. Slawin, *New J. Chem.*, 2000, **24**, 429-435.

[246] M. Knorr and C. Strohmann, *Organometallics*, 1999, **18**, 248-257.

[247] N.M.S. Ballester, M.R.J. Elsegood, M.B. Smith and G.M. Brown, *Acta Cryst.*, 2007, **E63**, m719-m721.

[248] V. Ravindar, H. Schumann, H. Hemling and J. Blum, *Inorg. Chim. Acta*, 1995, **240**, 145-152.

[249] S.-T. Liu, J.-T. Chen, S.-M. Peng, Y.-L. Hsiao and M.-C. Cheng, *Inorg. Chem.*, 1990, **29**, 1169-1172.

[250] Q.F. Mokuolu, P.A. Duckmanton, P.B. Hitchcock, C. Wilson, A.J. Blake, L. Shukla and J.B. Love, *Dalton Trans.*, 2004, 1960-1970.

[251] F. D'Souza, R. Chitta, A.S.D. Sandanayaka, N.K. Subbaiyan, L. D'Souza, Y. Araki and O. Ito, *Chem. Eur.J.*, 2007, **13**, 8277-8284.

[252] J. Bernstein, R.E. Davis, L. Shimoni and N.-L. Chang, *Angew. Chem. Int. Ed. Engl.*, 1995, **34**, 1555-1573.

[253] S.H. Dale, M.R.J. Elsegood, M. Hemmings and A.L. Wilkinson, *CrystEngComm*, 2004, **6**, 207-214.

[254] M.J. Palmer, J.A. Kenny, T. Walsgrove, A.M. Kawamoto and M.P. Wills, *J. Chem. Soc., Perkin Trans. 1*, 2002, 416-427.

[255] J.X. McDermott, J.F. White and G.M. Whitesides, *J. Am. Chem. Soc.*, 1976, **98**, 6521-6527.

[256] R. Urson, A. Laguna and M. Laguna, *Inorg. Synth.*, 1989, **26**, 85-89.

[257] C. Claver, E. Fernandez, A. Gillon, K. Heslop, D.J. Hyett, A. Martorell, A.G. Orpen and P.G. Pringle, *Chem. Commun.*, 2000, 961-962.

[258] M.T. Reetz and T. Sell, *Tetrahedron Lett.*, 2000, **41**, 6333-6336.

[259] M.T. Reetz and G. Mehler, *Angew. Chem. Int. Ed. Engl.*, 2000, **39**, 3889-3890.

[260] M.v.d. Berg, A.J. Minnaard, E.P. Schudde, J.v. Esch, A.H.M.d. Vries, J.G.d. Vries and B.L. Feringa, *J. Am. Chem. Soc.*, 2000, **122**, 11539-11540.

[261] B. Breit, *Angew. Chem. Int. Ed. Engl.*, 2005, **44**, 6816-6825.

[262] M.T. Reetz, T. Sell, A. Meiswinkel and G. Mehler, *Angew. Chem. Int. Ed. Engl.*, 2003, **42**, 790-793.

[263] M.T. Reetz and G. Mehler, *Tetrahedron Lett.*, 2003, **44**, 4593-4596.

[264] M.T. Reetz and X. Li, *Tetrahedron*, 2004, **60**, 9709-9714.

[265] M.T. Reetz and X. Li, *Angew. Chem. Int. Ed. Engl.*, 2005, **44**, 2959-2962.

[266] B. Breit and W. Seiche, *J. Am. Chem. Soc.*, 2003, **125**, 6608-6609.

[267] V.F. Slagt, P.W.N.M.v. Leeuwen and J.N.H. Reek, *Chem. Commun.*, 2003, 2474-2475.

[268] V.F. Slagt, P.C.J. Kamer, P.W.N.M.v. Leeuwen and H.N.J. Reek, *J. Am. Chem. Soc.*, 2004, **126**, 4056-4057.

Accompanying CD

A CD containing files for each of the structures determined by X-ray crystallography is included in the inside back cover of this thesis. For further information, see the instructions file on the CD.